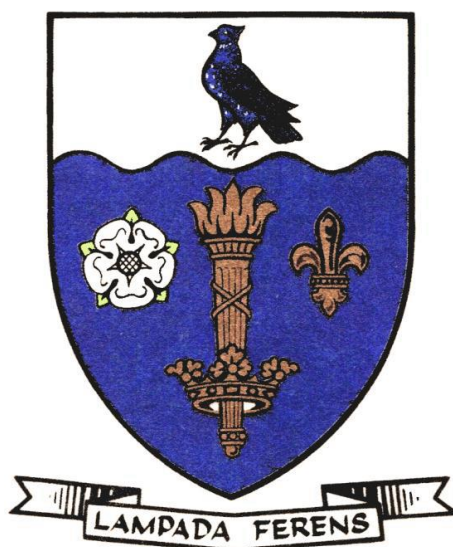


THE UNIVERSITY OF HULL



**POROUS MATERIAL PREPARATION VIA HYDROGEL SLURRY
TEMPLATING TECHNIQUE**

being a Thesis submitted for the Degree of

Doctor of Philosophy
in the University of Hull

by

Marius Rutkevičius, BSc (Hons) University of Warwick

March 2014

CONTENTS

ACKNOWLEDGEMENTS	VI
ABSTRACT	VII
PUBLICATIONS AND PRESENTATIONS	IX
ABBREVIATIONS	X
LIST OF FIGURES	XII
LIST OF TABLES	XVI

CHAPTER 1. INTRODUCTION TO COMPOSITE AND POROUS COMPOSITE MATERIALS 1

1.1 COMPOSITE MATERIALS: SCOPE AND CLASSIFICATION	1
1.2 POROUS MATERIALS: BENEFITS IN CONSTRUCTION AND HI-TECH APPLICATIONS	2
1.2.1 HIERARCHICAL STRUCTURED POROUS MATERIALS	6
1.2.2 AERATED FOOD PRODUCTS	12
1.3 HYDROGELS, THEIR TYPES AND MECHANISMS OF GELATION	14
1.3.1 CARRAGEENAN HYDROGELS	16
1.3.2 XANTHAN HYDROGELS	17
1.3.3 KONJAC HYDROGELS	19
1.4 METHODS FOR CHARACTERISATION OF POROUS MATERIALS	20
1.4.1 MECHANICAL PROPERTIES OF MATERIALS	20
1.4.2 RHEOLOGY: TESTING APPARATUS, VISCOMETRY, ANALYSIS OF MELTING AND GELLING OF A HYDROGEL	22
1.5 HYDROGEL TEMPLATING FOR THE FABRICATION OF POROUS MATERIALS	28
1.6 OBJECTIVES OF THE PRESENT THESIS	29
1.7 PRESENTATION OF THIS THESIS	29
1.8 REFERENCES	31

CHAPTER 2. EXPERIMENTAL

2.1 MATERIALS	36
2.1.1 HYDROGELS	36
2.1.2 FILLER MATERIALS (MATRICES)	36
2.1.3 WATER	39
2.1.4 ORGANIC SOLVENTS	39
2.1.5 CHEMICALS	39

2.2	CHARACTERISATION EQUIPMENT	41
2.2.1	MICROSCOPY	41
2.2.2	SOUND ABSORPTION ANALYSIS	41
2.2.3	MECHANICAL STRENGTH TESTING	43
2.2.4	HYDROGEL SLURRY FABRICATION EQUIPMENT	43
2.2.5	MEASUREMENT OF THE DISSOLUTION TIME OF COMPOSITES	45
2.2.6	OTHER MEASUREMENTS AND INSTRUMENTATION	46
2.3	METHODS	46
2.3.1	PREPARATION OF THE HYDROGELS	46
2.3.2	PREPARATION OF THE HYDROGEL SLURRY TEMPLATED COMPLEXES	48
2.3.3	PREPARATION OF THE POROUS SALT MARBLES	52
2.4	REFERENCES	53

CHAPTER 3. HYDROGEL SLURRY TEMPLATING TECHNIQUE USED TO PRODUCE POROUS CEMENT, GYPSUM, CLAY AND PDMS COMPOSITES **54**

3.1	FABRICATION OF POROUS CEMENT AND PDMS COMPOSITES	54
3.2	CHARACTERISATION OF THE HYDROGEL SLURRIES USED IN POROUS CEMENT, GYPSUM, CLAY AND PDMS COMPOSITE PREPARATION	55
3.3	DENSITIES OF POROUS CEMENT, GYPSUM, CLAY AND PDMS COMPOSITES	55
3.4	CHANGE IN THE VOLUME OF POROUS CEMENT, GYPSUM, CLAY AND PDMS COMPOSITES	62
3.5	SEM ANALYSIS OF THE POROUS CEMENT, PDMS, GYPSUM AND TALC COMPOSITES	64
3.5.1	COMPRESSIONAL STRENGTH ANALYSIS OF POROUS CEMENT AND PDMS COMPOSITES	65
3.6	CONCLUSIONS	67
3.7	REFERENCES	68

CHAPTER 4. FABRICATION OF SOUND ABSORBING MATERIALS USING A HYDROGEL SLURRY TEMPLATING TECHNIQUE **69**

4.1	INTRODUCTION TO SOUND POLLUTION	69
4.2	FABRICATION OF POROUS SOUND ABSORBING CEMENT AND PDMS COMPOSITES USING PAA AND GELLAN GUM HYDROGELS RESPECTIVELY	72
4.3	RESULTS OF POROUS SOUND ABSORBING CEMENT AND PDMS COMPOSITES PREPARED USING PAA AND GELLAN GUM HYDROGELS RESPECTIVELY	73
4.3.1	POROSITY OF THE PDMS AND CEMENT COMPOSITES TEMPLATED WITH HYDROGEL BEAD SLURRIES	73

4.3.2	ANALYSIS OF THE STRUCTURE OF THE SAMPLES: ELECTRON MICROSCOPY AND OPTICAL PHOTOGRAPHY ANALYSIS	75
4.3.3	SOUND ABSORPTION OF POROUS PDMS COMPOSITES	79
4.3.1	SOUND ABSORPTION OF POROUS CEMENT COMPOSITES	80
4.4	FABRICATION OF POROUS SOUND ABSORBING CEMENT COMPOSITES USING XANTHAN-KONJAC HYDROGEL MIXTURE	81
4.4.1	HYDROGEL BEAD SIZE DISTRIBUTIONS AND POROSITY OF THE COMPOSITES	81
4.4.2	SOUND ABSORPTION OF THE XANTHAN – KONJAC HYDROGEL SLURRY TEMPLATED CEMENT COMPOSITES	86
4.4.3	COMPRESSIONAL STRENGTH ANALYSIS OF THE PRODUCED SAMPLES	88
4.4.4	SEM ANALYSIS OF THE POROUS CEMENT COMPOSITES PRODUCED BY TEMPLATING XANTHAN – KONJAC AND ALGINATE HYDROGEL BEAD SLURRIES	91
4.5	CONCLUSIONS	93
4.6	REFERENCES	93

CHAPTER 5. STRUCTURING OF POROUS FOOD PRODUCTS THROUGH HYDROGEL SLURRY TEMPLATING **95**

5.1	INTRODUCTION TO FOOD CHEMISTRY: POROSITY AND TEXTURE	95
5.2	FABRICATION OF POROUS HYDROGEL-SLURRY-TEMPLATED BOUILLON CUBE SAMPLES	97
5.3	RESULTS	100
5.3.1	BOUILLON CUBE COMPOSITES WITH XANTHAN - KONJAC HYDROGEL AS A FILLER	100
5.3.2	BOUILLON CUBE COMPOSITES WITH K-CARRAGEENAN HYDROGEL	113
5.3.3	POROUS FAT - SALT COMPOSITES PREPARED WITHOUT FREEZE-DRYING	132
5.4	CONCLUSIONS	132
5.5	REFERENCES	134

CHAPTER 6. DEVELOPMENT OF HOLLOW-SHELL SALT MARBLES USING SPRAY-GELATION AND DRYING TECHNIQUE **135**

6.1	INTRODUCTION TO THE HEALTH ISSUES RELATED TO THE USE OF TABLE SALT	135
6.2	PREPARATION OF HOLLOW-SHELL SALT MARBLES	139
6.3	RESULTS	140
6.3.1	POROUS SALT MARBLE SIZE ANALYSIS	140
6.3.2	SEM ANALYSIS OF THE HOLLOW-SHELL SALT-HYDROGEL MARBLES	144
6.3.3	SALT-HYDROGEL MARBLE TASTE TESTING: MEASURING IONIC CONDUCTIVITY CHANGE UPON DISSOLUTION	147

6.4	CONCLUSIONS	151
6.5	REFERENCES	152
<u>CHAPTER 7. DEVELOPMENT OF NOVEL SOAP-HYDROGEL FORMULATIONS WITH IMPROVED SUSTAINABILITY</u>		<u>154</u>
7.1	THE NEED FOR SOAP WASTE REDUCTION IN THE DEVELOPED WORLD	154
7.2	RESULTS	155
7.2.1	ADJUSTMENT OF THE MELTING POINTS OF SOAP COMPOSITE	155
7.2.2	MORPHOLOGY ANALYSIS OF THE SOAP-HYDROGEL COMPOSITES	159
7.2.3	DISSOLUTION TIME OF THE SOAP COMPOSITES	161
7.2.4	RELEASE OF THE SOAP DURING DISSOLUTION OF THE SOAP-HYDROGEL COMPOSITES	163
7.3	CONCLUSIONS	166
7.4	REFERENCES	167
<u>CHAPTER 8. SUMMARY AND CONCLUSIONS</u>		<u>169</u>
8.1	REFERENCES	174

ACKNOWLEDGEMENTS

Firstly, and most importantly, I would like to thank my supervisors Prof. Vesko Paunov, Prof. Georg Mehl and Prof. Simeon Stoyanov. It was an excellent opportunity to learn from the countless ideas generator, Vesko, how to be a good researcher, the ideas suggested by him were always interesting for me to carry out. During the productive meetings with Vesko and Georg I learned to present my work effectively and solve scientific problems. I was always welcomed by Georg in his office to discuss any other problems, concerns and his second opinion always gave me the reassurance on my concerns. I would also like to thank him for the occasional jokes in the project review meetings and outside of the Department too. The work carried in Unilever under Simeon's indirect supervision has given me the opportunity to taste the work at an industrial company, which I found both interesting and active. I would like to also thank him for his constructive ideas and support expressed in the meetings and presentations.

Secondly, I would like to thank my colleagues who became friends during my studies: Josef, Anupam, Hamza, Baghali, Andy, Padina, Negar, Saeed, Luke as well as other S&CG Group members. It was good to discuss science and have a great free time together. This also goes to people in Unilever: Theo, Nicolas, Randi, Young, Kace, Viviana, Rita and Katherine. Thirdly, my students who also contributed to the science and life behind the scenes: Camille, Loelia, Marine, Zak, Sellva, Adam, Zoe, Michelle and Ben. I thank you all for your work and cooperation. Fourthly, I must say I would not be in Hull without Kara as my housemate at that time, who really inspired me in becoming a Doctor of Philosophy. It is impossible to say how fortunate I was to get into research.

I also thank all the people who were not in England during my studies, but kept in touch. My sister Viktorija and brother-in-law Saulius, with their son Bernardas, my Mother and Father. Also Monika, Kristina, Kristina, Dainius, Frida, Tomas, Tomas, Darius, Edgaras, Paulius and Vilius.

Last, but not least, I am grateful for the EPSRC and Unilever CASE studentship funding for this project.

ABSTRACT

A novel route for porous and composite material fabrication by templating materials over hydrogel slurries has been developed. The introduction of porosity was achieved by evaporating the water from the incorporated hydrogel particles and thus creating voids within the composite structure. The size of the hydrogel beads was tuned selectively making the technique particularly attractive due to the possibility to fabricate materials of different pore sizes. In addition to this, the technique is environmentally friendly as it does not require to use organic porogens or synthetic particles, but is based on naturally available gelling agents.

The technique was applied to produce porous building materials: cement, gypsum, clay-cement and PDMS. It was possible to introduce up to 75 vol% porosity within these materials using hydrogel slurry templating. The density reduction of these materials would allow easier transportation of building materials and the high porosity showed improved performance in acoustic absorbance of the materials and could lead to an efficient thermal insulation. Scanning Electron Microscopy analysis of porous cement composites showed formation of fibrous domains within the voids of the structure, which are believed to assist the classic sound absorption mechanisms by an additional dissipation of the sound energy. The sound absorption was particularly increased with smaller pore size and a higher degree of porosity within the composites. The reduced mechanical strength of these porous composites makes them suitable for fabrication of non-strength bearing soundproofing panels.

The technique was also applied to the production of porous food formulations: porous bouillon cubes and hollow-shell salt marbles. The porous bouillon cube composites dissolved faster compared to the non-porous samples, moreover, the reduction in the mechanical strength of the porous composites showed that they would be easier to crumble by the consumer, which makes them very attractive for industrial applications. Hollow-shell salt marbles were prepared by spray-gelling a hot hydrogel solution onto a bed of finely milled salt crystals. After coating the surface of the hydrogel with salt, the water from the core of the marble was evaporated producing

hollow-shell salt particles. Upon dissolution in water, these marbles changed the solution conductivity faster than table salt, showing that such marbles would give saltier taste to the consumer with less amount of salt used. The produced particles could find an application in seasoning of dry foods such as crisps and could also be used in baking.

Finally, the hydrogel slurry templating technique was applied to produce composite soap-hydrogel bars. The increase in the hydrogel content within the composites slightly reduced the release of surface active ingredients upon dissolution in water, but due to the change in the texture of the composites the release could also be increased if stress was applied to the composite. The application of hydrogel slurry templating in soaps could reduce the environmental impact of detergents released from the disposed unused soap bars in the hotels.

PUBLICATIONS AND PRESENTATIONS

The work presented in this thesis has given rise to the following publications and presentations:

"Fabrication of novel lightweight composites by a hydrogel templating technique". M. Rutkevičius, S. K. Munusami, Z. Watson, A. D. Field, M. Salt, S. D. Stoyanov, J. Petkov, G. H. Mehl and V. N. Paunov. *Materials Research Bulletin*, 2012, 47, pp 980-986.

"Sound absorption properties of porous composites fabricated by a hydrogel templating technique". M. Rutkevičius, G. H. Mehl, V. N. Paunov, Q. Qin, P. A. Rubini, S. D. Stoyanov and J. Petkov. *Journal of Materials Research*, 2013, 28, pp 2409-2414.

Presentations:

Oral presentation winning "Best Oral Presentation Colloquium Prize 2013"
"Introducing porosity through hydrogel slurry templating". M. Rutkevičius, V. N. Paunov, G. Mehl and S. S. Stoyanov. *Faculty of Science and Engineering, Department of Chemistry Colloquium*, 2013.

Poster presentation: **"Hydrogel Templating Technique to Fabricate Lightweight Meso-porous Composites"**. M. Rutkevičius, G. H. Mehl, S. K. Munusami, Z. Watson, A. D. Field, M. Salt, S. D. Stoyanov, J. Petkov and V. N. Paunov. *European Colloid Interface Society (ECIS)*, 2013.

Poster presentation: **"Fabricating lightweight meso-porous composites by templating hydrogels"**. M. Rutkevičius, G. H. Mehl, S. K. Munusami, Z. Watson, A. D. Field, M. Salt, S. D. Stoyanov, J. Petkov and V. N. Paunov. *Vth International Conference on Molecular Materials (MolMat)*, 2012.

Oral presentation: **"Porous and Composite Material Preparation via a Hydrogel Templating Technique"**. M. Rutkevičius, G. Mehl, V. N. Paunov, S. S. Stoyanov and T. Blijdenstein. *Unilever R&D, Vlaardingen, Netherlands*, March 2014.

ABBREVIATIONS

Abbreviation	Description	Units
UV-Vis	Ultra violet - visible	
KGM	Konjac glucomannan	
SEM	Scanning Electron Microscopy	
rpm	Revolutions per minute	
CNT	Carbon nanotube	
PDMS	Polydimethylsiloxane	
PAA	Polyacrylamide	
vol%	Volume percentage	
wt%	Weight percentage	
ω	Weight fraction	
LBG	Locust Bean Gum	
CMC	Critical micelle concentration	
GPC	Gel Permeation Chromatography	
DSC	Differential Scanning Calorimetry	
μ CT	X-ray microtomography	
FITC	Fluorescein isothiocyanate	
TRITC	Tetramethylrhodamine isothiocyanate	
BET	Brunauer–Emmett–Teller adsorption	
GC-MS	Gas chromatography mass chromatography	
PTR-MS	Proton transfer reaction mass spectrometry	
σ	Compressive strength	Pa
F	Load	N
A_{base}	Area of the base of the sample	m ²
τ	Shear stress	Pa
$\dot{\gamma}$	Shear rate	s ⁻¹
η	Viscosity	Pa s
ϵ_l	Strain	a.u.

γ	Shear strain	a.u.
Ω	Angular velocity	rad s ⁻¹
r	Radius of the base of the cone	mm
G^*	Complex shear modulus	Pa
η^*	Complex viscosity	Pa s
η'	Real (dynamic) viscosity	Pa s
η''	Out-of-phase viscosity	Pa s
G'	Storage modulus	Pa
G''	Loss modulus	Pa
λ	Wavelength	nm
α	Sound absorption coefficient	
f	Frequency	Hz
p_{MAX}, p_{MIN}	Sound pressure (maximum and minimum)	V
ρ_s	Density of a raw material (matrix)	kg m ⁻³
ρ_0	Density of a porous composite	kg m ⁻³
θ	Porosity	

LIST OF FIGURES

Figure 1.1. Classification of composite materials by their structure properties.	2
Figure 1.2. Image showing cement crack healing by the release of calcium carbonate from the micro-encapsulated bacteria spores.	4
Figure 1.3. An SEM image of concrete samples with carbon nanotubes.	5
Figure 1.4. Porous PDMS produced by using water as a porogen.	6
Figure 1.5. Image showing a typical natural hierarchical structure of collagen fibrils forming fibres in a bone tendon.	7
Figure 1.6: Schematic image showing the basic idea of a quadrumodal hierarchical porous material preparation.	9
Figure 1.7: TEM images of silica templated with a polymer and a fluorinated surfactant.	9
Figure 1.8. Porous hierarchical composites made by ice templating.	11
Figure 1.9. Chemical structures of carrageenans (μ and κ).	17
Figure 1.10. Chemical structure of Xanthan gum hydrogel.	18
Figure 1.11. The interaction of Xanthan gum with LBG.	18
Figure 1.12. Chemical structure of Konjac glucomannan.	19
Figure 1.13. The compressional strength analysis of the composites.	Error!
Bookmark not defined.	
Figure 1.14. Graph showing strength vs density of various materials.	22
Figure 1.15. Schematic representation of a fluid placed between two parallel plates, where one of them is stationary and one has a force applied parallel to x direction, resulting in a velocity gradient in the fluid.	24
Figure 1.16. Schematic showing the shear between two parallel planes.	25
Figure 1.17. Graph showing shear stress-rate of strain for materials.	26
Figure 1.18. Schematic image of a plate and cone rheometer.	27
Figure 2.1. Schematic showing an impedance tube.	43
Figure 2.2. Images showing Kenwood Chef mincing attachment.	44
Figure 2.3. Typical setup to determine the dissolution time of the composites.	45

Figure 2.4. Schematic representation of the hydrogel slurry templating technique to produce porous cement and PDMS composites for acoustic testing.	49
Figure 2.5. Schematic of the mould used for soap-gel and bouillon composites.	51
Figure 3.1. (a) Gellan hydrogel beads and (b) polyacrylamide hydrogel bead slurry. (c) The size distribution of the hydrogel beads.	57
Figure 3.2. Moulded samples of porous building materials produced.	59
Figure 3.3. The mass density of the composite porous materials as a function of the initial volume percentage of the hydrogel.	60
Figure 3.4. Schematic representation of the cross-section of a hydrogel slurry templated PDMS composite.	61
Figure 3.5. The volume shrinkage of the porous composite materials as a function of the initial volume percentage of the hydrogel.	63
Figure 3.6. SEM images of cement templated polyacrylamide hydrogel.	64
Figure 3.7. SEM images of PDMS control and porous composites.	65
Figure 3.8. Graphs showing the compressional strength variation of the PDMS samples versus the percentage of the hydrogel.	66
Figure 4.1. Cross sectional diagram of a porous solid with the different pore types.	71
Figure 4.2. SEM images of the solidified porous cement composites.	76
Figure 4.3. SEM images of the PDMS-hydrogel composite samples.	77
Figure 4.4. Schematic representation of the hypothesis of the sound energy dissipation by the fibrous domains present within the pores of the composites.	78
Figure 4.5. Sound absorption coefficient of the PDMS composites.	80
Figure 4.6. Sound absorption coefficient of cement composites as a function of the sound frequency.	81
Figure 4.7. Fluorescence microscopy images of the Xanthan – Konjac beads.	82
Figure 4.8. Histogram showing bead size distribution of the Xanthan – Konjac.	83
Figure 4.9. A photograph of the top of the sample of a porous cement sample.	84
Figure 4.10. Graphs displaying weight loss percentage and porosity.	85
Figure 4.11. Sound absorption of samples made with 50 vol% hydrogel.	87
Figure 4.12. Sound absorption of sample made with 60 vol% hydrogel.	88
Figure 4.13. Sound absorption of sample made with 70 vol% hydrogel.	88
Figure 4.14. Mechanical strength data of porous cement samples.	90

Figure 4.15. SEM images of cement composite samples composed of Xanthan – Konjac hydrogel and sodium alginate hydrogel beads. A photograph of a composite sample with alginate hydrogel beads after drying.	92
Figure 5.1. X-Ray microtomography of a cross-section of a bouillon cube sample.	97
Figure 5.2. Schematic showing the hydrogel slurry templating technique applied for bouillon cubes.....	99
Figure 5.3. DSC graph of palm oil stearin and rheology measurements of a Xanthan – Konjac hydrogel giving the first elastic modulus as a function of the temperature of the hydrogel.	102
Figure 5.4. SEM images of palm oil, table salt crystals and fat mixed with salt. ..	104
Figure 5.5. SEM images of fat - salt composites.	106
Figure 5.6. Images of different fat and salt composites.	107
Figure 5.7. A graph of weight loss and volume expansion after the evaporation. .	109
Figure 5.8. Compression strength analyses after freeze drying of different bouillon cube samples.	110
Figure 5.9. Graph of dissolution time as a function of the hydrogel percentage. ...	112
Figure 5.10. Photographs of typical bouillon composites after freeze-drying.	114
Figure 5.11. Fluorescence microscopy images of the hydrogel and salt-fat base. .	116
Figure 5.12. SEM images of salt-fat base templated with κ -carrageenan.	118
Figure 5.13. Weight loss of the salt-fat-hydrogel composites after freeze-drying..	120
Figure 5.14. The compressional strength of the dried composites.	121
Figure 5.15. Graph comparing the effect of chilling and freezing of the sample for the compressional strength of the composites.	123
Figure 5.16. Graph comparing the effect of initial freezing in a freezer and freezing of the composites with liquid nitrogen for their compressional strength.	124
Figure 5.17. The dissolution time of the porous fat-salt composites at various gelling agent content, for the 25 vol% and 40 vol% κ -carrageenan hydrogel.	126
Figure 5.18. The effect of the gelling agent (κ -carrageenan) content on the dissolution time of the samples.	128
Figure 5.19. The dissolution time vs hydrogel content for different methods of cooling the porous fat-salt composite.	129

Figure 5.20. The dissolution time of different fat-salt – hydrogel slurry composites for the 1.5 wt%, 2.25 wt% and 3 wt% κ -carrageenan within the hydrogels.	131
Figure 5.21. A photograph of a sample that was dried in open air at room temperature after freezing the sample at -20 °C.	132
Figure 6.1. SEM of hollow-shell particles of sodium bicarbonate and table salt. ..	138
Figure 6.2. The method used to produce porous salt marbles.	140
Figure 6.3. Photographs of salt marbles.	141
Figure 6.4. Graph for salt marble size of Xanthan-Konjac salt marbles.	142
Figure 6.5. Graph for salt marble size distribution for κ -carrageenan salt marbles.	143
Figure 6.6. SEM images of salt marbles.	144
Figure 6.7. SEM images showing salt marbles.	145
Figure 6.8. The possible outcomes of the spray gelation technique.	146
Figure 6.9. Conductivity of the aqueous medium vs time followed the introduction of a fixed amount of table salt.	148
Figure 6.10. Conductivity of the aqueous medium vs time followed the introduction of a fixed amount of table salt or alternatively hollow-shell salt marbles.	150
Figure 6.11. Graph showing the solution conductivity upon dissolution of different samples of salt or salt marbles 40 seconds after the addition of the sample.	151
Figure 7.1. UV-Vis spectra of raw soap at various temperatures and samples at molten state and soap base with varying glycerol content.	157
Figure 7.2. Images of hydrogel (Xanthan - Konjac) templated soap composites. ..	159
Figure 7.3. 3D Confocal laser scanning images reconstructing the structure of soap - hydrogel bead composite.	160
Figure 7.4. Images of hydrogel templated soap stirred in water for 20 hours.	162
Figure 7.5. Image showing soap-hydrogel composites.	164
Figure 7.6. Graph showing the change in the surface tension as a function of the time of the sample dissolution experiment.	165
Figure 7.7. Surface tension of soap base vs its concentration in water.	166

LIST OF TABLES

Table 1.1. Methods and their description for the formulation of different types of aerated food products.	13
Table 1.2. Classification of the hydrogels.	15
Table 2.1. Table showing major components of palmoil stearin.	37
Table 2.2. Table showing components of soap base.	38
Table 2.3. Chemicals used, their structure and supplier.	40
Table 2.4. Sound absorption coefficient values for typical materials.	42
Table 3.1. Summary of the templated matrix materials.	57
Table 4.1. Porosity, density and shrinkage of the cement and PDMS composites. .	74
Table 4.2. The standard deviation and the average size of the hydrogel beads after passing through different pore-size mincer plates.	83
Table 5.1. Melting point regions of different fats used for the fat base.	103
Table 5.2. Dissolution time of various hydrogels samples in hot water.	113
Table 7.1: Composition and setting temperature range of soap base with added glycerol.....	158
Table 7.2: Hydrogel composition for the soap-gel mixture.	159
Table 7.3: Hydrogel composition used in soap-hydrogel composites dissolution experiment.	161
Table 7.4. Size and weight change for the soap – hydrogel composites after the dissolution experiment.	162

Chapter 1. Introduction to Composite and Porous Composite Materials

“Writers do not read for fun.”

T. S. Garp, The World According to Garp

In this section of the thesis a literature overview is presented and some of the definitions used throughout the thesis are introduced. The concepts as well as the advantages of composite materials, porous and hierarchical materials, and hydrogels are described. Methods of porosity introduction both in foods and non-food materials are given. Xanthan, konjac and κ -carrageenan hydrogels are described. The Chapter also gives an insight into the main ideas behind this thesis and the objectives of the research.

1.1 COMPOSITE MATERIALS: SCOPE AND CLASSIFICATION

Composites are classically described as materials that consist of two or more individual phases, which when blended together yield a material with new functionalities and properties.¹ The continuous phase, also called *matrix*, usually is a weaker material that holds the *fibres*, which have a high stiffness and a relatively low density.^{1, 2} Examples of man-made matrices are cement, polymers, metals and etc.²⁻⁴ The matrix is often weaker and used to transmit externally applied loads.¹ Examples of fillers are glass, wood or cellulose fibres, clays and others.² Nature has created numerous examples of excellent composites: wood, where the chains of cellulose fibres are present in lignin matrix; bones and teeth, where hydroxyapatite and osteon crystals, respectively, form a tough matrix supported by collagen.² Both of these examples show anisotropy, where the properties of the composite are not the same in x, y and z directions.² Examples of man-made composites are steel rods reinforcing cement matrix in buildings, glass fibres in epoxy matrices in lightweight boats (which account for >80 % of the marine vessels)⁵ and many others. Laminates are stacks of lamina – thin layer of a composite material, with a thickness usually in the order of

0.125 mm.⁶ One can see a significant improvement in the individual material properties once a composite is formed. The scope of classification of the composite materials is quite wide. The main points of interest are described below in Figure 1.1:³

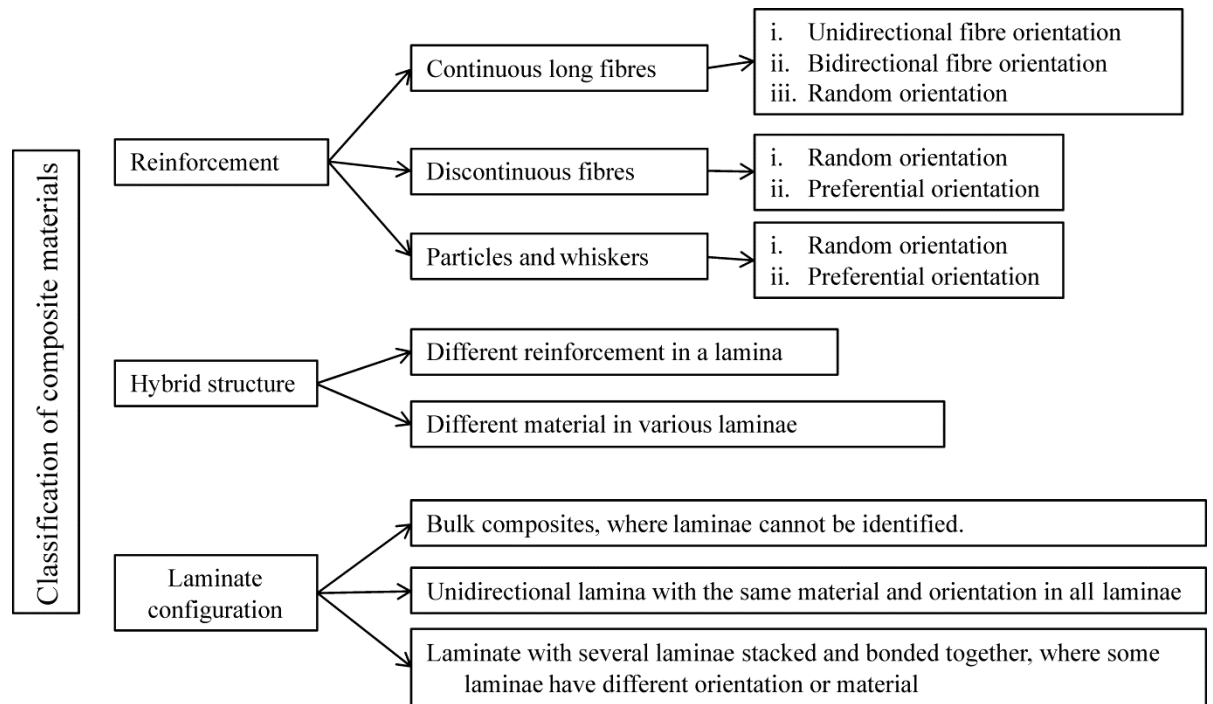


Figure 1.1. Classification of composite materials by their structure properties. Adapted from Introduction to composite materials.³

This thesis will focus on a new type of porous composite materials, where the pores are created by templating soft gel-based materials with a range of ‘scaffolding’ matrixes followed by the effective removal of the liquid from the gel phase by evaporation. This is achieved by templating a slurry of hydrogel microbeads in a self-crosslinking material slurry, such as cement or silicone elastomer with an added cross-linker forming PDMS. The formed materials have randomly dispersed particle composition, i.e. the pores do not show the formation of a distinct lamina.

1.2 POROUS MATERIALS: BENEFITS IN CONSTRUCTION AND HI-TECH APPLICATIONS

To understand the nature of porous materials, first their pores should be defined. A pore is an entrapped gas globule, otherwise defined as a gas quantity separated from environment by an interface.⁷ If the gas network is the continuous phase in a material,

air content can be called porosity.⁸ Porosity adds a new dimension of functionality to a variety of materials. Porous materials can be used in electronics, chemical filtration, biomedicine and pharmaceuticals.^{9, 10} Moreover, porous materials have a lower mass density and usually higher thermal insulation properties than the matrix itself. The improved properties makes the composite materials attractive for the use as building materials. Cement is a widely used building material with 2.8 million tonnes produced worldwide in 2009.¹¹ Apart from its traditional applications, a considerable research focus has been directed at porous cement composites for specific uses in radioactive waste storage,¹² sound¹³ and heat insulation.¹⁴ Improvement of the properties and production cost of current composite materials is beneficial which calls for new routes for their fabrication. Lightweight building materials have always been more appealing for having better thermal and sound insulation, cheaper transportation and sometimes their lower cost. Autoclaved aerated concrete (e.g. Ytong®) and polyurethane or polystyrene foams (e.g. Styrofoam®) resulted in a major breakthrough in the development of modern lightweight building and insulating materials. However, due to the significant flammability of polymer foams and a relatively high cost of production of aerated concrete, there is still a scope for development of alternative routes for fabrication of novel lightweight porous materials.¹⁵ Porous lightweight foamed cement made by introducing air into the cement slurry has shown to have good thermal and acoustic insulation.¹⁶ This cement has also been described as a feasible replacement of gypsum for flame insulation purposes.¹⁴

Recently, self-repairing cement formulations were designed by researchers in Netherlands, where bacteria spores were incorporated in cement mixtures. Once cracks were formed in the samples, water could pass through these channels and the bacteria were activated, producing calcium carbonate, thus healing the cracked cement.¹⁷ Similarly, *Bacillus sphaericus* spores were microencapsulated and released upon crack formation within cement, healing the cracks as shown in Figure 1.2.¹⁸ As well as such self-healing cements, self-cleaning and air-purifying cements have been designed by incorporation of titania nanoparticles.¹⁹ These nanoparticles have also improved the composite resistance to abrasion.²⁰ Other metal nanoparticles incorporated in cement composites showed improved compressional strength and elastic modulus.²⁰⁻²² Clay nanoparticles have also shown to improve the properties of

concrete, by reducing its shrinkage, permeability of chloride and enhancing mechanical properties of such samples.²³⁻²⁵ Carbon nanotubes (CNT) have been claimed as the most promising nanomaterial for strength enhancement and crack reduction in the review paper by Sanchez and Sobolev.²⁶ An image showing bridging of a crack with CNT is shown in Figure 1.3. Another example presented CNTs incorporated in a concrete composite, which was capable to sense pressure changes due to the change in the conductance of CNT.²⁷ To conclude, composites are much more interesting and lead to better results than bulk materials alone. Cement, however, is one of the most ubiquitous material known and research on improvement of its capabilities has been ongoing for thousands of years and will continue in the future.

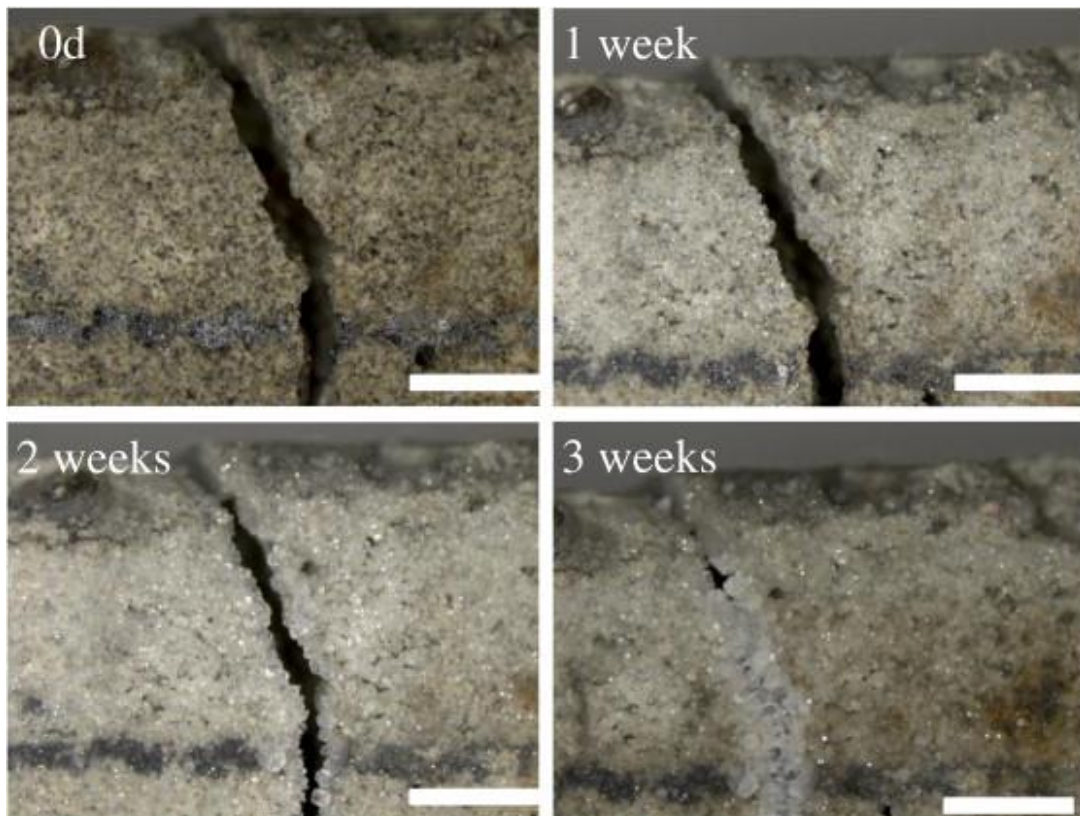


Figure 1.2. Image showing cement crack healing by the release of calcium carbonate from the micro-encapsulated bacteria spores. Scale bar represents 1 mm. Reproduced from Wang, et al.¹⁸

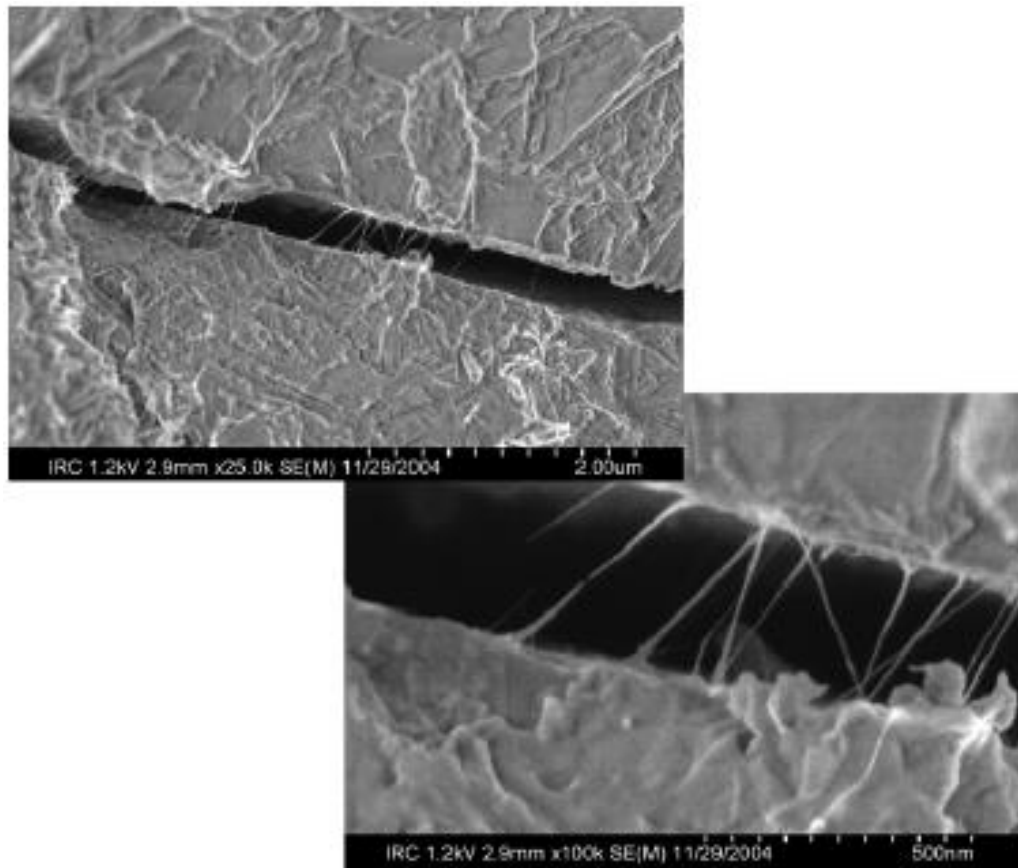


Figure 1.3. SEM images of concrete samples with carbon nanotubes, showing how the carbon nanotubes form bridges within a crack, thus strengthening the material. Reproduced from Makar et al.²⁸

Commercial silicone rubber, on the other hand, has only been available since the 20th century. PDMS (polydimethylsiloxane) is a synthetic polymer with a low glass transition temperature ($-125\text{ }^{\circ}\text{C}$)²⁹, a range of viscosities and can be cured to produce silicon rubber for a wide range of hi-tech applications, such as micro-contact printing, microfluidic device fabrication, as a sealant and an encapsulating material with a higher durability than other types of rubber. Recently, porous PDMS has been produced by emulsion polymerisation within a microfluidic device with water as a porogen which gives pore diameters in the range 2-6 μm (Figure 1.4).³⁰ Such materials could be used for enzyme encapsulation within the microfluidic devices. Surfaces of PDMS have also been made porous by CO_2 -pulsed laser and application of NaCl crystals to the surface prior curing.³¹

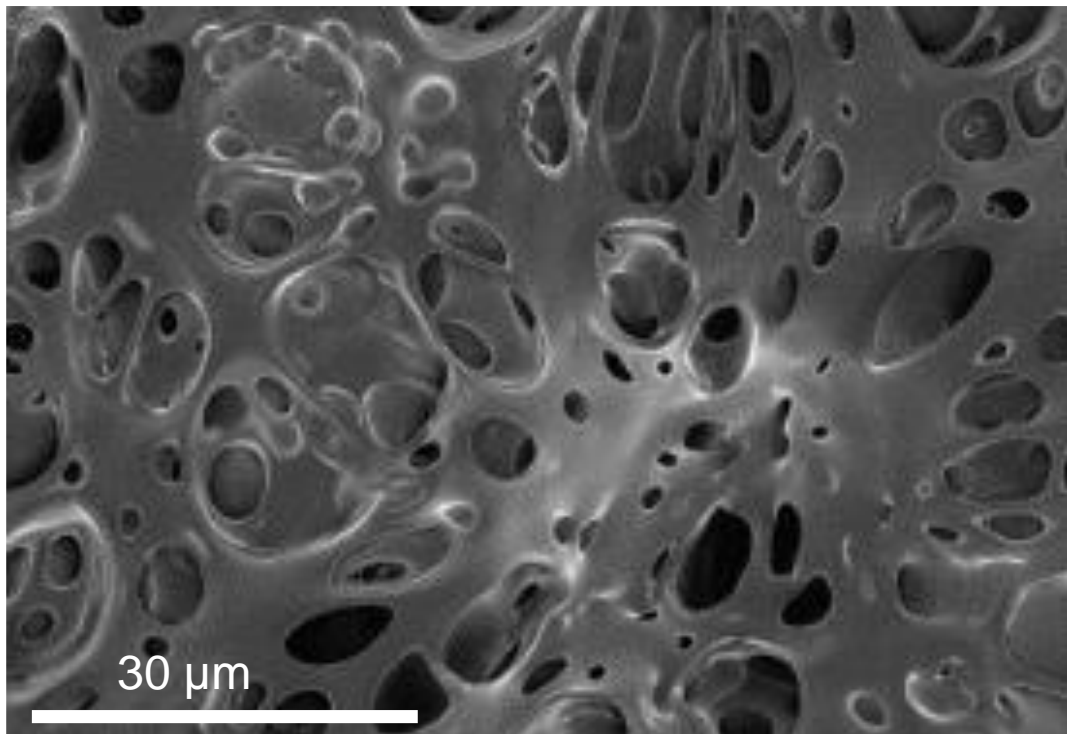


Figure 1.4. Porous PDMS produced by using water as a porogen. Reproduced from Juchniewicz et al.³⁰

1.2.1 Hierarchical Structured Porous Materials

Even more promising and potentially applicable in building and hi-tech applications seem to be hierarchical materials. Natural hierarchical structures are self-organisations of molecular units or their aggregates that are assembled with other phases, which in turn are self-organised at an increasing size levels.³² In other words, hierarchical structures are solids, which within them have structural elements with structure.³³ Such structures are divided into three categories (1D – fibres, 2D – layers and 3D – pores) and have unique properties.³² A cellular solid is a type of hierarchical structure where one of the phases is a solid and the other is an empty space, or possibly a fluid, with examples such as rocks, wood and bones.³³ A good example of 1D natural hierarchical cellular solid is collagen, which structure is shown below in Figure 1.5. Collagen fibrils are forming arrays of arranged structures, as shown by the parallel lines in the image. The structures overlap in different directions, which gives them a high strength and flexibility. The benefits of hierarchy include improvement of strength and toughness or unusual physical properties, e.g. having a negative Poisson's

ratio (auxetics).³³ Natural hierarchical structures possess the advantage of having very precise and complex structure, self-healing or self-repairing capabilities, but on the other hand, they also have negative features – they are stable only between a very narrow pH and temperature range, are only suited for specific moisture and pressure range.³² Hierarchical materials are valued for their high surface area and improved flow properties, as described in a review by Yang and others.^{34, 35}

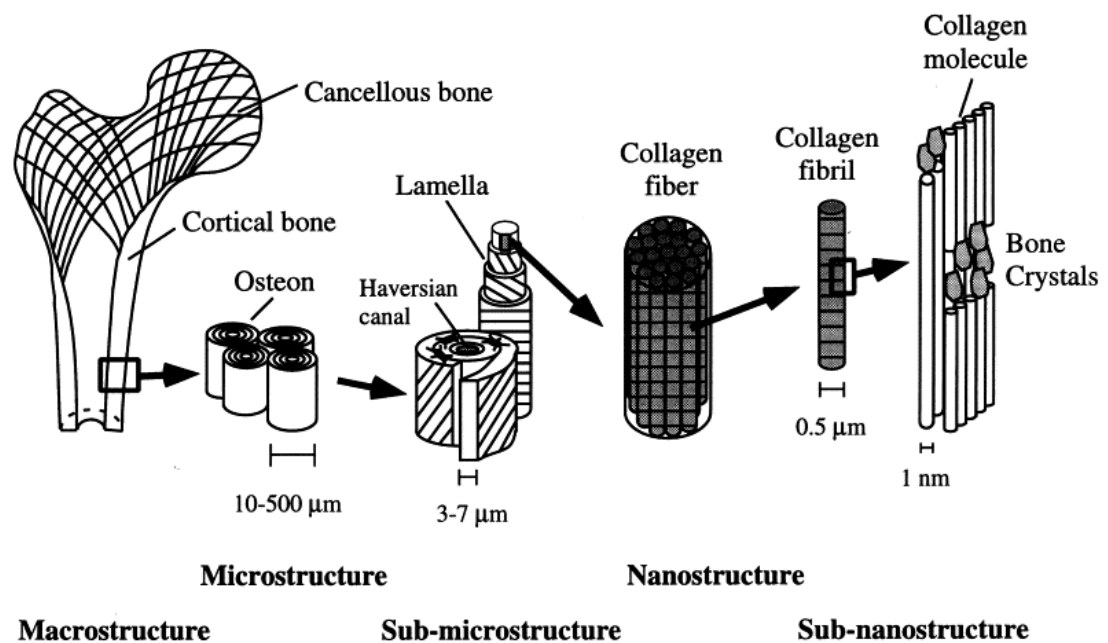


Figure 1.5. Image showing a typical natural hierarchical structure of collagen fibrils forming fibres in a bone tendon. Scale bars at the bottom of the images show the size guides of the structures. The collagen fibres in the Haversian canal form arranged structures that are long and straight, accounting for strength of the material, whereas the other layers form overlapped structures in different directions giving the material flexibility. Image reproduced from Rho et al.³⁶

Size of the pores in hierarchical materials can be controlled by the properties of the templating material. It has been found that nanopores (< 2nm) in zeolites can be controlled by small amine molecules;³⁴ mesopores (2-50 nm) can be controlled by surfactant assemblies^{37, 38} and block co-polymers;³⁸ macropores (>50 nm) have been reported to be formed by the lost wax casting templates.³⁸ Incorporating two different unimodal pore size materials, i.e. macropores into meso-/microporous structures helped to bring the properties from both structures into one for simultaneous

exploitation.³⁴ The synthesis of hierarchical materials was based on the incorporation of multi template systems. The templates can be solid particles, low boiling point liquid drops (alcohol molecules), gas bubbles, supramolecular aggregates, biomaterials and others.³⁴

The dual micellar templating approach has been explored by a number of researchers. Some general results found by them will be presented in this paragraph. The idea of a multi template (e.g. quadrumodal) is represented in Figure 1.6. Various small assembled structures were dispersed within silica gel, the gel was crystallised and then the dispersed structures were removed to create pores. Coppens and co-workers prepared bimodal mesoporous silica by first making mesoporous silica (≈ 2 nm) hydrothermally with cetyl trimethylammonium bromide and then introducing larger pores (16-50 nm) with a triblock co-polymer also by hydrothermal treatment.³⁹ However, these materials lacked a well-defined pore structure on at least one length scale. Antonietti and co-workers reported liquid-crystal templating under acidic conditions by a nanocasting technique.⁴⁰ They also reported templating small fluorosurfactant with poly(styrene)-poly-(ethylene oxide) copolymers, introducing small mesopores within large mesopores at certain concentrations of reactants, their result is displayed below in Figure 1.7.⁴¹ Another family of co-templates – ionic liquids was well researched. The polarisable head groups leading to highly ordered pore structures via a nanocasting technique, which could be used in a size-selective catalysis.^{34, 42} Trimodal meso-/macroporous materials were prepared by templating poly styrene beads (macropores of 360 nm, wall thickness 100 nm), block copolymer $[H(CH_2CH_2CH_2(CH)CH_2CH_3)_x-(OCH_2CH_2)_yOH]$ (large mesopores, spherical shape, size ca. 12 nm) and ionic liquid (1-hexadecyl-3-methylimidazolium chloride) (small elongated mesopores of 2-3 nm size).⁴³ The BET surface area of this material was determined to be $244 \text{ m}^2 \text{ g}^{-1}$ and there was no separation reported between the block copolymer and the ionic liquid.

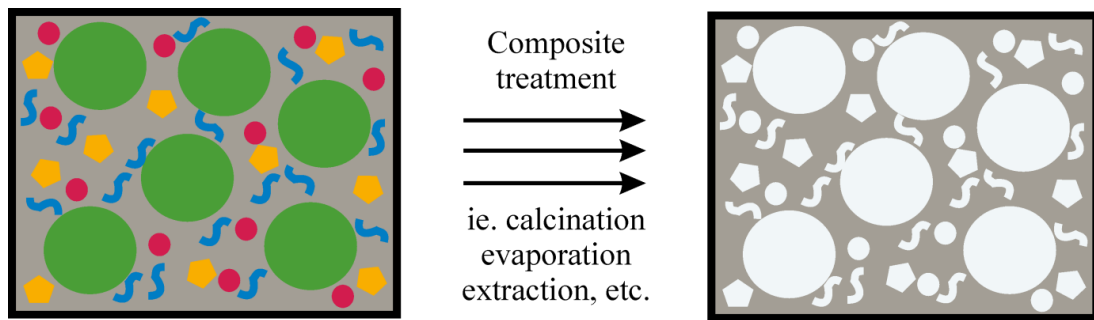


Figure 1.6: Schematic image showing the basic idea of a quadrumodal hierarchical porous material preparation. The left image shows all templates (large green spheres – polystyrene latex particles, orange pentagons – solvent drops, blue s-shaped lines – ionic liquid micelles, small red spheres – surfactant micelles) being incorporated within a silica matrix, whereas after removal of the templates (right image) various size and shape – hierarchic voids are produced. Even more anticipated result would be of a system where the larger pores are interconnected by the smaller pores.⁴³

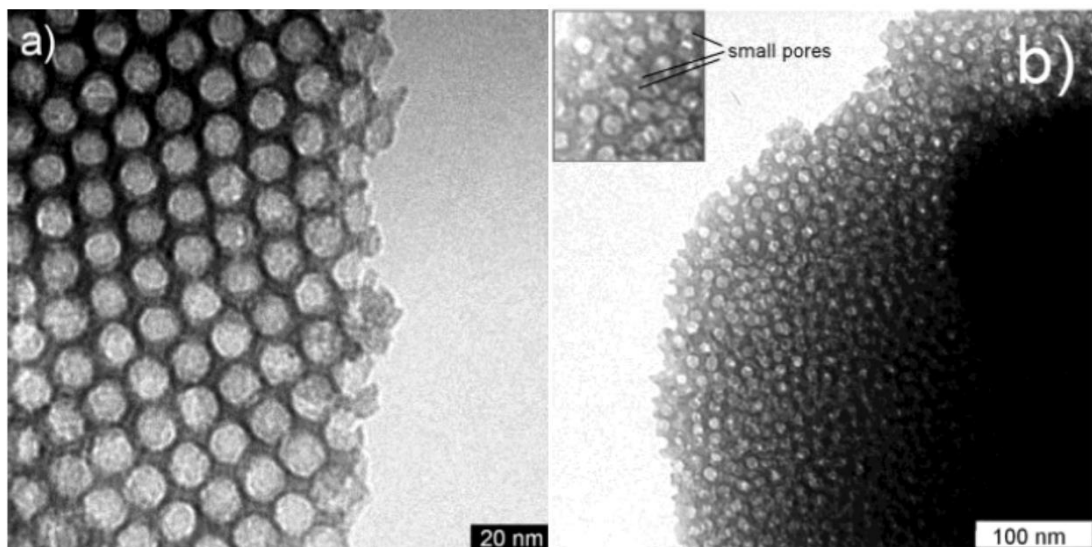


Figure 1.7: TEM images of silica templated with a polymer and a fluorinated surfactant. Both samples (a and b) had SiO_2 (1 g), tetramethylorthosilicate (TMOS, 2.56 g); (a) had 0.45 g polymer and 0.09 g surfactant, (b) – 0.31 g polymer and 0.29 g surfactant. It was observed that increasing the percentage of surfactant reduced the ordering of the sample. The small pores generated by the surfactant are shown in the inset. Reproduced from Groenewolt et al.⁴¹

Small solid particles, such as polystyrene latex beads, were also used by many researchers in hierarchical composite preparation. For example, titania, silica and niobia (Nb_2O_5) composites were prepared by aggregating latex particles in an ordered fashion and then adding an inorganic precursor and a surfactant micellar solution, followed by crystallisation of this phase and removal of the latex particles.⁴⁴ Also, inorganic salt solution droplets (NaCl , LiCl , KCl , NH_4Cl and NiSO_4) were used for the formation of macropores in silica structures, with the size being varied by the rate of evaporation of the solvent and amphiphilic block copolymer self-assembly at the interstices.⁴⁵ The structures were sponge-like, had a high thermal stability and a surface area of $660 \text{ m}^2 \text{ g}^{-1}$.⁴⁵

A versatile method to prepare hierarchical porous materials was reported by Nishihara and co-workers. Micrometre size ice crystals were used to template silica to prepare honeycomb structures.⁴⁶ Their method was based on a micrometre-size ice crystal templating, since thermally induced separation arise when hydrosols, hydrogels, or aqueous slurries of metal oxides are quickly frozen, causing the formation of micrometre-sized spheres within the matrix of the materials.⁴⁶ These spheres can then be templated within macroporous polymers or metal oxides.⁴⁶ Polygonal ice rods with fairly uniform diameters were also grown from hydrogels, as the freezing was unidirectional and there was enough solid material within the gels.⁴⁶ Such rods were then thawed, producing long, ordered silica macropores.⁴⁶ In addition to this, micro- and meso- pores were formed within the materials by drying the tert-butyl alcohol, which was previously soaked into the hydrogel. The size of the macropores was changed by varying the rate of immersion into the cold bath and the thickness by the concentration of SiO_2 .⁴⁶ The structures produced by this method are shown in Figure 1.8. Colard et al. used similar approach to produce a lightweight conducting polymer foam.⁴⁷ Here the researchers used large and small latexes (200-500 nm and 37 nm respectively), which were foamed and frozen in liquid nitrogen, forming soft armoured matrices. The procedure was followed by evaporation of the ice crystals and formation of a dried foam.

Other interesting methods were also used, such as templating within natural wood structure whilst leaching degraded lignin and hemicellulose,⁴⁸ emulsion templating for

macro-meso porous structures,⁴⁹ *Bacillus subtilis* threads were templated in silica⁵⁰ and other materials. Also, there are many examples showing successful hierarchical material preparation procedures by using physical or chemical methods, like chemical etching, physical deposition, leaching and others.⁵¹

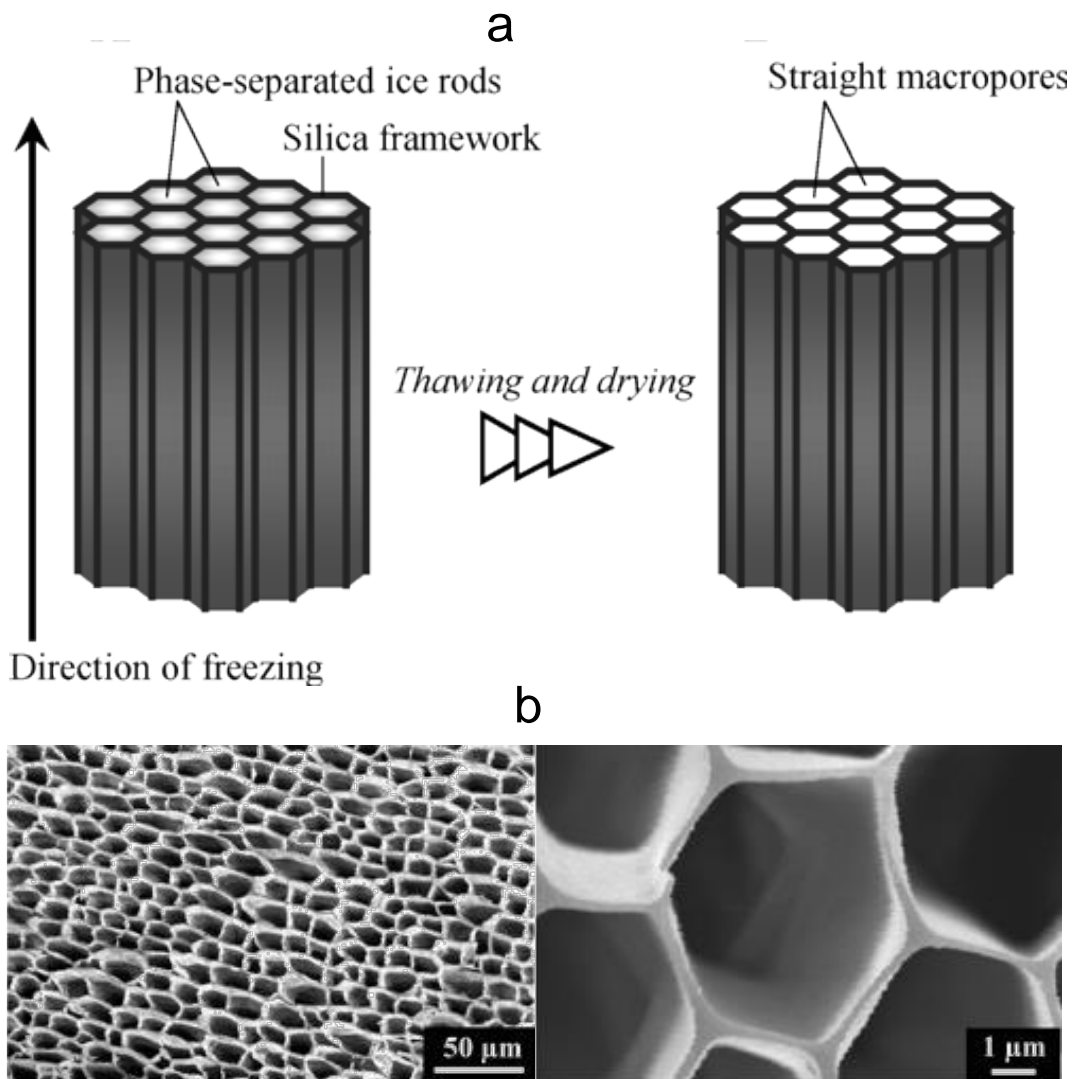


Figure 1.8. Porous hierarchical composites made by ice templating. (a) – schematic of the method, where a straight array of polygonal ice tubes is created and followed by formation of macropores by thawing and removing the ice crystals; (b) – SEM images of a cross-section of silica honeycombs at freezing rates of 6 cm hour^{-1} (left) and 20 cm hour^{-1} (right). Reproduced from Nishihara et al.⁴⁶

1.2.2 Aerated Food Products

It is important to introduce the methods of food aeration at this stage as part of the work described later in this thesis is applicable to foods. A variety of foods in our shopping baskets are actually aerated, i.e. they consist of bubbles. For example, bread, ice cream (that consist of around 50 vol% of air), beer and meringues.⁸ For a number of reasons food producers are particularly interested in the incorporation of bubbles into the products. The bubble interface allows a better exploitation of the ingredients, the density of the food is reduced, different texture of the food gives a different feel of the food, an enhanced surface area and a better digestibility,⁵² as well as a feeling of fullness with a lower mass of product used, even easiness of chewing and many others.⁵³ On the other hand, aeration may lead to the reduced shelf life of food due to the faster oxidation of the porous food and sometimes a loss in flavour and a loss in nutrients as in the baking of bread when sugars are transformed into CO₂ by the yeast.⁸ The methods for food aeration listed in a review paper by Campbell and Mougeot are presented in the Table 1.1 below.⁸ One must remember, that majority of the techniques presented in the previous section of the composite and porous materials preparation cannot be applied to food preparation, as the food industries have to follow strict guidelines in the use of chemicals. These materials have to be approved as being safe for the consumer and not to possess any negative effect endangering the health and safety of the consumer.

The ability to study aerated products in terms of the porosity effect to the product is thought to be largely outside the scope of food scientists.⁸ The contributions from different ingredients such as lipids, surfactants and proteins are well understood,^{54, 55} unlike the pore size distributions, coalescence mechanisms, dynamic behaviour of systems and others.⁸ Most of these systems are thermodynamically unstable and are prone to breaking down, especially at low viscosity. Various stabilisers, such as proteins, emulsifiers, solid particles (fat, calcium carbonate) and solidified matrix are thus used. Bubbles break or coalesce if the interface thins out too much, thus the emulsifiers stabilise the locally depleted areas by moving into these thin-liquid areas and drawing liquid with them. Lipids, on the other hand, form an interlinked network at the interface.⁸

Table 1.1. Methods and their description for the formulation of different types of aerated food products. Adapted from Campbell and Mougeot.⁸

Method	Description	Uses
Fermentation	Yeast produced carbon dioxide	Bread, beer, wine
Whipping or shaking	Air entrapment by low-medium viscosity liquids or fat crystals	Beaten egg whites, whipped cream
Mixing of high viscosity pastes and doughs	Bubbles are entrapped as surfaces come together	Bread, nougat
Steam generation	During cooking, baking or frying of water-containing foods	Doughnuts, waffles
Entrapment	Between sheeted layers	Croissants, pastries
Frying	Very hot oil causing internal steam to puff the product	Crisps
Chemical raising agents	Carbonated salt decomposition into CO ₂	Cakes, pancakes
Rapid dry heating	Small or thin products puff and blister	Corn flakes, crisps
Gas injection	Air, carbon dioxide or nitrogen injection	Ice cream, soft drinks, bubble gum
Expansion extrusion	Superheated product emerging from an extruder in which moisture vaporises	Crisps, cereals, marshmallow, pet food
Pressure beating	Dissolution of gas under pressure	Chocolate, syrup
Puffing	Sudden pressure release of a superheated product containing moisture	Cereals
Vacuum expansion	Vacuum is applied and the temperature lowered to solidify the product	Chocolate bars
Special cases	Microwave or pan use for the expansion of popcorns, dough mixing with carbonated water under high pressure, steam injection for cappuccino, widgets in beer cans for bubble nucleation	Popcorn, bread, cappuccino, canned and bottled beer

There are three broad categories of aerated food analysis: food quality (rheology, texture and appearance), foam behaviour, gas phase properties (bubble size, air, air content).⁸ The size of the bubble is the primary parameter in determining its stability and effect to the food texture and structure, often measured as a wide size distribution with some bubbles contributing more to the appearance and others to the texture.⁸

1.3 HYDROGELS, THEIR TYPES AND MECHANISMS OF GELATION

Hydrogels are polymer networks that can absorb and retain large quantities of water and are broadly classified into categories showed in Table 1.2.⁵⁶ The hydrogel structure is formed upon hydration of the hydrophilic groups (domains) that are present in the network.⁵⁷ Hydration of a hydrogel begins by water absorption by the most polar, hydrophilic groups, preferably ionic and hydrogen-bonding character bods.⁵⁷ Once these groups are hydrated, the polymers swell and the hydrophobic groups come in contact with water. These interactions lead to “coating” of these groups with bound water, also called “secondary bound water”. After these initial hydration steps, the polymer may absorb additional water (called free or bulk water) due to osmotic forces since the system driving for an infinite dilution of the polymer, which leads to further expansion until an equilibrium between the osmotic and elastic retraction forces (covalent and physical cross-links) is reached.^{57, 58}

Gelation refers to the formation of a polymeric or particle network (colloidal gel) in a liquid, where the individual polymer or particle chains start to link together. Initially this leads to the formation of higher molecular weight branched soluble macromolecules, such system is called *sol*. The continuation of the growth of the molecular weight of these macromolecules leads to a decreased solubility and formation of an ‘infinite polymer’ also denoted as a *gel*. The transition from finite branched polymer to the infinite molecule network is called ‘sol – gel transition’ or *gelation point*.^{59, 60} The crosslink density and the polymer-water interaction parameter determines the equilibrium swelling state of a hydrogel.^{57, 58} As the polymer solution starts to gel, its viscosity increases.

Table 1.2. Classification of the hydrogels. Adapted from Peppas.⁶¹

Type of connection	Permanent	Covalent linkages between the networks ⁶²
	Reversible	Hydrogen bonding, van der Waals interactions between chains
Preparation method	Homopolymer	Cross-linked networks of one type hydrophilic monomer unit
	Copolymer	Cross-linked two co-monomer units, with at least one hydrophilic
	Multipolymer	Cross-linked three or more co-monomers
	Interpenetrating polymer	First a network is swollen in a monomer and then reacts with a second intermeshing network structure
Ionic charges ^{63, 64}	Neutral hydrogels	Have no charge
	Anionic hydrogels	Have a negative charge, related to deprotonated carboxyl groups
	Cationic hydrogels	Have a positive charge
	Ampholytic hydrogels	Antipolyelectrolyte behaviour – increasing chain expansion in the presence of a salt solution due to the breakage of intra- and intermolecular attractions attributed to the salt screening ⁷
Physical structure	Amorphous hydrogels	The chains of the macromolecule are arranged randomly
	Semi-crystalline hydrogels	Have dense regions of ordered macromolecular chains (crystallites)
	Hydrogen-bonded or complex structures	These may be responsible for the three-dimensional structure of the macromolecule

Due to their hydrophilic nature, hydrogel beads in water possess a low interfacial free energy, which allows them to be used in living systems, since the cells are not likely to adhere to such surfaces.⁶⁵ The viscoelastic or sometimes purely elastic behaviour of the hydrogels is a result of the cross-linking between the polymer chains and provides the hydrogel with its structure (hardness), elasticity and stickiness.⁶⁰ Some hydrogels demonstrate *hysteresis* (when the liquefaction and the gelling point temperatures are not the same) and some hydrogels are subjected to *syneresis* (water release from the hydrogel and a simultaneous contraction of a hydrogel).

For example, syneresis is observed in yoghurt, when a layer of water is formed on top of the rest of the contracted casein gel particles. It is essential in production of cheese,⁶⁶ in poly(N-isopropyl acrylamide) (pNIPAM) when the gel particles are heated above their volume phase transition temperature, their contraction leading to water being expelled from the system.⁶¹ In thermodynamic terms syneresis is described as the reverse of hydration.⁶⁴ This phenomenon is widely studied. The rate of syneresis depends on the temperature, pH, ionic strength, mechanical treatment, concentration and type of the gel used.⁶⁶⁻⁶⁸ Syneresis may occur by one of the three mechanisms.⁶⁹ Firstly, the rearrangement in the network of the gel. Secondly, the shrinkage of the polymer chains as a result of charge neutralisation, change of pH or temperature. Thirdly, by decrease of the solvation of the bound water, due to the change in the hydrophobicity of the polymer. Syneresis is often treated as a negative property of the hydrogel, as the system is effectively unstable over time.

In this thesis hydrogels are used as templates for composite material production, therefore some of their properties are considered in more detail in the Sections below.

1.3.1 Carrageenan hydrogels

Carrageenans come from red seaweed and are sulphated galactans with the typical structures presented in Figure 1.9. Sulphated polysaccharides have shown antitumor, anticoagulant and antiviral effects,⁷⁰ in particular a good activity against many viruses was shown *in vitro*,⁷¹⁻⁷³ which could be used beneficially in foods. All carrageenans are soluble in hot water, but only λ -carrageenan and specific salts of κ - and ι -carrageenans swell in cold water.⁷⁴ Carrageenan solutions are viscous and show shear

thinning effects upon application of stress. κ -carrageenan forms hard but brittle hydrogels, which are non-elastic. However, κ -carrageenan exhibits syneresis. The presence of salts influence the gelling point temperature, which could be between 30-70 °C for a moderate concentration of the gelling agent solution.⁷⁴ Different ions influence the gelling properties of different carrageenans: calcium is responsible for ι -carrageenan being more elastic and potassium makes κ -carrageenan more brittle.⁷⁵

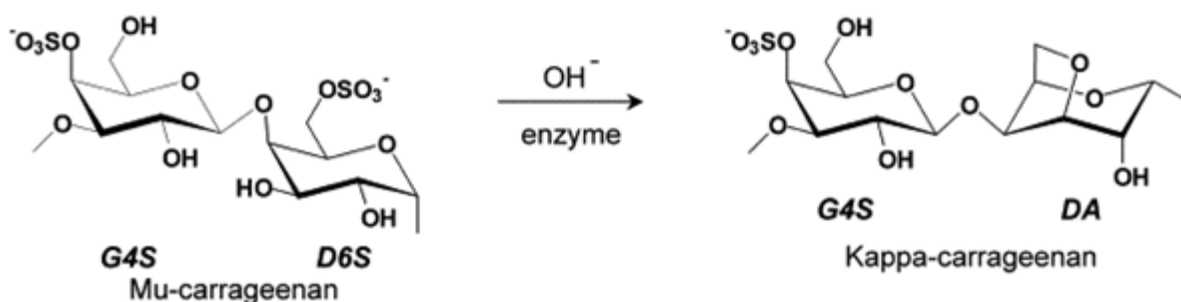


Figure 1.9. Chemical structures of carrageenans (μ and κ). μ -carrageenan is the biogenic precursor of the κ -carrageenan (4-Linked 3,6-anhydro- α -D-galactopyranose and 3-linked β -D-galactopyranose 4-sulphate). Reproduced from van de Velde, et al.⁷⁶

1.3.2 Xanthan hydrogels

Xanthan gum is a polysaccharide secreted by a plant microbe species *Xanthomonas campestris*. It is formed of repeated pentasaccharide units formed by glucose, mannose and glucuronic acid units, in the molar ratio 2.8:2.0:2.0 (shown in Figure 1.10) and the molecular weight is ranging from 2 MDa to 20 MDa.⁷⁷ Calcium ions (Ca^{2+}) can interact with the anionic moiety of pyruvic and acetic acids (COO^-) of two different chains of Xanthan gum and create a new bond between these two molecules. The more bonds there are in the hydrogel, the tougher it is. The viscosity of Xanthan gum depends on the temperature and three conformations of the polymer chain are apparently available, depending on this temperature: helix, double helix and random coil.^{8, 52, 78} Xanthan gum interacts with different plant polysaccharides (locust bean gum (LBG), Guar gum, Konjac gum) and this synergistic behaviour results in an increase of the viscosity of the mixture of the different hydrogels.^{77, 79, 80} A schematic representation of the interaction between Xanthan gum and LBG is shown in Figure 1.11, where it was reported that Xanthan side chains interact with LBG backbone thus

significantly increasing the viscosity of the solution, which is more than the sum of individual viscosities of Xanthan and LBG separately.⁵⁵

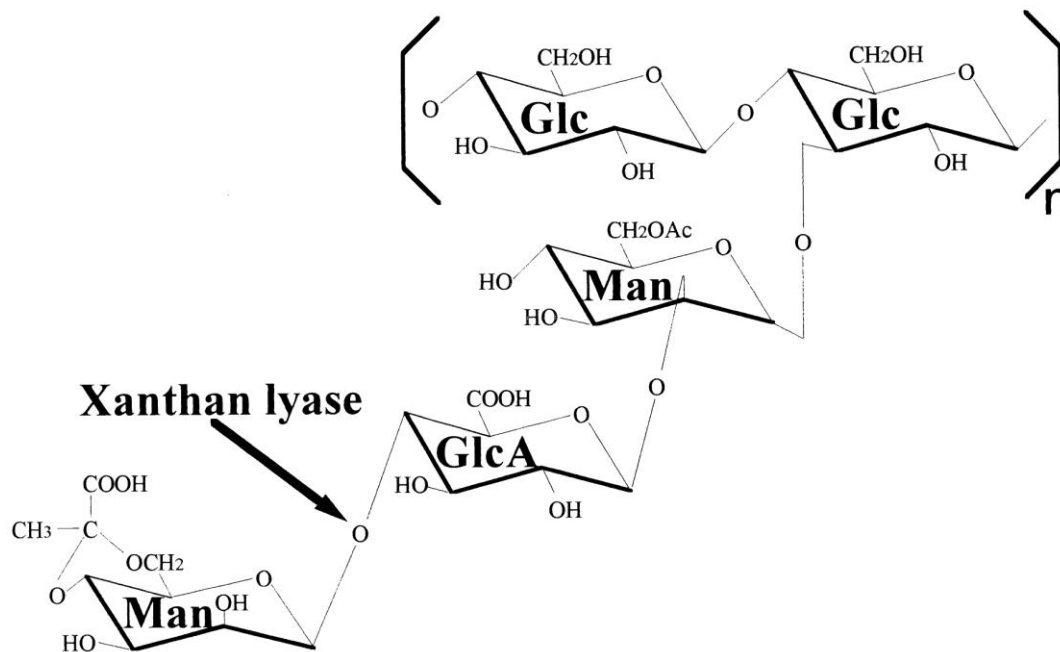


Figure 1.10. Chemical structure of Xanthan gum hydrogel. Glc, Man and GlcA represents glucose, mannose and glucuronic acid respectively. Reproduced from Hashimoto, et al.⁸¹

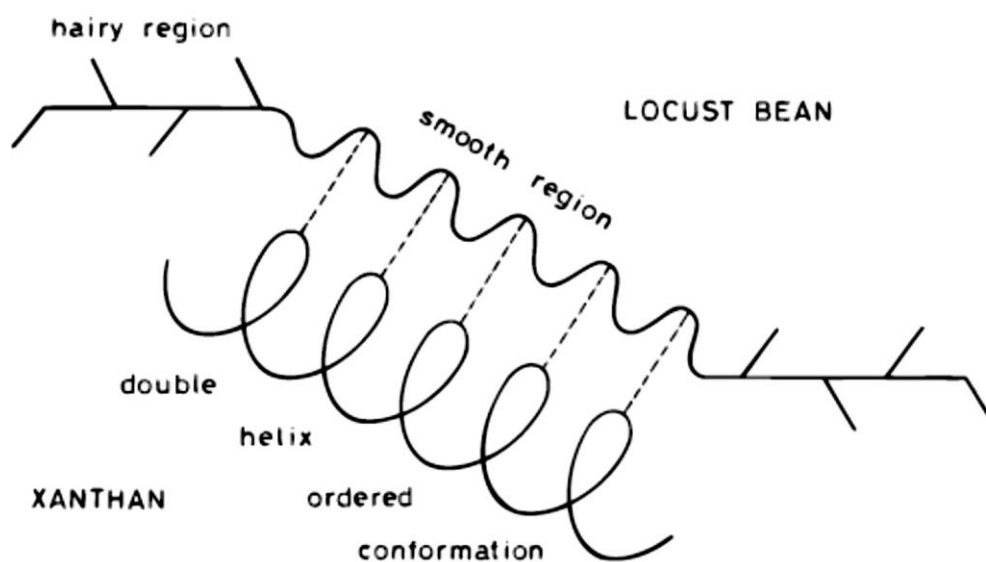


Figure 1.11. Schematic representation the interaction of Xanthan gum with LBG. Helically structured Xanthan side chains are interacting with the backbone of LBG. Reproduced from Casas and García-Ochoa.⁷⁹

1.3.3 Konjac hydrogels

Konjac is a perennial plant with an underground stem in a form of a corn and a leaf in a shape of an umbrella.⁸² Out of 170 species mainly distributed in the West African tropical region seven had been used in medicine, food and wine production, as dietary supplement and to treat obesity, with some of the species used in China for thousands of years.^{82, 83} Konjac glucomannan (KGM) extracted from *Amorphophallus konjac* plant (mannose and galactose conjugate: β -(1 \rightarrow 4) linked D-glucose and D-mannose in the molar ratio of 1:1.6 with a low degree of acetyl groups (see Figure 1.12))⁸⁴ is water-soluble.

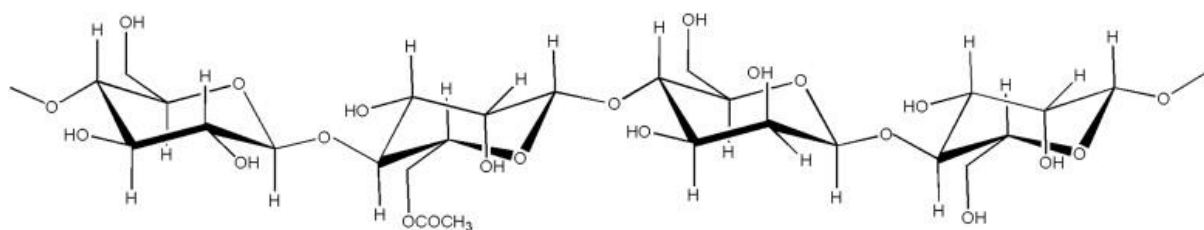


Figure 1.12. Chemical structure of Konjac glucomannan. Reproduced from Kk et al.⁸⁵

Konjac has unique rheological properties and is used in thickening and emulsifying drinks, as a binder in meat and poultry products as well as in a controlled drug delivery.⁸⁶ Konjac can absorb high quantities of water (1 g of Konjac can absorb up to 200 g of water)⁸⁷ thus it can be used in disposable nappies and sanitary towels.⁸⁵ A thermally stable hydrogel formation is triggered by the deacetylation of the acetyl groups in presence of alkali metal ions.⁸⁸ It has a firm consistency making it harder to dissolve compared to gelatine, which is more attractive for chewable snacks.⁸⁹

There are multiple theories for the mechanism of gelling of KGM. For a number of years hydrogen bonding has been predicted to aid the gelling of the deacetylated polysaccharide chains.⁹⁰ More recently hydrophobic interactions in the deacetylated polymer chains were proposed to lead to the gelation of deacetylated KGM and both hydrogen bonding and hydrophobic interactions playing a significant role in the gelation of acetylated KGM.⁹¹

1.4 METHODS FOR CHARACTERISATION OF POROUS MATERIALS

A significant part of this thesis comprises of material characterisation and analysis. This section will briefly introduce the basics of material analysis, particularly important in compressional analysis of composite materials and rheological behaviour of hydrogels.

1.4.1 Mechanical properties of materials

Chapters 3 and 4 of this thesis will present cement composites. Cement in practical applications is primarily designed to resist compressive strength.⁹² This is why compressional strength is used as a more significant property compared to the elastic (Young's) modulus by cement industries.⁹³ In compression analysis, a sample is compressed up to its bearing point. During the analysis, a curve of stress vs strain is obtained (see Figure 1.13) and the maximum stress is recorded. *Stress* is an intensity of load per unit area and *strain* is the displacement.⁶ Once the maximum stress is reached, the material behaves plastically and would not return back to its original shape. The compressive force can be calculated using equation:

$$\sigma = \frac{F}{A_{base}} \quad (1.1)$$

where σ is the compressive strength, F is the load applied to the sample and A_{base} is the area of the base of the sample.

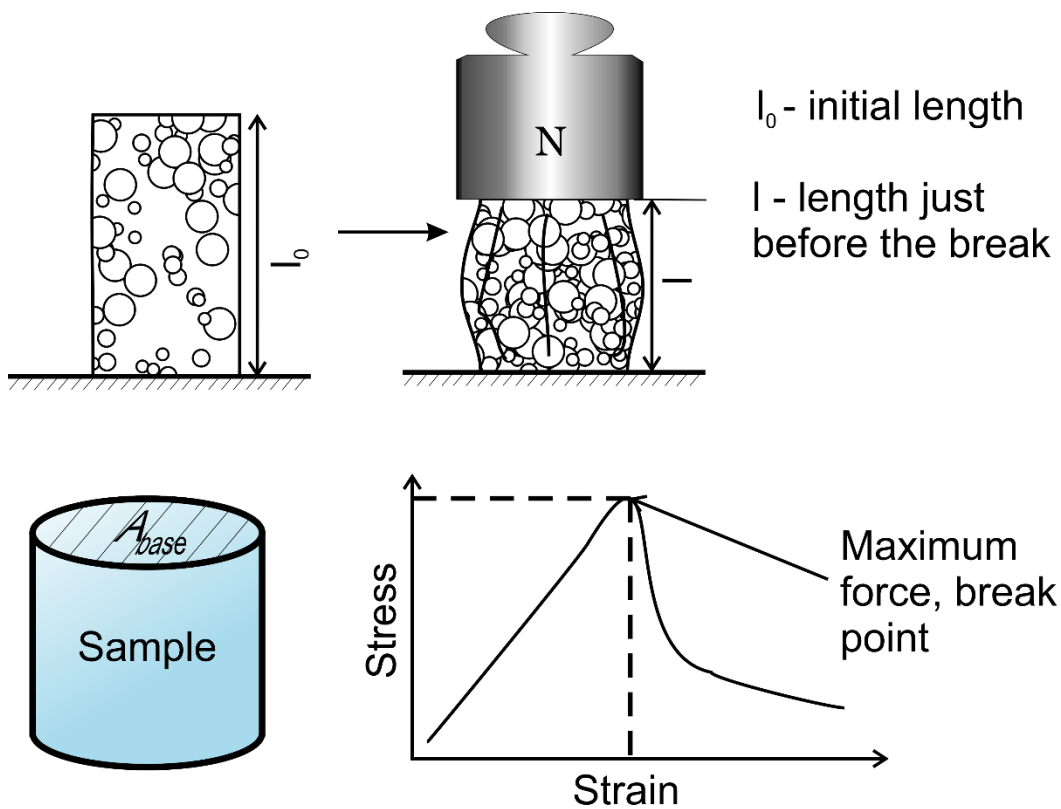


Figure 1.13. Schematic image showing the compressional strength analysis of the composites. Left to right: sample is placed on a flat surface and then a force is applied from the top. As the sample compresses, the force is increasing until a critical point where the sample crumbles. The force can be recorded at that point and using the equation above the compressional strength can be calculated.

The initial part of the slope of the curve shown in Figure 1.13 is the Young's modulus. This modulus can help to predict how much the material would extend or contract if being pressed or stretched. The units of this modulus are the same as for pressure N m^{-2} .

If the value of Young's modulus was divided by the density of the material, *specific modulus* would be calculated, similarly if compressional strength was divided by the density, giving *specific strength*.⁶ These values are particularly useful, as the compressional strength for ordinary steel and a glass-epoxy composite may be the same, but their density difference would clearly influence the choice of an architect. A graph showing the strength vs density of materials is shown in Figure 1.14.

Ceramics, metals and composites show highest strength, whereas foams and wood products have lowest densities.

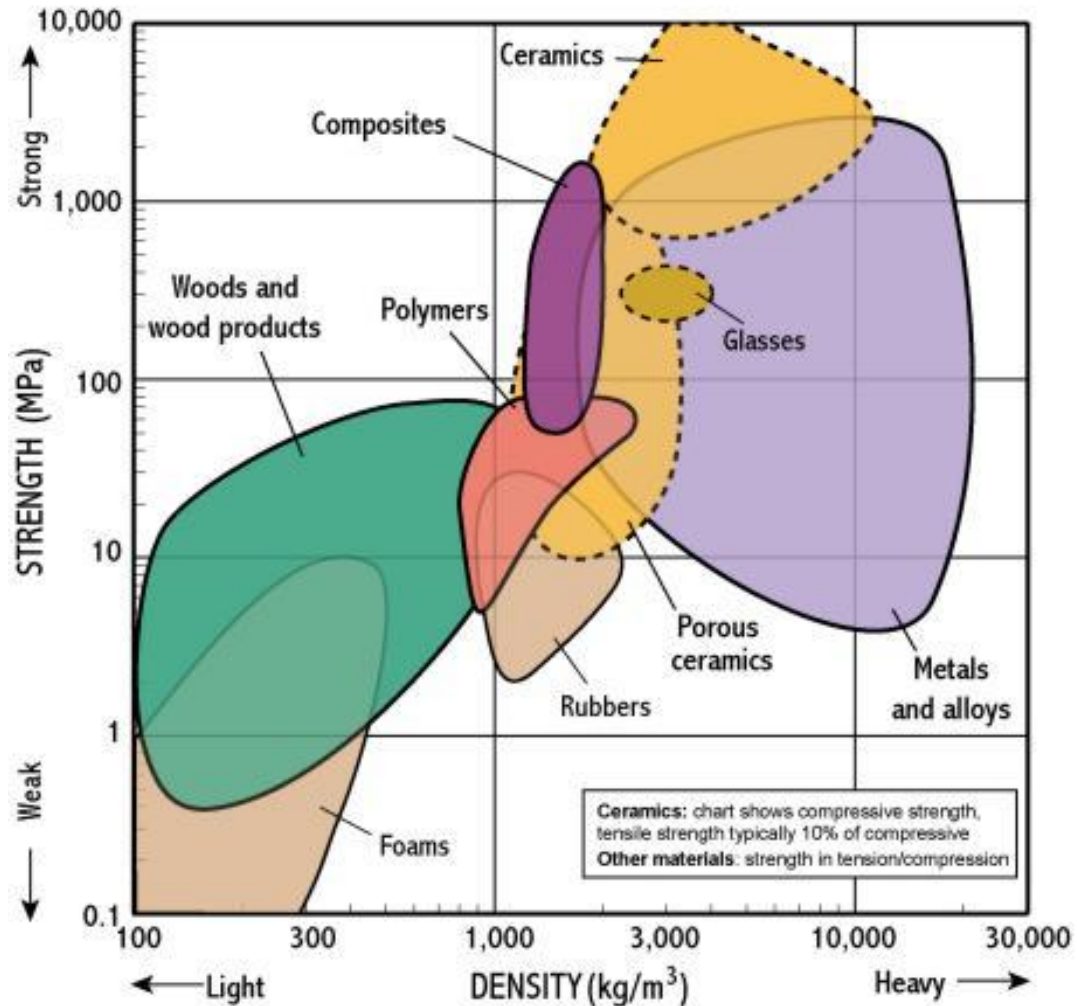


Figure 1.14. Graph showing strength vs density of various materials. Reproduced from “Material selection and processing”, Cambridge University.⁹⁴

1.4.2 Rheology: Testing Apparatus, Viscometry, Analysis of Melting and Gelling of a Hydrogel

One of the most obvious property of a material or a liquid is its reaction to deformation and flow behaviour. It is common to describe paints by their “levelling”, cream by its “thickness”, or bread dough by its “tackiness”. Such properties are studied by rheological techniques or in the case of liquids by viscometry. Rheology is the study of flow and deformation of materials, *rheos* meaning *stream* in Greek.^{95, 96} Rheology

can be used in measuring the flow properties of hydrogels, providing useful information on their melting, gelling, strength and elasticity properties. Indeed, solids show *elastic* behaviour, similarly to some sterically stabilised colloids. However, colloids may lose their elasticity upon even a minute shear and become viscous, just like an ordinary liquid. Such behaviour is known as *viscoelastic*. The following paragraph will look into the different possible behaviours of fluids and dispersions.

Let us imagine a fluid set between two non-slip plates as shown in Figure 1.15. One of the plates (bottom in this case) is stationary, and a force F is applied to the upper plate in the x direction, resulting in a velocity of the fluid at its boundary to be equal to the plate's velocity. The layers of the fluid lying between the plates have an intermediate velocity and the condition is called *laminar flow*. When the separation between the layers is set to dy , the velocity changes by the amount of dv . Velocity gradient can then be defined as dv / dy , which according to *Newton's law of viscosity* is proportional to the shear stress, $\tau = F / A$. The viscosity η of the sandwiched fluid is the factor of proportionality:

$$\tau = \frac{F}{A} = \eta \frac{dv}{dy} = \eta \dot{\gamma} \quad (1.2)$$

Here $\dot{\gamma}$ represents the rate of shear, $d(\text{shear}) / dt$, since the velocity is dx / dt and shear strain (flow deformation per unit length) is dx / dy . The units of shear rate are s^{-1} and the units of equation viscosity are $(\text{kg m}^{-1} \text{s}^{-1})$ or Pascal second (Pa s).

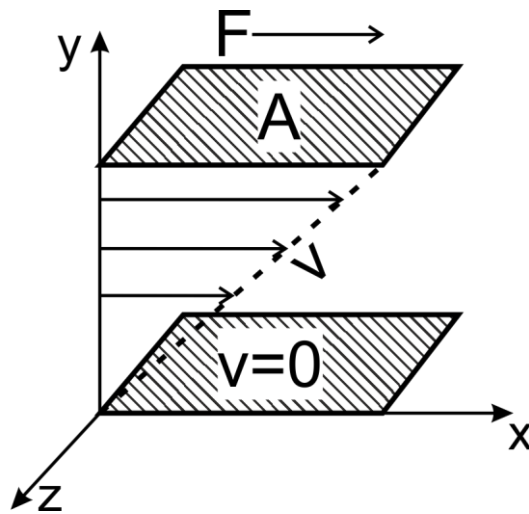


Figure 1.15. Schematic representation of a fluid placed between two parallel plates, where one of them is stationary and one has a force applied parallel to x direction, resulting in a velocity gradient in the fluid.

Some materials would only deform if an external force was applied (elastic behaviour), whereas some will start to flow (viscous behaviour). Rheology studies the relations between forces exerted on a material and the resulting deformations as a function of time.⁹⁷ Rheology becomes important when designing and constructing machinery for the manipulation of colloid systems (milk, paint, mineral slurries), spreading the colloids, presenting information about the structural properties of a material. After applying a stress to a viscous material it flows at a certain rate and once the stress is removed the material may retain the shape which was at the last moment when the stress was still applied. Elastic materials deform at once if the stress is applied, but will return to the original shape once the stress is removed. An ideal fluid would dissipate all the applied energy as heat, whereas for an ideal elastic material the energy would be stored and released afterwards to regain the initial shape.

Strain can be defined in the following way, which only applies for small deformations. When a force is applied to a system, where two points A and B (Figure 1.16) with a volume element of a material separated by a distance h , their relative position will change, the material will be displaced and deformed - B will move to B'. Considering only the elongation, the relative deformation between A and B is given by $(AB' - AB) / AB = \Delta x / x$. The strain ϵ_l can be defined as the infinitesimal elongation of x (in this

case, only involving change in length) as the relative deformation gradient $\epsilon_l = \delta\Delta x / \delta x$.

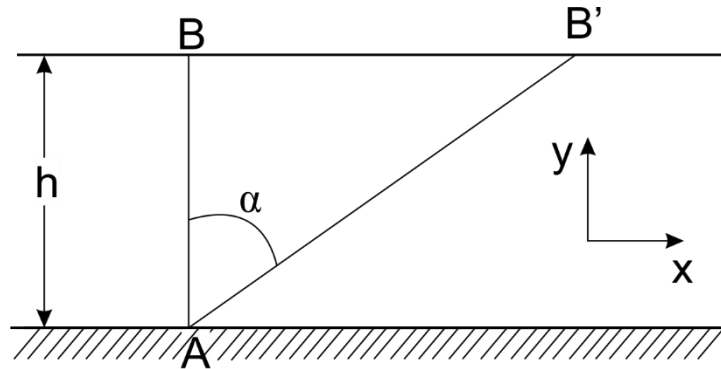


Figure 1.16. Schematic showing the shear between two parallel planes, where B changes location to B'. Adapted from Lyklema.⁹⁷

There are three main types of deformation: all-sided (isotropic) compression, shear and uniaxial compression or extension. The first one for isotropic materials will only lead to a change in the volume of a material.

Shearing refers to the shifting of material parts parallel to its other parts. For a homogenous material this shift will be even throughout the sample. The measure of shear is $\gamma = \Delta x / \Delta y$, with the x and y being the coordinates, e.g. in Figure 1.15. Elastic materials will deform, resulting in a shear strain γ , whereas viscous materials after a short initial interval will flow at a specific shear rate, $\dot{\gamma} = d\gamma / dt$.⁹⁷ Typical shear rates at room temperature of draining of paints under gravity are $10^{-1} - 10^1 \text{ s}^{-1}$, chewing and swallowing of food – $10-100 \text{ s}^{-1}$, blood flow – $10 - 10^3 \text{ s}^{-1}$, rubbing creams and lotions on the skin – $10^4 - 10^5 \text{ s}^{-1}$.⁹⁶ Viscosity of glass is 10^{40} Pa s , golden syrup 100 Pa s , water 0.001 Pa s , and air 10^{-5} Pa s .

The last one, uniaxial compression or extension occurs when only one side of a material is subjected to tensile or compressive stress. The other two sides of the material are not subjected to stress.

A graphical relationship between stress and strain is shown in Figure 1.17. Newtonian fluids show a linear relationship, thus they can be described by only knowing the viscosity η , as it is not dependant on the shear rate and shearing time. Most of the real

materials have multiple properties of the ones represented in Figure 1.17. For non-Newtonian fluids the relationship between the rate of shear ($\dot{\gamma}$) and shear stress (τ) is not linear. For shear-rate dependant systems a shear rate dependant viscosity is called an apparent viscosity, η_{app} , with $\eta_{app} = f(\dot{\gamma})$. Shear thinning (pseudoplastic) behaviour occurs when η_{app} decreases with increasing $\dot{\gamma}$, and when it increases, the behaviour is called shear thickening.

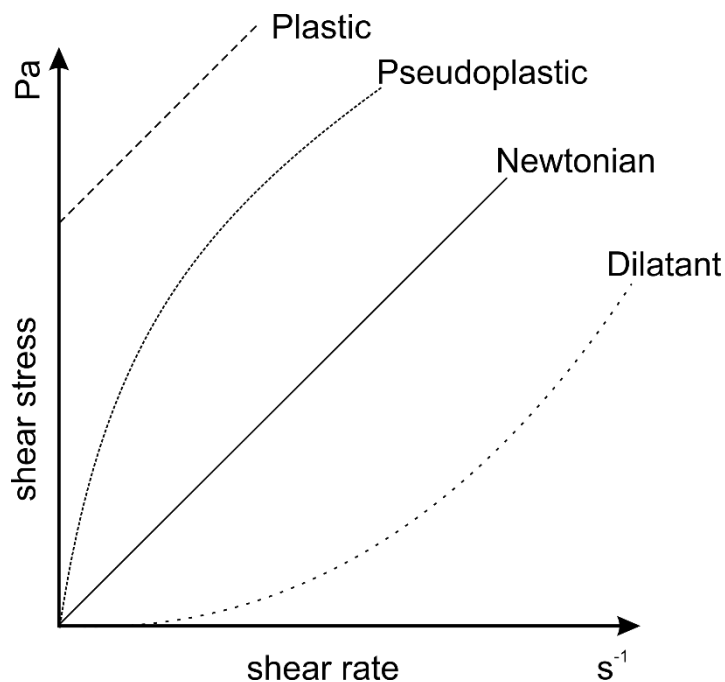


Figure 1.17. Graph showing shear stress-rate of strain for Newtonian, shear thickening (dilatant), pseudoplastic (shear thinning) and plastic materials. Adapted from Lyklema.⁹⁷

1.4.2.1 Rheology Measuring Techniques

The rheological properties of a gel can be measured by a number of viscometers, one of the most popular being rotational rheometers, one of which is the plate and cone rheometer (Figure 1.18). Rheometer in this case is used instead of a viscometer as apart from viscosity it can measure additional properties of a material. If the angle of the cone (θ) is smaller than 5° , the shear is approximately constant throughout the

analysed sample⁹⁶ and can be calculated knowing the angular velocity of the cone (Ω) using the following equation:

$$\dot{\gamma} = \frac{\Omega}{\theta} \quad (1.3)$$

The fact that the shear stress (τ), shear rate ($\dot{\gamma}$) and the time dependant shear rate ($\ddot{\gamma}$) are nearly uniform throughout the sample, the plate and cone geometry makes the method attractive to measure shear thinning liquids and materials with a yield stress.⁹⁷ The shear stress can also be calculated, knowing a constant C , specific to individual rheometer, calculated by the manufacturer of the instrument.⁹⁸ r is the radius of the cone.

$$\tau = \frac{3C}{2\pi r^2} \quad (1.4)$$

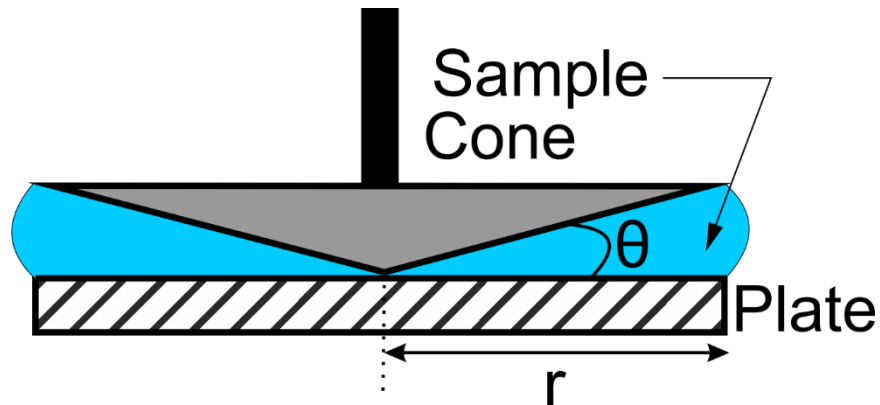


Figure 1.18. Schematic image of a plate and cone rheometer. θ is the angle between the plate and the cone and r is the radius of the cone (and plate).

At any point, strain can be measured from the generalised Hooke's Law:⁹⁹

$$\tau = G^* \gamma \quad (1.5)$$

Where G^* is the complex shear modulus (ratio of stress/strain) or a generalised form of Newton's Law:

$$\tau = -\eta^* \dot{\gamma} \quad (1.6)$$

Where η^* is the complex frequency - dependant viscosity function ($\eta^* = \eta' - i\eta''$), where η' is the real (dynamic) viscosity and η'' is associated with the solid-like behaviour. Complex shear modulus is $G^* = G' + iG''$, where G' is the storage or real shear modulus and G'' is the loss or imaginary shear modulus, associated with dissipation of the energy as heat during the deformation (viscous liquid property).

This brief rheology measurement technique introduction section did not aim to provide the reader with detailed derivations of the equations used in the measurement of properties of materials, but rather give an overview of what is possible to measure and what are the simplified calculations to obtain results. For those readers wishing to understand rheology in more detail, there are many books available and those referenced throughout this Section can be found in the references section of this Chapter.^{95-97, 99}

1.5 HYDROGEL TEMPLATING FOR THE FABRICATION OF POROUS MATERIALS

After describing the methods of introduction of porosity both in foods and non-foods, composite material preparation techniques and their uses, hydrogels and their properties it is time to introduce a specific technology of material preparation – hydrogel templating. As we shall see, majority of the research is focused on hydrogel templating, as well as entrapping particles within hydrogels and then removing such particles by various methods.

An excellent review on various processes and current trends in hydrogel templating has been recently published by Texter.¹⁰⁰ 3D close-packed composites prepared by latex particle templating have been proved to be excellent sensors. Barry and Wiltzius have templated polystyrene nanoparticles (450 nm) in a flow cell by polymerising acrylamide trapped between the nanoparticles.¹⁰¹ After the polymerisation, the particles were dissolved in toluene leaving an inverse opal hydrogel, capable of changing its reflectance spectra as the humidity was varied, thus showing capability of being used as a humidity sensor. Similar methods were used to design pH¹⁰² and glucose¹⁰³ responsive hydrogels. Much smaller than the latex nanoparticles, surfactant micelles and rod-like polyelectrolytes at 15-20 % concentrations have been templated

within acrylamide following similar procedures as above. The templates were then removed leaving defined pore size gaps within the polymer.¹⁰⁴ The different sizes of the pores gave specific electrophoretic mobilities for proteins that could pass through the porous polymer. These are expected to enhance the mobility of molecules of particular size range relative to smaller and larger molecules.¹⁰⁴

Hydrogel templating has also been studied theoretically for the application in Gel Permeation Chromatography (GPC) to separate globular proteins.¹⁰⁵ These gels have been predicted to have more sharply defined exclusion limits and improved resolution for the GPC purposes.¹⁰⁵ Gold nanoparticles have also been templated with poly(*N*-isopropylacrylamide) (pNIPAM), where after the polymerisation reaction the core of the particle was dissolved in potassium cyanide solution producing hollow hydrogel nanoparticles.¹⁰⁶ Even liposomes have been used to template relatively monodisperse alginate nanogels.¹⁰⁷ Hydrogel templating has been used in a range of methods for the preparation of materials for biomedical applications as bone replacement and cartilage substitutes. Skelton *et al.* reported an interesting approach of the hydrogel use in food products. Agar hydrogel swollen by water or alcohol was emulsified to reduce the fat content in chocolates.¹⁰⁸ Up to 80 vol% of the hydrogel was incorporated into the chocolate formulations. It is easy to see, that hydrogels have been widely used in various applications, but there are still many possible applications where hydrogels could be applied.

1.6 OBJECTIVES OF THE PRESENT THESIS

The objective of this Thesis is to present the design and application of a novel method of composite materials preparation. The main objective in this thesis was to develop a new technique for introducing porosity in solid formulations, which would allow a better control of the pore size distribution and related properties of the porous composites. This thesis is organised around several sub-objectives, which include the application of the hydrogel templating method for several classes of porous and composite materials. Part of the Thesis is directly linked to industrial projects and product development.

1.7 PRESENTATION OF THIS THESIS

This thesis presents the methodology of applying hydrogel slurry templating technique in building materials, foods and household products. The details about the reasons behind the need of developing particular composite materials are given in the beginning of each Chapter. Each of the Chapters is concluded with a list of references used in that Chapter. Firstly, in Chapter 2 the materials and methods used for the preparation of the composite materials by a hydrogel slurry templating technique are discussed.

In Chapter 3 the porous cement and porous PDMS production is presented and results are summarised. Chapter 4 reviews and optimises the methodology of these building materials preparation for sound absorption. The resulting porous cement samples are tested for a potential application as sound absorption panels and these results are presented and discussed.

In addition, the hydrogel slurry templating is applied to foods in Chapter 5, where the technology is adjusted to generate composite bouillon cube formulations. The reported data is for a model composition with a fat and salt base, which does not include all the flavours required in a consumer product.

Hydrogel templating was used as a way to reduce salt intake and is presented in Chapter 6. Spray gelation was used for the preparation of porous core-shell particles with an evaporable hydrogel core and salt microcrystal particle shell. These particles could be used as a table salt alternative in seasoning. Their saltiness is measured and compared to an ordinary table salt.

Finally, application of the hydrogel slurry templating methodology for sustainable soap bar development is presented in Chapter 7. The technique is tuned to fit a common household product modification. Soap bars with hydrogel beads are fabricated with the aim to reduce detergent pollution caused by the extensive use of this product.

The summary and plans for future work are presented in Chapter 8 of the thesis.

1.8 REFERENCES

1. P. A. Fowler, J. M. Hughes and R. M. Elias, *Journal of the Science of Food and Agriculture*, 2006, **86**, 1781.
2. D. Hull and T. W. Clyne, *An introduction to composite materials*, 2nd edn., Cambridge University Press, Cambridge ; New York, 1996.
3. E. J. Barbero, *Introduction to composite materials design*, 2nd edn., Taylor & Francis, Boca Raton, 2011.
4. M. Rutkevicius, S. K. Munusami, Z. Watson, A. D. Field, et al., *Materials Research Bulletin*, 2012, **47**, 980.
5. C. S. Smith, *Design of marine structures in composite materials*, Elsevier Applied Science ; Elsevier Science Pub. Co., London ; New York, 1990.
6. A. K. Kaw, *Mechanics of Composite Materials, Second Edition*, CRC Press, Boca Raton, New York, 1997.
7. J. Butterfield, *Collins English Dictionary*, HarperCollins Publishers Limited, Glasgow, UK, 2003.
8. G. M. Campbell and E. Mougeot, *Trends in Food Science & Technology*, 1999, **10**, 283.
9. M. L. K. Hoa, M. Lu and Y. Zhang, *Advances in Colloid and Interface Science*, 2006, **121**, 9.
10. X. Li, C. Zhang, Z. Du and H. Li, *Journal of Colloid and Interface Science*, 2008, **323**, 120.
11. H. G. van Oss, United States Geological Survey, January, 2010 edn., 2010, p. 39.
12. S. B. Eskander, S. M. Abdel Aziz, H. El-Didamony and M. I. Sayed, *Journal of Hazardous Materials*, 2011, **190**, 969.
13. F. Hernandez-Olivares, M. R. Bollati, M. del Rio and B. Parga-Landa, *Construction and Building Materials*, 1999, **13**, 179.
14. M. A. Othuman and Y. C. Wang, *Construction and Building Materials*, 2011, **25**, 705.
15. G. D. Welles, *Journal of Chemical Education*, 1945, **22**, 442.
16. M. S. Hamidah, A. I., M. R. A. Ruslan, K. Kartini, et al., *Optimisation of Foamed Concrete Mix of Different Sand-Cement Ratio and Curing Conditions in Use of Foamed Concrete in Construction*, ThomasTelford, London, 2005.
17. H. M. Jonkers, A. Thijssen, G. Muyzer, O. Copuroglu, et al., *Ecological Engineering*, 2010, **36**, 230.
18. J. Y. Wang, H. Soens, W. Verstraete and N. De Belie, *Cement and Concrete Research*, 2014, **56**, 139.
19. Y. Murata, H. Tawara, H. Obata and K. Takeuchi, *Journal of Advanced Oxidation Technologies*, 1999, **4**, 227.
20. H. Li, M. H. Zhang and J. P. Ou, *Wear*, 2006, **260**, 1262.
21. Z. Li, H. Wang, S. He, Y. Lu, et al., *Materials Letters*, 2006, **60**, 356.
22. H. Li, H. G. Xiao and J. P. Ou, *Cement and Concrete Research*, 2004, **34**, 435.
23. T. P. Chang, J. Y. Shih, K. M. Yang and T. C. Hsiao, *Journal of Materials Science*, 2007, **42**, 7478.
24. W. Y. Kuo, J. S. Huang and C. H. Lin, *Cement and Concrete Research*, 2006, **36**, 886.
25. X. He and X. Shi, *Transportation Research Record*, 2008, 13.

26. F. Sanchez and K. Sobolev, *Construction and Building Materials*, 2010, **24**, 2060.
27. G. Y. Li, P. M. Wang and X. Zhao, *Cement and Concrete Composites*, 2007, **29**, 377.
28. J. M. Makar, J. C. Margeson and J. Luh, 3rd International Conference on Construction Materials: Performance, Innovations and Structural Implications, Vancouver, B.C., 2005.
29. S. J. Clarson and A. J. Semlyen, *Siloxane polymers*, Prentice Hall, Englewood Cliffs NJ, 1993.
30. M. Juchniewicz, D. Stadnik, K. Biesiada, A. Olszyna, et al., *Sensors and Actuators B: Chemical*, 2007, **126**, 68.
31. M. T. Khorasani, H. Mirzadeh and Z. Kermani, *Applied Surface Science*, 2005, **242**, 339.
32. B.-L. Su, C. Sanchez and X.-Y. Yang, Insights into Hierarchically Structured Porous Materials: From Nanoscience to Catalysis, Separation, Optics, Energy, and Life Science in *Hierarchically Structured Porous Materials*, Wiley-VCH Verlag GmbH & Co. KGaA, Weinheim, Germany, 2011, pp. 1.
33. R. Lakes, *Nature*, 1993, **361**, 511.
34. X. Y. Yang, Y. Li, A. Lemaire, J. G. Yu, et al., *Pure and Applied Chemistry*, 2009, **81**, 2265.
35. X. Y. Yang, A. Leonard, A. Lemaire, G. Tian, et al., *Chemical Communications*, 2011, **47**, 2763.
36. J.-Y. Rho, L. Kuhn-Spearing and P. Zioupos, *Medical Engineering & Physics*, 1998, **20**, 92.
37. A. Stein, *Advanced Materials*, 2003, **15**, 763.
38. M. E. Davis, *Nature*, 2002, **417**, 813.
39. J. H. Sun, Z. P. Shan, T. Maschmeyer and M. O. Coppens, *Langmuir*, 2003, **19**, 8395.
40. M. Antonietti, B. Berton, C. Goltner and H. P. Hentze, *Advanced Materials*, 1998, **10**, 154.
41. M. Groenewolt, M. Antonietti and S. Polarz, *Langmuir*, 2004, **20**, 7811.
42. Y. Zhou and M. Antonietti, *Advanced Materials*, 2003, **15**, 1452.
43. D. B. Kuang, T. Brezesinski and B. Smarsly, *Journal of the American Chemical Society*, 2004, **126**, 10534.
44. P. D. Yang, T. Deng, D. Y. Zhao, P. Y. Feng, et al., *Science*, 1998, **282**, 2244.
45. D. Y. Zhao, P. D. Yang, B. F. Chmelka and G. D. Stucky, *Chemistry of Materials*, 1999, **11**, 1174.
46. H. Nishihara, S. R. Mukai, D. Yamashita and H. Tamon, *Chemistry of Materials*, 2005, **17**, 683.
47. C. A. L. Colard, R. A. Cave, N. Grossiord, J. A. Covington, et al., *Advanced Materials*, 2009, **21**, 2894.
48. Y. Shin, L. Q. Wang, J. H. Chang, W. D. Samuels, et al., *Nanotechnology in Mesosstructured Materials*, 2003, **146**, 447.
49. T. Sen, G. J. T. Tiddy, J. L. Cascic and M. W. Anderson, *Chemical Communications*, 2003, 2182.
50. S. A. Davis, S. L. Burkett, N. H. Mendelson and S. Mann, *Nature*, 1997, **385**, 420.

51. Z. Wang, D. Luan, C. M. Li, F. Su, et al., *Journal of the American Chemical Society*, 2010, **132**, 16271.
52. M. L. Parker, A. Grant, N. M. Rigby, P. S. Belton, et al., *Journal of Cereal Science*, 1999, **30**, 209.
53. J.-C. Arboleya, M. García-Quiroga, D. Lasa, O. Oliva, et al., in *International Journal of Gastronomy and Food Science*.
54. J. B. German, Properties of Stabilising Components in Foams in *Food emulsion and foams: theory and practice*, American Institute of Chemical Engineers, New York, USA, 1990, vol. 86, pp. 62.
55. C. E. Stauffer, *Emulsifiers*, American Association of Cereal Chemists, Eagan Press, St Paul, Minnesota, USA, 1999.
56. B. D. Ratner, A. S. Hoffman, F. J. Schoen, J. E. Lemons, et al., *Biomedical Engineering e-Mega Reference*, Elsevier Science, San Diego, CA, 2009.
57. J. M. Rosiak and F. Yoshii, *Nuclear Instruments and Methods in Physics Research Section B: Beam Interactions with Materials and Atoms*, 1999, **151**, 56.
58. N. A. Peppas, *Hydrogels in Medicine and Pharmacy*, CRC Press, Boca Raton, Florida, 1986-1987.
59. R. Murakami and A. Bismarck, *Advanced Functional Materials*, 2010, **20**, 732.
60. B. P. Binks and R. Murakami, *Nature Materials*, 2006, **5**, 865.
61. T. Gan, Y. Guan and Y. Zhang, *Journal of Materials Chemistry*, 2010, **20**, 5937.
62. W. Hennink and C. Van Nostrum, *Advanced Drug Delivery Reviews*, 2012, **57**, 13.
63. B. D. Ratner and A. S. Hoffman, Hydrogels for Medical and Related Applications, ACS symposium series, 1976.
64. T. Vliet, H. J. M. Dijk, P. Zoon and P. Walstra, *Colloid and Polymer Science*, 1991, **269**, 620.
65. I. A. Challen, S. East and G. R. Sanderson. Process for preparation of algin or pectin gels, *U. P. Office*, 1982.
66. X. L. Geng, F. W. J. van den Berg, A. N. Bager and R. Ipsen, *International Dairy Journal*, 2011, **21**, 711.
67. C. Daviau, M.-H. Famelart, A. Pierre, H. Goudédranche, et al., *Lait*, 2000, **80**, 397.
68. C. L. Hansen, Å. Rinnan, S. B. Engelsen, T. Janhøj, et al., *Journal of Agricultural and Food Chemistry*, 2009, **58**, 513.
69. P. F. Fox, P. L. H. McSweeney, T. M. Cogan and T. P. Guinee, *Cheese: Chemistry, Physics and Microbiology: General Aspects, 3rd Ed.*, Elsevier Science, London, UK, 2004.
70. G. Franz, *Planta Medica*, 1989, 493.
71. S. Girond, J. M. Crance, H. Vancuyckgandre, J. Renaudet, et al., *Research in Virology*, 1991, **142**, 261.
72. M. Baba, R. Snoeck, R. Pauwels and E. Declercq, *Antimicrobial Agents and Chemotherapy*, 1988, **32**, 1742.
73. M. E. Gonzalez, B. Alarcon and L. Carrasco, *Antimicrobial Agents and Chemotherapy*, 1987, **31**, 1388.
74. A. Imeson, *Food Stabilisers, Thickeners and Gelling Agents*, John Wiley & Sons Ltd., Chichester, UK, 2011.
75. A. I. Usov, *Food Hydrocolloids*, 1998, **12**, 301.

76. F. van de Velde, S. H. Knutsen, A. I. Usov, H. S. Rollema, et al., *Trends in Food Science & Technology*, 2002, **13**, 73.
77. Unilever, *Unilever Sustainable Living Plan: Progress Report 2012*, 2013.
78. C. Wandrey, A. Bartkowiak and S. E. Harding, *Materials for Encapsulation in Encapsulation Technologies for Active Food Ingredients and Food Processing*, Springer, New York, NY, 2009.
79. J. A. Casas and F. García-Ochoa, *Journal of the Science of Food and Agriculture*, 1999, **79**, 25.
80. C. Inoue, S. Silva Paes, M. E. Perrine, A. K. Popp, et al. Savoury Food Concentrate, *U. P. Office*, 2011, 20100143550.
81. W. Hashimoto, H. Miki, N. Tsuchiya, H. Nankai, et al., *Applied and Environmental Microbiology*, 1998, **64**, 3765.
82. M. Chua, T. C. Baldwin, T. J. Hocking and K. Chan, *Journal of Ethnopharmacology*, 2010, **128**, 268.
83. C. Williams, *Medicinal Plants in Australia Volume 3: Plants, Potions and Poisons*, Rosenberg Publishing, 2012.
84. K. Nishinari, P. A. Williams and G. O. Phillips, *Food Hydrocolloids*, 1992, **6**, 199.
85. M. S. Kök, A. S. Abdelhameed, S. Ang, G. A. Morris, et al., *Food Hydrocolloids*, 2009, **23**, 1910.
86. M. Alonso-Sande, D. Teijeiro-Osorio, C. Remunan-Lopez and M. J. Alonso, *European Journal of Pharmaceutics and Biopharmaceutics*, 2009, **72**, 453.
87. X. Wen, T. Wang, Z. Wang, L. Li, et al., *International Journal of Biological Macromolecules*, 2008, **42**, 256.
88. M. Maeda, H. Shimahara and N. Sugiyama, *Agricultural and Biological Chemistry*, 1980, **44**, 245.
89. S.-L. Yeh, M.-S. Lin and H.-L. Chen, *Planta Medica*, 2007, **73**, 1384.
90. K. Maekaji, *Agricultural and Biological Chemistry*, 1974, **38**, 315.
91. J. Chen, J. Li and B. Li, *Carbohydrate Polymers*, 2011, **86**, 865.
92. J. F. Lamond, *Making and Curing Concrete Specimens in Significance of Tests and Properties of Concrete and Concrete-making Materials*, ASTM, Bringeport, New Jersey, 2006, pp. 80.
93. D. Bentz, J. Bullard, C. Ferraris, E. Garboczi, et al., *Virtual Testing of Cement and Concrete in Significance of Tests and Properties of Concrete and Concrete-making Materials*, ASTM, Bringeport, New Jersey, 2006, pp. 38.
94. *Material Selection Charts*, http://www-materials.eng.cam.ac.uk/mpsite/interactive_charts/strength-density/NS6Chart.html.
95. P. C. Hiemenz and R. Rajagopalan, *Principles of Colloid and Surface Chemistry, Third Edition, Revised and Expanded*, Taylor & Francis, New York, NY, 1997.
96. H. A. Barnes, J. F. Hutton and K. Walters, *An Introduction to Rheology*, Elsevier, Amsterdam, Netherlands, 1989.
97. T. van Vliet and H. Lyklema, *6 Rheology in Fundamentals of Interface and Colloid Science*, Academic Press, Amsterdam, Netherlands, 2005, vol. Volume 4, pp. 6.1.
98. A. U. Khan, N. Mahmood and A. A. Bazmi, *Materials Research*, 2009, **12**, 477.
99. J. C. Berg, *An Introduction to Interfaces & Colloids: The Bridge to Nanoscience*, World Scientific, 2010.
100. J. Texter, *Colloid and Polymer Science*, 2009, **287**, 313.

101. R. A. Barry and P. Wiltzius, *Langmuir*, 2005, **22**, 1369.
102. Y. J. Lee and P. V. Braun, *Advanced Materials*, 2003, **15**, 563.
103. Y. J. Lee, S. A. Pruzinsky and P. V. Braun, *Langmuir*, 2004, **20**, 3096.
104. R. L. Rill, B. R. Locke, Y. Liu, J. Dharia, et al., *Electrophoresis*, 1996, **17**, 1304.
105. R. L. Rill, D. H. Van Winkle and B. R. Locke, *Analytical Chemistry*, 1998, **70**, 2433.
106. N. Singh and L. A. Lyon, *Chemistry of Materials*, 2007, **19**, 719.
107. J. S. Hong, W. N. Vreeland, S. H. DePaoli Lacerda, L. E. Locascio, et al., *Langmuir*, 2008, **24**, 4092.
108. T. S. Skelton, P. K. A. Olsson, A. R. Morgan and S. A. F. Bon, *Food & Function*, 2013, **4**, 1314.

Chapter 2. Experimental

“Great things are not done by impulse, but by a series of small things brought together.”

Vincent van Gogh

This Chapter outlines the different experimental procedures used in the hydrogel templating methods across this thesis. Various hydrogel samples have been made and blended into beads; slurries of cement, PDMS, fat – salt mixture and soap were fine-tuned as well as their temperatures, in order to produce desirable composites. To analyse these composites, they were fluorescently stained, observed with the help of various microscopy techniques, compressed, dissolved and tested for acoustic and other properties. This Chapter gives a detailed description of materials and procedures used in the research outlined above.

2.1 MATERIALS

2.1.1 Hydrogels

Xanthan gum (Vanzan® NF) was kindly supplied by R. T. Vanderbilt Company, Inc., Norwalk, CT, USA, Konjac gum (Nutricol® GP 312) and κ -carrageenan (Gelcarin GP911 NF) were supplied by FBC BioPolymer, Philadelphia, PA, USA. Agar (bacteriological, NO. 1) was purchased from Oxoid Ltd., England, polyacrylamide granules as water retaining plant gel (MiracleGel®) were produced by The Scotts Company LLC, Marysville, Ohio and purchased from a local garden shop. Gellan gum (KELCOGEL LT100) was provided by CP Kelco, Prescott, Merseyside, UK.

2.1.2 Filler Materials (Matrices)

Lafarge extra rapid curing cement and gypsum powder were purchased in a local store. Silicon elastomer SYLGARD® 184 (Base oil) and silicon elastomer curing agent SYLGARD® 184 were purchased from Dow Corning GmbH, Wiesbaden, Germany.

EXPERIMENTAL

Palmoil stearin (fat base) (batch 13-15529; 3588598 (the main components within this material are listed in the Table 2.1 below)), vegetable fat with a lower melting point region (batch LEN200204-025) and potato starch (9 % moisture, batch: 12-10050; 3587023) were kindly provided by Unilever research

Soap base as “Melt & Pour, clear” was purchased from Hobby Craft and contained ingredients listed in Table 2.2. Exact quantities of the ingredients have not been disclosed by the manufacturer.

Table 2.1. Table showing major components of palmoil stearin.

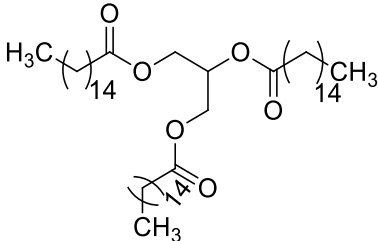
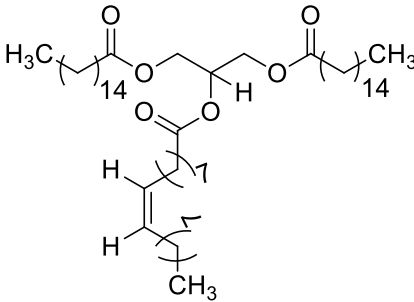
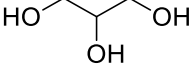
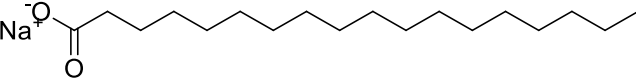
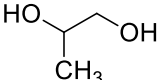
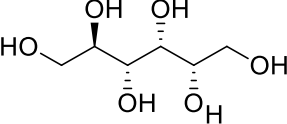
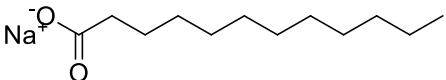
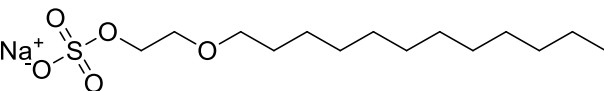
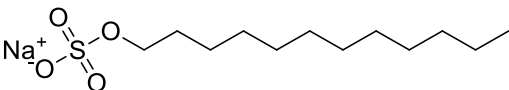
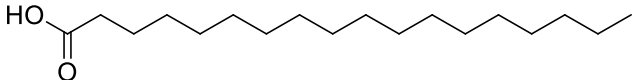
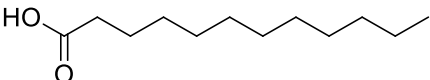
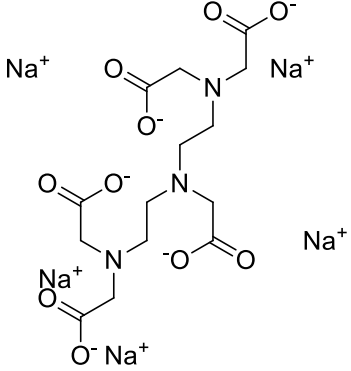
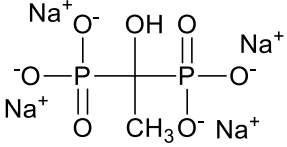
Name	Structure
Glyceril tripalmitate	
Glycerol dipalmitate monooleate	

Table 2.2. Table showing components of soap base.

Name	Structure
Water	H_2O
Glycerin	
Sodium stearate	
Propylene glycol	
sorbitol	
sodium laurate	
sodium laureth sulfate	
sodium lauryl sulfate	
sodium chloride	$NaCl$
stearic acid	
lauric acid	
pentasodium pentetate	
tetrasodium etidronate	

2.1.3 Water

Purified water was obtained using an Elgastat Prima reverse osmosis unit, with a conductivity below 50 μ S.

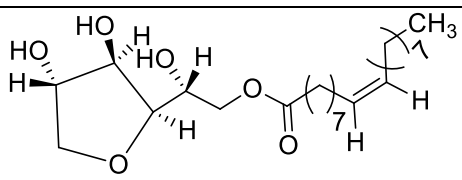
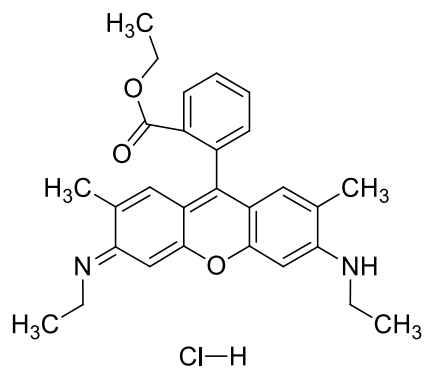
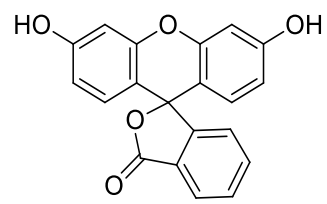
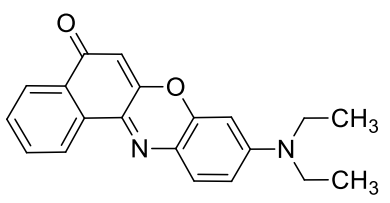
2.1.4 Organic Solvents

Solvents used for washing microscope slides, dissolving hydrophobic dyes and other applications included acetone, isopropanol, ethanol and methanol. All were laboratory reagent grade, purchased from Fisher Scientific, UK.

2.1.5 Chemicals

Calcium chloride dihydrate was purchased from Fisher Scientific, UK, CaCO_3 was purchased from Fluka Chemika, UK. Table salt was used in experiments with food formulations, which was supplied by 3663, UK, with an added anti caking agent (Sodium Hexacyanoferrate II). Potato starch (food grade) was provided by Unilever Research, The Netherlands. Silicone oil was purchased from Sigma Aldrich, UK. Other chemicals are listed below in Table 2.3.

Table 2.3. Chemicals used, their structure and supplier

Compound, purity	Structure	Supplier
Span 80		KOCH-LIGHT Ltd, UK.
Rhodamine 6G (99%)	 Cl-H	Across Organics, UK.
Fluorescein disodium salt, microscopy grade		Sigma, UK.
Nile Red (technical grade)		Sigma, UK.

2.2 CHARACTERISATION EQUIPMENT

2.2.1 Microscopy

2.2.1.1 Optical Microscopy

The bright field and fluorescence images were obtained using a BX-51 fluorescence microscope equipped with a DP70 digital camera. Objectives of 2x, 4x, 10x, 20x, 50x and 100x (oil immersion) were used. For fluorescence microscopy, an Hg-arc lamp housed in a U-RFL-T power supply was used to as an excitation light source. All filters and equipment above were manufactured by Olympus, Japan. For Rhodamine 6G and Nile red treated samples a MW1G2 filter set ($\lambda_{\text{excitation}} = 520\text{-}550\text{ nm}$, $\lambda_{\text{emission}} = 570\text{ nm}$) was used and for Fluorescein treated samples a MWIBA2 filter set ($\lambda_{\text{excitation}} = 460\text{-}490\text{ nm}$, $\lambda_{\text{emission}} = 510\text{-}550\text{ nm}$). Where samples were treated with both fluorophores, the individual images were merged in post-processing using Corel PhotoPaint X6 software. Microscope images were captured and particle sizes were analysed using an image analysis software Image Pro Plus 6.

2.2.1.2 Scanning Electron Microscopy (SEM)

SEM images were obtained using a bench-top Hitachi TM-1000 SEM. Samples for analysis were prepared by attaching analytes onto an adhesive carbon sticker, which was pre-attached onto an aluminium SEM stub (Agar, UK). None of the samples were coated prior to their examination.

2.2.1.3 Confocal Laser Scanning Microscopy

Confocal microscopy images were obtained using an inverted confocal microscope (Carl Zeiss AG, Oberkochen, Germany), equipped with a LSM Axiovert 510 laser scanning device using a 10x Plan Apochromat objective, with an automated z-stack functionality. To excite the dyes an Argon laser operating at $\lambda = 488\text{ nm}$ was used.

2.2.2 Sound Absorption Analysis

In order to reduce noise in apartments, offices etc. it is important to know how well particular building materials reduce sound amplitude. Materials interact with sound

waves by reflecting and absorbing them. If the sound energy is absorbed by a material, it is converted to heat. Porous materials absorb sound better than non-porous and the sound absorption extent varies for the same material at different sound wave frequencies. *Sound absorption coefficient*, α , which ranges from zero (no sound absorption) to one (full sound absorption) is typically used to describe materials acoustic performance. Typical values of sound absorption for some common materials are detailed in Table 2.4 below.

Table 2.4. Sound absorption coefficient values for typical materials.^{1,2}

Material	250 Hz	500 Hz	2000 Hz
Painted drywall	0.08	0.05	0.03
Carpet	0.05	0.10	0.30
Flexible polyurethane foam (density of 34 kg m ⁻³ , thickness 25 mm)	0.25	0.45	0.97

To determine porous composite sample acoustic properties, i.e. sound absorption ability, samples were analysed with an acoustic impedance equipment. The measurement revealed the materials performance in terms of sound absorption. Composite samples were inserted into an acoustic impedance tube and their sound absorption coefficients were analysed at different sound frequencies. An impedance tube with a single microphone was used in this test, where the microphone was attached to a slider (see Figure 2.1) according to the published standards.³ The sound impedance tube was made from aluminium, its inner diameter was 76 mm and the distance from the sound source to the plunger was 3.0 meters. Computer based software analysed the measured sound pressure amplitude of the combined waves (the sum of the incident wave and the reflected wave). The slider was used to change the position of the microphone within the tube to find the highest (MAX) and the lowest (MIN) sound pressure of the combined waves. The collected p_{MAX} and p_{MIN} pressures (converted to Volts by the digital microphone) were then used to calculate the sound absorption coefficient, α , using equation (2.1)

$$\alpha = 1 - \left\{ \frac{[(P_{MAX} / P_{MIN}) - 1]^2}{[(P_{MAX} / P_{MIN}) + 1]^2} \right\} \quad (2.1)$$

The lower frequency for the test was set to 200 Hz and the upper to 2000 Hz. Data points were taken every 100 Hz for frequencies below 1000 Hz and every 200 Hz for the higher frequencies.

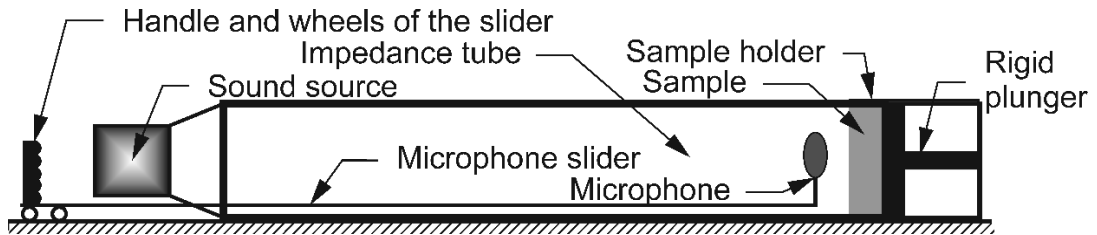


Figure 2.1. Schematic showing an impedance tube fitted with a single microphone for the sound absorption measurement. The microphone was connected to a computer, which analysed the signal, and a slider was used to find the highest and the lowest sound pressure spots (p_{MAX} , p_{MIN}) within the impedance tube. The length of the tube was 3 m, inner diameter 76 mm.

2.2.3 Mechanical Strength Testing

The mechanical strength testing was conducted by compressing the sample materials using a Lloyds LD50 mechanical strength apparatus equipped with a 5 kN cell or Lloyds LR100KPlus mechanical strength apparatus equipped with 100 kN cell. The apparatus was controlled using software and a force was applied onto the sample (4 mm / min) until the sample crumbled. The pressure was calculated by measuring the diameter of the sample and then calculating the area of the base. Typically, samples had a diameter of 32 mm and a height of around 5 cm. The force per unit area was calculated following the equation (1.1) ($\sigma = F/A$).

2.2.4 Hydrogel Slurry Fabrication Equipment

Various methods of cutting hydrogels down to millimetre and sub-millimetre sizes were used. For the porous materials described in Chapter 3 and partially in Chapter 4 as well as for bouillon composites with Xanthan – Konjac hydrogel mixture and soap composites, a hand-held kitchen blender was used (Wilkinson, UK), whereas in later

EXPERIMENTAL

experiments (the porous materials in Chapter 4 with Xanthan – Konjac hydrogel, bouillon cubes with κ -carrageenan) Kenwood Chef mixer equipped with a grinder accessory (shown in Figure 2.2a) was used. The pores in the plates were either 2 mm or 3 mm (Figure 2.2b).



Figure 2.2. Images showing (A) Kenwood Chef mincing attachment used for the fabrication of hydrogel bead slurries, (B) the mincer plates with diameter 3 mm and 2 mm of the plate holes on the left and right respectively used to produce different bead size distributions within hydrogel slurries.

2.2.5 Measurement of the Dissolution Time of Composites

To measure the time required for soap and bouillon composites to dissolve, the following methodology was developed and used in this thesis. A 2 L beaker containing 1500 mL of distilled water previously heated to 90 °C (40 °C for soap composites) was stirred with a magnetic stirrer (diameter of 4 cm, 800 rpm). A cylinder-shaped stainless steel mesh (diameter: 5 cm) containing a set amount of sample was then lowered down so that the sample was 4 cm above the surface of the bottom of beaker as represented in Figure 2.3. The speed of stirring was constant (800 rpm) and the evaporation of water was prevented by covering the beaker with an aluminium foil. The disintegration time corresponds to the time from immersing the samples of the same shape to the moment when fragments of the sample were no longer visible.

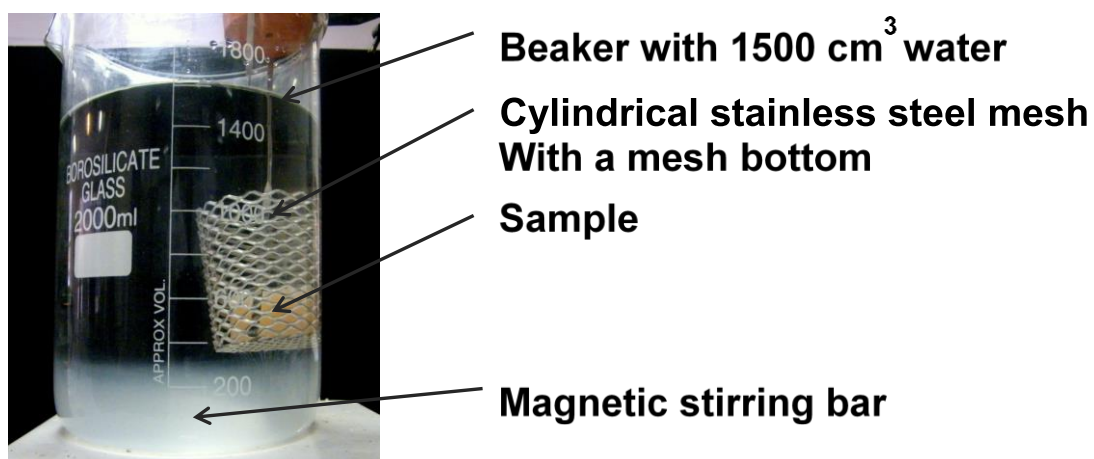


Figure 2.3. Image of the typical setup used to determine the dissolution time of the composites. A cylindrical shaped mesh with a sample (in this photograph a soap composite sample) was lowered into a stirred beaker and the dissolution of the sample was monitored. Time taken to fully dissolve the sample was recorded, or if the sample did not dissolve, it was taken out and measured.

2.2.6 Other Measurements and Instrumentation

Surface tension was measured using a Kruss 10 Mk2 tensiometer by the pendant drop method using a 1.651 mm thickness needle. The final result was averaged out of at least three surface tension measurements.

Rheology analyses were performed using a Bohlin Instrument (CVO 120). Parallel plates (rough surfaces, 40 mm diameter) with a gap set to 150 μm were used. Frequency of oscillation was 0.1 Hz, strain controlled experiments of 0.1 % were used. The sample evaporation was reduced by the use of a plastic cover.

Differential Scanning Calorimetry (DSC) measurements were recorded using Perkin-Elmer DSC 7 (cooling-heating cycle; scan rate of 5 $^{\circ}\text{C}/\text{min}$).

Standard deviation of the results (s_N) was calculated using the equation below:

$$s_N = \sqrt{\frac{1}{N} \sum_{i=1}^N (x_i - \bar{x})^2} \quad (i = 1, 2, \dots, N) \quad (2.2)$$

Where N is the number of the values, x_i is the observer value, \bar{x} is the mean observed value.

2.3 METHODS

2.3.1 Preparation of the Hydrogels

2.3.1.1 Preparation of Xanthan – Konjac Hydrogel Bead Slurries with Sodium Chloride

Xanthan – Konjac hydrogel compositions were prepared using a temperature controlled water bath: NaCl (132.75 g) and calcium chloride dehydrate (6.50 g) were dissolved in water (500.0 mL). To some solutions Fluorescein sodium salt (1 mM, 10 mL) was added at this stage and the solution was heated to 95 $^{\circ}\text{C}$, followed by the addition of Xanthan gum (11.50 g, 2.3 wt%) and Konjac gum (5.50 g, 1.1% wt) whilst mixing with an Ultraturrax homogeniser at 12 000 rpm and further mixing for 5 minutes. The hydrogel was then centrifuged at (3000 g, 3 min, twice) whilst hot in order to remove any air trapped during the hydration of the materials, and left to set

overnight (4 °C). The hydrogel was then turned into a slurry by passing it three times through a food processor (Kenwood Chef) equipped with a grinder kit for sound absorbing materials. For the application in porous bouillon cube preparation it was blended using a Silverson LR4 homogeniser.

2.3.1.2 Preparation of the κ -carrageenan Hydrogel Bead Slurries

The hydrogels were prepared using a temperature controlled water bath. Water was heated (500 cm³, 85 °C) and optionally solutions were stained with fluorescein sodium salt (1 mM, 10 mL). Then κ -carrageenan (1.5 – 3.0 wt%) was added whilst mixing with an Ultraturrax homogeniser at 12, 000rpm and homogenised further for 1 minute. The hydrogel was then centrifuged at (3000 g, 1 min) whilst hot and left to set at room temperature. It was then kept at 5 °C. After the gel was set it was blended into a slurry by passing it three times through a food processor equipped with a grinder kit (plate pore size was 3 mm).

2.3.1.3 Preparation of Polyacrylamide Hydrogel Slurries

Polyacrylamide gel was prepared by adding polyacrylamide granules (12 g or 20 g) into water (400 cm³) thus producing 3 wt% or 5 wt% gel slurry respectively. After allowing the gel beads to swell for 20 min, 12.5 cm³ of 1% wt CaCl₂ (aq) was added and the mixture was blended (using a hand-held kitchen blender) for 3 minutes to produce a slurry of PAA hydrogel microbeads.

2.3.1.4 Preparation of Gellan Gum Hydrogel Bead Slurries

Gellan gum powder (10 g) was added to water (1000 cm³). The resulted mixture was heated in a water bath at 90 °C for about 2 hours. After allowing to cool down to room temperature the set hydrogel was blended for 3 minutes to produce a slurry of Gellan gum microbeads. Hand-held kitchen blender was used in this case.

2.3.1.5 Production of Monodisperse Sodium Alginate Hydrogel Beads

The beads were produced by a drop wise addition (plastic syringe with a standard needle, 0.5 cm³ min⁻¹) of the pre-hydrated (using methods detailed above) hot sodium

alginate solution (4 wt% gelling agent) into a beaker containing calcium chloride (10 wt%). The beads were then drained and used in composite production.

2.3.1.6 Hydrogel Beads Produced by Spray-gelation

These samples were produced by spraying a hot hydrogel solution through a cold tube (-7 °C, or -17 °C resulting in +8±5 °C and -1±4 °C tube inner temperature respectively). The tube was 1.5 m high and 15 cm diameter, with a nitrogen flow from top and bottom of the tube to reduce water condensation within the system. Xanthan - Konjac 2:1 hydrogels (0.3, 0.6, 0.9, 1.0, 1.2 and 1.5 wt% of gelling agent) and κ -carrageenan (1.0, 1.2, 1.5 wt% of gelling agent) hydrogels were used. A hand-held sprayer was used to atomize the hydrogel solutions into fine droplets.

2.3.2 Preparation of the Hydrogel Slurry Templated Complexes

The technique was applied throughout the range of matrices (cement, PDMS, fat-salt base, etc.) and fillers (different hydrogel formulations). The image with a schematic summary of this technique can be found below in Figure 2.4. The methodology was tuned for specific matrices and hydrogels.

2.3.2.1 Hydrogel Slurry Templating with Cement Slurry

Dry powder of cement was mixed with water in a 2.175:1 ratio to produce a thick cement slurry. This slurry was hand-mixed with a polyacrylamide gel slurry (3 wt% or 5 wt%), Xanthan – Konjac hydrogel mixture (2-3.5 wt% gelling agent) or sodium alginate hydrogel beads in various ratios. The samples were poured into paper cups or cylindrical moulds and were allowed to cure at room temperature for 24 hours followed by drying at 50 °C for 5 days. Cement slurry mixtures at eight different volume ratios of added hydrogel were prepared and moulded at the same conditions as the control sample (100% cement slurry).

2.3.2.2 Hydrogel Slurry Templating with PDMS

Two different types of PDMS templating phases were prepared and studied: Sylgard 184 with added 10% of silicon oil and 5% Span 80 surfactant and separately Sylgard 184 without further additions. The first set was prepared by mixing the silicon

elastomer and curing agent in a 10:1 ratio, adding silicon oil (10 %), surfactant Span 80 (5 %) and finally adding various percentages of blended Gellan gum hydrogel. The mixture was hand-mixed and degassed under vacuum for 2 h. The mixture was allowed to cure for 24 hours at room temperature prior to drying of the sample at 50 °C for 5 days. The second (see Figure 2.4) set was made following the same procedure except that silicon oil and surfactant were not added to the mixture. PDMS-to-hydrogel slurry mixtures at several different PDMS-to-hydrogel volume ratios were prepared, moulded and cured at the same conditions as the control sample of PDMS.

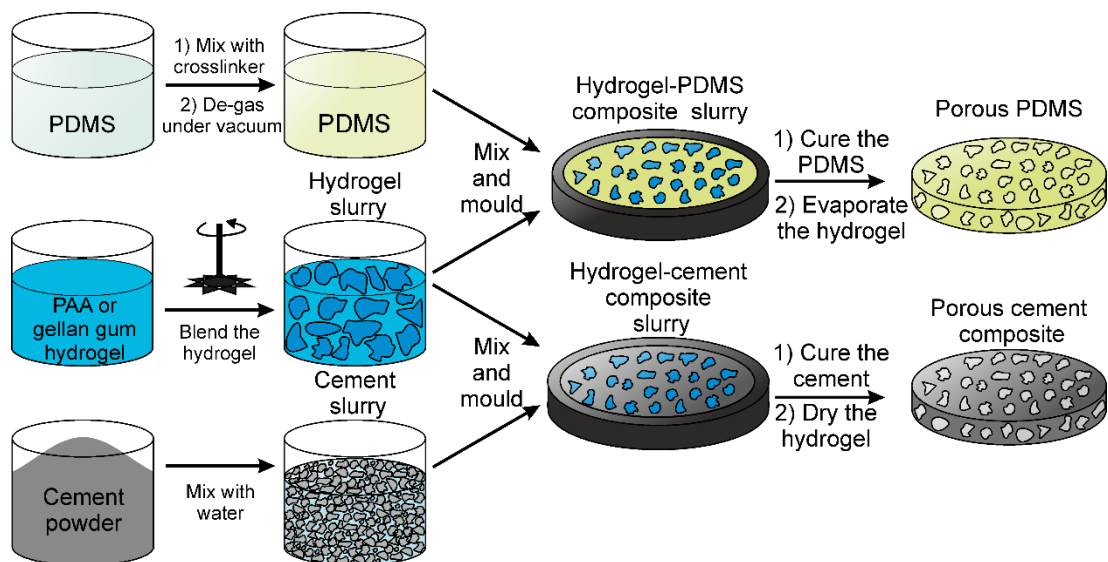


Figure 2.4. Schematic representation of the hydrogel slurry templating technique to produce porous cement and PDMS composites for acoustic testing. The slurries of the matrices were mixed with the hydrogel slurries and moulded into cylindrical moulds, engineered to match the sample holder in the sound impedance tube. The evaporation of the water from the hydrogel was carried out at 60 °C once the matrix was solidified under ambient temperature and the mould was removed after drying of the sample to evaporate the hydrogel.

2.3.2.3 Hydrogel Slurry Templating with Clay-Cement Slurries.

Talc was chosen as a clay material to make composite cement-talc templating of hydrogel slurries. Dry powder of talc (70 wt%) and dry powder of cement (30 wt%) were mixed prior to the hydrogel templating process. The procedure in the preparation of this talc-cement slurry was similar to that of cement as outlined in section 2.3.2.1. A control sample of talc-cement slurry was also prepared. As for the hydrogel templating of talc-cement slurry, 3 wt% of polyacrylamide hydrogel gel was used after blending for 3 minutes. The procedure was similar to that with the cement. Six different ratios of talc-cement slurry to hydrogel (50:50, 40:60, 30:70, 20:80, 10:90, and 5:95) by volume were prepared and studied at the same conditions as the control sample (100% talc-cement slurry).

2.3.2.4 Hydrogel Slurry Templating with Gypsum Slurry

The methodology in the hydrogel templating with gypsum resembled that of cement. Gypsum in the form of dry powder was mixed with water (typically in 2.175:1 ratio by weight) to prepare the aqueous slurry of gypsum. This slurry was used to prepare the control sample of gypsum after curing at room temperature. Polyacrylamide hydrogel (4 wt%) was mixed with the gypsum slurry. Gypsum – hydrogel slurry mixtures at eight different volume ratios were prepared and moulded at the same conditions as the control sample of gypsum slurry.

2.3.2.5 Preparation of Salt – Fat – Starch Composite Templating with 3.4 wt% Xanthan-Konjac Hydrogel Slurries

The composites were prepared by first melting the fat mixture consisting of palm oil stearin (14 wt%, 56 g) and vegetable fat (1 wt%, 4 g) at 40-45 °C, followed by addition of the potato starch (4 wt%, 16 g) and then water (drop wise, 4 wt%, 16 g) and lastly sodium chloride crystals (77 wt%, 300 g, cooking salt, further ground by pestle and mortar). The salt – fat slurry was kept at 40-45 °C until it was mixed with the blended hydrogel and homogenised with a hand-held mixer. All final samples corresponded to 40 mL and various ratios of salt-fat slurry – hydrogel were used to analyse the influence of the hydrogel beads on the final material. The samples were moulded in cylinder-shaped tubes (d= 37mm, cut lengthwise and joined by clamps with a

EXPERIMENTAL

removable base made of PDMS) as shown in Figure 2.5. The composites were exposed to vacuum for degassing purposes and then recompressed by hand. The samples were then left in a fridge for 2 hours (4 °C) and freeze dried overnight (-40 °C, 6mmHg, samples in moulds) followed by freeze drying when the moulds were removed.

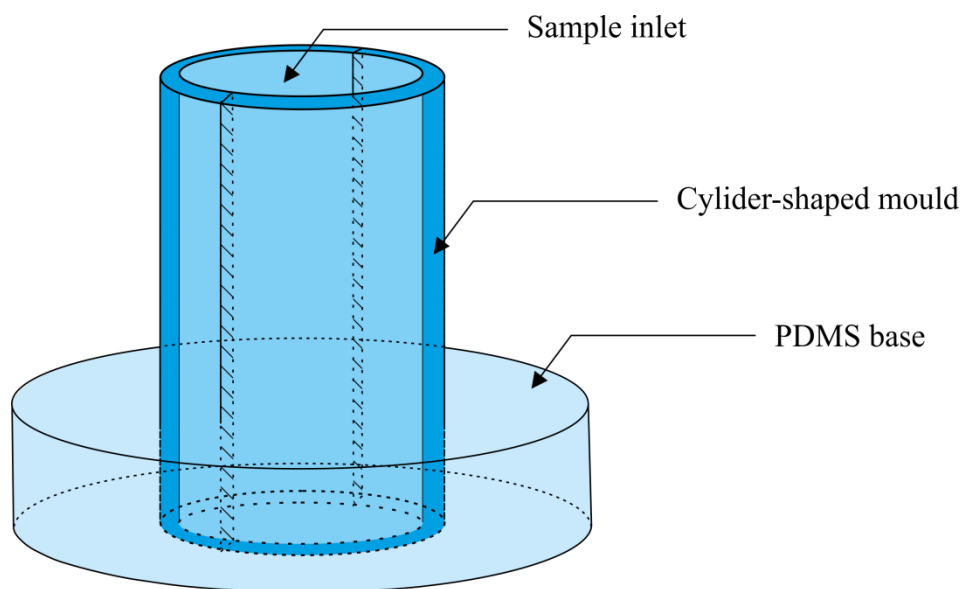


Figure 2.5. Schematic of the mould used for soap-gel and bouillon composites. The diameter of the sample inlet was 36 mm.

2.3.2.6 Preparation of Fat-salt Composites by Templating with Hydrogel Slurries

The basic principle of this method was outlined in Section 2.3.2.1 and Figure 2.4. The composites were prepared by first melting the fat mixture consisting of palm oil stearin (16 wt%, 56 g) and vegetable fat (1wt%; 4 g) at 40-45 °C (with an optional addition of Nile Red (1 mM, 2 cm³) in acetone), followed by addition of sodium chloride crystals (83 wt%; 300 g, table salt, further ground by pestle and mortar). The salt – fat slurry was kept at 39-42 °C until it was mixed with the blended hydrogel and homogenised with a hand-held mixer. All final samples corresponded to 40 mL and various ratios of salt-fat slurry – hydrogel were used to determine the influence on the final material. The samples were moulded in cylindrical tubes (d = 37 mm, cut lengthwise and joined by clamps with a removable base made of PDMS). The samples were then left in a fridge for at least 4 hours (5-6 °C) or frozen in a freezer for at least 6 hours at -20 °C, or immersed in liquid nitrogen (-196 °C, 2 minutes) and then freeze-dried overnight (-40 °C, 6 mmHg, samples in moulds) followed by freeze-drying for another night when the moulds were removed.

2.3.2.7 Preparation of Soap Bars Structured with Hydrogel Slurries

The composites were prepared by first melting the soap base at 80 °C and then after allowing it to cool to 45 °C pouring the cooled soap (45 °C) on the blended hydrogels (either Xanthan - Konjac 2:1 mixture with sodium chloride or κ -carrageenan) and homogenising with a spatula. Various ratios of soap – hydrogel were used. Samples were moulded in cylinder tubes (d=36 mm) cut lengthwise and joined by clamps with a detachable base made of PDMS as shown in Figure 2.5. Samples were allowed to cool down for at least 3 hours before removing from the moulds.

2.3.3 Preparation of the Porous Salt Marbles

Table salt was pre-dried in an oven at 80 °C for 24 hours, milled using a ball mill for 1 hour, sieved and dried again for 24 hours, milled for the second time for 30 minutes, dried, sieved through 300 μ m or 38 μ m pore-size sieve onto a flat glass dish and placed below the cold tube, where the hydrogel was sprayed down. A PVC tube was used as a column in these preliminary experiments as detailed in Section 2.3.1.6.

EXPERIMENTAL

Salt marbles were produced by spraying hot hydrogel through the cold tube. Xanthan-Konjac (2:1 ratio, 0.4% to 1.5 wt%), κ -carrageenan (1.0-2.0 wt%) and Agar (1.5% and 3.0 wt%) hydrogels were used to spray on salt microcrystals using a hand held plastic spray bottle. The glass dish with finely milled salt crystals was then shaken by hand (10 s) to facilitate the covering of the gel beads with salt microcrystals. The powder was then sieved through 0.6mm and 0.3mm sieves, to remove the unused salt crystals and to separate large and small salt marbles. Then the marbles were left in glass bottles to dry at 30 °C for 2 days. This way of drying is hardly optimal, as passing air through a bed of marbles would result in a much faster drying, but the latter was out of the scope of for these pioneering experiments.

2.4 REFERENCES

1. M. T. Bomberg and J. W. Lstiburek, *Spray Polyurethane Foam in External Envelopes of Buildings*, Taylor & Francis, 1998.
2. T. D. Rossing, *Springer Handbook of Acoustics*, Springer, 2007.
3. I. S. Organisation, *Geenva*, Switzerland, 1996.

Chapter 3. Hydrogel Slurry Templating Technique Used to Produce Porous Cement, Gypsum, Clay and PDMS Composites

“It is not titles that honour men, but men that honour titles”

Niccolo Machiavelli

In this Chapter an alternative method for the sustainable introduction of porosity by hydrogel slurry templating is introduced, where the preparation of porous materials based on cement, PDMS, gypsum, and clay will guide the reader into further understanding of the importance of this methodology. These materials were chosen due to their high applicability in construction, chemical and medical fields and their well-defined properties. Changes in the density, volume shrinkage of samples, porosity and strength of the materials at different hydrogel volume fractions are discussed and SEM images presented. For an introduction to cement and PDMS the reader should refer to Section 1.2 in Chapter 1.

The basis of this Chapter have already been published as a peer-reviewed publication in Materials Research Bulletin.¹

3.1 FABRICATION OF POROUS CEMENT AND PDMS COMPOSITES

In this Chapter several routes of hydrogel templating for the fabrication of porous materials based on inorganic and organic matrices are explored. The focus of the Chapter is on the preparation of a range of porous materials by templating aqueous slurries of hydrogel microbeads with: (i) aqueous slurries of inorganic microparticles (cement, gypsum, clays) as well as (ii) PDMS formulations. A schematic representation the methodology for the preparation of these materials was presented in Chapter 2 Figure 2.4. In both cases (i) and (ii) the blended hydrogel microbeads play the role of the template around which the continuous phase (aqueous slurry of

cement, gypsum or clay) or PDMS solidifies. After the curing (solidification) of the continuous phase, the hydrogel phase was dried resulting in the introduction of pores in the produced composites. This approach allows in principle fine tuning the pore sizes by using hydrogel beads with a particular size and the material porosity by controlling the hydrogel to matrix volume fraction. The effect of the hydrogel initial volume fraction on the density (porosity) and the volume contraction of the obtained porous materials was examined. A summary of the morphological and microstructural differences between the various lightweight porous materials produced by this technique and some data on the compressional strength of the porous PDMS as a function of the initial volume fraction of the hydrogel will be presented below.

3.2 CHARACTERISATION OF THE HYDROGEL SLURRIES USED IN POROUS CEMENT, GYPSUM, CLAY AND PDMS COMPOSITE PREPARATION

The hydrogel microbeads size distribution strongly depends on the power of the blender and the blade geometry. The Gellan gum and polyacrylamide hydrogels were doped with Fluorescein disodium salt and Rhodamine 6G and after blending with a hand-held blender were examined with fluorescence microscopy using FITC/TRITC filter set (see **Figure 3.1**). The hydrogel slurry was mixed with silicone oil and spread over a microscope glass slide and images were taken, which allowed to assess the size distribution of the hydrogel particles. The later was not possible by prior dilution of the slurry with water as the hydrogel particles absorbed the added water almost instantaneously. The average diameters of polyacrylamide and Gellan gum hydrogel beads were determined to be $130 \pm 100 \mu\text{m}$ and $750 \pm 500 \mu\text{m}$, respectively, both showing a high polydispersity. The range of the hydrogel particle size varies from 20 to $350 \mu\text{m}$ for the polyacrylamide and 250 to $1300 \mu\text{m}$ for the Gellan gum hydrogels. These bead sizes depend on the method of blending of the prepared hydrogels to form hydrogel beads of appropriate size and determines the pore size of the porous materials obtained by their templating.

3.3 DENSITIES OF POROUS CEMENT, GYPSUM, CLAY AND PDMS COMPOSITES

It has been reported, that PDMS has a density of 0.97 kg/m^3 ,² which corresponds well to the control sample (1.01 g/cm^3 and 0.98 g/cm^3 for PDMS without silicone oil and

with respectively, determined by measuring the weight and volume of the samples as truncated cones). The reported density of Portland cement varies and the density of the sample after drying was 1.74 g/cm^3 . The densities of all samples were calculated by assuming that the structure after shrinkage was still a truncated cone and are summarized in Table 3.1. Typical samples are shown in Figure 3.2. Both samples of the porous PDMS (with and without dilution with silicone oil) follow a linear relationship between the percentage of the hydrogel used in each sample and their density, with the samples becoming uniformly less dense with the increase in the hydrogel concentration, as shown in Figure 3.3. It was unexpected that the moulded samples of the hydrogel and PDMS without the silicon oil and the surfactant were more homogenous than the samples with oil and surfactant. It is known that the combination of hydrophobic and hydrophilic components separate phases if they are not pre-stabilised. The better result was due to the lack of silicon oil decreasing the viscosity. This experiment was carried out for 50%, 60%, 70%, 80%, 90%, and 95% hydrogel volume fractions. The 90% and 95% samples collapsed during the curing process due to the lack of supporting material (matrix) and were not used in further analysis.

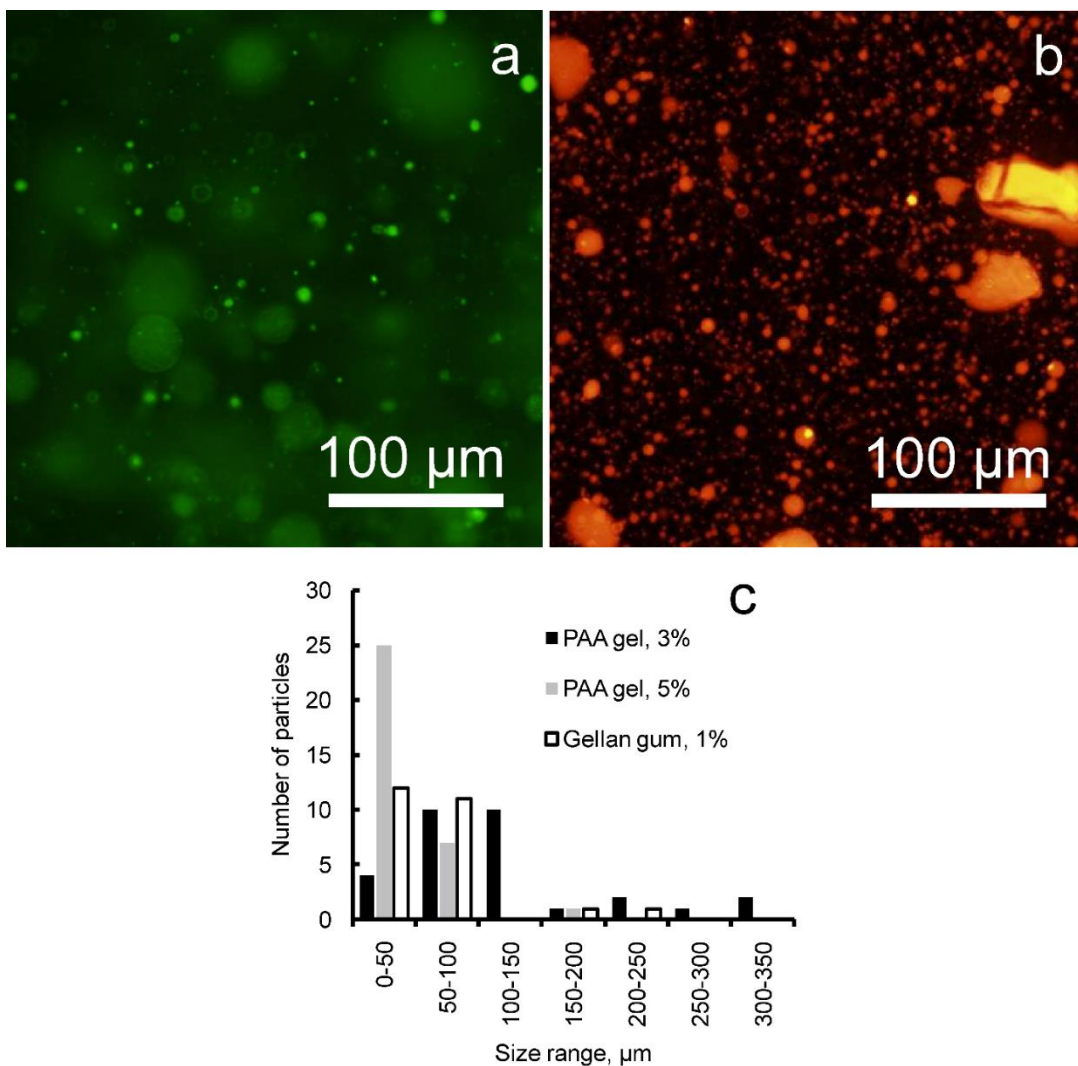


Figure 3.1. Fluorescence microscope images of (a) Gellan hydrogel beads and (b) polyacrylamide hydrogel bead slurry produced by blending the hydrogel. (c) The size distribution of the hydrogel beads in the hydrogel slurries prepared by following a blending procedure with a hand-held blender. The bead size was measured using the fluorescence microscopy images.

Table 3.1. Summary of the templated matrix materials, showing the sample density, the reduction in density and the reduction in volume. Reduction in volume was measured as a volume ratio of sample with hydrogel (assuming isotropic contraction of the truncated cone) and the control sample.

Volume percentage of hydrogel mixed with the material	Density, g cm⁻³	Reduction in density, %	Reduction in volume, %
Cement (C) 0%	1.74	-	-
C ^a 50 %	0.96	45.2	5.2
C ^a 67 %	0.72	58.5	5.2
C ^a 75 %	0.60	65.6	5.2
C ^a 80 %	0.40	77.2	17.0
C ^b 50 %	1.00	42.3	5.2
C ^b 67 %	0.80	54.2	5.4
C ^b 75 %	0.65	62.8	3.2
C ^b 80 %	0.53	69.4	5.2
PDMS ^c 0 %	0.98	-	-
PDMS ^c 50 %	0.48	51.0	2.5
PDMS ^c 60 %	0.39	60.2	4.4
PDMS ^c 70 %	0.31	68.4	6.4
PDMS ^c 80 %	0.22	77.6	8.2
PDMS ^d 0 %	1.01	-	-
PDMS ^d 50 %	0.60	40.6	0.0
PDMS ^d 60 %	0.39	61.4	4.8
PDMS ^d 70 %	0.29	71.3	5.7
PDMS ^d 80 %	0.21	79.2	7.3
Clay-cement 0%	1.23	-	-
Clay-cement 50%	0.56	54.8	37.5
Clay-cement 60%	0.53	57.3	44.1
Clay-cement 70%	0.58	53.2	49.1
Clay-cement 80%	0.60	51.3	61.5
Clay-cement 90%	0.76	38.8	80.1
Clay-cement 95%	0.76	38.5	86.7
Gypsum 0%	1.11	-	-
Gypsum 50%	0.79	29.0	29.0
Gypsum 60%	0.62	44.7	44.7
Gypsum 70%	0.43	61.3	61.3
Gypsum 80%	0.37	66.7	66.7

^a 5 wt% gelling agent was used. ^b 3 wt% gelling agent was used. ^c PDMS sample with silicone oil and Span 80. ^d PDMS sample without silicone oil and Span 80

HYDROGEL SLURRY TEMPLATING TECHNIQUE USED TO PRODUCE POROUS CEMENT, GYPSUM, CLAY AND PDMS COMPOSITES



Figure 3.2. Moulded samples of:(A-E) PDMS with no silicone oil or surfactant, (A) control, (B) 50% gel, (C) 70%, (D) 80%, (E) 90%; (F-J) PDMS with surfactant and oil, (F) control, (G) 50%, (H) 60%, (I) 80%, (J) 90%; (K-O) cement: (K) control, (L) 66% hydrogel of 3 wt% gelling agent (M) 90% hydrogel of 3 wt% gelling agent, (N) 66% of 5 wt% gelling agent hydrogel, (O) 90% of 5 wt% gelling agent hydrogel; (P-T) talc-cement composite: (P) control, (Q) 50%, (R) 60%, (S) 90%, (T) 95%; (U-Y) gypsum: (U) control, (V) 40% hydrogel, (W) 50% hydrogel, (X) 60% hydrogel, (Y) 75% hydrogel.

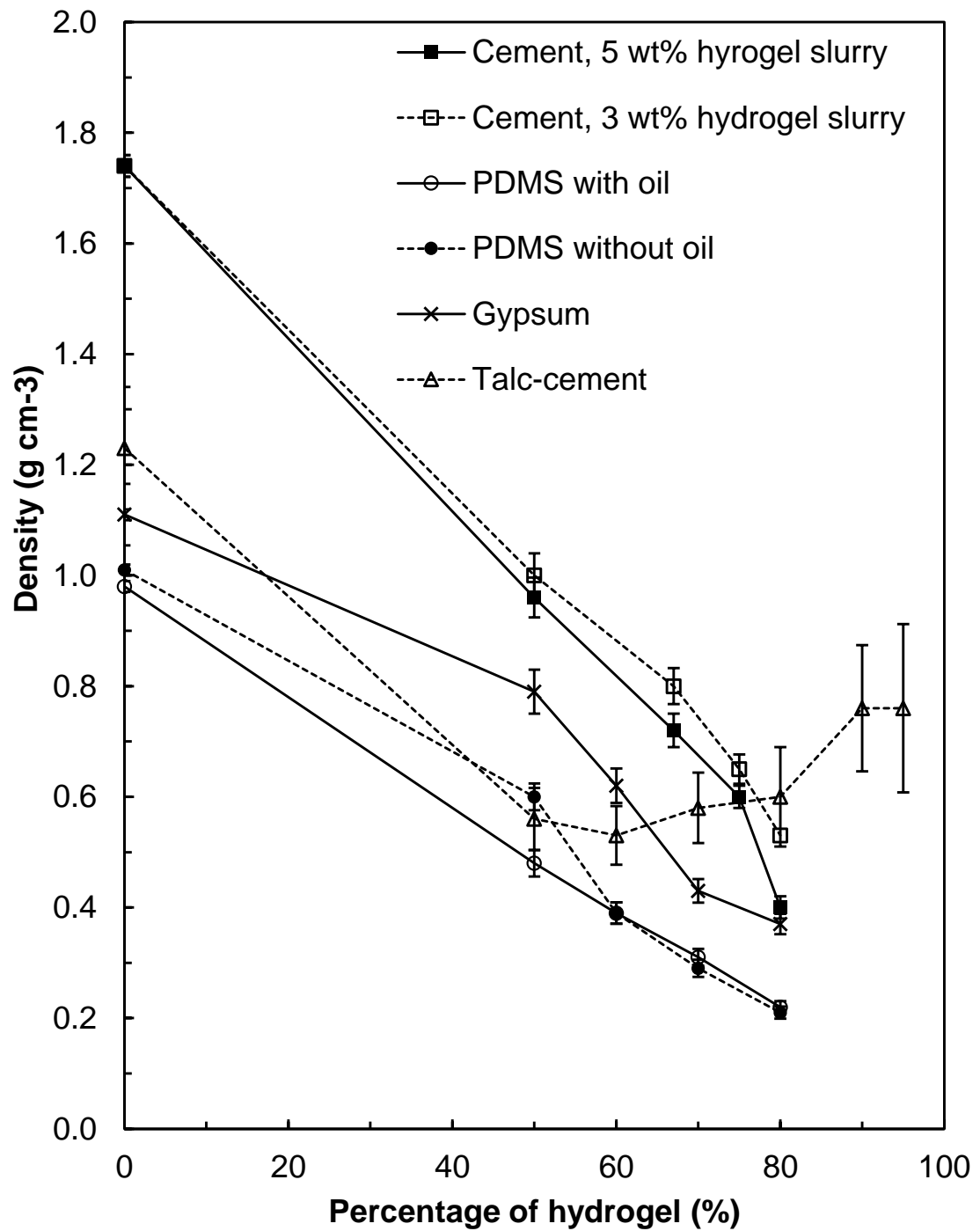


Figure 3.3. The mass density of the (cement, gypsum and clay templated with PAA, PDMS with Gellan) composite porous materials as a function of the initial volume percentage of the hydrogel.

The sample of 50 vol% hydrogel and no surfactant had been found to retain the water of the hydrogel even after curing in the oven and after being dried in a vacuum oven for 3 days at 80 °C. This result brings both a challenge for adjusting the density to the expected value and also a useful property – preventing the evaporation of the solvent by keeping it in a porous medium, as shown in a schematic representation in Figure 3.4. If the low density of a material is the desirable property, the data suggests that the volume percentage of the hydrogel in the composite should be higher than ~50 vol%, so that a continuous porosity would be present within the sample. This volume fraction will depend on the packing and size of the blended beads within the PDMS matrix.

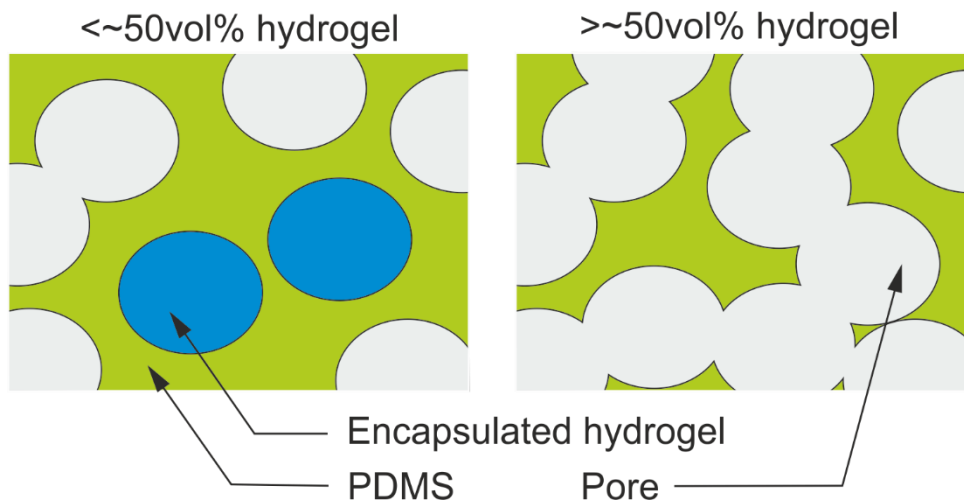


Figure 3.4. Schematic representation of the cross-section of a hydrogel slurry templated PDMS composite, where the hydrogel beads are trapped within the matrix (left) and where an interconnected network of the hydrogel beads allow a successful evaporation of the water from the composite.

The density of the cement samples has decreased for both 3wt% and 5wt% Gellan gum hydrogel concentrations with increasing hydrogel volume. This decrease follows the linear trend well with samples of up to 80 vol% of the gel, as shown in Figure 3.3. However, when the hydrogel volume fraction exceeded 80 vol% the samples were not stable enough to retain their volume, thus the densities were not calculated for these samples. However, the samples that contained 80 vol% of the hydrogel showed significant decrease in their densities with 69% and 77% decreases for the 3 wt% and 5 wt% of Gellan gum present in the hydrogel respectively. The density of the moulded

samples with gypsum had also been reduced. Up to 67% reduction in the density was observed in the porous gypsum samples.

The samples of talc-cement did not show a linear trend in the density reduction. However, the density was reduced for all the samples, compared to the control. This was likely because talc is not an excellent construction material alone and thus the composite shrinks during the curing process. The material requires an additional cross-linker, such as cement for the high volume of the hydrogel to be stable during the curing process.

3.4 CHANGE IN THE VOLUME OF POROUS CEMENT, GYPSUM, CLAY AND PDMS COMPOSITES

The volume shrinkage was most significant in the porous talc-cement samples, followed by gypsum samples, as shown in Figure 3.5. The samples had shrank with the increase in the initial hydrogel volume percentage following a near-linear trend, with a significant reduction in the volume even for 1:1 templating material-to-hydrogel ratio sample. The porous PDMS and cement samples showed a lower reduction of their volumes upon drying, with cement sample templated with 3 wt% Gellan gum hydrogel showing the lowest shrinkage. The difference in the percentage of volume shrinkage between this sample and the one with a higher gelling agent concentration in the hydrogel was around 15 vol%. This identifies that the volume retention in the cement-hydrogel samples is highly dependent on the gelling agent concentration in the hydrogel, especially when a high volume of the hydrogel is templated. The PDMS samples without silicone oil and Span 80 surfactant were more stable in terms of their volume retention. The sample with half the volume of the hydrogel showed no volume shrinkage upon drying. Samples with up to 80% of the hydrogel shrank less than 10%, however when the hydrogel volume fraction was increased further, the samples collapsed as shown in Figure 3.2 (e, j).

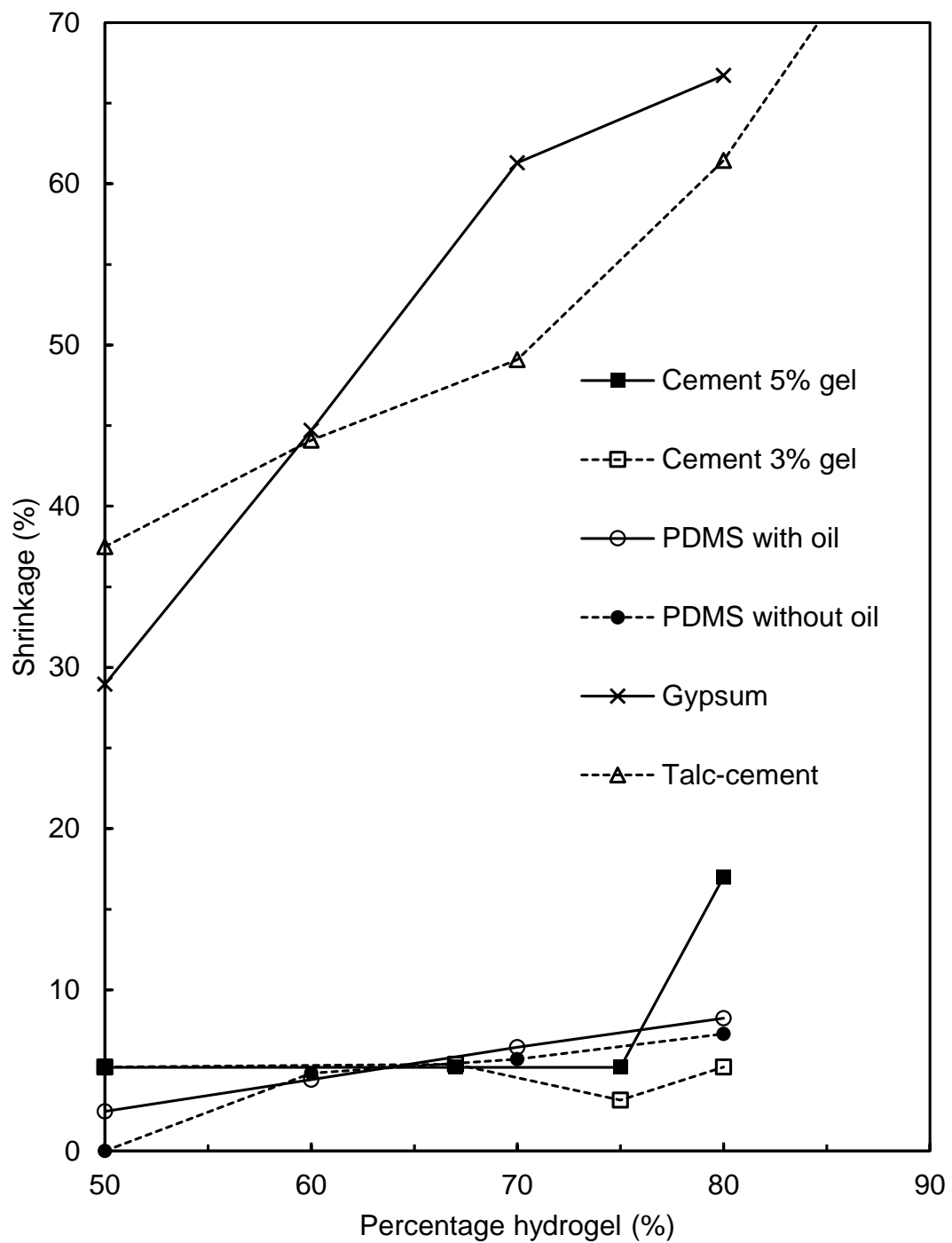


Figure 3.5. The volume shrinkage of the porous composite materials as a function of the initial volume percentage of the hydrogel. The shrinkage was calculated by measuring final volumes of the control and hydrogel templated composites, assuming isotropic contraction of the truncated cone shaped samples.

3.5 SEM ANALYSIS OF THE POROUS CEMENT, PDMS, GYPSUM AND TALC COMPOSITES

The Scanning Electron Microscopy (SEM) images in Figure 3.6 show hydrogel slurry templated cement composites. Various materials are present in the porous composites produced from the cement-polyacrylamide hydrogel formulations. In the solidified cement, fibrous domains (voids) could be observed at the places where the hydrogel beads were placed within the cement slurry. This interesting material possess an enhanced sound insulation properties due to the dissipating effect of the fibrous domains adjacent to the hard cement domains which may enhance the absorption and dissipation of the sound waves, as explained in greater detail in Chapter 4 of this thesis.

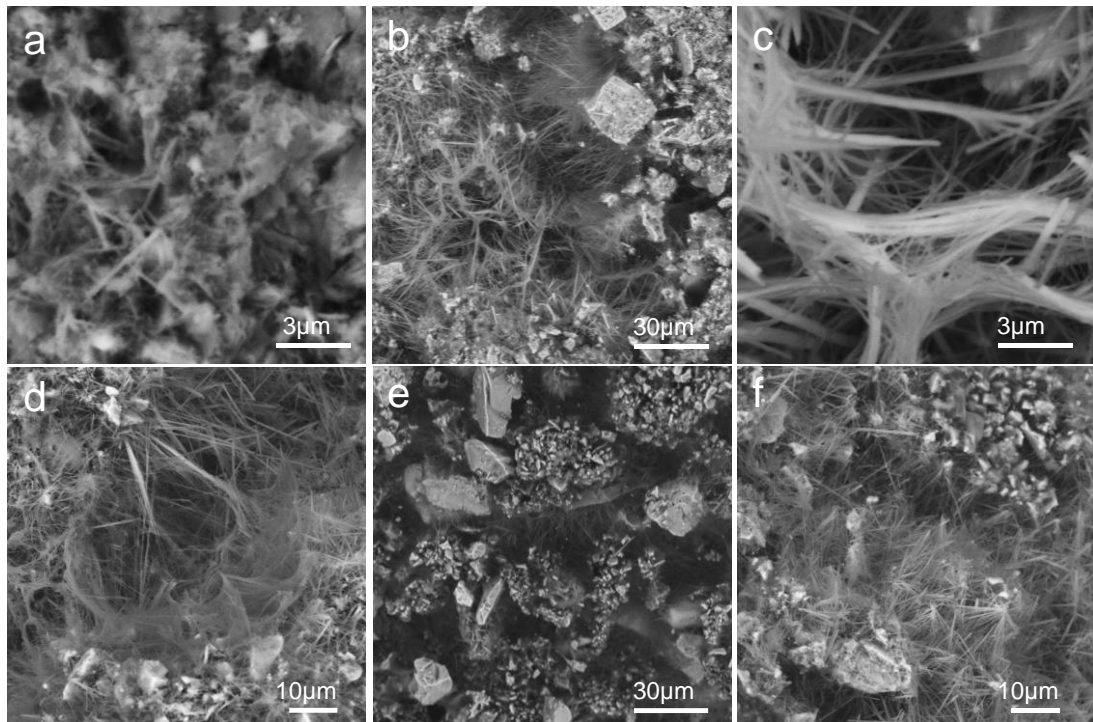


Figure 3.6. SEM images of cement templated with CaCl_2 containing polyacrylamide hydrogel (3 wt%): (a) control sample of solidified cement slurry (0% hydrogel), (b)-(c) 66 vol% hydrogel, (d) 75 vol% hydrogel, (e)-(f) 80 vol% hydrogel. The polyacrylamide hydrogel was loaded with CaCl_2 to counteract the osmotic pressure of the cement slurry, which causes the pure PAA hydrogel (without CaCl_2) to shrink when mixed with the slurry.

The SEM images of the porous PDMS samples (Figure 3.7 b and c) show that the porosity was highly increased when the concentration of the hydrogel was increased from 60 vol% to 80 vol%. The sample with the lower hydrogel content exhibited a continuous structure of PDMS, with a high number of pores present, whereas the 80 vol% sample did not show individual pores, because both the hydrogel and the PDMS were continuous throughout the sample. The non-continuous structures with the lower hydrogel content also lead to the hydrogel being trapped within the sample and excessively long drying times. The cement samples, unlike PDMS, did not show a clear change between the samples of different hydrogel content.

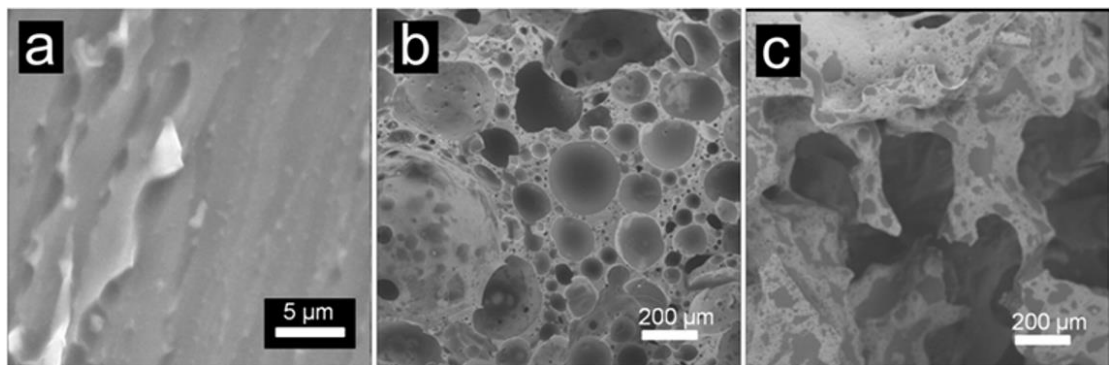


Figure 3.7. SEM images of PDMS with no surfactant and no oil, (a) control (PDMS only, no hydrogel), (b) PDMS with 60% volume of hydrogel; (c) PDMS with 80% volume of hydrogel.

3.5.1 Compressional Strength Analysis of Porous Cement and PDMS Composites

PDMS samples were pressed between two plates as was done with cement samples, but since the fracture force could not be detected, the force required to press the samples to 50% of their original height was measured and the compressional strength calculated. The resulting graphs are shown in Figure 3.8. The average force was calculated from at least 3 measurements and it was noticed, that it decreased with each experiment by around 2%. However, it did not decrease significantly after applying the compression to the samples for 24 hours and then measuring the force again. From the graphs in Figure 3.8 it is apparent that the compression strength decreases with increasing hydrogel initial volume fraction and thus also with decreasing the sample

mass density. Both graphs showed a logarithmic relationship between the measurements. The PDMS sample without addition of silicone oil and surfactant exhibited almost two times higher compressional strength compared to the sample with added 10% of silicone oil and surfactant (Span 80) at similar porosity. This is likely to be due to the higher cross-linking of non-diluted PDMS.

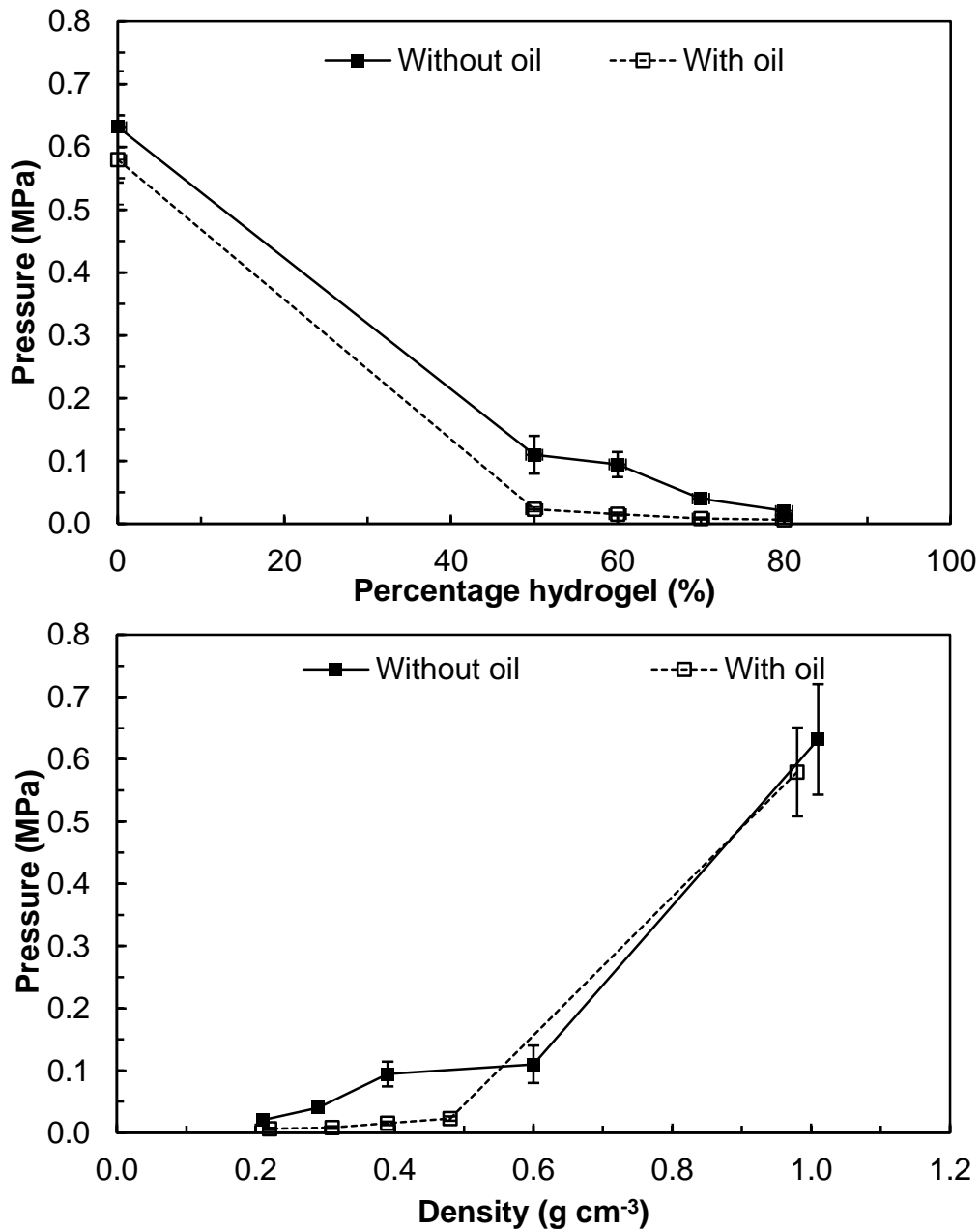


Figure 3.8. Graphs showing strain variation of the PDMS samples versus the percentage of the hydrogel (top); compression strength variation of the PDMS samples with density (bottom) of the porous PDMS material. Lines are guides to the eye.

3.6 CONCLUSIONS

Slurries of hydrogel beads from two different types of hydrogels, polyacrylamide and Gellan gum were templated with four different materials to produce porous materials after drying the hydrogel. Micro-porous PDMS was produced by templating Gellan gum microbeads with a curable PDMS to produce a material with a high porosity, which was elastic and retained its structure almost completely after being compressed. The measured volume shrinkages of the composite samples before drying were of less than 10% of their original volume during the setting and drying of the hydrogel for 50% - 80% volume content of the hydrogel in the initial composition of the hydrogel-PDMS composites. The porous PDMS samples produced without dilution of the original PDMS formulation with silicone oil had a lower mass density (higher porosity) and a lower total volume shrinkage. These samples also required a smaller force to be mechanically compressed to half volume at the same percentage of the hydrogel. The use of an oil-soluble surfactant (Span 80) in the PDMS did not improve the dispersability of the hydrogel in the PDMS. Ultra porous cement samples were produced by templating 3 wt% and 5 wt% polyacrylamide hydrogel beads with cement slurries at various volume fractions of the hydrogel. Although the 5 wt% polyacrylamide hydrogel – cement sample had a lower density, it shrunk more than the 3 wt% sample. Porous gypsum and talc-cement samples produced by this method showed a significant volume shrinkage upon drying of the polyacrylamide hydrogel templates. Although the densities were reduced after templating the hydrogels with both slurries, the porous composites shrank significantly upon drying. These materials were also much more fragile, especially the porous talc-cement sample. The stability could be increased with cross-linking additives. This method for preparation of porous materials by templating hydrogels has the potential to find application for preparation of a range of porous plastics, lightweight ceramics, reduced weight insulation and building materials as we shall see in the following Chapters of this thesis.

3.7 REFERENCES

1. M. Rutkevičius, S. K. Munusami, Z. Watson, A. D. Field, et al., *Materials Research Bulletin*, 2012, 47, 980.
2. J. E. Mark, *Polymer Data Handbook*, Oxford University Press, New York, NY, 1999.

Chapter 4. Fabrication of Sound Absorbing Materials Using a Hydrogel Slurry Templating Technique

“Chop your own wood and it will warm you twice”

Henry Ford

This Chapter investigates and explores the properties of sound absorption of porous materials fabricated using a hydrogel slurry templating technique. This was achieved by the development of the hydrogel templating technique in order to produce samples that can be accurately and reliably tested for their acoustic absorption. The mechanical strength of the samples was tested so that any dual property behaviour (useful sound absorption and mechanical strength) of the material could be displayed.

In addition, methods of controlling pore size of samples produced using this technique shall be investigated. This investigation will include research into the methods of controlling hydrogel bead distribution which ultimately dictates the size of the pores and their distribution. The subsequent effects of this pore size variability in terms of acoustic absorption and mechanical strength will be explored in order to demonstrate the extent to which control was exhibited over the properties.

Part of the results in this Chapter can be found as a published paper in the Journal of Materials Research.¹

4.1 INTRODUCTION TO SOUND POLLUTION

Many factors contribute to an increase in the noise pollution, including general population increase, growth of transport infrastructure and the increased use of heavy duty machinery for industrial purposes.² The demand for materials which have multiple uses is increasing as industries attempt to solve more of the problems facing

a rapidly advancing society. One of the problems which is caused by these advances in the society is noise pollution. Undesirable and potentially hazardous noise is treated as a type of environmental pollution and can cause a risk to public health.³ Noise pollution is an issue due to a serious health hazard, with a potential to cause issues such as hypertension, ischemic heart disease and severe hearing difficulties if subjects are exposed to noise for prolonged time.⁴ An article by Godlee suggests that noise produced in the working environment is a major cause of the hearing loss in adults throughout the industrialised world.⁵ Noise levels of a volume of 90 dB and over appear to be the most damaging, especially over long periods of time. Industrial noise is the most intense between the frequency ranges of 250 – 500 Hz,⁶ noises due to automotive sources tend to peak at 800-1200 Hz.⁷ Improving the noise absorption, especially at low frequencies, is considered very important in the transport industry and the construction of buildings.

There are several methods to reduce noise: one may try to obstruct the noise using a barrier or try to reduce the noise by interfering with the source of the sound waves/vibrations.⁸ However, the most common solution for reducing noise is to use the passive method of a sound absorbing material. It is recommended that the sound absorbing materials are always used in conjunction within enclosures and alongside barriers in order to optimise their efficacy. A passive sound absorber requires no additional external energy in order to absorb sound. Typical sound absorbing materials come in forms of various foams, fibres, boards, mats, perforated metals, aerogels and others,^{7, 9} as a high sound absorption coefficient is usually only observed in porous materials.¹⁰

As shown in Figure 4.1, several different pore types can be identified and characterised. It is clear that the closed pores on this diagram are not connected to the outside of the material. However, they still have bearing on the overall properties of the material in terms of density, mechanical strength and capacity for heat absorption. The lack of outside interconnectivity means that the closed pores are much less efficient than the open pores for the purpose of sound absorption. This serves to demonstrate the importance of interconnectivity. Open pores may be split into two types: blind pores and through pores. It can be seen that through pores are open at two or more ends of

the cavity and blind pores are akin to a “dead end” and have no through connectivity. Both of these pore types have a large effect on the sound absorbing effects of a porous material.

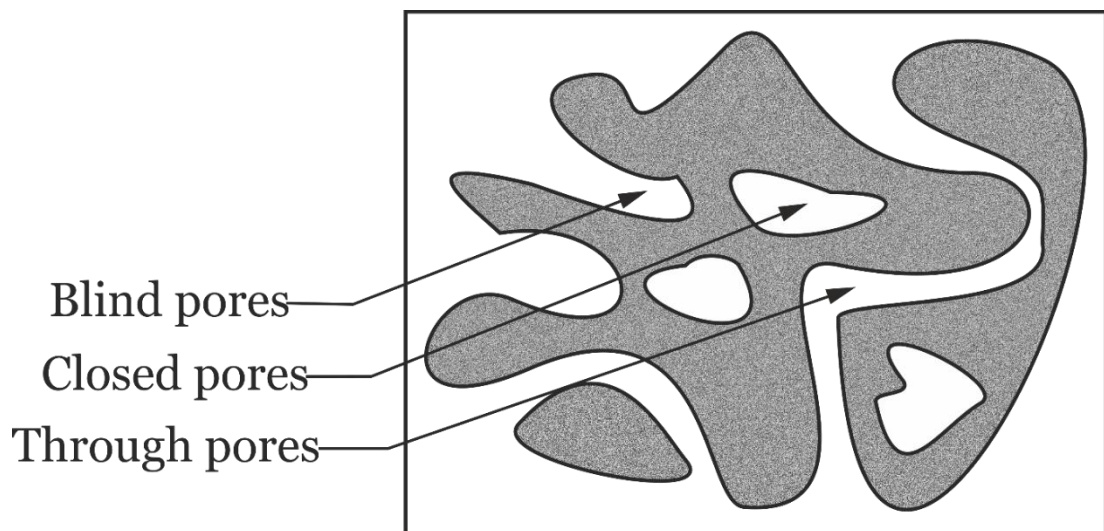


Figure 4.1. Cross sectional schematic diagram of a porous solid showing the three different pore types. Closed pores are completely surrounded by a matrix and have little bearing on properties such as sound absorption but still contribute to an overall density. Blind pores have connection to the outside of the material and therefore have some influence on sound absorption. Through pores are interconnected pores which have multiple paths through the material and have the largest effect upon the sound absorption of the material. Reproduced from Arenas and Crocker.⁷

An empirical equation developed by Delany and Bazley shows that porous materials can absorb sound much better than monolith materials, especially at medium and high frequencies.^{11, 12} The typical pore size of a sound absorbing material is below 1 mm, which is much smaller than the wavelength of sound (5 cm – 15 m).⁹ The sound pressure creates oscillations between air molecules within the porous material, resulting in a frictional loss of momentum of these molecules. This way the porous structure reduces the momentum of the propagating high frequency sound wave.⁹ Efficient conduction of heat within a porous composite result in an energy loss for a low frequency sound wave, as the air pressure in the pores undergoes periodic compression and decompression resulting in a change of temperature.⁹ In general,

porosity, tortuosity and air flow resistivity have been claimed as the most important properties for the efficient sound absorption.^{13, 14}

Recent trends in porous sound-absorbing materials have been reviewed by Arenas and Crocker.⁷ There are known methods to introduce porosity in the materials and improve their sound absorption at low frequencies. For example, Atalla *et al.* found that a hierarchical porosity of macro (porosity in the periodic cylindrical hole fashion) and micro (natural porosity of rock) can be created in a mineral rock and thus improve its sound absorption properties.¹⁵ Cuiyun *et al.* studied the absorption properties of porous cylindrical zeolites made by sintering zeolites with polymer foam particles and simultaneously burning the polymer to create voids in the structure.¹⁶ It was found that increased porosity improves the sound absorption at frequencies around and below 600 Hz, but slightly decreases the absorption at frequencies higher than 1200 Hz; also, thicker samples shifted the absorption towards lower frequencies by approximately 100 Hz per 5 mm increase in thickness. Sodium bicarbonate as a blowing agent was used to prepare porous rubber, which had different pore sizes corresponding to different blowing temperatures.¹⁷ The authors of this study found that the smallest pores (approx. 0.8 mm) had the best sound absorption behaviour. Other researchers investigated acoustic behaviour of surface-modified polymeric porous microspheres,¹⁸ needle punctured nonwovens,⁸ porous road pavements,¹⁹ micro-perforated panels,²⁰ concretes²¹ and others.

In this Chapter the sound absorption properties of porous Polydimethylsiloxane (PDMS) and porous cement obtained by hydrogel templating are explored. These materials are described in the previous Chapter as well as the technique to make porous samples by hydrogel bead slurry templating. In this Chapter the sound absorption properties of the porous cement and PDMS composites produced at various degrees of porosity using different volume fractions of the hydrogels are presented and discussed.

4.2 FABRICATION OF POROUS SOUND ABSORBING CEMENT AND PDMS COMPOSITES USING PAA AND GELLAN GUM HYDROGELS RESPECTIVELY

The sound absorbing composites were prepared following similar methodology as described in the previous Chapter, the only difference being that some of the composites were prepared using different hydrogels. Section 4.3 focuses on the cement and PDMS composites prepared with PAA and Gellan hydrogels, where the hydrogels were blended using a hand-held blender as in the previous Chapter, whereas Section 4.4 looks into the properties of porous cement composites produced using salt resistant Xanthan – Konjac hydrogel mixture, which was blended using different pore-size meat mincer attachments, allowing better control of the hydrogel bead size distributions within the slurries.

A relatively fundamental and well documented method was used for the testing of sound absorption.^{9,22} The use of a sound impedance tube alongside some fairly simple calculations allowed to measure quite accurate values of the sound absorption of a material. The experiment consisted of an aluminium tube with a sliding microphone as described in Chapter 2 Section 2.2.2.

4.3 RESULTS OF POROUS SOUND ABSORBING CEMENT AND PDMS COMPOSITES PREPARED USING PAA AND GELLAN GUM HYDROGELS RESPECTIVELY

4.3.1 Porosity of the PDMS and Cement Composites Templated with Hydrogel Bead Slurries

Before and after drying the composites, their sizes and weights were measured. The reduction of the composite volume after evaporating water is shown in Table 4.1 and was not significant, but was still accounted for when calculating the densities of the materials after drying the composites. The porosity of the composites, θ , was calculated using the following formula:

$$\theta = \left(1 - \frac{\rho_0}{\rho_s}\right) \times 100\% \quad (4.1)$$

where ρ_0 is the apparent density of the porous composite, calculated from the volume and mass after drying the samples and ρ_s is the density of the pure matrix without the hydrogel. The calculated porosity is shown in Table 4.1. As expected, the porosity

increased with the initial hydrogel content within the composite. For cement, the porosity was approximately 10 % lower than the hydrogel content, whereas for PDMS, the porosity correlated with the hydrogel content very closely. This could be due to the syneresis effect in the cement composites, which is discussed later in detail in Section 4.3.2.

Table 4.1. Porosity, density and shrinkage of the analysed cement and PDMS composites.

<u>Cement</u>			
Hydrogel content (vol%)	Reduction in volume (%)	Density (g cm ⁻³)	Porosity (%)
0	-	1.74	0
50	5.2	1.0	43
80	5.2	0.53	70
<u>PDMS</u>			
Hydrogel content (vol%)	Reduction in volume (%)	Density (g cm ⁻³)	Porosity (%)
0	-	1.01	0
50	0	0.60	41
70	5.7	0.29	71
80	7.3	0.21	79

The average hydrogel particle size prior mixing the slurry with the matrix material was measured by doping the hydrogel with Rhodamine 6G or Fluorescein sodium salt dye and using an optical microscope equipped with a FITC/TRITC filter as in Chapter 3. The pore size of the final composite reflects the hydrogel particle size, assuming that the hydrogel size does not change upon mixing with the matrix material and the moulding of the sample. The hydrogel bead size was lower for Gellan gum gels (mean particle size for Gellan gum was found to be 50 μm and for PAA it was 100 μm).

4.3.2 Analysis of the Structure of the Samples: Electron Microscopy and Optical Photography Analysis

Porous composites were cut and analysed with a Scanning Electron Microscope. The SEM images of the cement composites are displayed in Figure 4.2 and those of PDMS composites – in Figure 4.3. The SEM images show the morphology of the different domains that are present in the porous composites produced from cement-polyacrylamide hydrogel. Fibrous domains (voids) were observed at the places where the hydrogel beads have been trapped in the solidified cement slurry. The fibrous domains in the porous cement composites resulting from the evaporation of the polyacrylamide hydrogel were bordered by the more compact domains of the cement slurry. In addition to the traditional mechanisms of sound absorption mentioned in the introduction section, the hypothesis for the dissipation of energy involves a more significant deformation of the fibrous domains during exposure to sound, whose elastic and dampening response leads to a more efficient absorption of the sound energy. The latter is possibly due to the friction within the fibrous domains and the adjacent more compact cement particles (Figure 4.4).

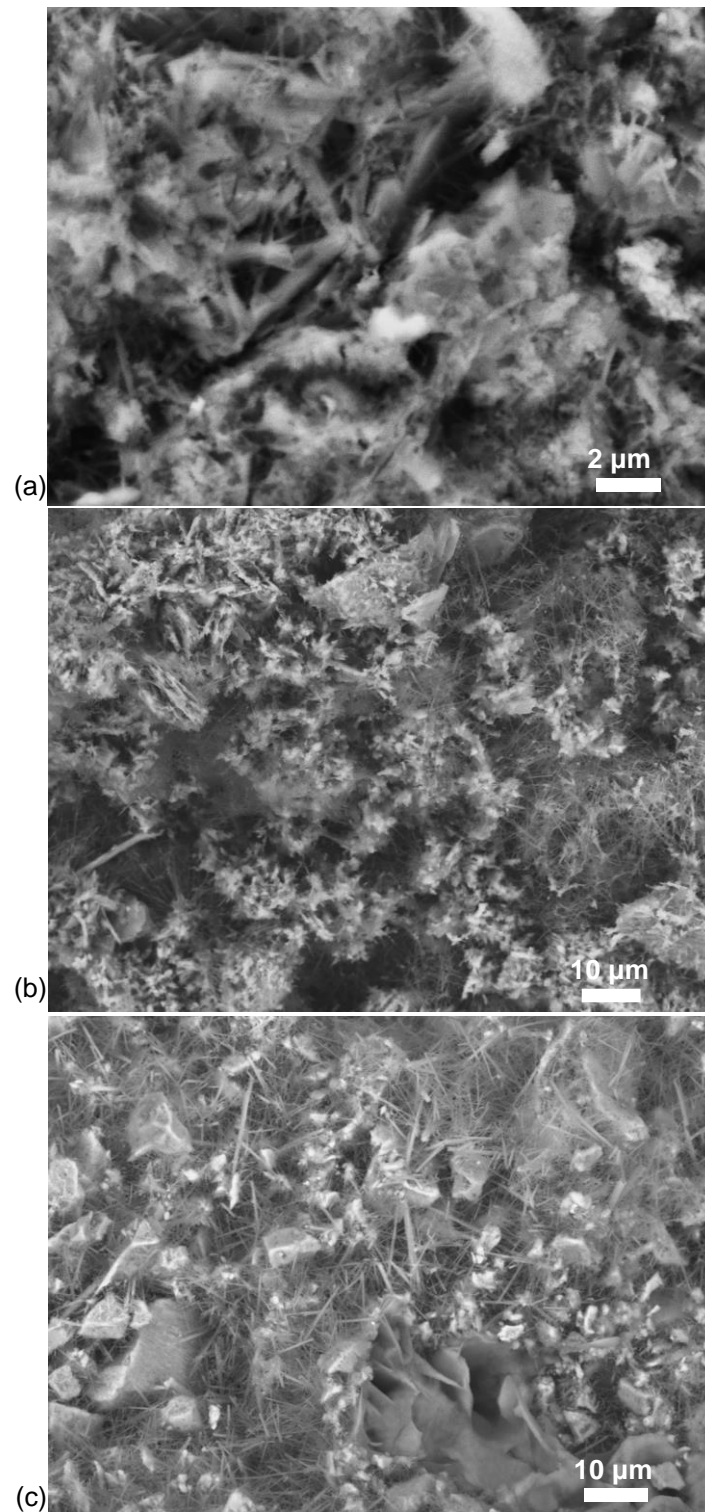


Figure 4.2. SEM images of the solidified cement composites after the evaporation of the water phase (a) without hydrogel (0% hydrogel), (b) 50 vol% hydrogel and (c) with 80 vol% hydrogel. The voids from the evaporated hydrogel appear as darker regions and the fibrous domains can be observed within.

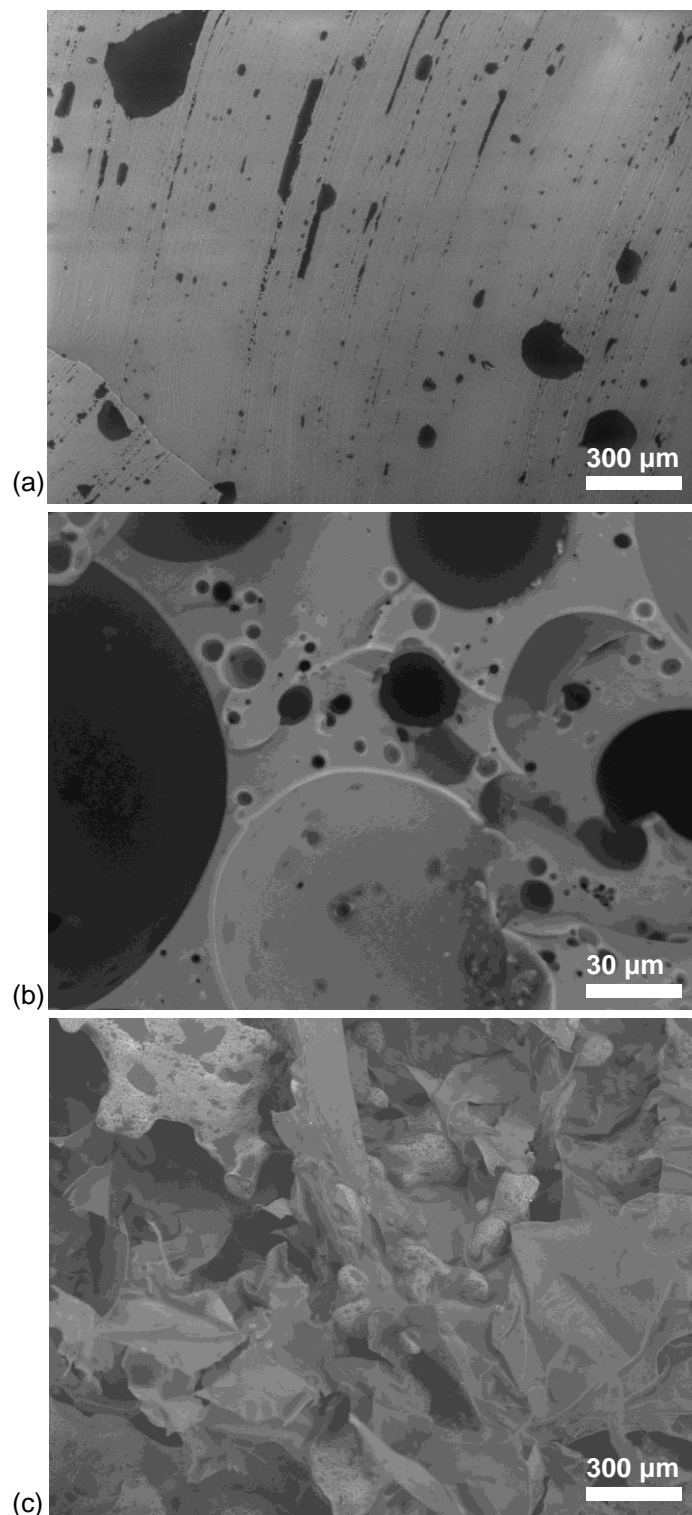


Figure 4.3. SEM images of the PDMS-hydrogel composite samples after evaporating water, where (a) pure PDMS without the hydrogel, (b) 60 vol% Gellan gum hydrogel templated within the PDMS composite and (c) 80 vol% of Gellan gum hydrogel templated within the PDMS composite.

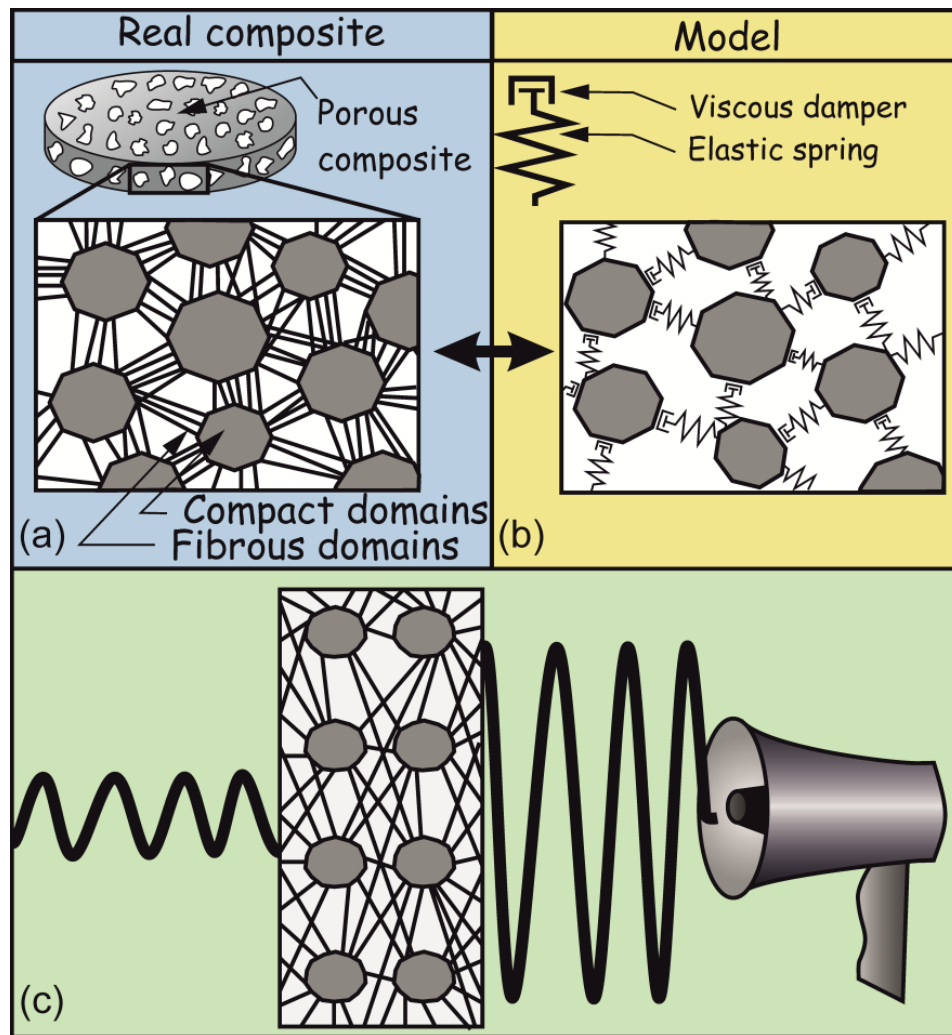


Figure 4.4. Schematic representation of the hypothesis of the sound energy dissipation by the fibrous domains present within the pores of the composites. (a) Represents the simplified structure of the cement composites, corresponding to the SEM images and (b) is a model structure of the composite, where the compact cement domains are linked with fibrous domains represented as a combination of springs and dampeners, which can absorb the energy of the sound wave and reduce the output amplitude (c).

At a high porosity the compact cement domains [Figure 4.4 (a)] are bordered by the fibrous domains (pores) [Figure 4.4 (b) and (c)] acting as energy dissipating elements, dampening the amplitude of the incoming sound waves passing through the material. This seems to be most effective when an open-pore structure is formed above the critical volume percentage of the hydrogel, which is approximately 70 vol%.

The SEM images of the porous PDMS sample (Figure 4.3) show that the porosity was highly increased when the initial concentration of the hydrogel was increased from 60 vol% to 80 vol%. The sample with a lower hydrogel content exhibits a continuous structure of PDMS with a high fraction of voids present, whereas the 80 vol% sample did not show individual voids, as both the hydrogel and PDMS were continuous phases throughout the sample. Previously, in Chapter 3 Section 3.5.1, a rapid decrease in the compression strength was observed with the increasing porosity. In the present sound absorption experiments, the structure of the 80 vol% hydrogel composite (79% porosity) remained mechanically stable for a range of sound frequencies used. The non-continuous structures of PDMS composites with a lower hydrogel content to the hydrogel beads being encapsulated within the sample and excessively long drying times. The cement samples, unlike PDMS, did not show such a clear change between the samples of different hydrogel contents. This could be attributed to the water exchange between the cement slurry and the hydrogel domains occurring in order to match the osmotic pressure of the environment. This effect was tackled by adding a small amount of calcium salt into the hydrogel and using a non-ionic hydrogel polyacrylamide (PAA).

4.3.3 Sound Absorption of Porous PDMS Composites

The absorption coefficients as a function of the sound frequency for the PDMS composites are plotted in Figure 4.5. These data show that the PDMS composites absorb sound well in the lower frequency range. As expected, composites absorb better than the pure PDMS, especially at frequencies >800 Hz, although the 1:1 hydrogel : PDMS sample showed poorer absorption at frequencies above 1000 Hz. Composites with a lower hydrogel content formed discontinuous structures, where the hydrogel was entrapped in the PDMS matrix and could not evaporate to form pores. As discussed in the literature, porous materials with an open network of pores show a better sound absorption than those with closed pores, which do not have a good sound absorption.⁷ The 1:1 hydrogel : PDMS sample did not have a continuous porosity and the energy of the sound was also not absorbed well by the sample, but mostly reflected back as it was the case for the control sample of pure PDMS. Surprisingly, porous

samples showed a high absorption in the low frequency range around and below 300 Hz.

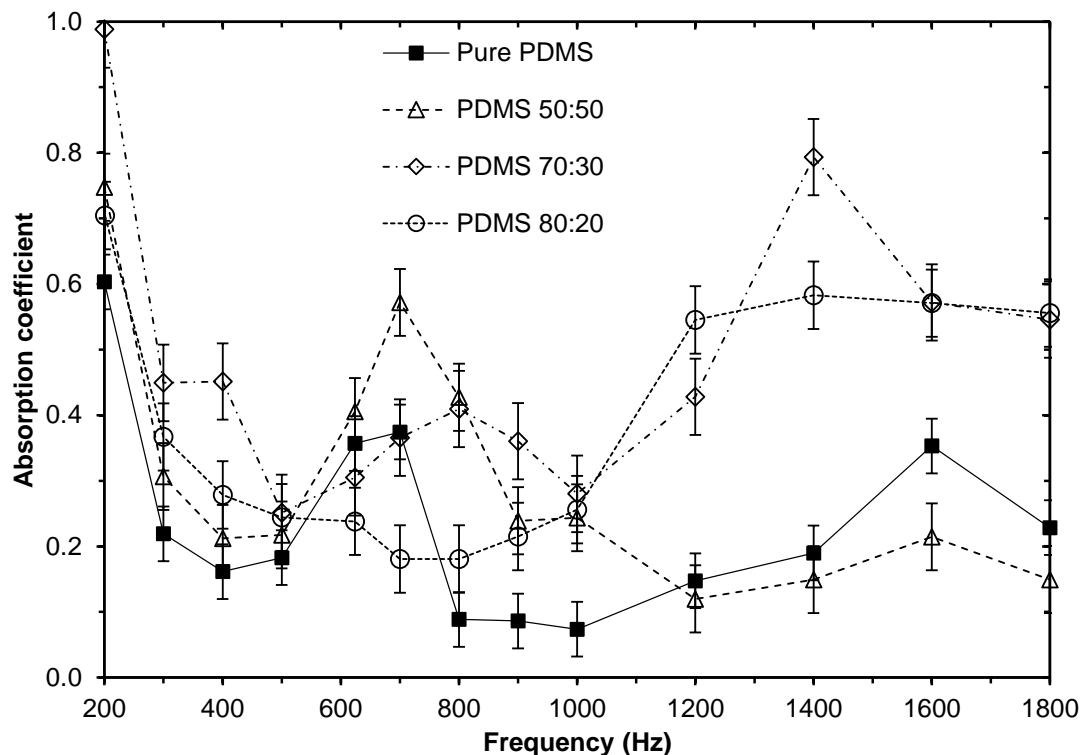


Figure 4.5. Sound absorption coefficient of the PDMS composites having 0, 50, 70 and 80 vol% hydrogel content as a function of the sound frequency.

4.3.1 Sound Absorption of Porous Cement Composites

The cement samples showed a similar trend (Figure 4.6): the increase in the initial hydrogel content increased the sound absorption, but unlike the PDMS composites this was observed through a wider frequency range. Since the cured cement paste is also a microporous material,²³ the bigger pores created by the templating of the hydrogel domains are likely to increase the ability of the material to absorb the sound energy, as these two networks of pores are interconnected (as shown in the SEM images in Figure 4.2). The sound absorption of the 80 vol% hydrogel was also high (up to 0.65) in the low frequency range (200-300 Hz), then decreased through the mid-frequencies and increased again to approximately 0.5 in the higher frequencies (>1000 Hz). The absorption coefficient of the composites could be increased by reducing the

polydispersity of the hydrogel particles and thus forming monodisperse pore-size composites, which could be applied for a specific frequency range.

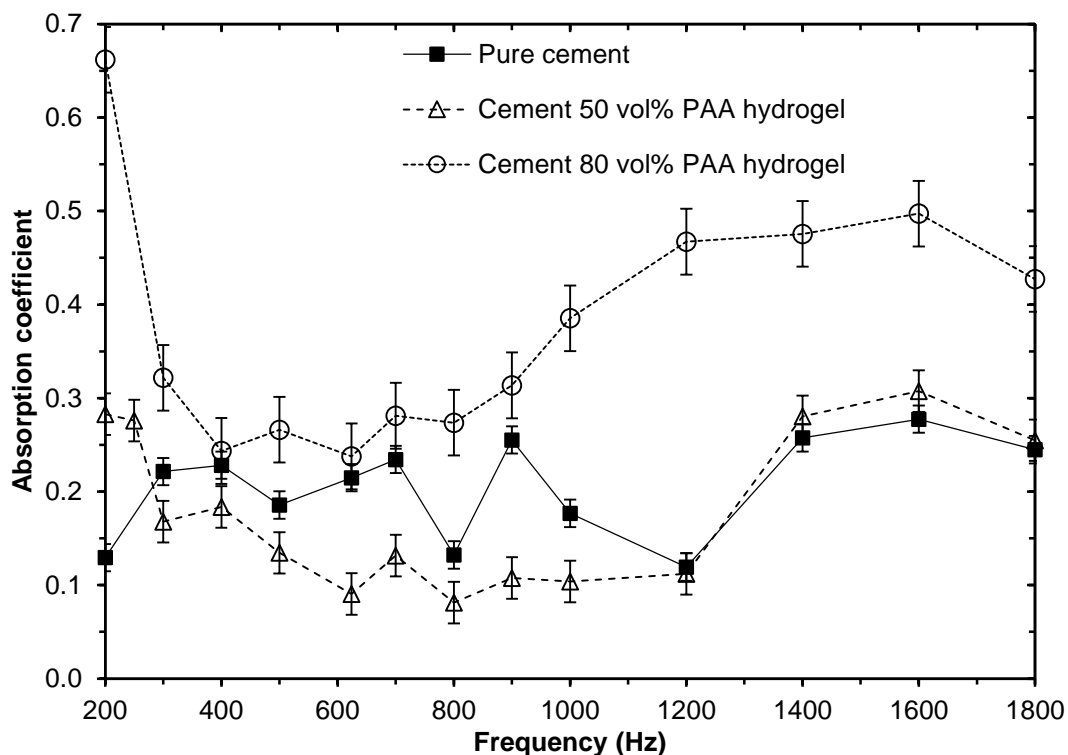


Figure 4.6. Sound absorption coefficient of (pure cement, 50:50 and 80:20 hydrogel : cement) composites as a function of the sound frequency.

4.4 FABRICATION OF POROUS SOUND ABSORBING CEMENT COMPOSITES USING XANTHAN-KONJAC HYDROGEL MIXTURE

4.4.1 Hydrogel Bead Size Distributions and Porosity of the Composites

In order for the samples to have tuneable properties, it was important to investigate a method of controlling the bead size of the Xanthan – Konjac hydrogel. Upon production of the hydrogel beads using the mincing method, a distribution range of the bead sizes was obtained by analysing fluorescent microscope images of the beads. The way to control the distribution was to use different Kenwood Chef mincing attachment plates with either 2 mm or 3 mm sized holes for the production of the hydrogel bead slurries. These hydrogel beads were then spread on separate microscope slides and observed under x2 magnification with a fluorescent light (Figure 4.7). The mean size of the bead was recorded and around 100 beads were measured.

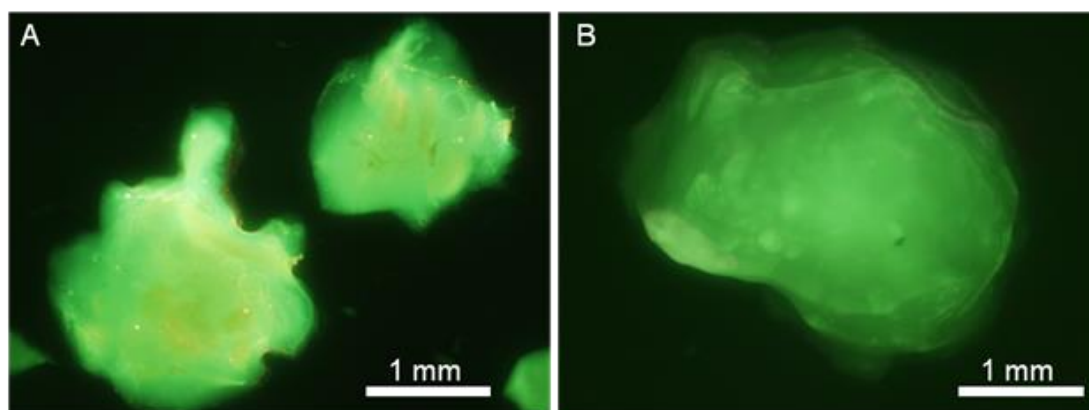


Figure 4.7. Fluorescence microscopy images of the Xanthan – Konjac hydrogel beads produced by mincing hydrogel through plates with 2 mm holes (A) and 3 mm holes (B) respectively.

Plotting the measured data gives very useful, statistic information as to which extent of control was exhibited through the use of different sized mincing holes. Given these data it can be observed that the two different mincing plates produced markedly different distributions of the hydrogel beads (Figure 4.8). This is significant for the development of the material as many other current techniques in the chemical literature allow control of bead size, e.g. control of the pore size through lattice.²⁴ Therefore this method allowed a reliable control of the bead size distribution. Figure 4.8 and Table 4.2 show that the 3 mm hydrogel samples had a wider distribution of bead sizes and the standard deviation. This increased distribution range could be attributed to the logical assumption that a wider hole was letting through a greater range of smaller beads and larger beads were potentially only "pushed through" only to regain size once they had passed the plate. It is clear from observing the data that the use of different sized holes in the mincing plates allowed to control the Xanthan – Konjac hydrogel bead size.

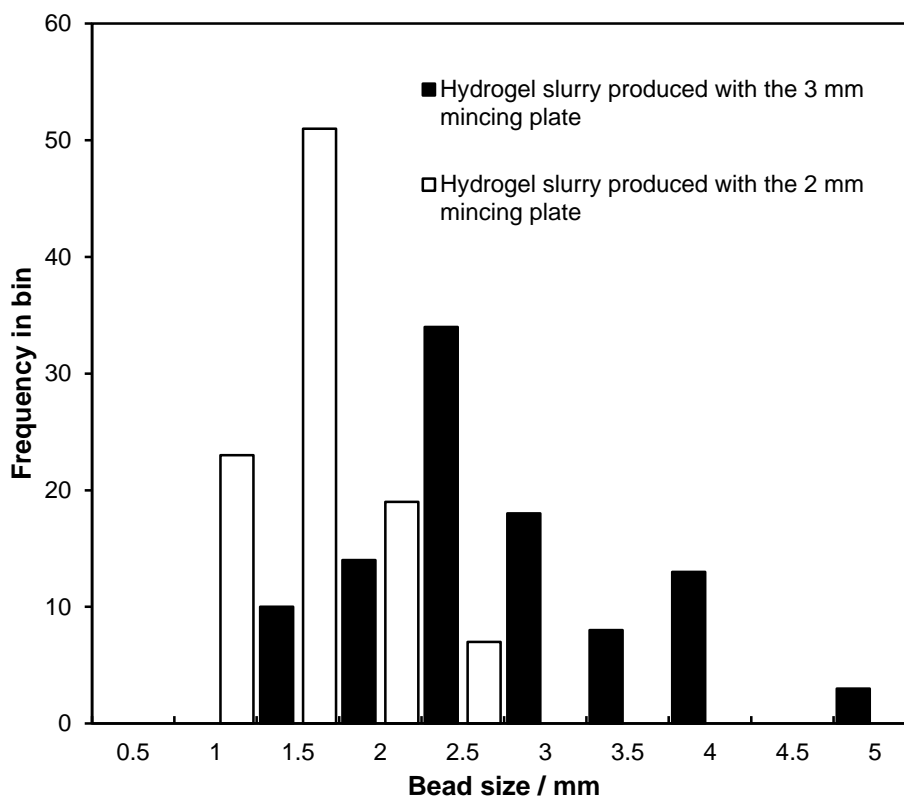


Figure 4.8. Histogram showing bead size distribution of the Xanthan – Konjac hydrogel beads created with 2 and 3 mm pore-size of the mincing plates.

Table 4.2. The standard deviation and the average size of the hydrogel beads after passing through different pore-size mincer plates.

Sample	Standard Deviation (mm)	Average Value (mm)
3 mm hydrogel	0.796	2.5
2 mm hydrogel	0.375	1.3



Figure 4.9. A photograph of the top of the sample of a porous cement sample (70 vol% hydrogel content) produced using 3 mm pore size mincer plate minced hydrogel. Sample diameter was 7.6 cm and thickness 2.0 cm designed to fit the sound impedance apparatus.

Porosity of the composites was calculated using equation (4.1). Samples were measured using a Vernier calliper in order to calculate their volume and subsequently density. A typical composite obtained is shown in Figure 4.9. The results from Figure 4.10 show that the porosity was highly controlled by the hydrogel templating technique. The weight loss data was consistent with the increase in the porosity through the evaporation of the hydrogel.

FABRICATION OF SOUND ABSORBING MATERIALS USING A HYDROGEL SLURRY TEMPLATING TECHNIQUE

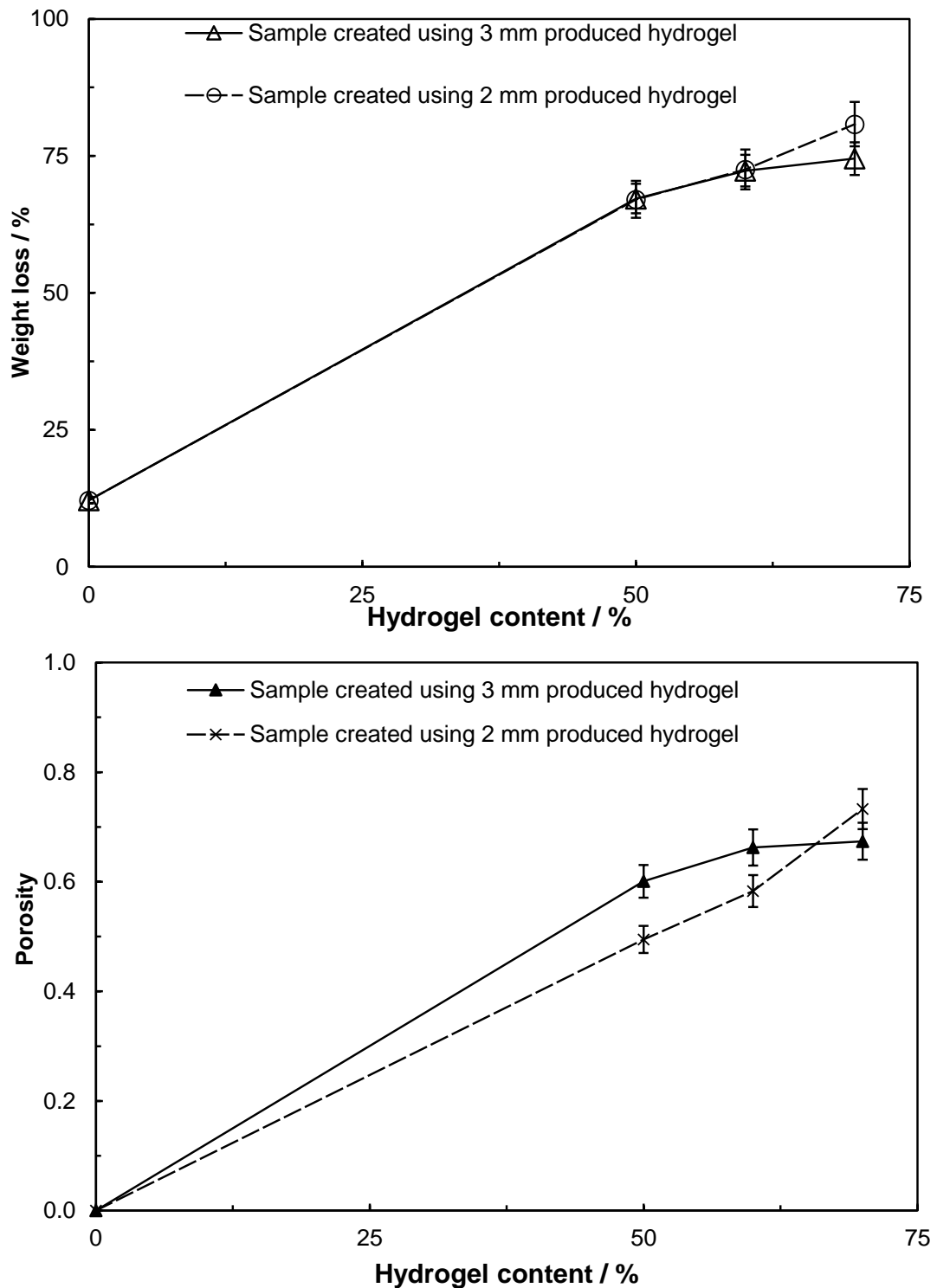


Figure 4.10. Graphs displaying weight loss percentage (top) and porosity (bottom) as functions of the percentage composition of hydrogel in the porous cement sample produced with minced hydrogel (2mm and 3mm mincer plate pore size). It can be observed that both porosity and weight loss increase with the higher hydrogel content in the samples.

4.4.2 Sound Absorption of the Xanthan – Konjac Hydrogel Slurry Templated Cement Composites

The resulting absorption coefficients of the various cement samples have been plotted on the graphs below (Figure 4.11, Figure 4.13 and Figure 4.12). It can be seen from these data that the porous cement samples had a markedly higher sound absorption coefficient than the cement control sample, particularly towards the higher sound frequency range (1000-2000 Hz). It is also clear by looking at the plots that decreasing the hydrogel bead size affected the sound absorption. The data suggest that as the hydrogel bead size is decreased, the absorption increases in several frequency ranges. These data are significant as they put the hydrogel templated material on the same level to the other materials in the literature, which have controllable sound absorbing properties.

It can be seen, particularly for the 50:50 and 60:40 hydrogel : cement samples, that decreasing the hydrogel bead size to 2 mm had a profound effect in the 500 - 800 Hz region. The graphs indicate a trend of the rising absorption in these regions, which show how changing the bead size may be used as a targeting tool for sound absorption of specific frequencies. This is especially promising for the capture of the traffic noise as a lot of traffic based noise occurs in this frequency region. In addition to this, the samples also proved to be effective at absorbing the sound at around 1200 Hz area, where the majority of the industrial noise occurs.

It is possible that some particular bead size produced using the 2 mm mincer plate was affecting distribution pattern and causing an increased absorption in this region. Reducing the polydispersity of the hydrogel and identifying this particular bead size could allow the fabrication of a very specific, monodisperse noise absorbing material, which could be valued in the construction industry. For all samples, sound absorption is very high at 2000 Hz. Measurements in this region were difficult due to the wave fluctuations and this could be caused by a very high level of absorption resulting in a sound wave with an amplitude which is too small to measure accurately. The error in some regions is clearly significant, however the trends are still visible and should be confirmed by carrying out repeat tests under very careful controlled conditions. In

conclusion, the outlook is very positive for a material that has sound absorption properties that are controllable through a novel technique.

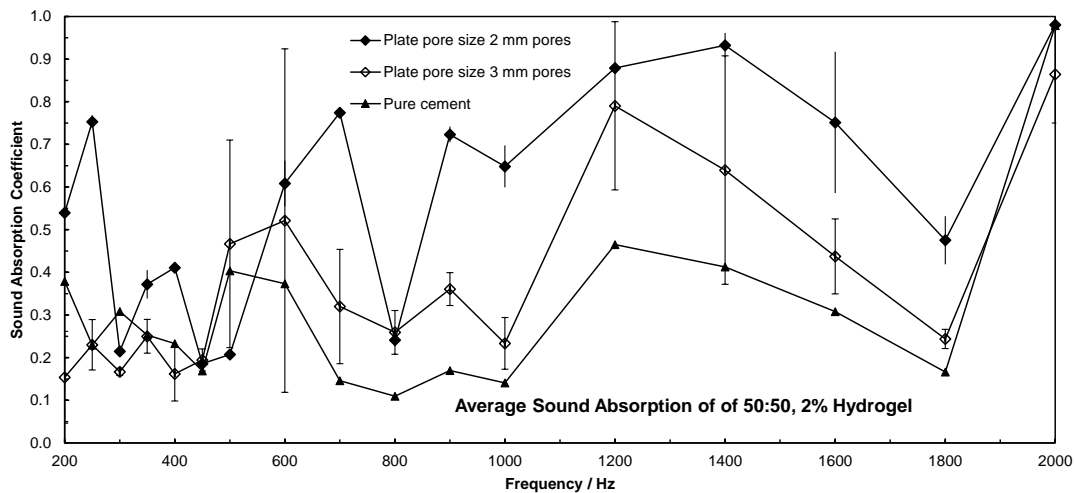


Figure 4.11. Sound absorption of samples made with 50 vol% hydrogel. The graph shows increased sound absorption of the samples made with 2 mm hydrogel beads.

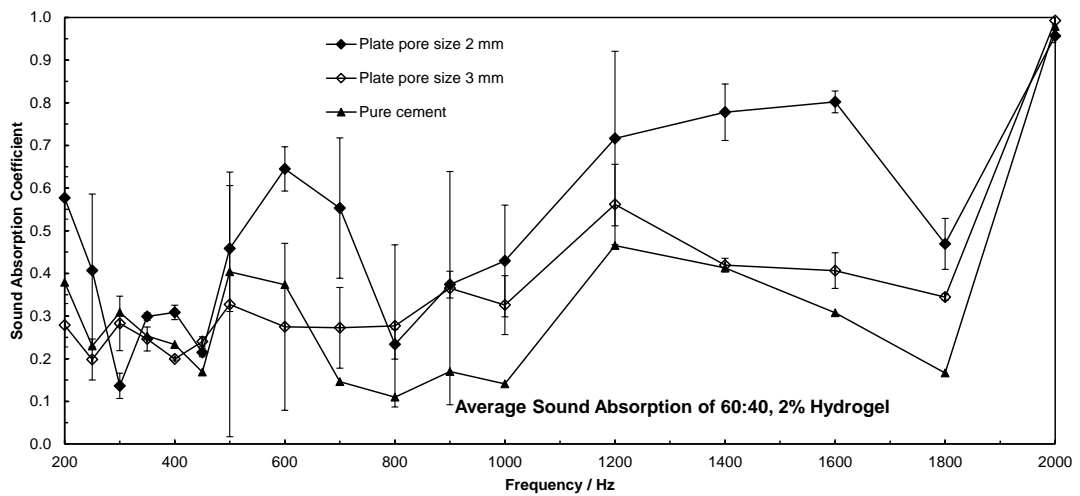


Figure 4.13. Sound absorption of sample made with 60 vol% hydrogel. This graph shows a similar trend to that observed for the 50 vol% sample but has a more distinct region of increased absorption.

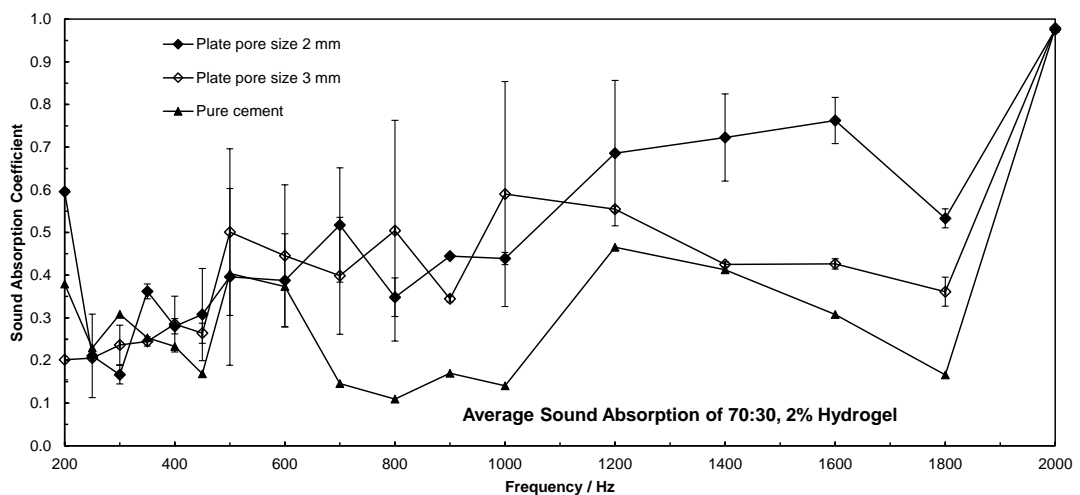


Figure 4.12. Sound absorption of sample made with 70 vol% hydrogel. The trend is similar to 50 vol% and 60 vol% samples towards the higher frequencies, but is quite hazy at low frequencies. The systematic errors were larger at low frequencies.

4.4.3 Compressional Strength Analysis of the Produced Samples

Similar samples for compressional strength analysis were prepared in the laboratory and analysed using a Lloyds compression strength analysis instrument. It can be seen in Figure 4.14 that there was a relatively linear trend with decreasing mechanical

strength and the increase in the porosity in the material as a larger quantity of the hydrogel was used. As expected, it is clear that the strongest material was the 100% cement sample due to a lack of induced pores. According to the literature, cement samples strength ranges from around 3-33MPa, depending on the type of cement and its curing stage, with rapid hardening Portland cement having a 33 MPa compressive strength after 28 days.²⁵ It can be seen that even the control sample did not match up to this value and the other samples showed considerably lower strength. The high compression strength cited in the literature could be due to the addition of structure enhancing components such as sand or gravel, whereas the samples for the current study were made of pure cement and added hydrogel bead slurries. Also, this study was aiming to compare like-to-like curing methods of the composites and controls, so the low compressional strength of the control sample indicates that the strength of the porous composites could be increased by 6 times using a more standardized method of preparation, setting and curing of the samples, as it was done in a specialised laboratory focused in the materials for construction purposes.

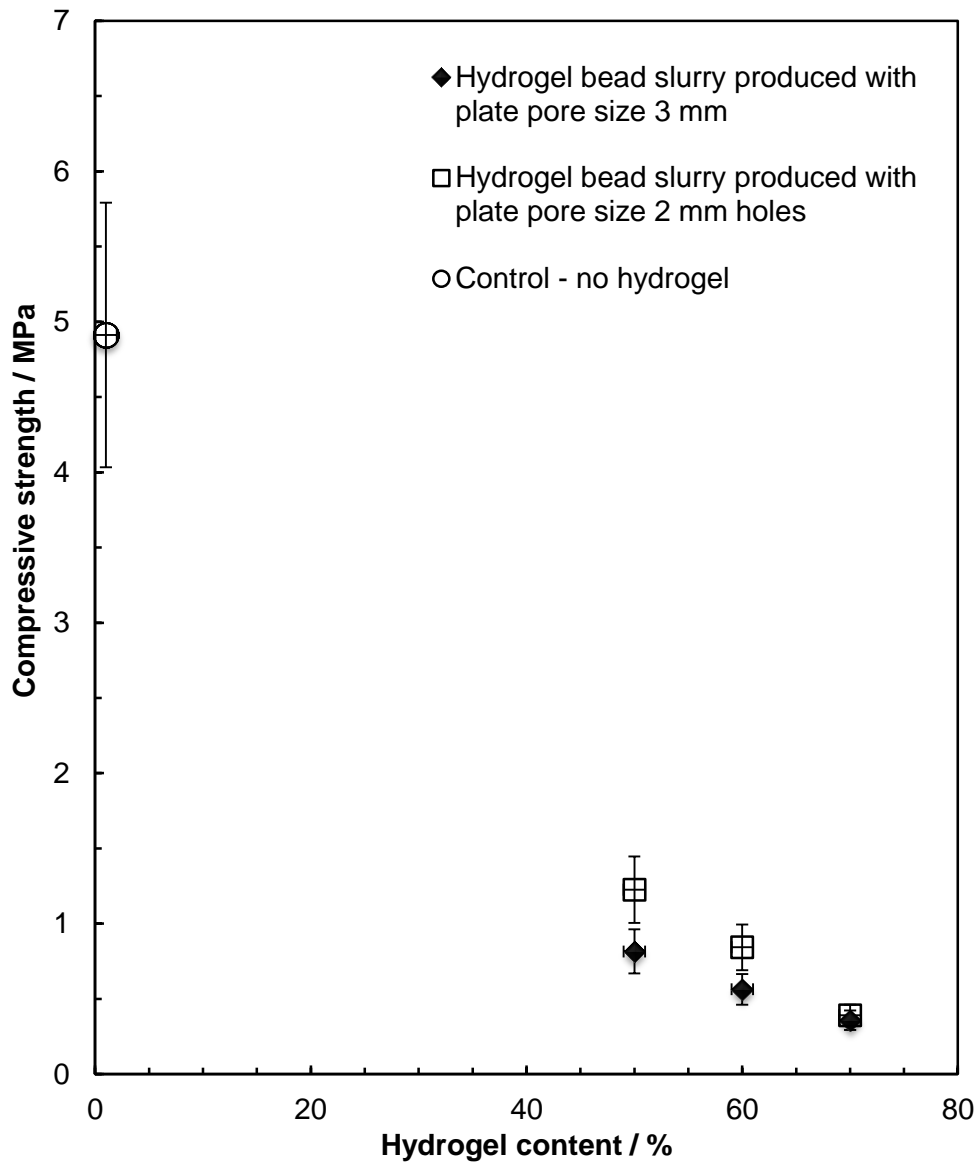


Figure 4.14. Mechanical strength data showing that as the hydrogel content in porous cement samples was increased, the mechanical strength decreased in a linear fashion. Using 2 mm pore size mincer plate the hydrogel produced appears to increase the mechanical strength over the 3 mm pore size plate samples.

Upon observation of the experiment, it was clear that the high porosity of the samples lead to a lower mechanical strength. However, this appeared to be due to the crumbling nature of cement only, the samples seemed to have a well-defined shape to handle the high force but limited internal binding. If the samples were made from concrete (cement with sand or some other aggregate), then the mechanical strength is likely to improve significantly, but for this proof of principle study, the focus was set to the investigation of the acoustic properties of the samples.

4.4.4 SEM Analysis of the Porous Cement Composites Produced by Templating Xanthan – Konjac and Alginate Hydrogel Bead Slurries

SEM images of the cement composites with Xanthan – Konjac hydrogel slurries are displayed in Figure 4.15 (a-c). Pores within cement can be observed in all samples. The micrographs display some of the microstructure around pores in the cement which were filled with the hydrogel residue. The images show pores partly bridged by the hydrogel residue, where the hydrogel bead slurry was used and flake-like (or film-like) microstructure of the non-bridged part. It could be argued that these hydrogel residual films aid the sound absorption of the material and assisted in the increased absorbance at the specific frequencies as they resonated.

The structure of the samples produced using the sodium alginate hydrogel (produced by dropping hydrogel solution into CaCl_2 solution to gel the drops) was found to be quite weak. This was due to the more discreet nature of the pores shown in Figure 4.15 (d, f) within the samples due to the very well formed beads. This discreet nature could encourage fracture lines to form in the material under very little stress and hence reduce the strength of the material. An image of one of these dried hydrogel particles is shown in Figure 4.15(e). It was possible to image the dried beads as the beads remained within the sample, since they had no through pores to evaporate effectively and had a tendency to contract. It can also be observed that the hydrogel production technique was not refined enough to eliminate the "tail" structure observed here that occurred when the beads hit the surface of CaCl_2 . Since the images did not show interconnected pore structure within the composite, these samples were not analysed for the sound absorption, as the wave of the sound would not percolate the sample, but instead bounce back to the detector, similarly to the cement control samples.

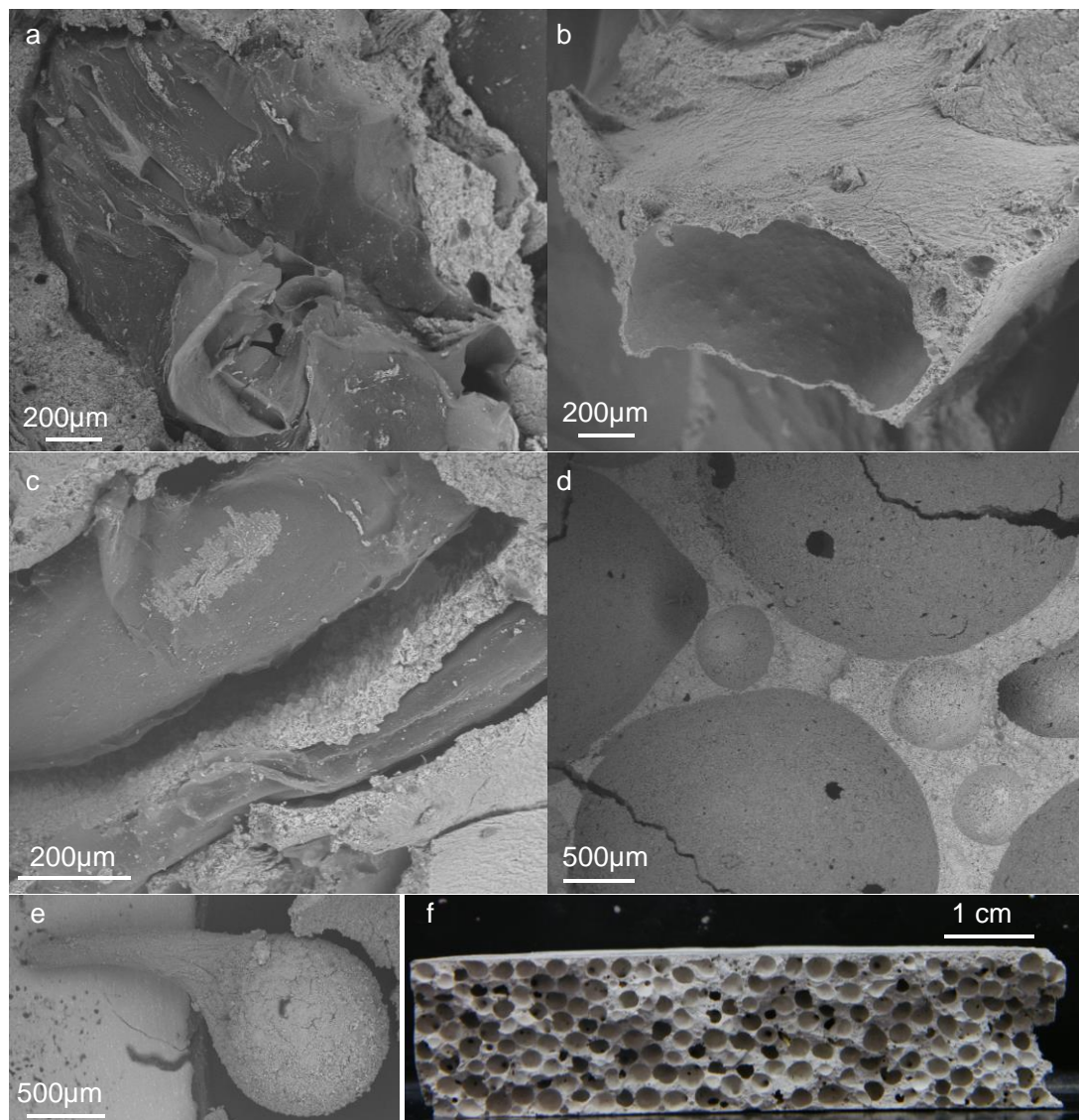


Figure 4.15. SEM images of cement composite samples (a - c) composed of Xanthan – Konjac (2:1 ratio, total 2 wt% gelling agent) hydrogel, where a 3 mm mincing plate was used to make the hydrogel slurry. (a) 50 vol% hydrogel, (b) 60 vol% hydrogel, (c) 70 vol% hydrogel slurry. (d) SEM image of a sample where sodium alginate (4 wt% gelling agent) hydrogel beads prepared by the syringe dripping method and gelled in CaCl_2 solution were used (66 vol%) with (e) SEM of a typical hydrogel particle after drying. (f) A photograph of a composite sample with alginate hydrogel beads after drying.

4.5 CONCLUSIONS

Here several developments in the field of hydrogel templated cement materials are presented, which are relevant as porous sound absorbing materials. Porous cement materials were produced by a hydrogel templating technique using various percentages of hydrogel bead slurries, composition and different hydrogel bead sizes. The investigation of these samples through various experimental techniques resulted in the following key findings.

Firstly, the technique has been extended and the moulding techniques improved to produce samples that are consistently sized and of good homogeneity, which had been substantiated by the SEM analysis and size measurements. Secondly, the hydrogel bead distribution for batches of hydrogels produced using 2 mm and 3 mm pore-size mincing plates has been investigated and proved to be significantly different and therefore a method by which the hydrogel bead size may be controlled has been proven to be valid.

It has also been shown that the initial hydrogel bead size has an effect on the sound absorption properties of the final porous material, with specific regions (500-800 Hz) being absorbed much more effectively (α between 0.6 and 0.8) using the 2 mm hydrogel. These findings are very significant for the material as they put it on the same field as many other porous materials in the literature which do not have such simple and green fabrication methods.

It was found that increasing the hydrogel content (and therefore porosity) reduces the mechanical strength of the material.

4.6 REFERENCES

1. M. Rutkevičius, G. H. Mehl, V. N. Paunov, Q. Qin, et al., *Journal of Materials Research*, 2013, 28, 2409.
2. L. Goines and L. Hagler, *Southern Medical Journal*, 2007, 100, 287.
3. W. Passchier-Vermeer and W. F. Passchier, *Environmental Health Perspectives*, 2000, 108, 123.
4. M. N. Mead, *Environmental Health Perspectives*, 2007, 115, A536.
5. F. Godlee, *British Medical Journal*, 1992, 304, 110.
6. P. V. Bruel, *Noise Control Engineering Journal*, 1977, 8, 52.
7. J. P. Arenas and M. J. Crocker, *Sound and Vibration*, 2010, 44, 12.

8. N. D. Yilmaz, P. Banks-Lee, N. B. Powell and S. Michielsen, *Journal of Applied Polymer Science*, 2011, 121, 3056.
9. L. L. Beranek and I. L. Vér, *Noise and vibration control engineering: principles and applications*, John Wiley & Sons, New York, New York, 1992.
10. M. J. Crocker, *Handbook of Noise and Vibration Control*, John Wiley & Sons, Hoboken, New Jersey, 2007.
11. M. R. F. Kidner and C. H. Hansen, *International Journal of Acoustics and Vibration*, 2008, 13, 112.
12. M. E. Delany and E. N. Bazley, *Applied Acoustics*, 1970, 3, 105.
13. T. J. Cox and P. D'Antonio, *Acoustic Absorbers and Diffusers: Theory, Design and Application*, Taylor & Francis, London, UK, 2004.
14. F. J. Fahy, *Foundations of Engineering Acoustics*, Elsevier Science, London, UK, 2000.
15. N. Atalla, R. Panneton, F. C. Sgard and X. Olny, *Journal of Sound and Vibration*, 2001, 243, 659.
16. D. Cuiyun, C. Guang, X. Xinbang and L. Peisheng, *Applied Acoustics*, 2012, 73, 865.
17. N. N. Najib, Z. M. Ariff, A. A. Bakar and C. S. Sipaut, *Materials & Design*, 2011, 32, 505.
18. Y. H. Ng and L. Hong, *Journal of Applied Polymer Science*, 2006, 102, 1202.
19. H. Olms and B. Breuer, *Inter-Noise 99: Proceedings of the 1999 International Congress on Noise Control Engineering*, Vols 1-3, 1999, 213.
20. J. Kang and M. W. Brocklesby, *Applied Acoustics*, 2005, 66, 669.
21. H. K. Kim, J. H. Jeon and H. K. Lee, *Construction and Building Materials*, 2012, 29, 193.
22. I. S. Organisation, Geenva, Switzerland, 1996.
23. N. M. Alford and A. A. Rahman, *Journal of Materials Science*, 1981, 16, 3105.
24. B. T. Holland, C. F. Blanford, T. Do and A. Stein, *Chemistry of Materials*, 1999, 11, 795.
25. A. J. Charlett and M. T. Craig, *Fundamental Building Technology*, Taylor & Francis, Oxon, UK, 2006.

Chapter 5. Structuring of Porous Food Products through Hydrogel Slurry Templating

“For me, I’m focused on what I want to do. I know what I need to do to be a champion, so I’m working on it.”

Usain Bolt

Porous hydrogel bead slurry templated bouillon cube formulations are explored in this Chapter. Existing bouillon cube formulations are introduced first and then followed by the methodology and reasons for the need of innovation in this area of food formulations. Two matrices were explored: fat with salt and starch; and the less strong, fat with salt only; two hydrogel formulations were analysed: salt resistant Xanthan – Konjac hydrogel mixture introduced in the previous Chapter and a more brittle κ -carrageenan hydrogel.

After establishing the melting temperature of the hydrogels and the solidification temperature of the fat, the two phases were mixed together at a particular temperature, moulded and finally freeze-dried. The dissolution time, texture (strength), volume contraction and changes in the density of the porous hydrogel templated bouillon cubes were assessed in terms of the initial content of the hydrogel. Finally, porous bouillon cube produced without freeze drying is presented.

A patent application has been submitted to protect part of this work.

5.1 INTRODUCTION TO FOOD CHEMISTRY: POROSITY AND TEXTURE

A soup preparation method from meat and spices has been known for centuries and valued by the Egyptian and Greek physicians, especially for the sick and recovering patients due to its good protein metabolism and digestion properties.¹ Nowadays the higher standards of living and existing technologies made the bouillon available to

nearly everyone. The main improvements in the technology of bouillon preparation came during the First World War as a replacement for the most important meals.¹ These formulations became so popular, that, for example, bouillon cubes are now used on a regular basis by 92% of Italian families to season their first and second courses.²

The main ingredients in bouillon cube formulations are salts (sodium chloride and monosodium glutamate), vegetable fats (palm oil stearins), animal fats, bouillon (produced by hydrolysis of vegetable and animal proteins), meat (chicken or beef) and yeast extracts (product of protein hydrolysis of yeast) and lastly vegetables, such as carrots, celery, onion and parsley are added to suit the taste of a particular region.¹ The preparation procedure of bouillon cubes involves blending of fats with other ingredients. Saturated fats, such as palm, palm kernel or coconut are used to prepare the cubes, since they are at least semi solid at room temperature and do not leak out of the product whilst packaging and transporting. As an alternative to these fats hydrogenated fats may be used, as their melting temperature is elevated due to their lowered fraction of unsaturated chains.¹

For bouillon cubes and similar type of food products, a complete release of the flavour and complete dissolution should be rapid, i.e. within seconds. The solubility of the bouillon tablets is often not satisfying for the consumer.³ The presence of lumps or a non-homogeneous cube causes hardness variations within the tablet structure leading to problems during the dissolution. Some idea of the structure of the samples can be gained after looking into X-ray microtomography (μ CT) images presented in Figure 5.1. The image shows that salt particles are trapped between the fat matrix in a random packing.⁴ Therefore, the introduction of porosity could lead to a better solubility, as water could then penetrate throughout the interconnected pore system thus dissolving the cube from within as well as from outside.

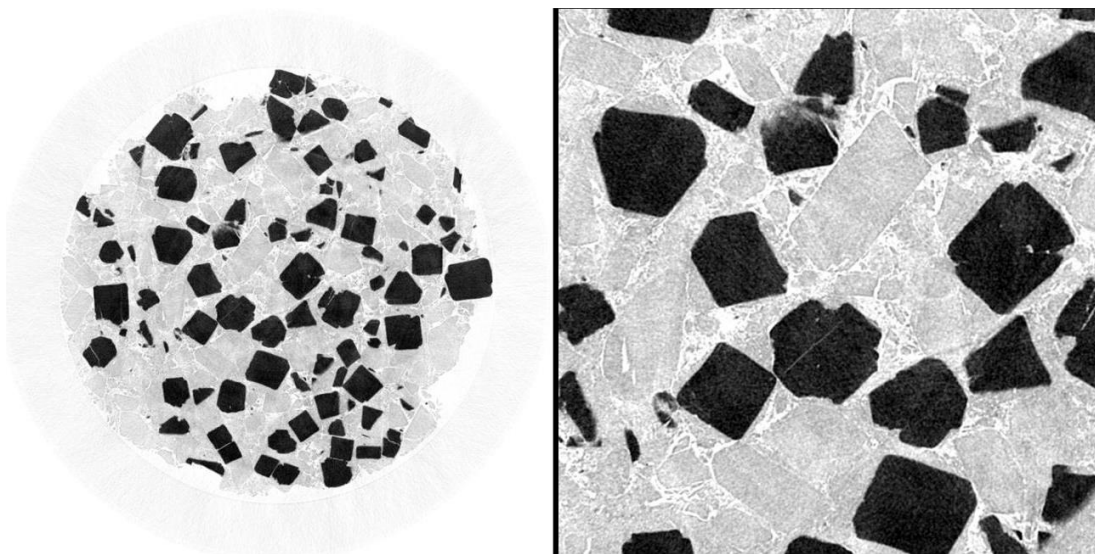


Figure 5.1. X-Ray microtomography images of a horizontal cross-section of a bouillon cube sample, where the left-hand side image had an area of 10.2 mm^2 and the right-hand side image is a zoom-in image representing 3.6 mm^2 area. Salt crystals are visible as dark particles and the fat is shown in grey. Reproduced from Koster and van Dalen.⁴

There is a considerable interest in the hydration/dissolution times of these formulations in the literature, focusing on the salt particle distributions within the cubes,⁴ reduction of the dissolution time of the cubes.^{3, 5} Fibrous materials like cellulose fibres from carrots were used in order to reduce the dissolution time,³ or alternatively using granulation machinery for the preparation of cubes, similarly to sugar cubes.⁵ However, most of the research presented focuses on other areas of the cube production, e.g. reduction in complexity and cooling times,^{6, 7} selective colouring,⁸ and others^{9, 10}. Other studies showed the importance of a binder in these tablets and in particular the addition of starch.^{11, 12} However, up to now there has not been reported bouillon cube formulations, where part of the volume is replaced by a hydrogel. The methodology of the production of such cubes is presented below followed by the discussion of the results obtained.

5.2 FABRICATION OF POROUS HYDROGEL-SLURRY-TEMPLATED BOUILLON CUBE SAMPLES

As presented in the previous Chapters of this thesis, hydrogel templating method can be used to produce porous composites. Fat - salt composites with evaporated hydrogel

beads, which are essentially porous bouillon cube composites have been produced and the schematics detailing the procedure are presented in Figure 5.2 below, which shows that the later stages of the preparation of the composites were essentially the same as in the previously described applications. In this method, a large proportion of the material had been substituted by addition of the hydrogel slurry. The hydrogel can then be evaporated to produce a porous composite, or alternatively left in the composite, which keeps the density of the composite high. In any case, boiling the composites in water facilitated hydrogel (re)hydration and potentially introduced a better rheology and taste for the end product, reducing both the fat and the salt quantity per unit volume and benefitting from the residual hydrogel, which added extra taste of a thick soup, since the texture is one of the main attributes in determination of the overall food quality.¹³ Moreover, some hydrogels have antibacterial properties (as shown in Chapter 1 Section 1.3), which could add an extra shelf-life to the product thus reducing the costs.

The main difference in the methodology used in this Chapter with the ones described for building and sound absorbing materials was the use of solely food grade hydrogels. The matrix of bouillon cube was composed majorly of salt, which lead to the hydrogel syneresis for most of the hydrogels, which was not beneficial in this application. The first objective in this research was to find a hydrogel, which could tolerate a high salt content. It was found in the literature that Xanthan gum - Konjac gum or Xanthan gum – Locust bean gum mixtures can produce stable hydrogels in the presence of salt.¹⁴ Xanthan-Konjac mixture (3.5% gelling agent, ratio 2:1 Xanthan : Konjac in NaCl solution containing (90% of the maximum solubility of sodium chloride, 26.55 wt% and calcium chloride (1 wt%)) was selected, or separately κ -carrageenan (1 – 3.5 wt%) was used.

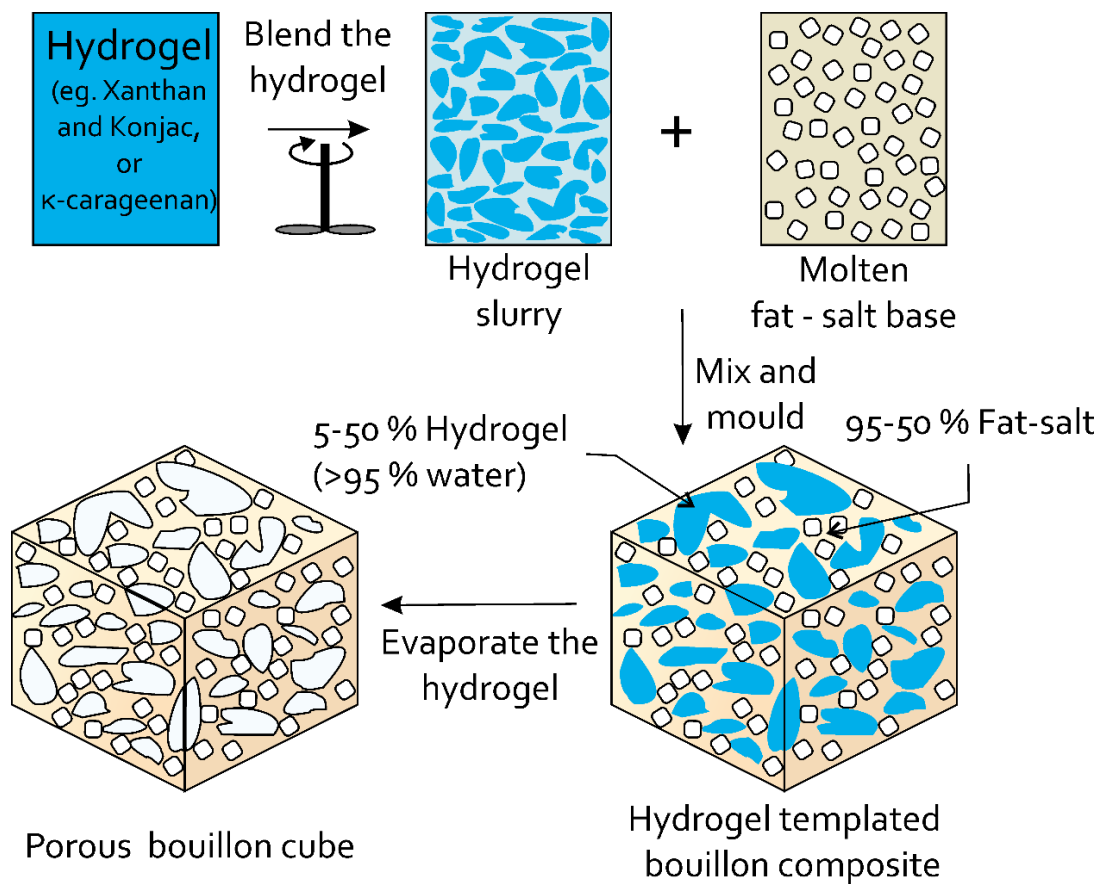


Figure 5.2. Schematic showing the hydrogel slurry templating technique applied for bouillon cubes. First, a hydrogel was prepared and allowed to set, then it was blended into a hydrogel slurry and mixed with fat/salt slurry. The composite was moulded and the water was then evaporated (optional) from the hydrogel domains.

The second difference, was that the samples had to be dried in a relatively short time, i.e. less than a week. Since the matrix consisted of palm oil, which softens at around 40 °C it was not possible to dry the samples effectively in an oven. Thus freeze drying was used as a way to dry the samples. Freeze drying has been developed in 1944 for drying blood plasma and penicillin.¹⁵ Samples are first frozen, and then placed in a vacuum chamber to be dried under sub-freezing temperatures. This method brings the system below the triple point (solid – liquid – gas), avoiding the direct liquid-gas translation seen in ordinary drying procedures. The frozen water passes directly from the solid sample into the gas phase, minimising the changes in the sample shape or shrinkage. An additional advantage of the hydrogel templating technique applied in foods is that water based flavours can be encapsulated in the hydrogel slurry which

allows more flexibility in the formulation, when it is difficult to incorporate hydrophilic taste enhancers within the fat – salt base.

5.3 RESULTS

This section will characterise the properties of the following types of model bouillon cubes, which were produced using these formulations:

1. With added starch solution to the fat – salt base using Xanthan – Konjac hydrogels.
2. With no starch added to the fat – salt base, where
 - a. Xanthan – Konjac (2:1) hydrogel mixture with added salt was used
 - b. κ -carrageenan hydrogel was used.

The Results section contains images of the samples, the dissolution times of the various composites and their compressional strength, which is an indication of the crumbliness of the sample.

5.3.1 Bouillon Cube Composites with Xanthan - Konjac Hydrogel as a Filler

5.3.1.1 Analysis of the Raw Materials Used in the Preparation of Salt – Fat Composites with Hydrogel Slurries: Melting Temperature and Strength Analysis

The amounts of gelling agent and salt influenced the strength of the hydrogel, i.e. stronger gels were formed with larger amounts of gelling agent and in the absence of salt. Indeed, for the same amount of gelling agents the mixture without salt produced a slightly stronger gel. However, Xanthan gum has a good compatibility and stability in the presence of salts. Likewise, being non – ionic, LBG and Konjac gum were not affected by ionic strength of the solution. Experiments showed that in the presence of salt (NaCl) the stronger Xanthan - Konjac gels are formed with a ratio 2:1. This result supports the work of P. A. Williams and co-workers.¹⁶ Furthermore, addition of calcium chloride solution (1 wt%) improved the hardness of the gels as confirmed by visual observation.

Blending of the hydrogel was an important step in the preparation of the porous cubes, since it determines the size of the hydrogel beads, which influence directly the pore size of the final material. Rheology measurements (Figure 5.3) allowed to estimate that the hydrogel melts at around 40 – 60 °C. The first elastic modulus did not go to zero when the gel was melted because the mixture was still visco-elastic. The curve obtained did not decrease drastically during the liquid – gel transition. By visual observation of the samples at the end of each measurement (each temperature), the hydrogel became soft above 40 °C. Thus, the temperature of the fat during the mixing step had to be lower than 42 °C as the hydrogel beads play the role of a template and should not melt whilst being mixed with the molten fat-salt base.

It was also hypothesised that the addition of Gellan gum (a polysaccharide, which produces hydrogels with a high melting point) into hydrogel solution would rise the melting temperature of the mixture. However, it did not increase the melting point of the hydrogel. Even more, it decreased the hardness of the gel when a large amount (approximately 2 wt%) of Gellan gum was used.

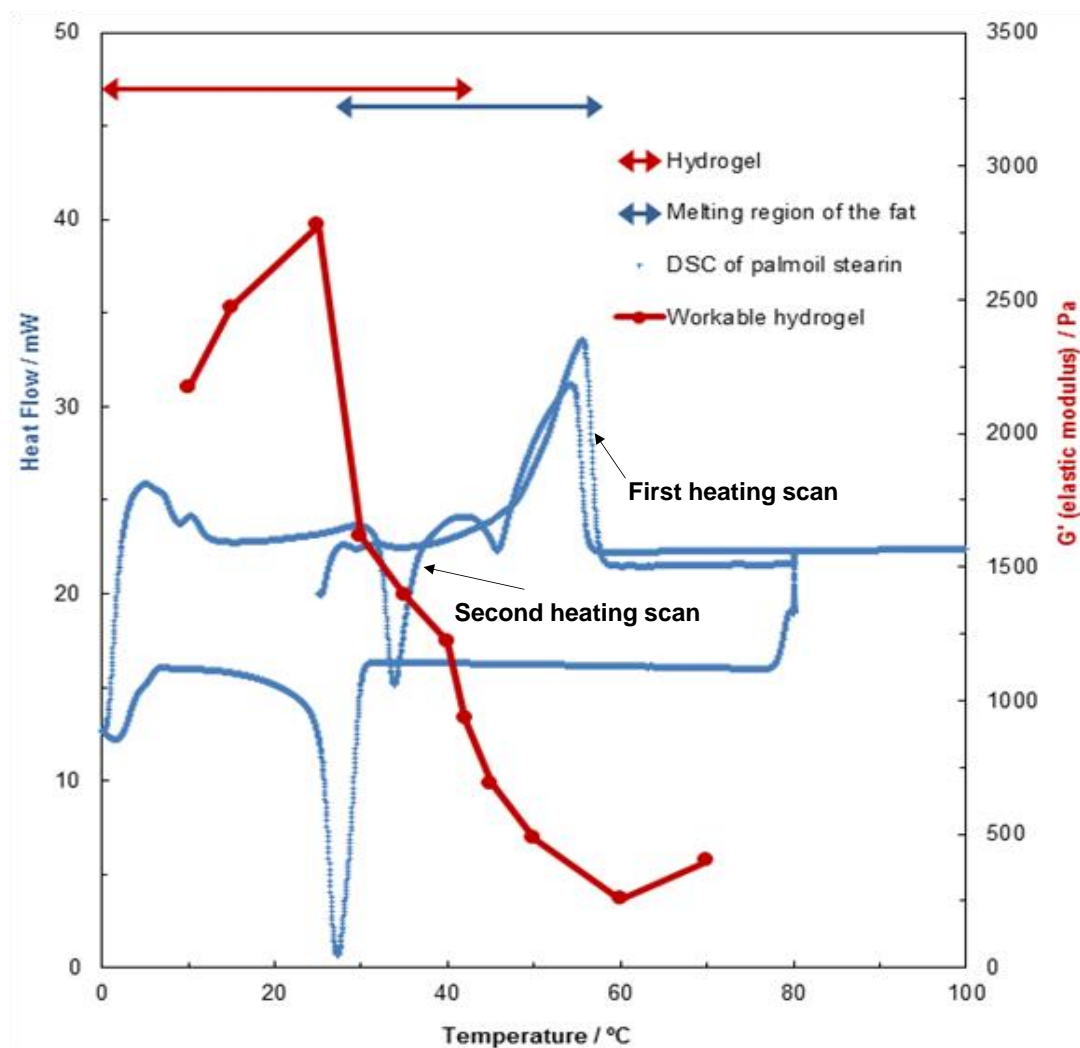


Figure 5.3. The left axis in blue shows the Differential Scanning Calorimetry (DSC) graph of palm oil stearin (heating and cooling rate at 5 °C/min); The right axis shows rheology measurements of a Xanthan – Konjac hydrogel (3.5 wt% gelling agent in NaCl solution (265.5 g/L), ratio 2:1 Xanthan : Konjac, with 1 wt% Calcium Chloride); this graph gives the first elastic modulus as a function of the temperature of the hydrogel; the frequency used to analyse the modulus for this graph was 0.1 Hz. The lines are a guide to the eye and the points are results recorded by the rheometer. Top double arrow (red) vaguely shows the temperature, at which hydrogel was still in the gelled state, and the double arrow below (blue) shows the region, where the fat is in the partially molten state. The temperature overlap region was used in the sample preparation (30-42 °C).

Analysis of the different fat melting temperature was done using DSC and is presented in Table 5.1. In order to reduce the overall *fat base* melting temperature, the palm oil stearin melting temperature had to be reduced and this was done by adding vegetable fat (6.6 wt% of palm oil stearin). The vegetable fat is soft at room temperature but it allows adjusting the melting point of the Palmoil stearin. This mixture provided a lower melting point region fat slurry, which was workable at 40 °C, the higher temperature region of a gelled hydrogel. Mixing different samples of salt and fat slurry yielded that the best ratio was 15 wt% of fat and 85 wt% of salt. Samples of 90 wt% had a fragile structure, which collapsed during the de-moulding process due to the lack of the binding material (fat). Likewise, more than 25 wt% of fat produced non-homogeneous samples, because the sedimentation of the salt occurred before the solidification of the composites. Figure 5.4 (c) shows a SEM image of a salt – fat composite without hydrogel and with the selected salt – fat ratio. Also, in order to distinguish between the salt and the fat, individual images of the raw materials were taken and shown in Figure 5.4 (a, b).

Table 5.1. Table showing melting point regions of different fats used for the fat base.

Fat	Melting temperature region / °C
Vegetable fat (Unilever)	18-40
Palm Kernel oil (other supplier)	37-51
Palm oil stearin (Unilever)	27-58

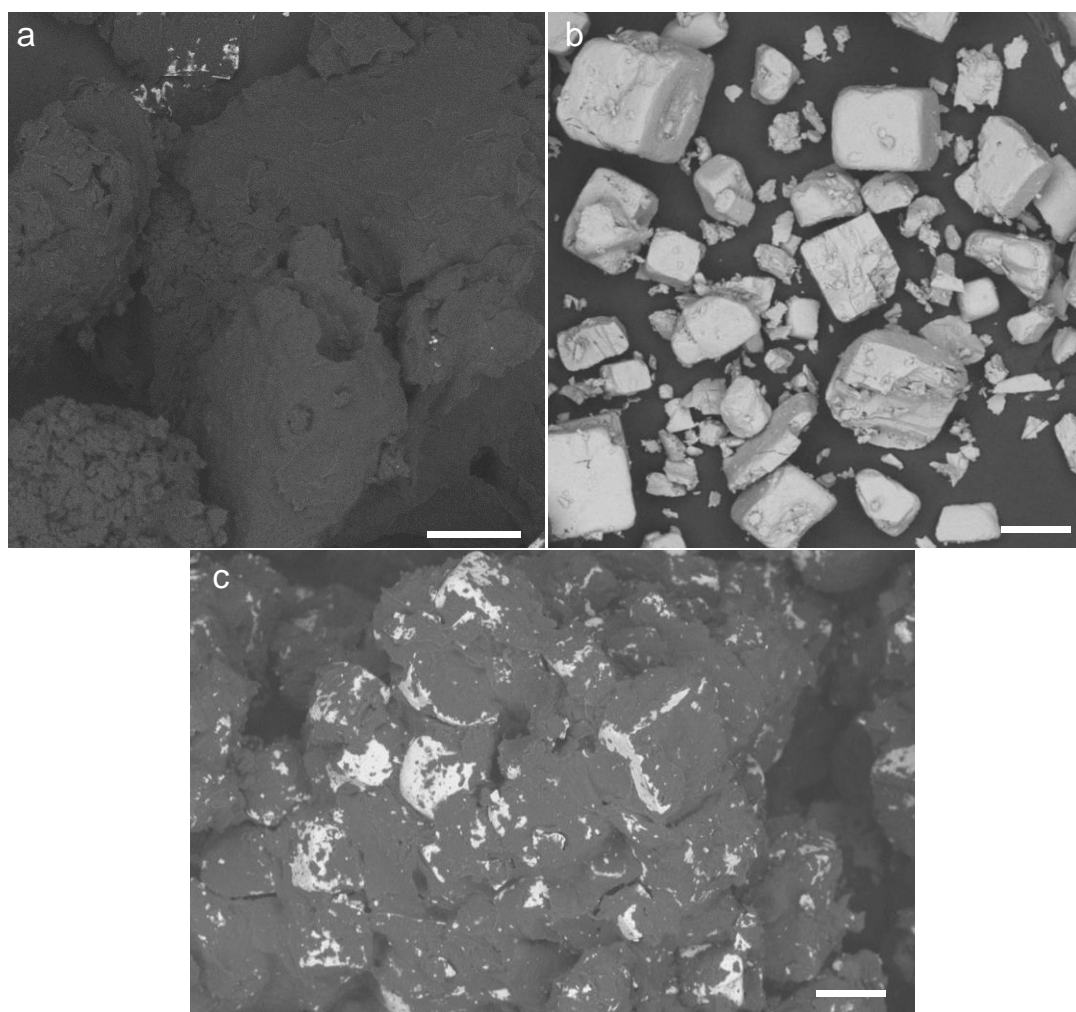


Figure 5.4. SEM images of (a) palm oil stearin, (b) table salt crystals and (c) fat (85%) mixed with salt (15%) (the fat - salt base). Scale bar is 200 μm .

5.3.1.2 Structure of the Porous Bouillon Cube Samples with Added Starch: Electron Microscopy Analysis

Samples were weighed regularly during the drying process in order to estimate the extent of drying. The different drying processes gave different results. It was found that the complete drying using a vacuum oven (where a pressure of 30 mmHg was used at 25 °C) was very slow (several weeks) as well as the technique using a vacuum desiccator (20 mmHg). These methods were taking long time as the temperature had to be below 30 °C in order to avoid the melting of the fat. Moreover, when the fraction of the hydrogel was too low, the pore system was not interconnected and continuous channels within the composite could not be formed. This resulted in some of the hydrogel beads being isolated and essentially trapped into the structure, which slowed down the evaporation of water.

On the other hand, freeze drying (-40 °C, 6 mmHg) was the quickest method (1 night) to dry the samples. However, freezing the samples in the liquid nitrogen (-196 °C) prior to the drying step fragmented the composites, so instead the samples were directly placed in the freeze dryer to evaporate, excluding the liquid nitrogen step commonly used with this method.¹⁷ Moreover, freeze drying when the samples were kept in the mould prevented the samples from shrinking. As the pressure was reduced in the vacuum chamber, the samples experienced swelling, due to the trapped air within the hydrogel, which was expanding at the lower pressure. In later stages, where starch was eliminated from the formulation, this issue was tackled by pre-centrifuging the hot hydrogel before it was allowed to gel, which eliminated most of the air bubbles trapped in the hydrogel solution. The swelling was directly measured by a difference in the height using a caliper.

Structures of the salt - fat slurries with hydrogel beads were observed visually after being dried. Illustrated in Figure 5.5 are SEM images of a porous salt – fat composite templated with 25 vol% and 50 vol% of hydrogel after freeze drying. The sodium chloride deposit from within the hydrogel demonstrates the evaporation of the water phase and the formation of the cavities within the structure. The deposited crystals of the salt were very small and had been precipitated during the drying process. The amorphous appearance of the deposit was due to the dried hydrogel.

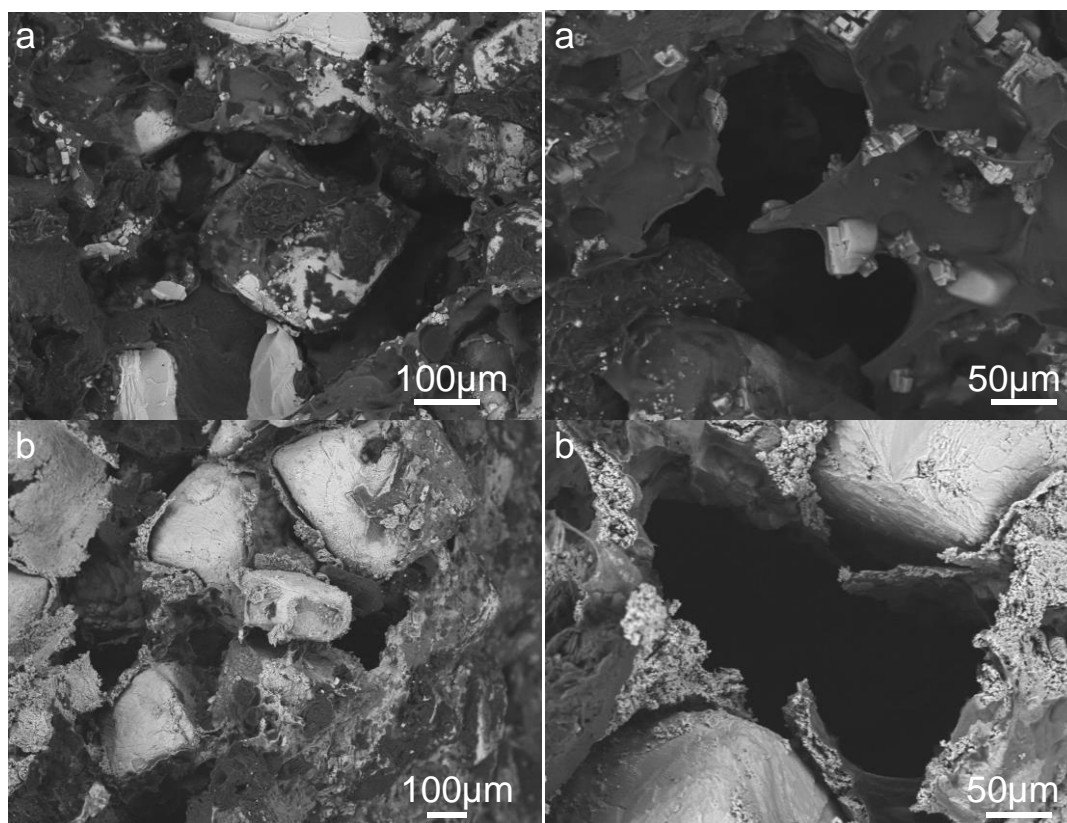


Figure 5.5. SEM images of fat - salt composites (15% fat, 81% salt, 4% starch) templated with Xanthan – Konjac hydrogel bead slurries: (a) 25 vol% hydrogel, (b) 50 vol% hydrogel. Images were taken after freeze drying the samples. The hydrogel contained NaCl (26.5 wt%).

5.3.1.3 Structure of the Samples with Added Starch: Porosity, Weight Loss and Compressional Strength

As expected, an increase in the initial volume percentage of the hydrogel increased the porosity of the composites, as shown in Figure 5.6(a-f). Two series of samples were prepared: with starch and without starch added to the salt-fat base or the hydrogel. Visually there was no significant difference between the series, however, the addition of starch (with water to produce a solution of starch) into the salt - fat slurry increased the strength and the rigidity of the composites. On the other hand, without prior hydration of starch in water, or adding starch into the hydrogel solution (not the matrix, 4 wt%) did not result in any significant increase in the strength of the samples.

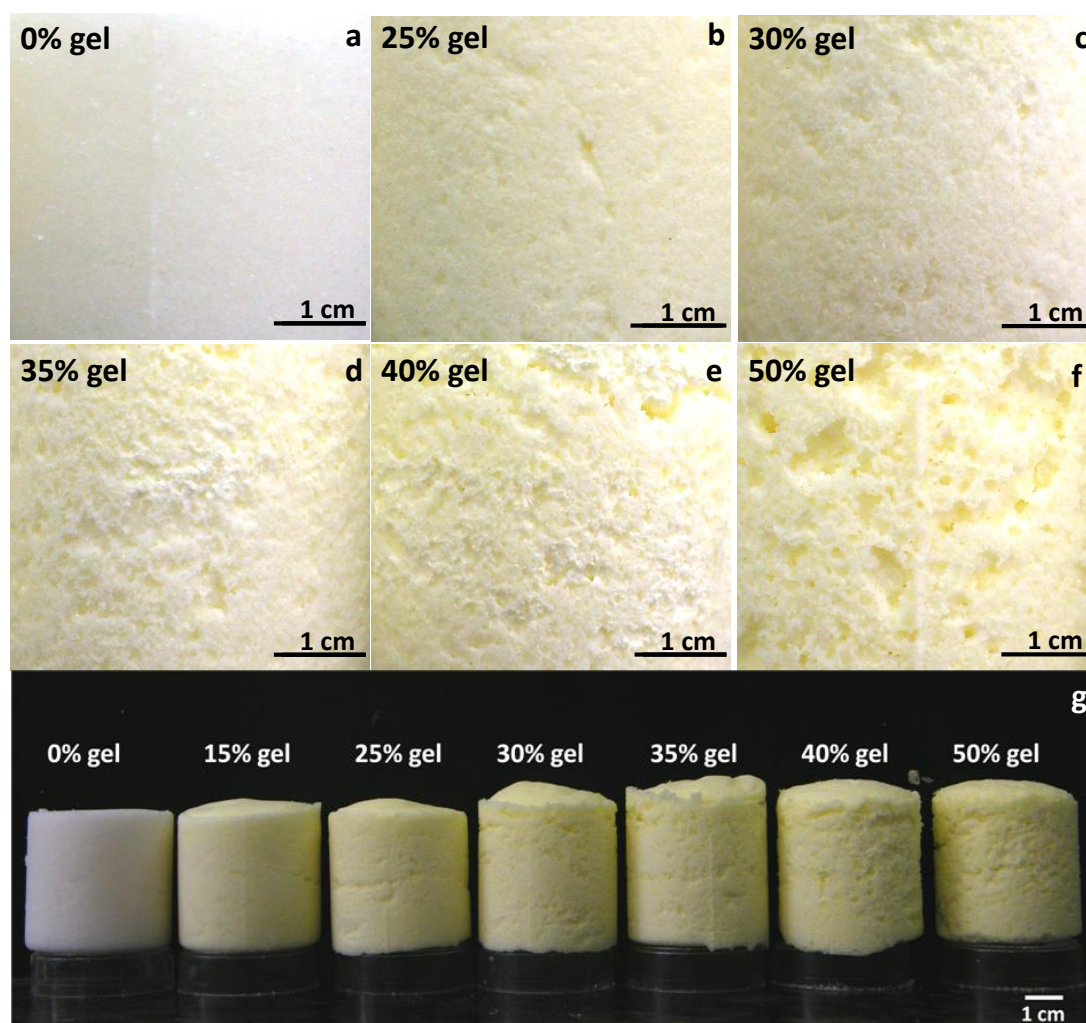


Figure 5.6. Images of different fat and salt composites (15 wt% Palmoil stearin, 1 wt% vegetable fat, 84 wt% salt) after freeze drying; the samples were not previously frozen with liquid nitrogen; these images show the porosity change upon different percentages of Xanthan – Konjac hydrogel (3.5 wt% gelling agent in NaCl solution, ratio 2:1, with 1 wt% Calcium Chloride and stained with fluorescein sodium salt). Different hydrogel volume percentages used are indicated in the images. (a-f) close-up images, (g) shows all samples lined together. The increase in their size with the increase in hydrogel was caused due to the expansion in vacuum of the air bubbles trapped within the hydrogels.

The weight loss and the volume difference of the samples as a function of the hydrogel percentage were calculated and are shown in Figure 5.7. The amount of lost water after freeze-drying was proportional to the percentage of the hydrogel (in the presence and in the absence of starch). Only the non-cracked samples were analysed, although they had expanded and were brittle. The samples expanded during the evaporation step and sometimes even cracked. This came as a result of microbubbles trapped within the hydrogel bead slurry during the preparation of the hydrogels. These bubbles were then subjected to the reduced pressure and caused structural expansion of the semi-solid fat-salt-hydrogel slurry composite. It was estimated that the volume for one air bubble under the freeze drying conditions (-40 °C, 6 mmHg versus 25 °C, 760 mmHg) would increase (about 100 times). The effect was not beneficial in this particular case of a food product, but could be used in the preparation of aerated chocolates. This issue with bouillon cube samples was addressed by degassing using a vacuum desiccator prior to the solidification and freeze drying. More results will be presented later in this Chapter. When the samples were degassed, as shown in Figure 5.7, there was a considerable decrease in swelling compared to the non-degassed samples, however the drying of the samples became slower.

Figure 5.8 shows the compressional strength results in the presence and in the absence of starch. Comparing the control samples of these two cases (without any hydrogel) the pressure which the sample could handle with added starch was higher than the sample without starch, which confirms the role of starch as a binder. With a low initial percentage of the hydrogel (<25 vol% without starch and <35 vol% with starch), the cubes became stronger than the control samples (0% hydrogel). Beads of Xanthan - Konjac hydrogel mixture played the role of a binder up to a certain volume percentage, but after increasing hydrogel volume further, the composites lost their strength and become more brittle with the increase of the hydrogel volume content. This effect was more vivid in the case when starch was added to the fat-salt base.

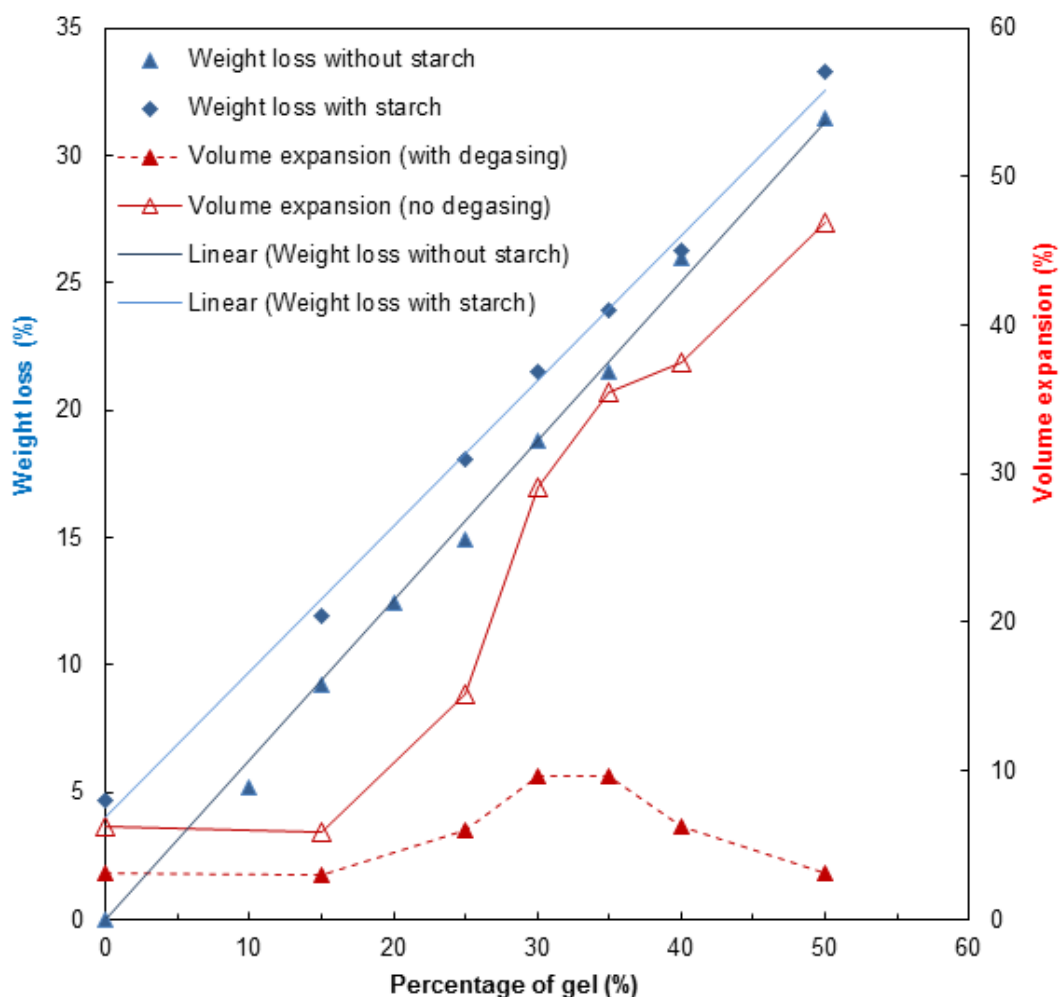


Figure 5.7. A graph of weight loss and volume expansion after the evaporation of the hydrogels as a function of the hydrogel percentage using samples with starch (14% Palmoil stearin, 1% vegetable fat, 4% starch, 4% water, 77% salt) and without starch (14% Palmoil stearin, 1% vegetable fat, 85% salt); the volume expansion was analysed for samples without starch, where one set of samples was subjected to vacuum prior freeze-drying and the other was freeze-dried directly after moulding; the lines are a guide to the eye and the points are the data.

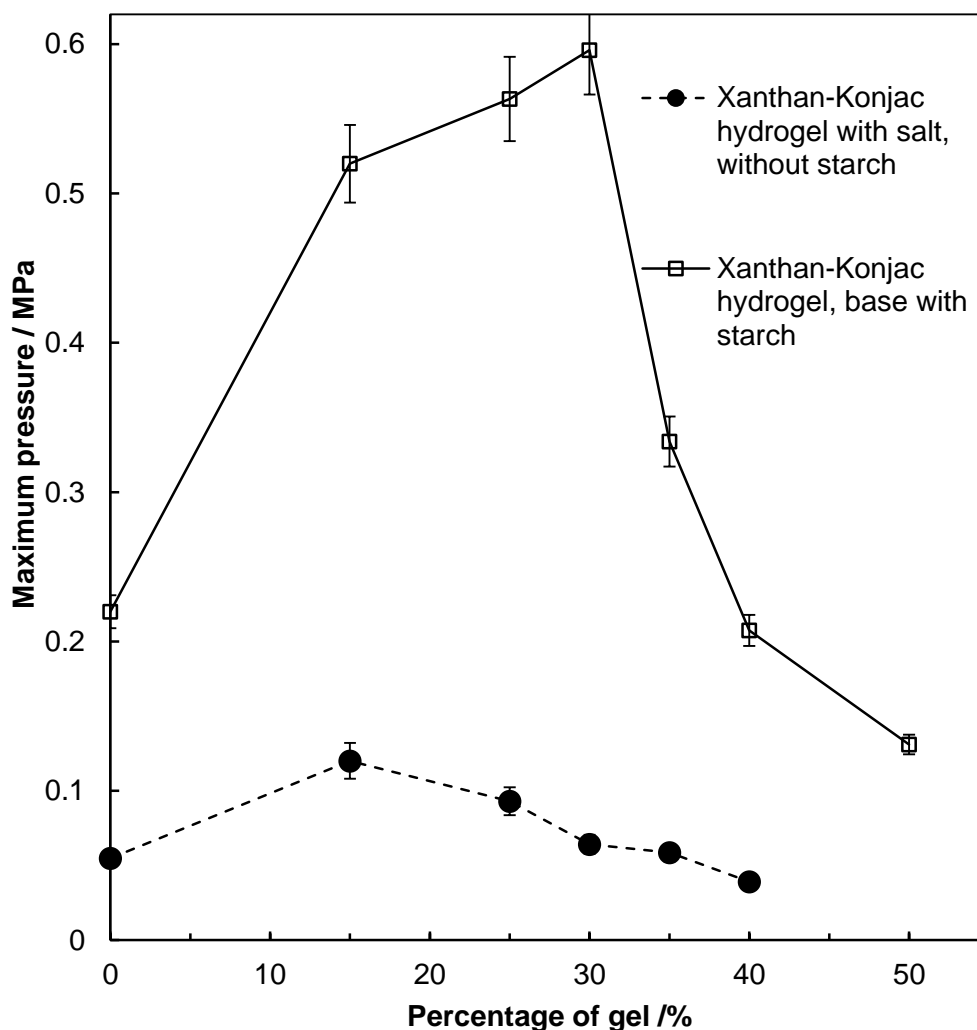


Figure 5.8. Compression strength analyses after freeze drying (no liquid nitrogen treatment) of different samples (filled points) without starch (15 wt% Palmoil stearin, 1 wt% vegetable fat, 84 wt% salt) and (unfilled points) with starch (15 wt% Palmoil stearin, 1 wt% vegetable fat, 4 wt% potato starch, 4 wt% water, 76 wt% salt); the different curves correspond to the different percentages of Xanthan – Konjac hydrogel (3.5 wt% gelling agent in NaCl solution of 265.5 g/L, ratio 2:1, 1 wt% Calcium Chloride, fluorescein sodium salt); the pressure was calculated using: $\sigma = \text{Load} / \text{area}$; the area was a disk with a diameter of 3.7 cm and the load was measured by the machine; the lines are a guide to the eye and the points are the data.

5.3.1.4 Dissolution Time of the Porous Bouillon Composites

The dissolution time of the samples was measured as described in Chapter 2 Section 2.2.5. Typically, a sample was immersed in a beaker of hot water, which was stirred and the time to disintegrate the composite was recorded. In the absence of starch the dissolution time increased for the low percentage of the hydrogel content samples (<30 vol% hydrogel) as shown in Figure 5.9. Afterwards the dissolution time decreased as the amount of the hydrogel was increased. The increase observed was likely to be due to the hydrogel deposits within the composite pores, which in presence of hot water started to rehydrate (and then form a gel). This prevented the hot water from being in contact with the core of the composite and the disintegration was delayed. When the percentage of the hydrogel exceeded 30 vol%, the porosity was higher and the composite had an open-pore structure. Thus the rehydration of the deposit did not affect the dissolution time to such extent. Also, the structure became more fragile, causing easier rupturing of the cubes. As the hydrogel volume in the sample was in the region of 25-30 vol% of hydrogel, this corresponded to the percolation of the gel inside the composite. The samples with starch did not show a similar behaviour, because of the difference in the preparation of the samples. It was observed that the the dissolution time increased much more for samples with starch, thus they were not tested to a large extent and the data is not reported in this thesis. Compared to the control sample, composites with evaporated hydrogel took much longer times to dissolve. As it will be shown later in this thesis, the type of hydrogel used had a vast effect on the dissolution time of the composite.

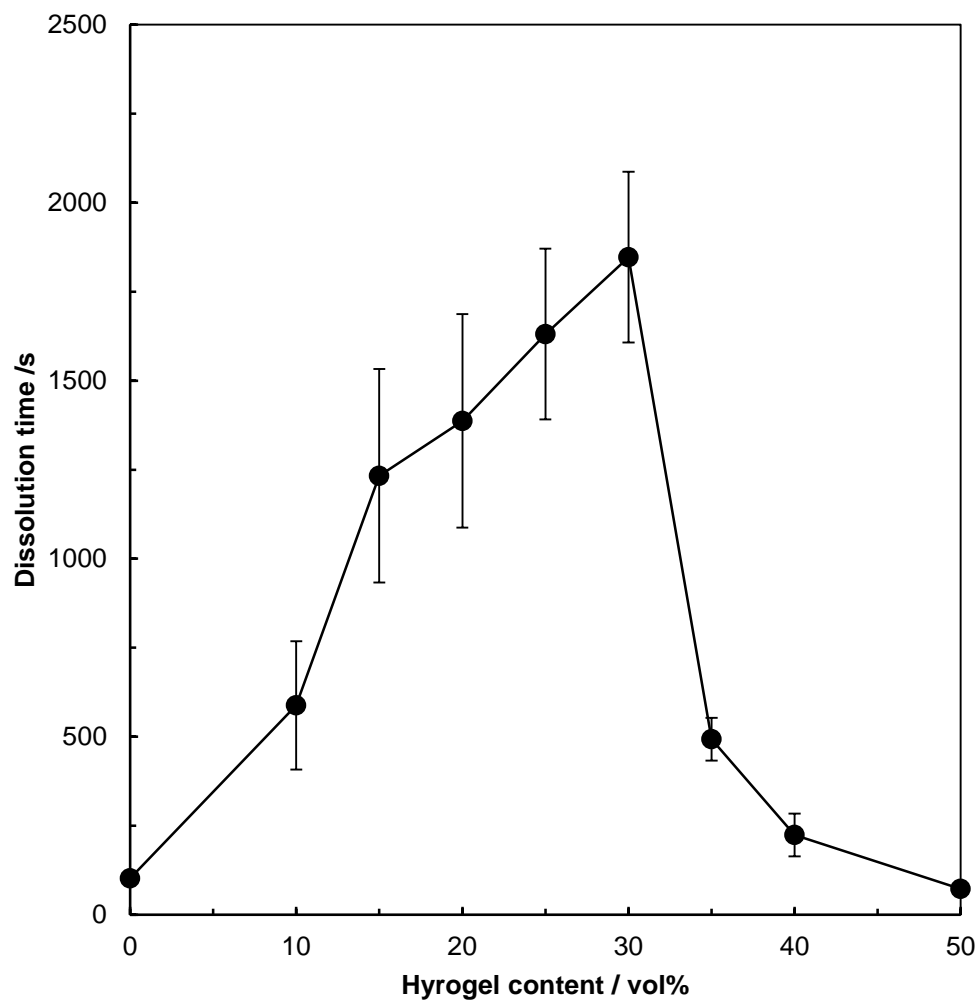


Figure 5.9. Graph of dissolution time as a function of the hydrogel percentage using samples without starch; Xanthan-Konjac hydrogel was used in the samples and they were not degassed before drying; the lines are a guide to the eye and the points are the data.

5.3.2 Bouillon Cube Composites with κ -carrageenan Hydrogel

In addition to the Xanthan-Konjac hydrogel based composites, another formulation was tested, which would still produce porous composites, but reduce their strength and, especially, their dissolution time. Removing starch from the fat-salt base showed a good improvement, but then it was decided to analyse different hydrogels and compare their dissolution times without any base. The results are presented below in Table 5.2. Previously used Xanthan-Konjac hydrogel mixture had shown the longest times for its dissolution, followed by Gellan gum, κ -carrageenan and gelatine. However, Gellan gum and gelatine were found not to be stable enough in the presence of salt, making them unsuitable hydrogels for the bouillon cube formulations. It was κ -carrageenan that was selected for the new study and the data that was collected is presented below. No salt was added to the hydrogel, which even though causes a significant osmotic pressure difference, due to the texture of carrageenan gels, did not cause significant syneresis (although significant syneresis was observed during the moulding process of the composites). Another difference from the previously discussed formulation was that instead of blending using a Silverson LR4 homogeniser to produce hydrogel beads, the hydrogel was passed through a Kenwood mincer with 3 mm or 2 mm pore size plate, used in the preparation of hydrogels reported in Chapter 4.

Table 5.2. Dissolution time of various hydrogels samples in water at 90 °C. All samples had a volume of $40 \pm 1 \text{ cm}^3$.

Gelling agent	Gellan gum 1.5 wt%	Gelatine 1.5 wt%	κ -carrageenan 1.5 wt%	Xanthan-Konjac 1.5 wt%
Time to dissolve	$101 \pm 2 \text{ s}$	$0.5 \pm 0.4 \text{ s}$	$50 \pm 1 \text{ s}$	$145 \pm 1 \text{ s}$

5.3.2.1 Typical Images of the Porous Fat / Salt Composite Samples

Sets of samples were photographed after the preparation and the images of them can be seen in Figure 5.10. The height of the samples varies due to the slightly different pressure applied to compress the composites in the moulds and hence sometimes releasing water from the hydrogel due to the hydrogel syneresis. In these images, one

can see pores produced from the entrapped evaporated hydrogel. The hydrogels were centrifuged whilst hot in order to eliminate all the air bubbles that were entrapped during the hydration of the hydrogel.

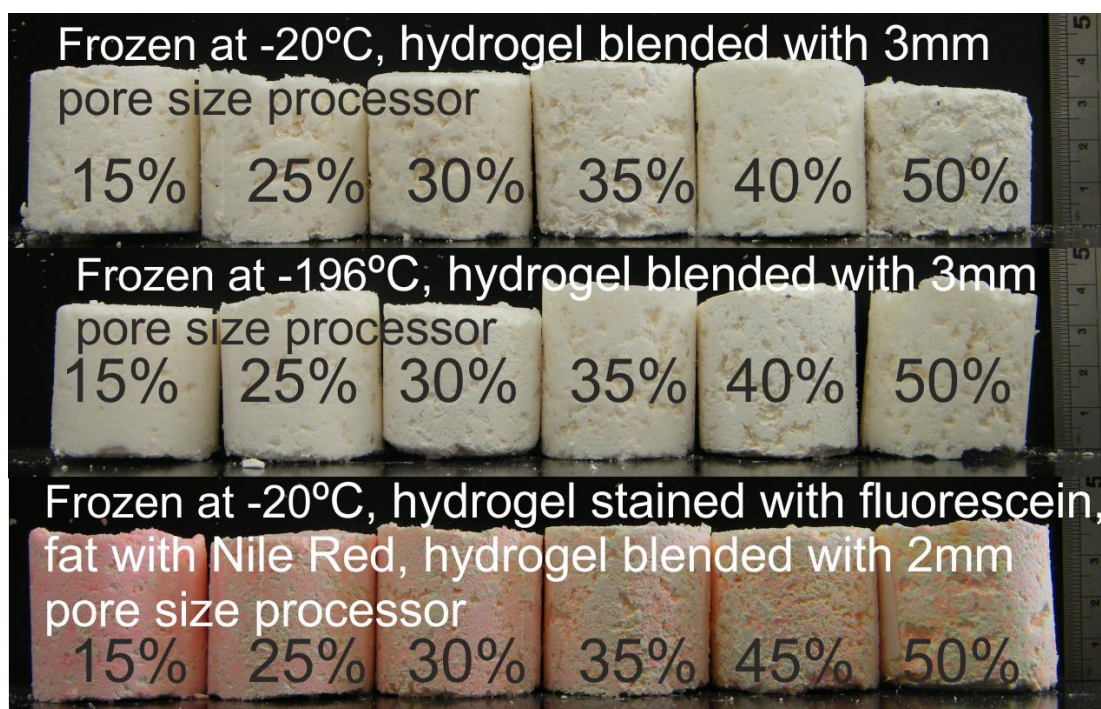


Figure 5.10. Photographs of typical bouillon composites after freeze-drying. All samples had a hydrogel with 3 wt% κ -carrageenan as a gelling agent. Top and bottom sets were frozen at $-20\text{ }^{\circ}\text{C}$ before freeze-drying, middle set was frozen at $-196\text{ }^{\circ}\text{C}$. Bottom image had Fluorescein sodium salt present in the hydrogel and Nile Red in the fat phase. Also, the hydrogel used for the bottom set of composites was passed through a smaller mincer plate (2 mm), compared to 3 mm used in the top two composites. Numbers on the samples represent initial hydrogel volume content in the composite before freeze-drying.

Composite samples before drying were cut and placed on a dimpled slide with a cover slip and were analysed under a reflected light microscope equipped with a FITC and TRITC filter set. Hydrogel was doped with Fluorescein sodium salt and the fat base with Nile Red. Images were taken using both filters separately and were merged together in the post-process. These micrographs are shown in Figure 5.11. From the images it was easy to distinguish between the hydrogel beads and the fat base. The sizes of the hydrogel beads were around 1-2 mm and they had been surrounded by the fat - salt base. This assured that the beads would not disintegrate during the sample preparation and were intact for the freezing process. Also, it was observed that the increase in the hydrogel content to 45 vol% decreased the fat content, but the fat was still visible around and on the hydrogel beads, which produced a bi-continuous structure where both fat -salt and hydrogel phases were interconnected. As we see later in this section, this formulation lead to the reduction of the dissolution time and the compressional strength of the composites.

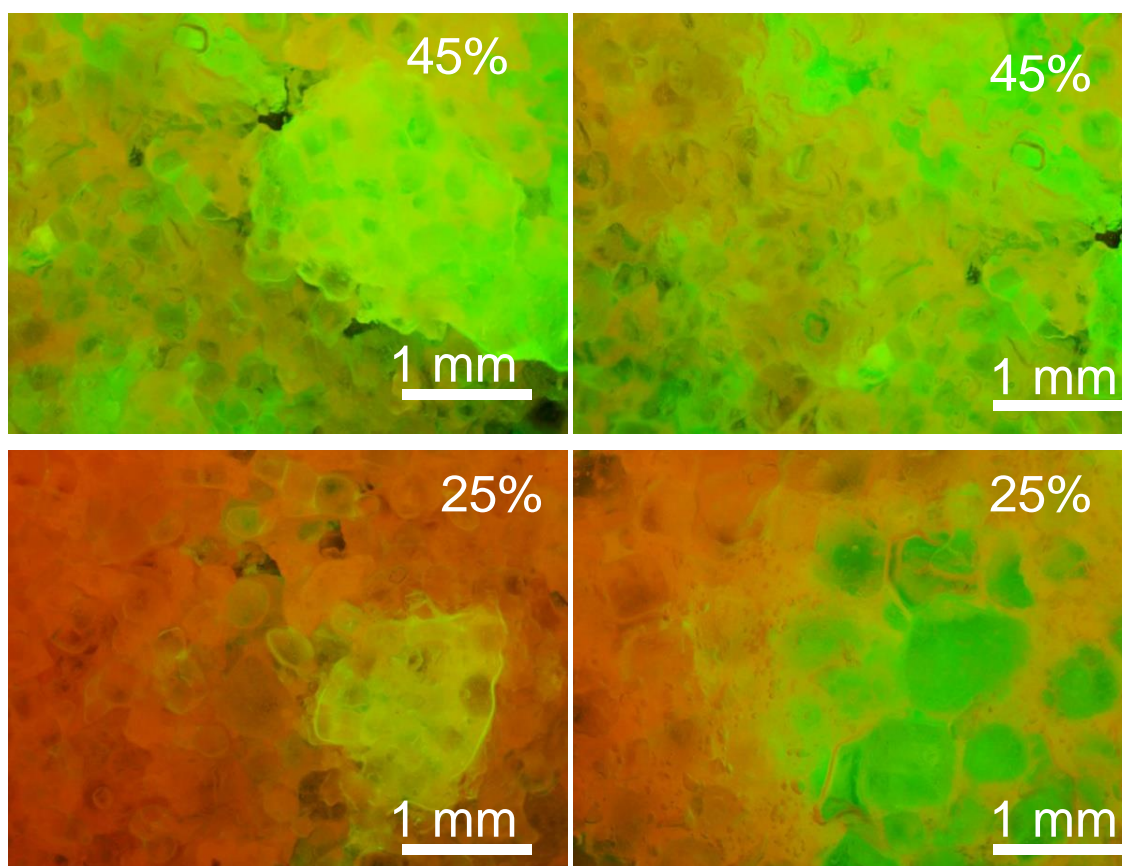


Figure 5.11. Merged fluorescence microscopy images of the κ -carrageenan hydrogel (green, image taken using FITC filter set) and salt-fat base (red, image taken using TRITC filter set) composite before drying. Top images are of the sample where 45 vol% of the hydrogel was templated and the bottom images are of a sample where 25 vol% of the hydrogel was used. A thin slice of the composite was placed on a dimple slide to obtain the images. 2mm mincer plate was used to blend the hydrogel.

5.3.2.2 SEM Analysis of the Porous Fat / Salt Composites with κ -carrageenan Hydrogel Beads

Dried samples have been sliced and analysed using SEM. The images of the typical samples are presented in Figure 5.12. These images show that the porosity increased with the increasing amount of the hydrogel added to the composite. It was observed that some of the gelling agent was deposited within the pores of the composite and partially dissolved salt had re-crystallised on the hydrogel residue. Also, the salt crystals were observed with extra salt deposited on them, which originated from the partially dissolved salt crystals in contact with the hydrogel beads, as some syneresis had occurred. The precipitated salt dissolved faster in the hot water solution rather than the embedded salt crystals, which could be treated as a beneficial property. It is not very straight forward to distinguish between the fat base and the residual hydrogel in these images, where the darker pixels of the image represent the fat base. Assuming this, it can be concluded that the fat phase was dispersed between the salt crystals and the hydrogel acted as filler.

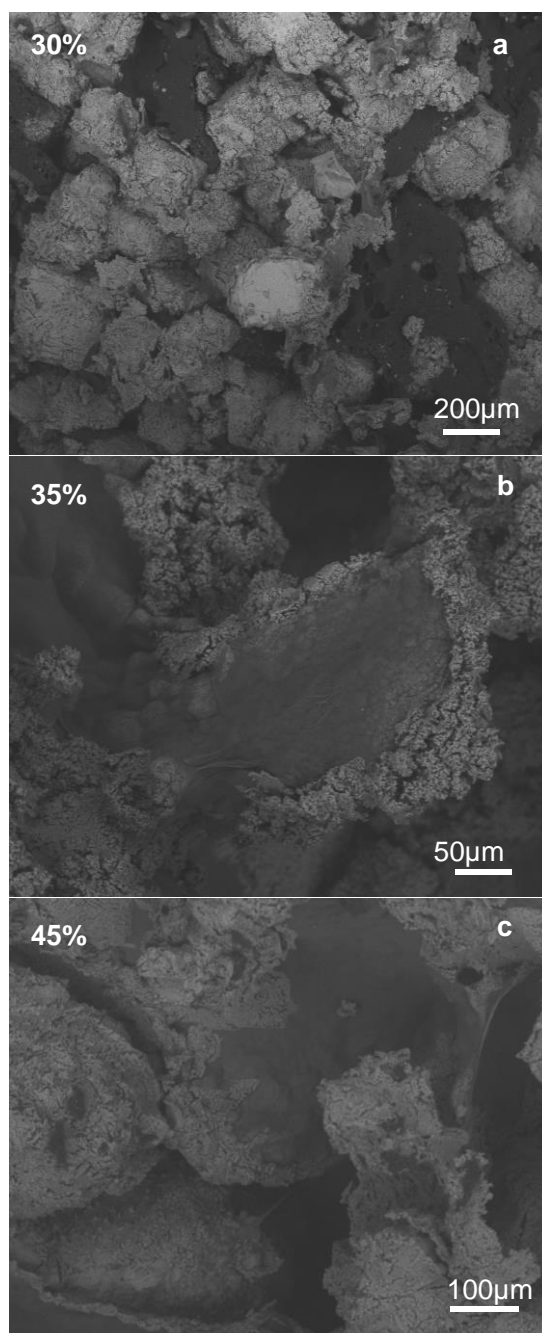


Figure 5.12. SEM images of salt-fat base templated with κ -carrageenan (1.5 wt% gelling agent) hydrogel beads (a) 30 vol%, (b) 35 vol% and (c) 45 vol%. Composites after freeze-drying. Hydrogel vol% shown in top corner of each image.

5.3.2.3 Weight Loss of the κ -carrageenan Templated Fat - Salt Composites

Samples have been weighted before and after drying process and their weight loss was calculated from the reduction in the mass compared to the initial mass of the composite. A graph showing the weight loss variation as a function of the hydrogel content is shown below in Figure 5.13. The weight loss was not linear, as was observed in the previous samples of Xanthan - Konjac – fat - salt composites. This was because some of the water from the hydrogel had been drained due to the partial syneresis of the κ -carrageenan hydrogel before the samples were actually chilled or frozen. The larger hydrogel concentrations within the sample showed larger effect of the syneresis, as the weight loss seems to have reached a plateau for the freezer-frozen samples at 45 vol% of the hydrogel. In large scale experiments, the effect could be reduced by reducing the time intervals between preparation of the composite and its freezing, for example doing it simultaneously or at a higher rate of cooling.

5.3.2.4 Compressional Strength of the Porous Bouillon Cube Formulations with κ -carrageenan

After pressing the composites with a compressional strength analysis machine, the compressional strength was plotted against the percentage of the gelling agent in the hydrogel sample (see Figure 5.14). In this image the effect of the gelling agent content is shown. Three gelling agent concentrations were analysed (1.5, 2.25 and 3.0 wt%) for the 25 vol% and 45 vol% hydrogel content samples, where the samples were first frozen at -20 °C for 6 hours and then placed in a freeze-dryer for two days. This graph shows that the increase in the gelling agent content within the hydrogel decreased the strength of the sample. This means, that the consumer could crumble the samples easier if a stronger hydrogel was used. However, the 3.0 wt% hydrogel was quite strong and even though it was brittle, the production of the beads was not as easy as for the lower gelling agent content samples. Also from this graph a decrease in the strength of the samples as the total volume of the hydrogel used was increased from 25 vol% to 45 vol% was observed. This result corresponds well to the expected outcome, as the increase in the hydrogel increased overall porosity of the sample, making it more brittle and easier to crumble.

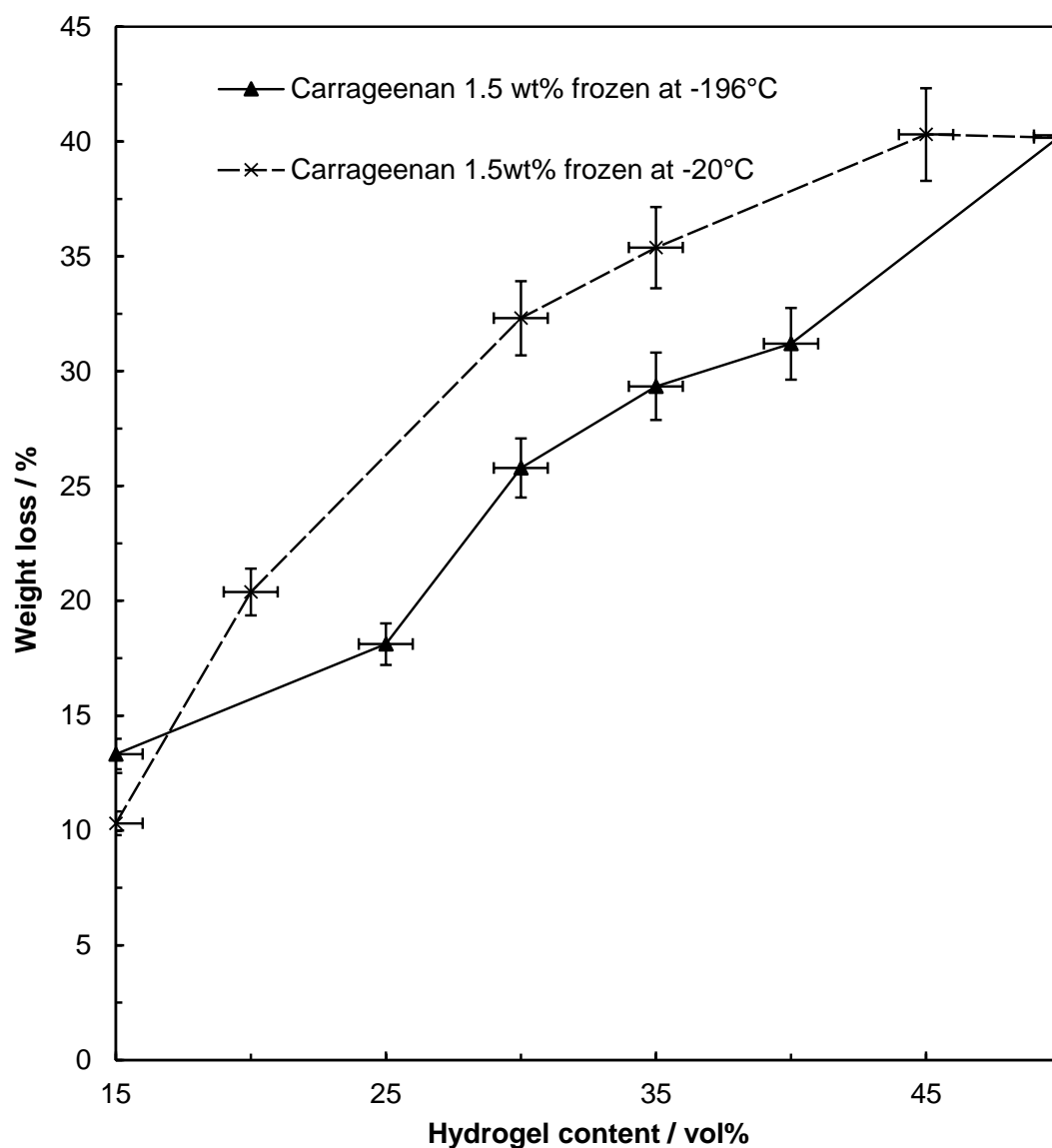


Figure 5.13. Weight loss (%) of the salt-fat-hydrogel composites after freeze-drying. Two different methods of freezing were explored: with liquid nitrogen and in a freezer. Lines are a guide to the eye.

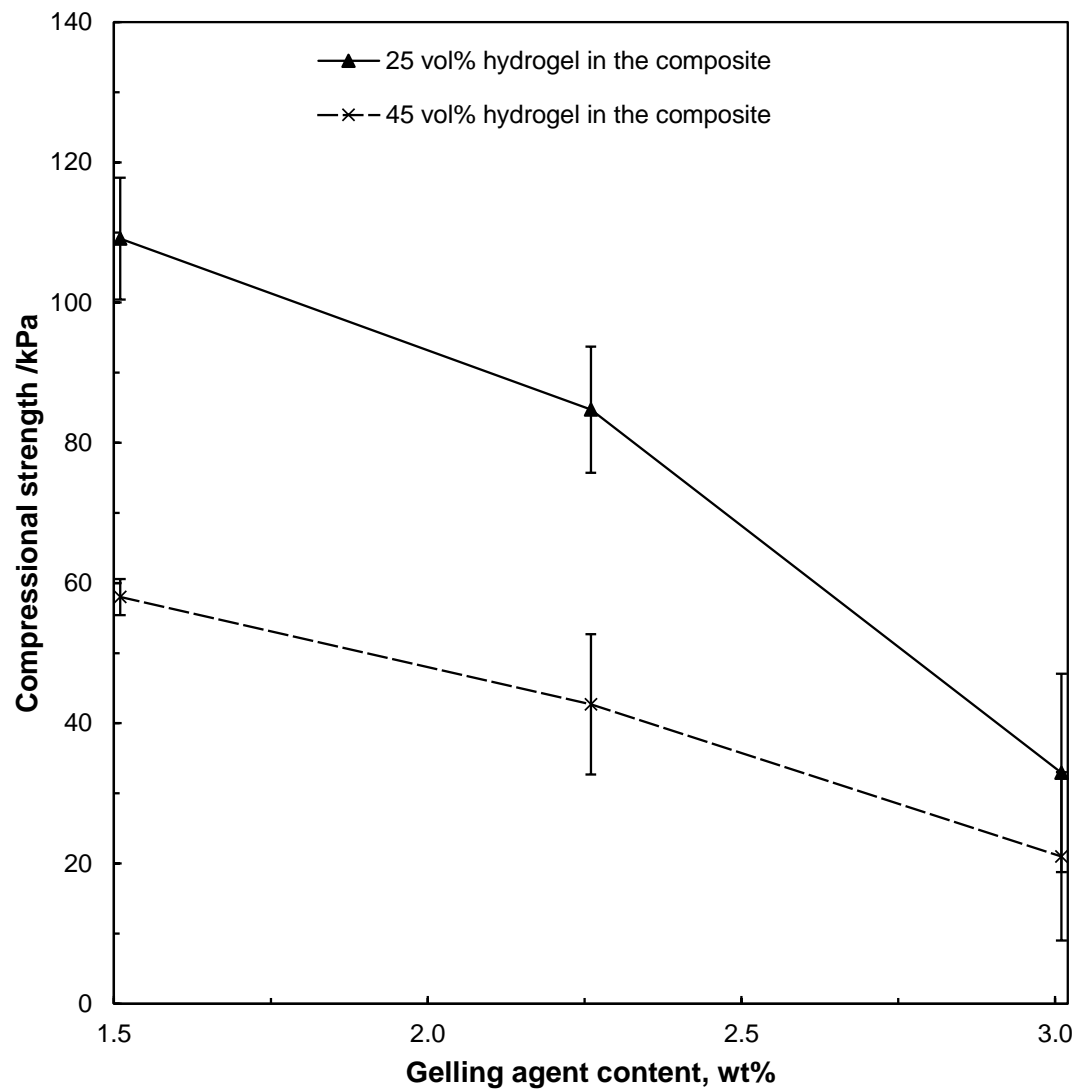


Figure 5.14. The compressional strength of the dried composites plotted for the three different gelling agent concentrations of κ -carrageenan (1.5, 2.25 and 3.0 wt%) at two hydrogel concentrations (25 and 45 vol%) of the total porous composite.

The compressional strength is plotted against hydrogel content in Figure 5.15 showing how the compressional strength varied with hydrogel content for the 1.5 wt% gelling agent content samples. Two different cooling methods after mixing the fat-salt base with the hydrogel were applied: chilling the samples at 6 °C for 4 hours and freezing the samples at -20 °C for 6 hours. In both of these cases, the samples were placed in a freeze-drier for a complete dehydration as a final step prior to their analysis. The frozen samples had a slightly higher compressional strength throughout the range of the hydrogel volume ratios used. This points towards the use of chilling procedure rather than freezing, however, the preparation procedure should be modified (i.e. less pressure used to compress the composites before the chilling process) so that the water within the hydrogel slurry would not be pressed out of the composites due to the partial syneresis of the composites.

Similarly, the effect to the strength of the sample due to the variation of freezing of the composites at -20 °C and at -196 °C was investigated. The dependence of the compressional strength against the hydrogel content is shown in Figure 5.16. The samples frozen in a freezer were in general easier to crumble, compared to those obtained by freezing in liquid nitrogen. This corresponds to the previous graph (Figure 5.15), where the lower temperature chilled samples were stronger as well. The sample containing 15 vol% hydrogel frozen in liquid nitrogen had the highest compressional strength among the analysed κ -carrageenan samples (170 kPa).

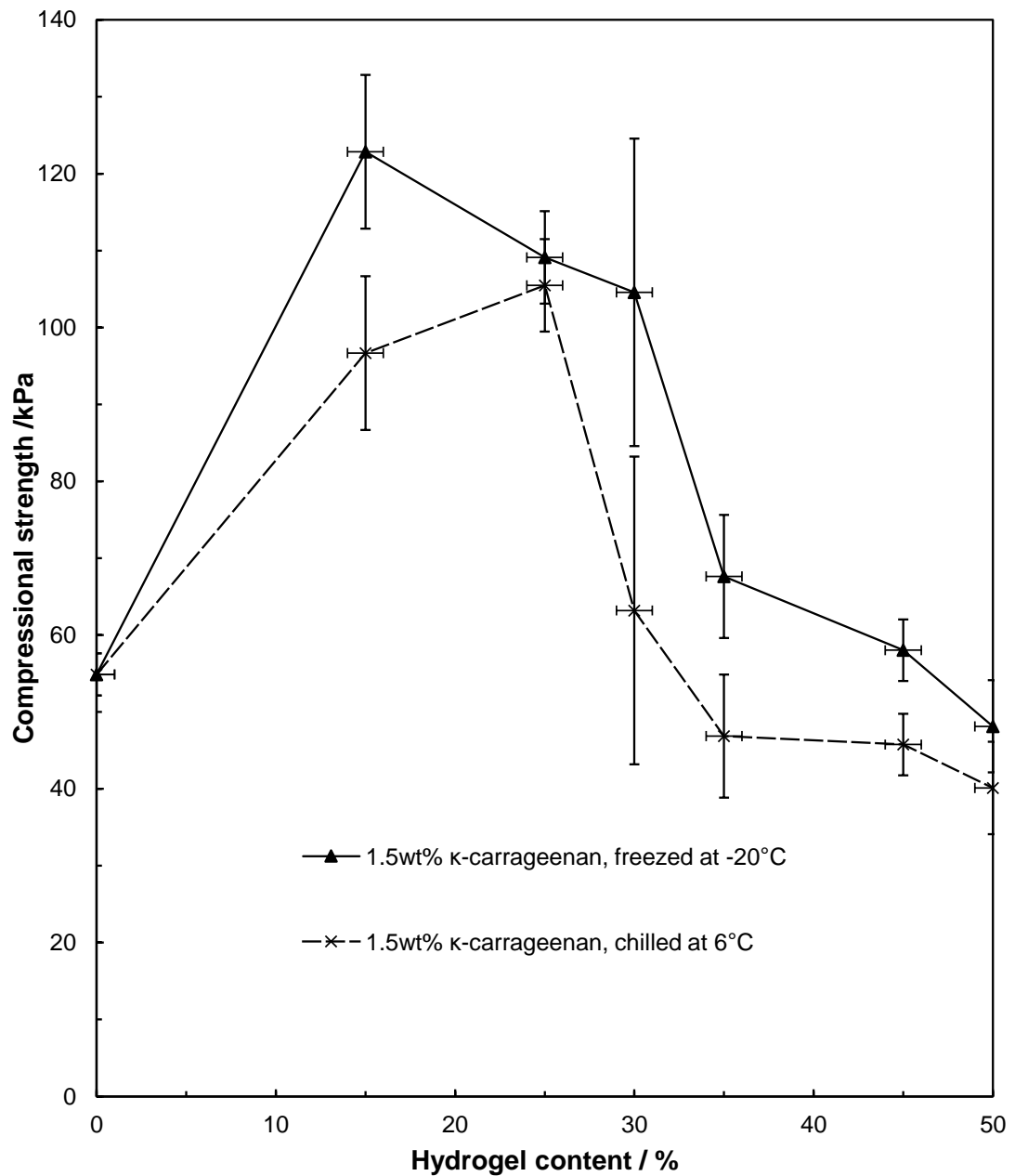


Figure 5.15. Graph comparing the effect of chilling and freezing of the sample for the compressional strength of the composites. The compressional strength of the dried composites is plotted against the hydrogel content within the composites. Gelling agent content within the κ -carrageenan hydrogel was kept as 1.5wt%.

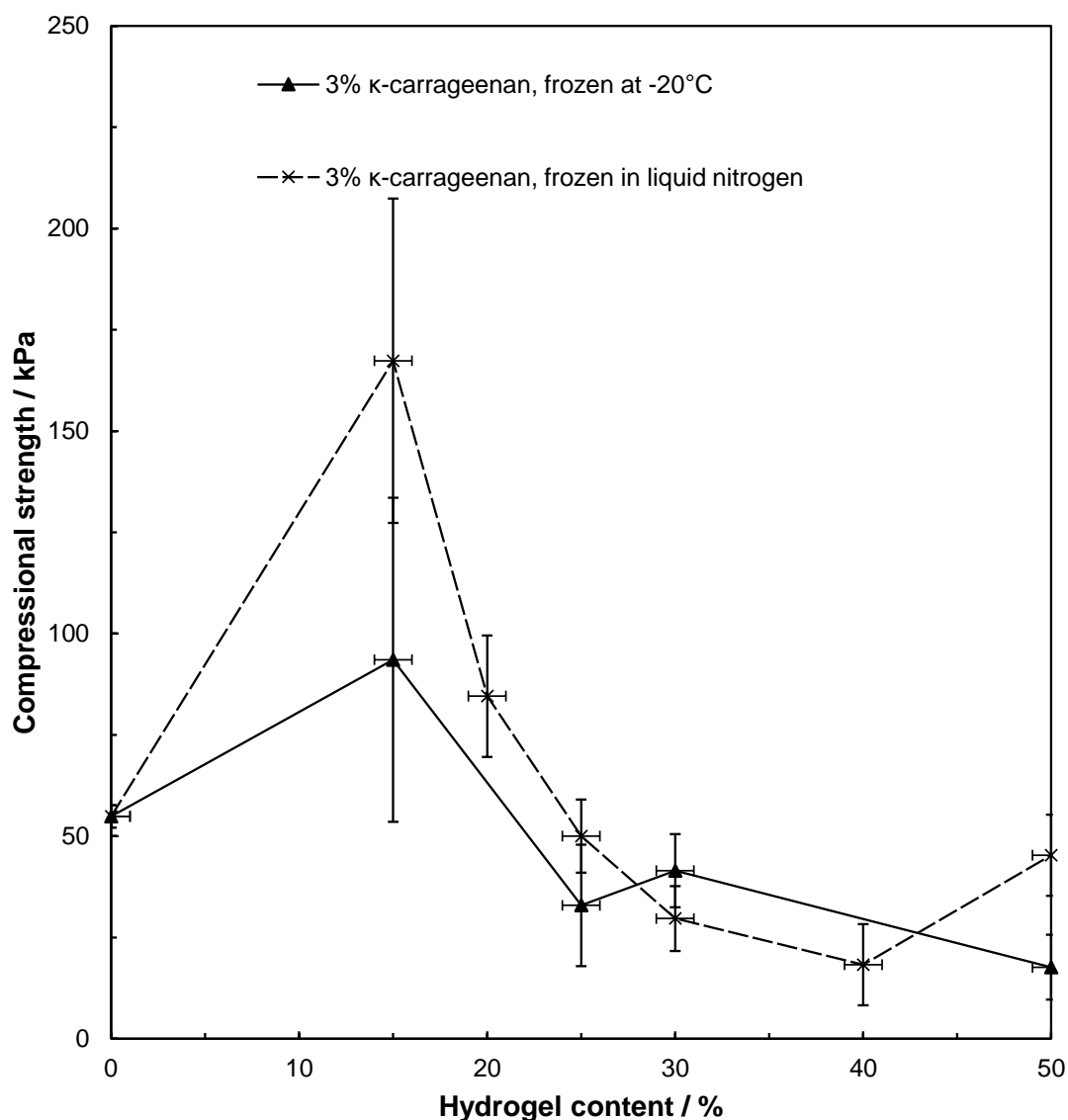


Figure 5.16. Graph comparing the effect of initial freezing in a freezer and freezing of the composites with liquid nitrogen for their compressional strength. The compressional strength of the dried composites is plotted against hydrogel content within the composites. Gelling agent content within the κ -carrageenan hydrogel was kept as 3.0wt%.

5.3.2.5 Dissolution Time of the κ -carrageenan Hydrogel Bead Slurry and Salt-Fat Composites

To measure the dissolution time of the samples, a method described previously was used. Typically, samples were placed in a cylindrical mesh and submerged into a stirred beaker (800 rpm) with water at 90 °C and the time to dissolve the samples completely was measured. Figure 5.17 shows the variation of the dissolution time as the gelling agent content was varied for 25 vol% and 40 vol% hydrogel content composites. From the graph it can be observed, that unlike for the compressional strength (where the higher gelling agent resulted in weaker samples) the samples dissolved slower with the increase in the gelling agent content, especially for the lower vol% of the hydrogel in the composite. However, same as in the Xanthan – Konjac case, as the hydrogel volume percentage was increased, the samples dissolved much faster. Comparing the Xanthan – Konjac with κ -carrageenan a much shorter dissolution time was measured for κ -carrageenan samples.

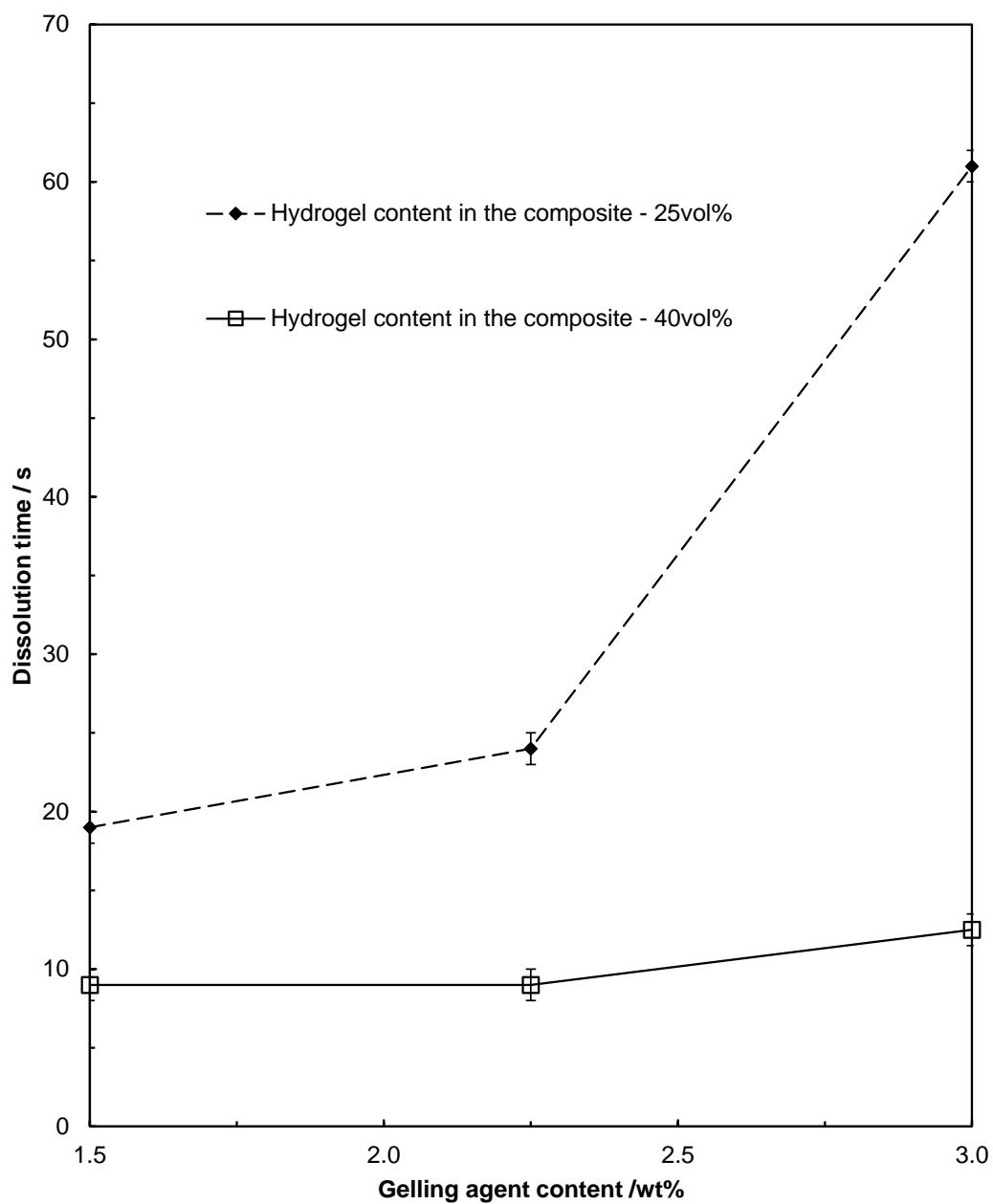


Figure 5.17. The dissolution time of the porous fat-salt composites at various gelling agent contents, for the 25 vol% and 40 vol% κ -carrageenan hydrogel content within the composites. Samples were exposed to stirred water at 90 °C at 800 rpm.

The influence of the gelling agent content to the composites throughout the hydrogel slurry volume content variation is shown in Figure 5.18, where it can be seen that the dissolution time variation of the 1.5 wt% and 3 wt% gelling agent content samples. It can be seen, that as the gelling concentration was increased, the dissolution time slightly increased for the samples where the hydrogel content within the composite was below 30 vol%, but did not change for both concentrations when the volume of hydrogel was higher than 30 vol%. For both gelling agent concentrations, where a low hydrogel slurry content was used (≤ 15 vol%), the composite dissolution time was around 15 times higher when compared to the higher hydrogel slurry content in the composites. This means that addition of the hydrogel (> 30 vol%) to the composites drastically reduces the dissolution time of the composites in hot water and could be useful in practical applications.

Figure 5.19 shows how the dissolution time of the composites changed upon different methods of cooling of the composites just after moulding them. One set of samples was placed in a fridge at $+6$ °C, whereas the other was placed in a freezer at -20 °C. Once the temperature of the samples was equilibrated, they were moved into a freeze-dryer. The dissolution time was shorter for samples with the hydrogel volume fraction below 20 vol% for the chilled samples, but above this volume fraction of the hydrogel the dissolution time became marginally longer for the chilled samples compared to the frozen ones. It can be concluded, that above 20 vol% of the hydrogel, the sample dissolution time was not much influenced by the cooling method, however was slightly shorter for the lower temperature method. This could be because of ice crystals, which were formed from the hydrogel in addition to the fat crystals. These created a solid structure that after evaporation produced a highly porous material, through which water could easily penetrate, disintegrate the structure both internally and externally. In addition to this, faster dissolution of the composites may be due to the freezing of the water within the hydrogel, which could have caused crack formation within the composite, as the tightly-packed beads were expanding.

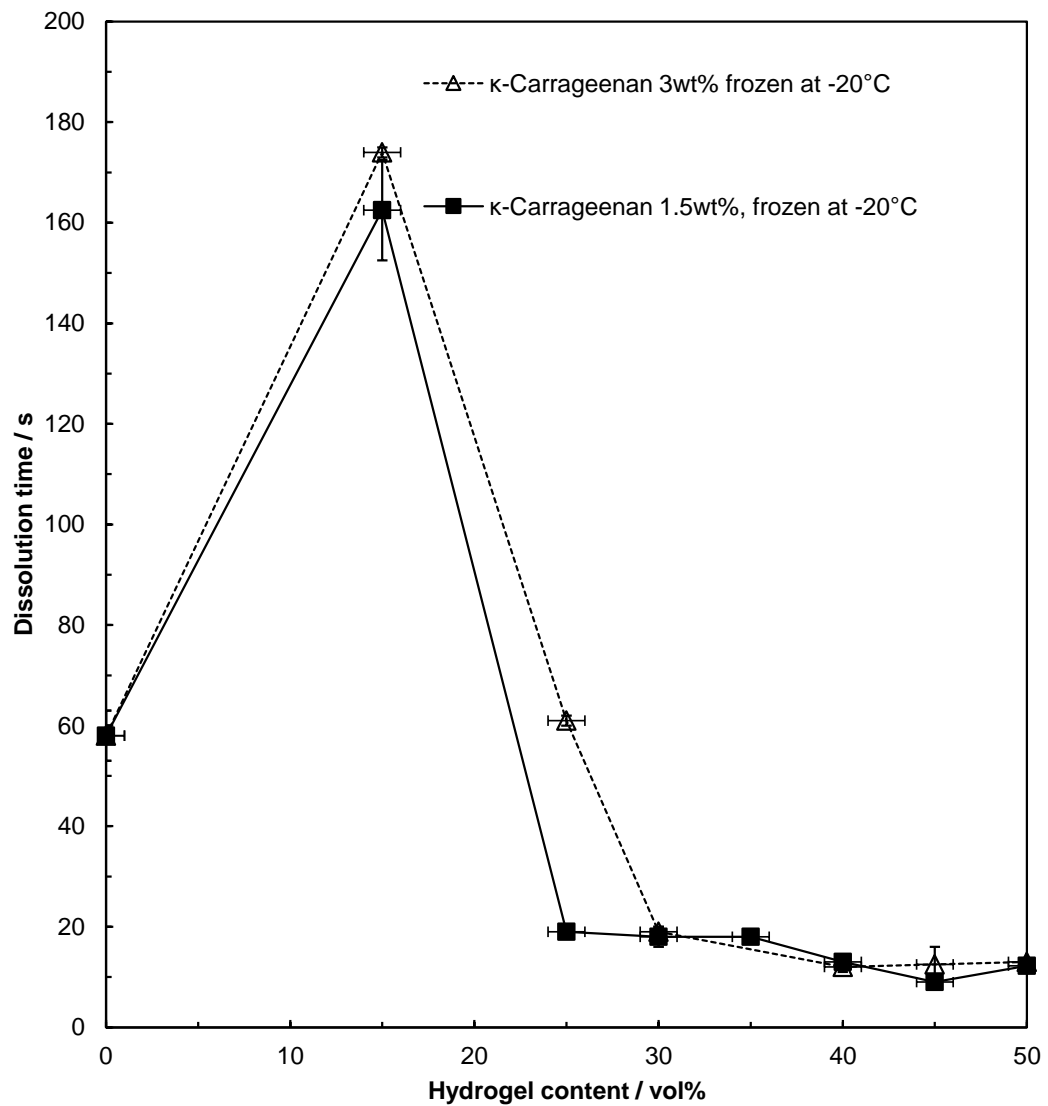


Figure 5.18. The effect of the gelling agent (κ -carrageenan) content on the dissolution time of the samples prepared by freezing both sets at $-20\text{ }^{\circ}\text{C}$ and only changing κ -carrageenan content.

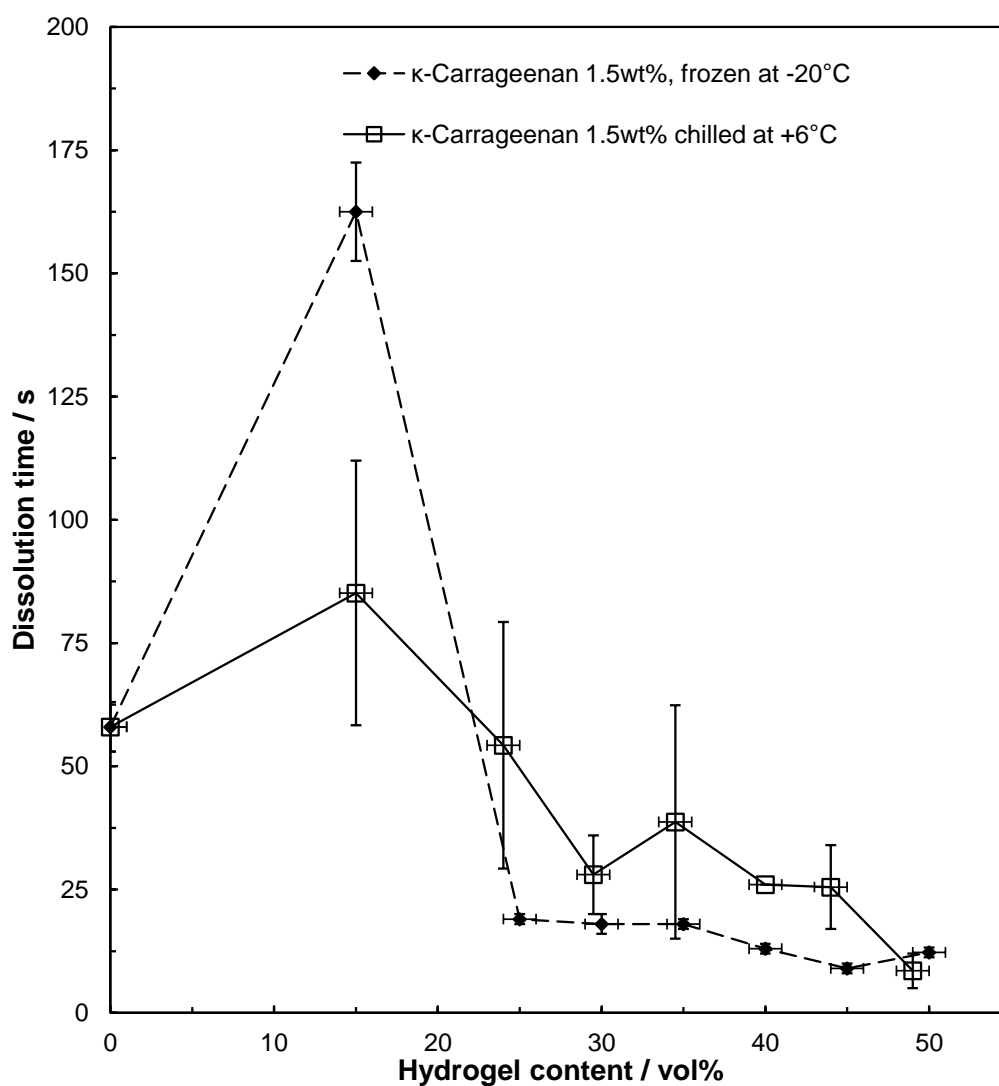


Figure 5.19. The dissolution time vs hydrogel content for the different methods of cooling the porous fat-salt composites just after mixing fat-salt phase with the hydrogel slurry. Chilling the composites in a fridge is compared with the freezing the samples in a freezer. Both sets were completed using 1.5 wt% gelling agent hydrogel. Error bars represent variation of the dissolution time, which was measured at least twice for each of the average point shown in the graph.

Figure 5.20 shows all the dissolution time data obtained for the κ -carrageenan hydrogel bead slurries templated with fat and salt base. In general, samples having hydrogel concentrations above 30 vol% dissolved in less than 30 seconds and the dissolution time increased as the gelling agent content was lowered. Also, in this graph the data of a set of samples, where smaller mincer plate pores (2mm instead 3mm) were used, is presented. A decrease in the dissolution time of the composites when the hydrogel slurry was prepared with smaller pore sizes of the mincer plate was observed, which corresponded to smaller pores within the composite. The faster dissolution could be caused by the higher capillary pressure effect caused by smaller pores leading to faster water penetration in the hot solution, thus faster disintegration of the porous composite.

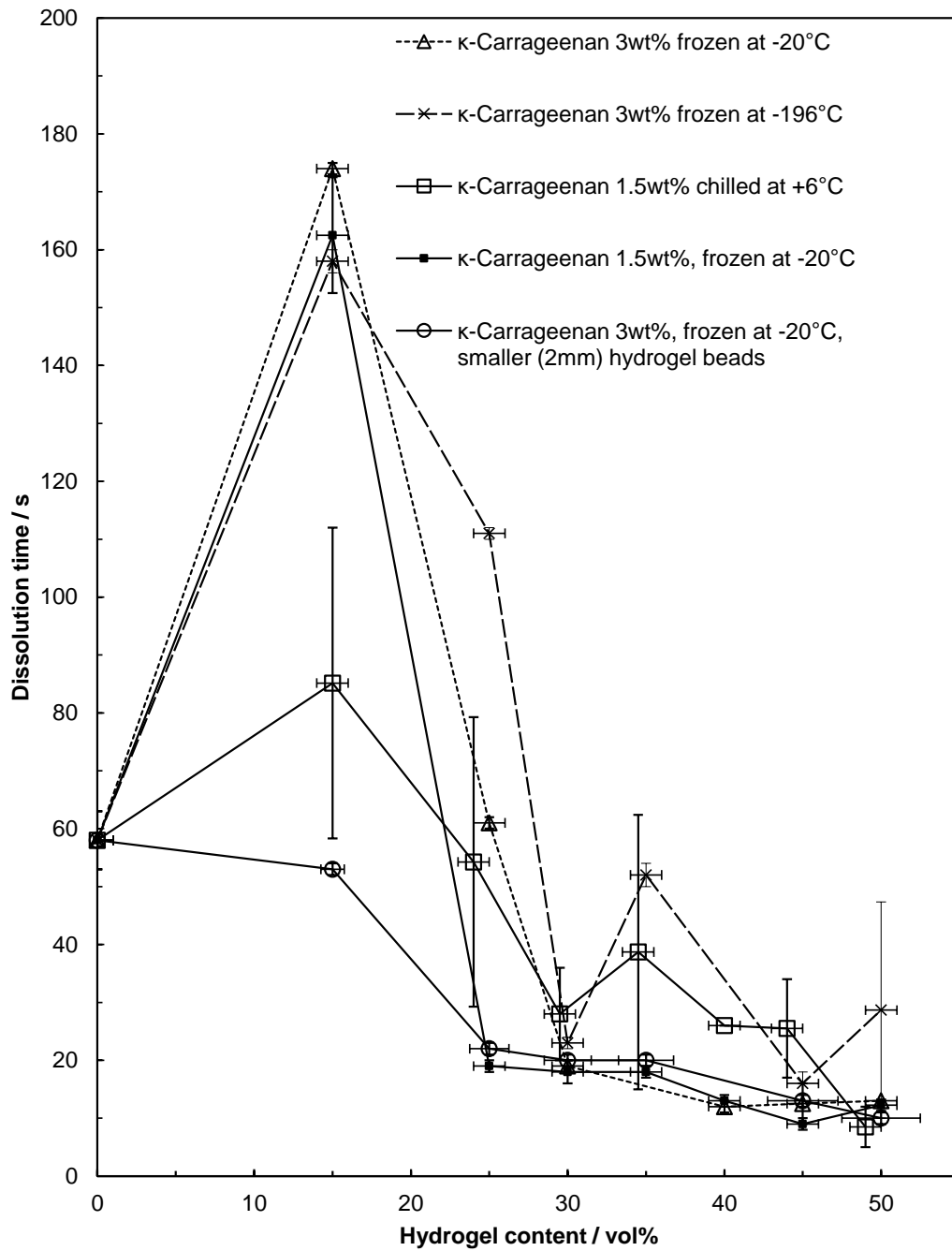


Figure 5.20. The dissolution time of different fat-salt – hydrogel slurry composites for the 1.5 wt%, 2.25 wt% and 3 wt% κ -carrageenan within the hydrogels. Samples were dissolved in a stirred beaker at 90 °C. Lines are guides to the eye.

5.3.3 Porous Fat - Salt Composites Prepared Without Freeze-Drying

In this experiment a composite with fat-salt base matrix and κ -carrageenan hydrogel bead slurry was frozen as described before, but instead of evaporating the hydrogel in a freeze-dryer, the composite was left on a piece of tissue at room temperature and open air for five days. The sample was photographed and an image is shown in Figure 5.21. Sample had not lost significant amount of the volume, compared to its freeze-dried equivalent. Future work will involve further analysis of the samples prepared this way, which could save energy costs related to freeze-drying of the porous bouillon cube formulations, as after the initial freezing of the sample it was dried at room temperature.



Figure 5.21. A photograph of a sample that was dried in open air at room temperature after freezing the sample at $-20\text{ }^{\circ}\text{C}$. The fat base was stained with Nile red and the hydrogel (1.5 wt% gelling agent, 50 vol% of the composite) with Fluorescein sodium salt.

5.4 CONCLUSIONS

The hydrogel slurry templating technique was successfully applied for the fabrication of porous foods in the form of porous bouillon cubes. The porosity of the composites

of fat-salt base with κ -carrageenan hydrogel slurry increased with increasing hydrogel content within the composites. Moreover, samples in most cases keep their volume and did not show significant, if any, shrinkage. The issue that should be taken into account in the formulation and the production of the composites is the need for fast moulding of the composites, while the composite is still a slurry, so that the syneresis of the hydrogel is not triggered after the mixing step with the fat-salt base. The fluorescence microscopy images of the composite slurry show a clear difference between the hydrogel beads and the fat base. This indicates that the hydrogel beads stay intact during the sample preparation. Similar conclusions can be drawn from the SEM images, which showed a likely deposit of the fat and salt on the evaporated hydrogel beads. Also, some of the dissolved salt recrystallising within the composite whilst the water was being evaporated was observed.

The compressional strength analysis of the composites showed that the strength of the composites was reduced with the increase in the hydrogel content. Comparing the strength of the composites to the control sample (with no hydrogel) a great reduction of the sample strength was recorded, which would make the product for the end user easier to crumble. The compressional strength of the composites compared to the previously reported Xanthan-Konjac hydrogel formulations was reduced as well. The density of the composites was decreased with the increase in the hydrogel content. For Xanthan – Konjac hydrogel system the decrease was linear, but for κ -carrageenan it did not follow linearity, as some of the water from the hydrogel was lost during the preparation of the composites and thus reduced the final volume of the composite.

The dissolution time of the composites was greatly reduced compared to the control samples. This was because water could penetrate easier through the open pore structure and disintegrate the sample not only from the outside moving inwards, but also simultaneously from the core of the composite. The reduced dissolution time also came from the κ -carrageenan hydrogel, which was easier to hydrate and which did not assist in binding the composite as well as the previous formulations based on the Xanthan/Konjac hydrogels.

The bead size of the hydrogel slurry had an influence to the composite properties. Careful formulation of the hydrogel slurry, so that the beads are monodisperse or a

particular size, could allow tuning the properties of the composites towards the ideal structure and texture. The size of the beads can be changed simply by changing the pore size of the mincer plate, multiple passes through the mincer, or alternative methods of spraying hydrogels could be designed and used. Finally, drying the composite in air or increasing the melting point of the fat could allow the use of oven drying. Alternatively, the beads could be left within the cubes and act as a filler and encapsulate flavours.

5.5 REFERENCES

1. F. Caponio, T. Gomes and M. T. Bilancia, *Journal of the Science of Food and Agriculture*, 2003, **83**, 1331.
2. M. Mariani, *Largo Consumo*, 1992, **12**, 42.
3. V. Kehlenbeck and S. Palzer. A Bouillon and/or Seasoning Tablet Containing Cereal, Vegetable and/or Fruit Fibers, *W. I. P. Organization*, 2007.
4. M. Koster and G. Van Dalen, Skyscan User Meeting, Brussels, Belgium, 2012.
5. R. M. Herreid and V. E. Lippert. Method for making fast dissolving bouillon cubes, *U. P. Office*, 2000, US6126979 A.
6. S. Gupta and P. Bongers, *Chemical Engineering and Processing: Process Intensification*, 2011, **50**, 9.
7. S. Gupta. Process to prepare seasoning cubes, *W. I. P. Organization*, 2009.
8. G. Achterkamp, J. Doyle and M. Gehrman. Marbled Bouillon, Broth, Soup, Sauce or Seasoning Cube and Process for Preparing the Same, *E. P. Office*, 2004.
9. M. H. M. Baggen and R. F. Kellerman. Bouillon or Seasoning Concentrate and Process for Preparing the Same, *EPA*, 2011.
10. K. Okada. High quality dried bouillon and methods for preparation thereof, *U. P. Office*, 2004, US20040005397 A1.
11. E. Weisser, J. J. Kasica and M. K. Okoniewska. Starch hydrolysis products for size enlargement, *U. P. Office*, 2005, US20070054027.
12. H. E. Smorenburg and T. Yamson. Fortified Bouillon Cube, *W. I. P. Organization*, 2009.
13. J. B. Hutchings and P. J. Lillford, *Journal of Texture Studies*, 1988, **19**, 103.
14. C. Inoue, S. Silva Paes, M. E. Perrine, A. K. Popp, et al. Savoury Food Concentrate, *U. P. Office*, 2011.
15. *Chemical & Engineering News Archive*, 1944, **22**, 1432.
16. P. Williams, D. Day, M. Langdon, G. Phillips, et al., *Food Hydrocolloids*, 1991, **4**, 489.
17. J. L. Vickery, A. J. Patil and S. Mann, *Advanced Materials*, 2009, **21**, 2180.

Chapter 6. Development of Hollow-Shell Salt Marbles Using Spray-Gelation and Drying Technique

“It's important to have a plan, a big picture. You can deviate from it or change it completely, but it gives you something to work for.”

Shannon Miller, Gymnast

This Chapter focuses on a method of production of hollow-shell particles, which are templated over hydrogel beads and the shell is finely milled salt. The core is further dried-up to yield a hollow-shell structure. This essentially is a modification of the previously described hydrogel bead templating technology aimed to reduce the amount of the table salt intake without reduction in saltiness of the food. After evaporation of the water from the hydrogel a shell of finely milled salt is produced and the end consumer benefits from a faster release of salt, yet a lower overall amount of salt is used in this way. Apart from the methodology, electronic microscopy images of the marbles are presented, the size distributions and dissolution time of the marbles analysed and discussed.

6.1 INTRODUCTION TO THE HEALTH ISSUES RELATED TO THE USE OF TABLE SALT

Salt intake from consumption of processed foods is currently above the recommended doses, US having a particularly high usage of salt. Recommendations not to exceed 5.8 g of salt per day were established by the departments of Agriculture and Health and Human Services with an even lower target of 3.7 g for those above 40 years old, blacks and persons with hypertension.¹ However, it was found that an average American man and woman between 2005 and 2006 had consumed 10.4 g and 7.3 g of salt per day respectively.² Within the UK, the figures were somewhat similar with an

average salt intake of 8.6 g per day in 2008.³ High salt intake causes many health issues in the modern World, typically hypertension, increase in the risk of stroke and others. Reduction in dietary salt leads to lower blood pressure and reduction in the risk of developing a cardiovascular disease.⁴

Reduction of salt was recently acknowledged by Unilever as a key challenge. According to the Unilever Sustainable Living Plan Report, 2011: “The scientific and marketing challenges of reducing salt are complex” and three possible approaches were suggested: “we find alternative to sodium salts; we reformulate with herbs, spices and other ingredients <...> for a salty flavour; we gradually wean the consumer off the taste of salt by reducing levels slowly over time”, showing that reduction of salt for Unilever is one of the main priorities.⁵

Various methods of salt reduction have been described in the literature. For example, sodium chloride reduction in bread dough was achieved by simply reducing or eliminating salt,⁶ replacing sodium salt with potassium and magnesium,⁷ reducing salt over long (three years) periods of time,⁸ but all these methods showed that the salt reduction come with either the loss of taste in the baked bread, loss of strength of the dough or only a limited amount of salt reduction (up to a quarter) could be achieved. In a different study it was noticed that delivering a salty solution to the tongue between intervals when normal water is passed gives a more salty taste compared to this salt solution first mixed with water (essentially diluted) and then passed through the tongue for the same time.⁹ This alternating delivery of sodium ions enhances saltiness perception for humans, meaning that faster dissolution of salt on a tongue should enhance the saltiness feeling. Also, inhomogeneous salt distribution within a particular food enhances the saltiness (up to 117%), as was shown with bread where layers of salty and non-salty dough were baked as one loaf with an average saltiness lowered.¹⁰
¹¹ One could elaborate on this knowledge and build porous or hollow crystals of salt, in order to eliminate the core, which takes long time to dissolve and does not lead to a sharp increase in the ionic conductivity over a short period of chewing time.

Liquid marbles were first described in a patent in 1968 and only in 2001 as a scientific paper.^{12, 13} The concept of liquid marbles has been extensively investigated in the recent years, where water (or oil) droplets were stabilised with hydrophobic

particles,¹⁴⁻¹⁷ as well as hydrophilic particles,¹⁸ producing non-stick droplets of liquid. Liquid marbles may be produced by rolling liquid droplets over a hydrophobic particle bed, where these particles are picked up by the droplets essentially encapsulating them by forming a shell around the drops.¹⁹ These marbles are valued for their low friction while moving the droplets, i.e. the droplets coated with particles can typically reach speeds of 100-1000 times faster than uncoated droplets, which is beneficial in the microfluidic devices, as well as in such cases where low temperature of the liquid and high viscosity is required, e.g. conservation of biological specimens.¹⁹ Smaller particles of the marble shell have been reported to come into contact with the liquid, whereas the larger ones tend to form the outer layers of the liquid marbles.²⁰ Marbles with their interface coated with hydrophobic model drug particles have been dried and their structure showed a hollow core as determined by X-ray tomography.²¹ Specifically designed liquid marbles have been shown to have HCl and NH₃ sensing capabilities.¹⁷ Substituting the liquid phase with a hydrogel and replacing the hydrophobic particles with salt crystals would allow to produce so called *salt marbles*.

Recently, researchers in Nottingham have developed hollow-shell sodium bicarbonate and separately salt particles using a different technique.^{22, 23} These particles were produced by first dissolving a gelling agent (e.g. Carboxymethyl cellulose or Gum Arabic) in water and then also dissolving a particular salt in the same solution. To produce the hollow-shell particles, these solutions were spray-dried. Typical samples can be seen in Figure 6.1. Thus, the production of these particles is significantly different from the production of liquid marbles or the production of salt marbles described in this Chapter.

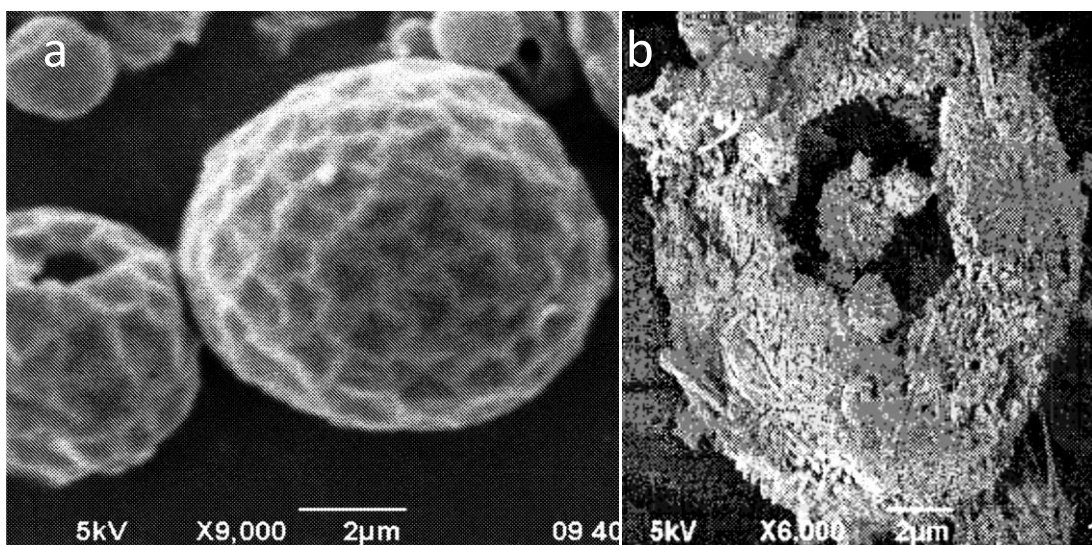


Figure 6.1. SEM images of hollow-shell particles of (a) sodium bicarbonate and (b) table salt. Reproduced from Minter et al.^{21, 22}

6.2 PREPARATION OF HOLLOW-SHELL SALT MARBLES

In the previous Chapters the hydrogel bead slurry templating technique was used to make porous composite materials by replacing part of a material with hydrogel beads and later evaporating the water. The amount of the matrix material was reduced by filling the composite volume with air and the results were extensively discussed. The technique was shown to be capable to reduce the density of cement, PDMS and fats in different products. Here a similar technique was used to reduce the salt content within the table salt. A hot hydrogel solution was sprayed down a cold column and gelled before landing on a finely milled salt particles, where the particles attach to the surface of the hydrogel beads, similarly as in the production of liquid marbles (see Figure 6.2). The water from the hydrogel beads was then removed by drying the marbles, leaving a cavity within a salt coated particle. The salt microcrystals on the surface are held together partially by the residual gelling agent and by a partial dissolution and re-crystallisation of the crystals in contact with the hydrogel surface. The amount of the salt would be reduced per unit volume, compared to the ordinary table salt, and the time of the dissolution of the salt content of the marble was shortened. This shorter dissolution time results in a steeper change of ionic strength and essentially a more salty perception for the consumer with the same amount of the sodium chloride used, since the sensitivity to salt on the tongue is enhanced by a high momentarily concentration of sodium chloride ions, rather than the overall mass of salt taken.⁹

The detailed methodology of preparation of the porous salt marbles was described in Chapter 2 Section 2.3.3. Here a summary of the equipment and technique used for the first time (to our best knowledge) will be given. A hot solution containing a hydrated gelling agent above the solution gelling temperature was sprayed down a chilled column. A tray with pre-milled table salt (particle size <300 μm) was placed at the bottom of the tube and after a required volume of hydrogel was delivered the tray was shaken to ensure the full coverage of the hydrogel beads with the salt particles shown in Figure 6.2.

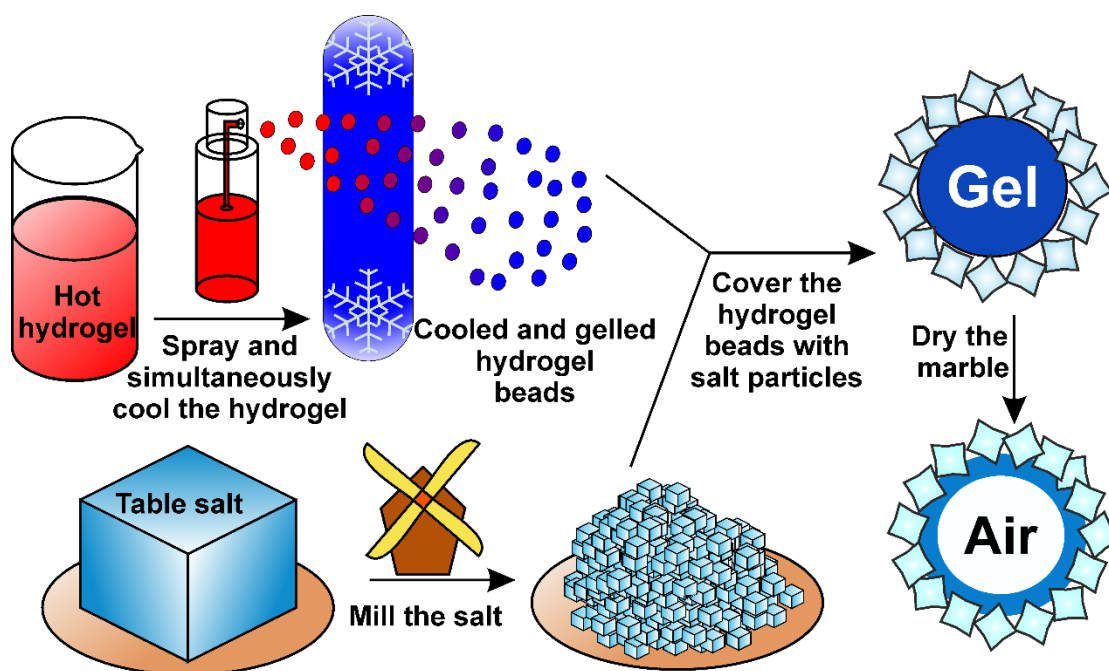


Figure 6.2. Schematic representation of the method used to produce porous salt marbles. A hot hydrogel solution was atomized by a stream of compressed air, producing droplets of hydrogel, which were subjected to a chilled column, where the droplets gelled before reaching a surface in the bottom of the column with finely milled salt crystals. As the salt bed was vibrated, a layer of salt crystals was deposited on the hydrogel beads. These were then removed and dried, producing porous salt marbles, with a hollow-shell structure.

6.3 RESULTS

6.3.1 Porous Salt Marble Size Analysis

The salt marbles were imaged with a digital camera (see Figure 6.3) prior to drying at 50 °C for 2 days. The size of the produced salt marbles was polydisperse, and a sieving step was introduced to separate the different size fractions of the marbles, which are shown in Figure 6.3. Alternatively, a less polydisperse production of the hydrogel beads should be introduced, for example an industrial or laboratory scale atomizer should be used for the viscous hydrogel solution bead preparation and an efficient spray of droplets of size <math><100 \mu\text{m}</math>. It was observed that as the gelling agent concentration exceeded 1.2 wt% for Xanthan-Konjac, the sprayer became incapable to separate the stream of hydrogel into individual droplets, producing a jet of a

hydrogel, which yielded a higher salt marble mean size, polydispersity and potentially a thicker salt deposit layer on the marbles surface.

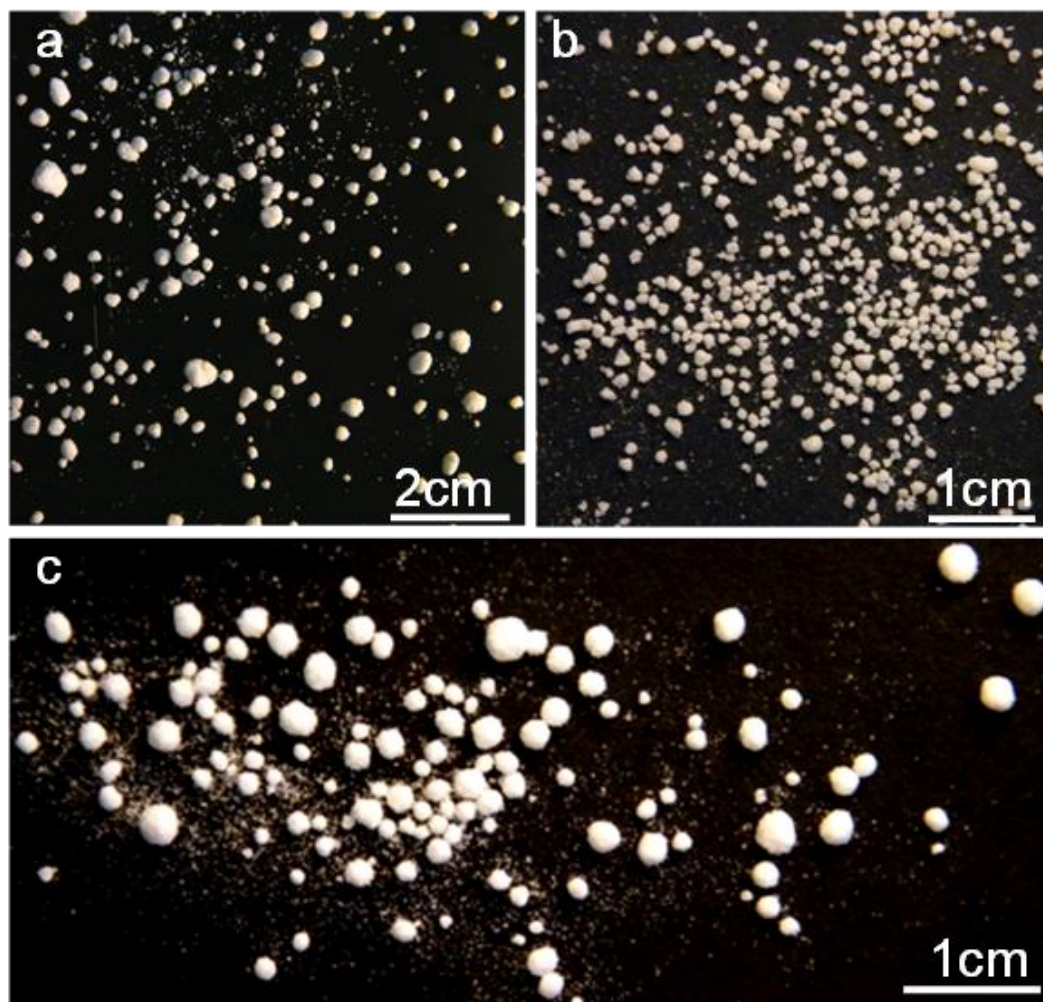


Figure 6.3. Photographs of salt marbles produced from (a) 3 wt% and (b) 1.5 wt% κ -carrageenan, (c) 0.5 wt% Xanthan-Konjac hydrogel.

As the gelling agent content within the hydrogels was increased, the viscosity of the hot hydrogel solution also increased. This changed the size distribution of the produced atomized drops of the hydrogel, changing the size of the produced salt marbles. Salt-gel marbles with different gelling agent concentrations within the hydrogels were prepared and analysed. The salt-gel marble size was analysed using photographs and image analysis software. The results are shown in Figure 6.4 and Figure 6.5 below for the samples with Xanthan-Konjac and κ -carrageenan hydrogels respectively. A broad size distribution was observed in the majority of the samples

analysed, especially as the amount of the gelling agent was increased. This could be tackled by using a more robust solution atomization technique. The mean size of the marbles was around $600 \pm 200\mu\text{m}$ for both κ -carrageenan and Xanthan-Konjac hydrogel salt marbles, varying slightly due to the different gelling agent concentrations used. The size of the marbles produced after drying of the hydrogel cores was not within the typical size of the table salt crystals ($280 \pm 100 \mu\text{m}$ in this case), which varies according to the preparation and grinding techniques, but would be within the range of sea salt crystals.

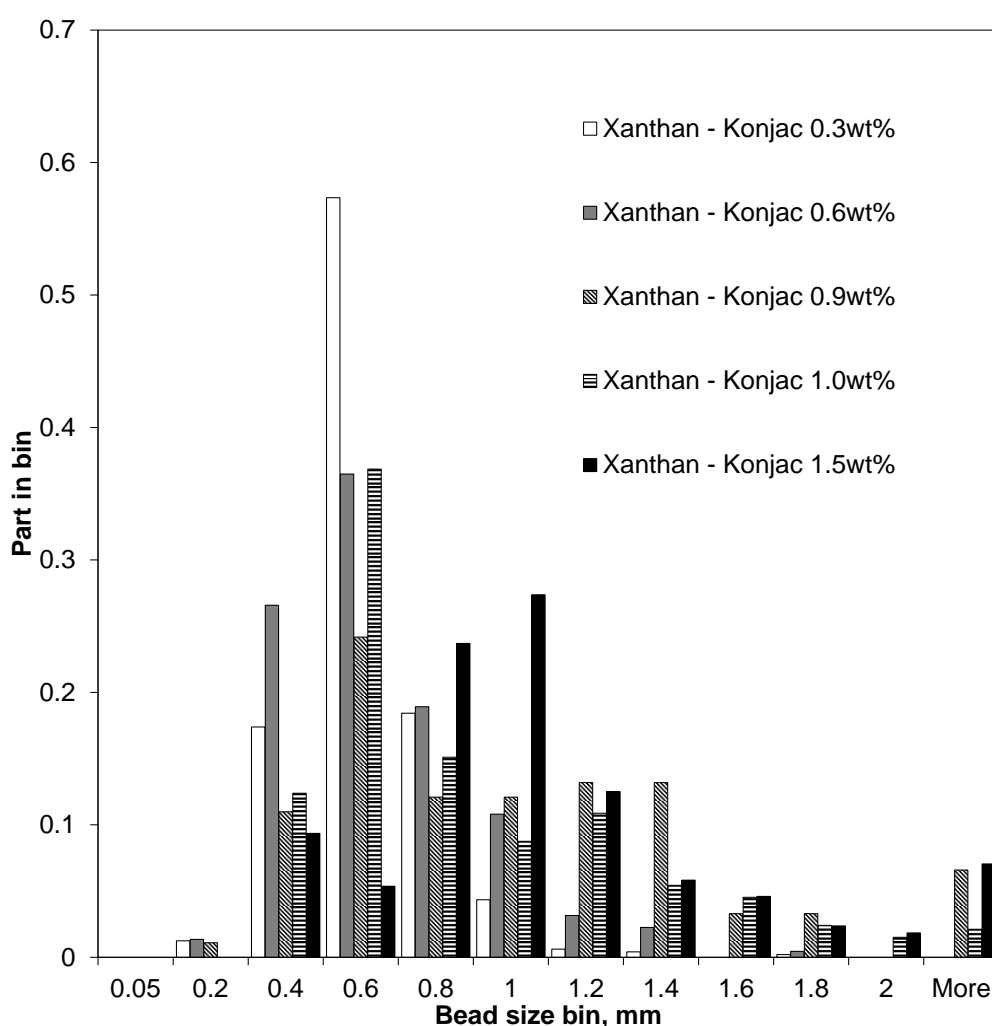


Figure 6.4. Graph showing salt marble size distribution diagram for samples where Xanthan – Konjac hydrogel was used as the core of the marble. For the gelling agent and its content refer to the legend. The columns of the histogram represent the size range of the x-axis between the numbers.

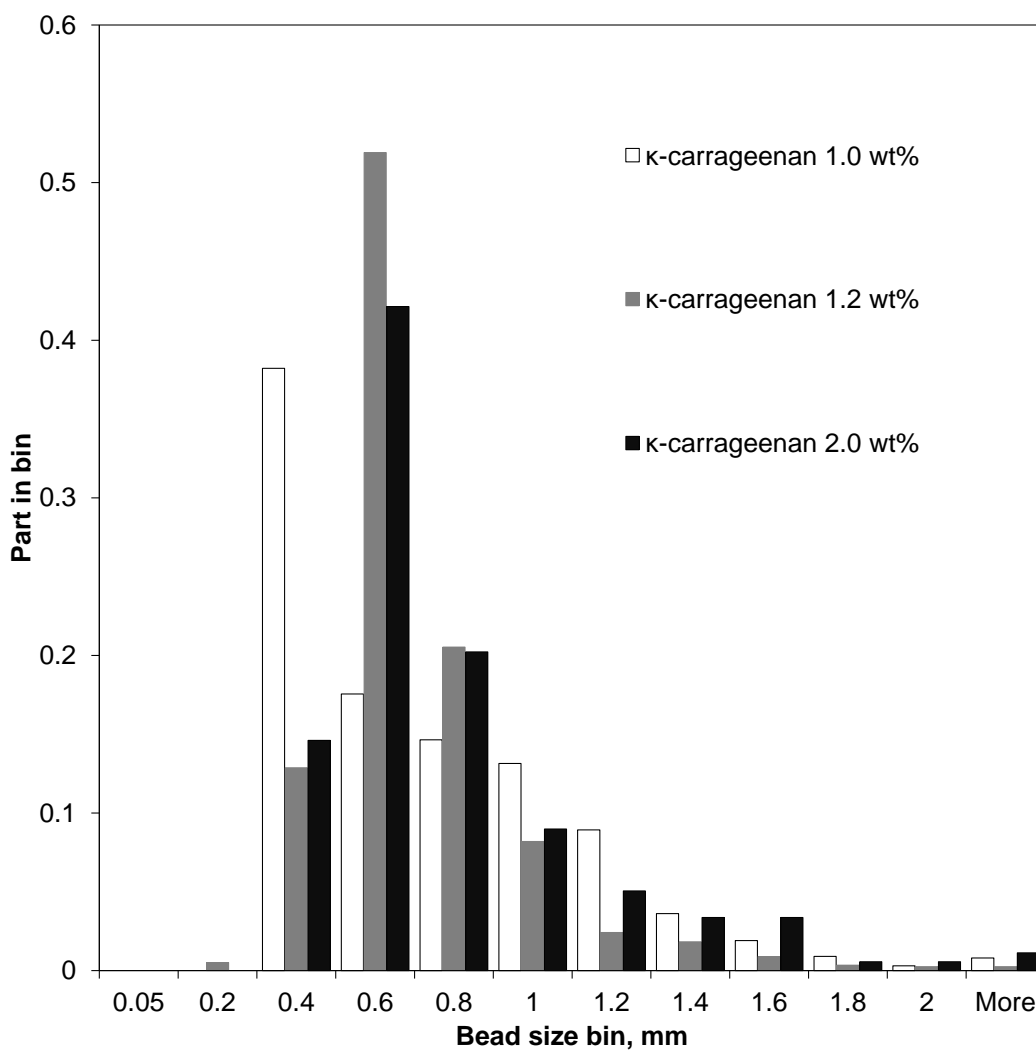


Figure 6.5. Graph showing salt marble size distribution diagram for samples where κ -carrageenan hydrogel was used as the core of the marble. For the gelling agent content refer to the legend. The columns of the histogram represent the size range of the x-axis between the numbers.

6.3.2 SEM Analysis of the Hollow-Shell Salt-Hydrogel Marbles

The SEM images are shown in Figure 6.6 and Figure 6.7 below. Some of the marbles show a layer of the dried gelling agent within the inner part of the salt layer (walls of the core) after drying. This was typical for Xanthan-Konjac hydrogels, which have film forming properties upon mixing with other hydrogels.^{24, 25} Such residue could be used to encapsulate flavours or taste enhancing compounds as they are first introduced into the hydrogel solution. This would give an additional taste for the salt and an additional way to make the final product more attractive to the customer.

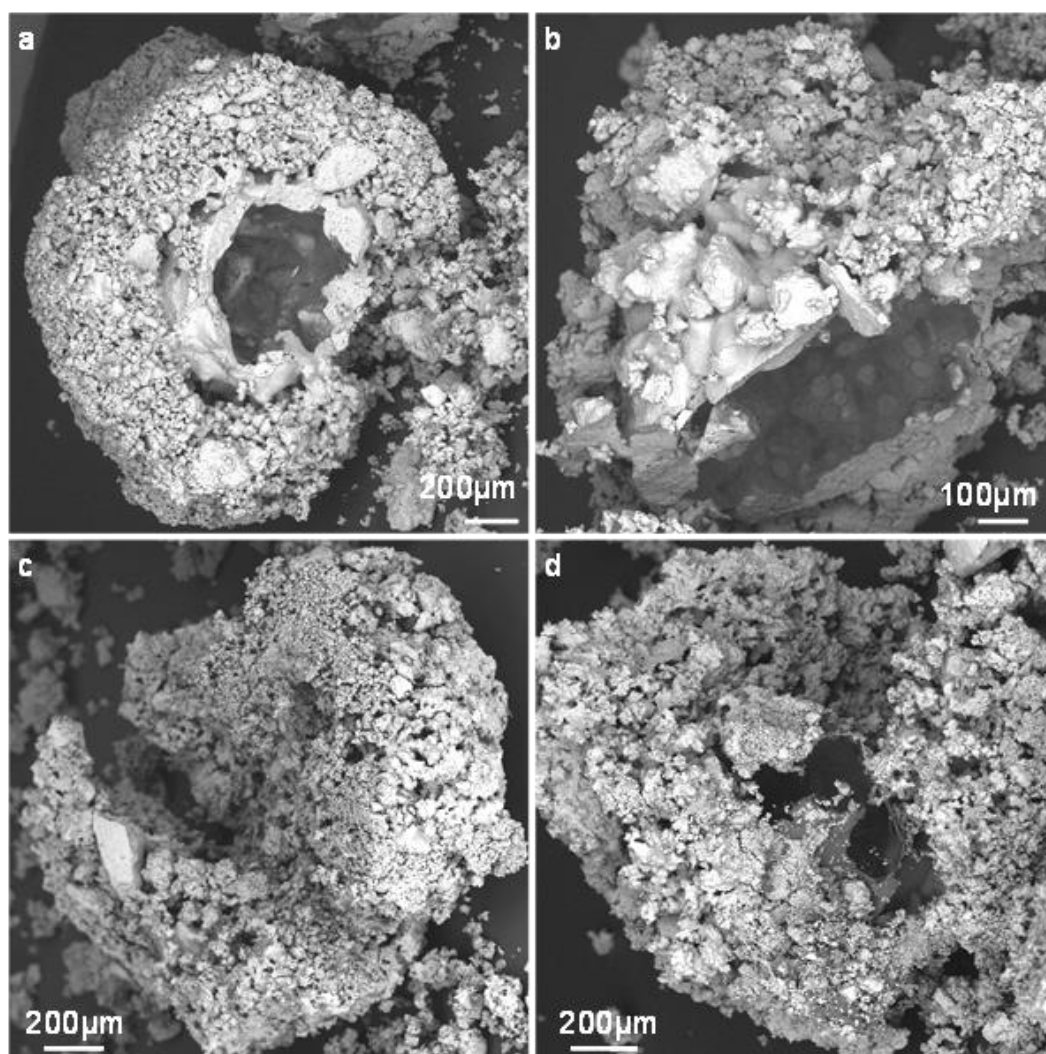


Figure 6.6. SEM images of salt marbles produced with 1.0 wt% Xanthan-Konjac hydrogel beads. (a-b) column surface temp. $\sim 6^{\circ}\text{C}$, (c-d) column temp. $\sim 1^{\circ}\text{C}$. Samples have been cracked open with a scalper whilst on the SEM grid. Larger marbles were selected for the analysis due to the easier sample preparation.

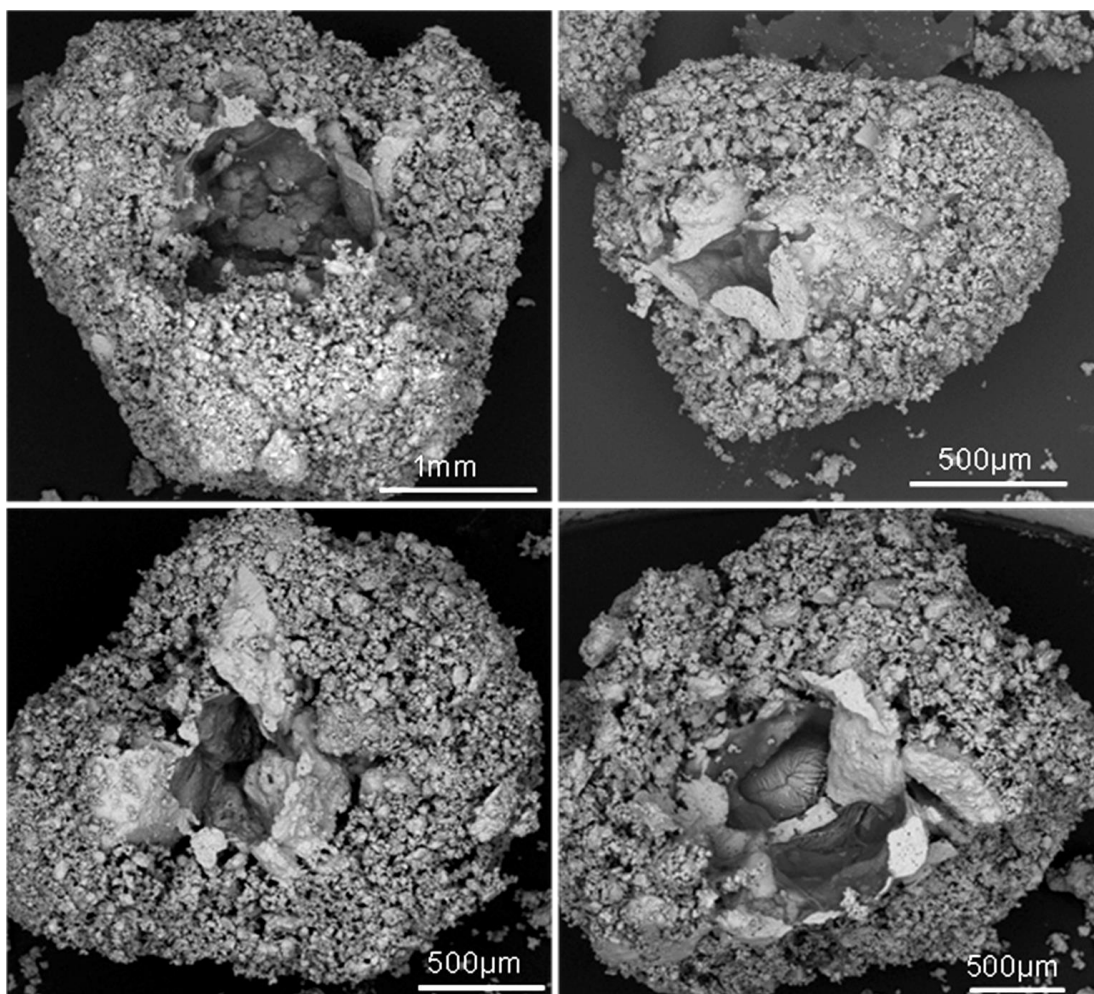


Figure 6.7. SEM images showing salt marbles produced by spraying hot 0.5 wt% Xanthan-Konjac hydrogel. Samples have been cracked open with a scalper whilst on the SEM grid. Larger marbles were selected for the analysis due to the easier sample preparation.

If the hydrogel was not fully gelled upon contact with salt particles, it did not form marbles, but produced salt granules instead (a continuous core of salt, e.g. Figure 6.6c), as shown in Figure 6.8. This was likely to be caused by the hydrogel syneresis, when water was leaked out of the hydrogel, thus removing the hydrogel core and making the salt deposit layer much thicker. One way to reduce this effect could be by increasing the gelling agent content within the hydrogel. This would make the hydrogel stronger and less likely to release water through syneresis. Another way to tackle the granulation process in the marble production could be addition of some salt to the hydrogel in order to balance the osmotic pressure between the hydrogel core and the surface, which was in contact with salt crystals. Also, the hydrogel could be cooled to near-freezing temperatures before coming in contact with salt crystals and then freeze-dried. The water in this case would be physically captured within the core and should be able not to wet excessive amounts of salt crystals, thus keeping the thickness of the salt shell low.

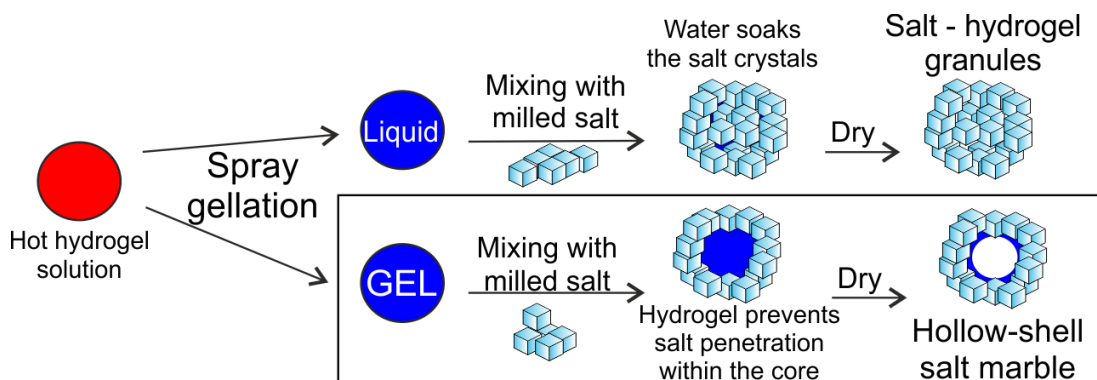


Figure 6.8. The process and the possible outcomes of the spray gelation technique for the fabrication of porous salt marbles. Top mechanism shows production of the salt granules, where water from the solution attracted the salt particles to form salt granules throughout the drop, due to the drop of the hydrogel being not fully gelled at the time of contact with the particle of milled salt. The bottom example shows a successful procedure for the preparation of the salt marbles, where a gel is formed before mixing with the milled salt step, thus salt crystals cannot penetrate to the core of the particle and instead form a shell. The water from the hydrogel was removed upon drying, thus producing a porous salt marble. The colours represent temperature. “Liquid” means cold, but not fully gelled solution of a hydrogel.

6.3.3 Salt-hydrogel Marble Taste Testing: Measuring Ionic Conductivity Change upon Dissolution

This experiment aimed to test the rate of release of salt from the marbles. Instead of tasting the samples, an experiment was designed, where the salt marbles were added to a fixed amount of water and the conductivity was measured over a period of time. First, the conditions of the stirrer bar rotation were set using a control sample (table salt). The conductivity was measured of a set amount of salt in a set volume of water, for different speeds of agitation.

Samples of table salt (0.2500 ± 0.0004 g) were placed into a beaker with distilled water (50 cm^3), so that $[\text{NaCl}]_{\text{final}} = 0.08696 \text{ M}$, or weight fraction (ω) $\omega_{\text{NaCl}} = 0.005$. In the first experiment, salt was allowed to dissolve on its own, without agitation, which was followed by experiments where a magnetic stirrer was stirred at various rotation speeds (50-200 rpm) (control experiments). The conductivity was measured as a function of the time elapsed from adding the salt to the water and plotted as a function of the time elapsed from adding the salt to the water and plotted in Figure 6.9. From this data, the optimum stirring speed was selected (60 rpm) and the experiment was repeated three times to determine the standard error of these measurements.

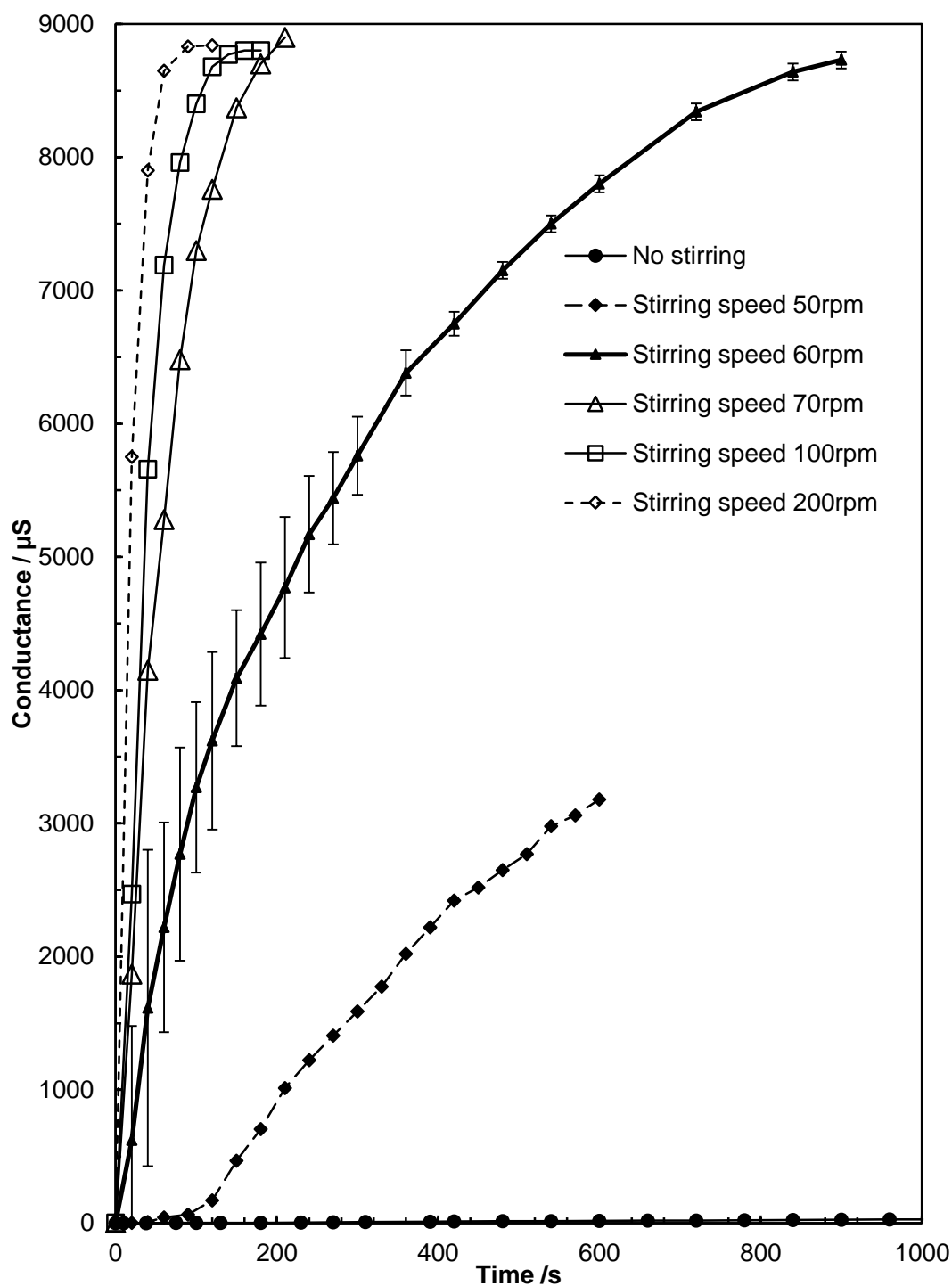


Figure 6.9. Conductivity of the aqueous medium vs time followed the introduction of a fixed amount (0.2500 g) of table salt to determine the optimum speed of stirring for the future analysis. From this data, the optimum stirring speed was selected (60 rpm) and the experiment was repeated three times to measure the standard error.

As a comparison, the salt marbles were added to water following the same procedure and the conductivity was plotted in Figure 6.10. This graph shows a more rapid increase in the conductivity of the salt marble solution compared to the table salt. This graph also shows the conductivity of the milled dried salt (particle size $30 \pm 20 \mu\text{m}$), used to produce the marbles. The difference in the conductivity of the pre-milled salt solution and the porous salt marble samples upon dissolution was low, the former having a slightly higher conductivity due to the crystals being loose rather than trapped on the surface of a marble. Also, as the gelling agent concentration was increased within the hydrogels, the conductivity seemed to change more rapidly, suggesting that these samples would feel saltier for the consumer. Another graph was plotted to show the conductivity of salt marbles after 40 s since the start of their dissolution and is presented in Figure 6.11. The conductivity of the marbles was higher at this time point of the dissolution experiment, compared to the unmilled table salt ($280 \pm 100 \mu\text{m}$). This allows to speculate that the taste of the saltiness would be stronger, as the concentration of the dissolved salt ions on the consumer tongue would be higher at the same time after start of the consumption of the product. Looking at this result from other side, a smaller amount of sodium chloride would be required to trigger the same saltiness effect, which would reduce the total amount of salt used for a particular seasoning.

Both κ -carrageenan and Xanthan-Konjac hydrogel formulations could be used in the production of the marbles for food grade products, providing a satisfactory level of flavour encapsulation. The marbles should have consumer evaluation analysis experiments before commercial production. It may be interesting to test both compositions for saltiness in future studies employing a double blinded experiment.

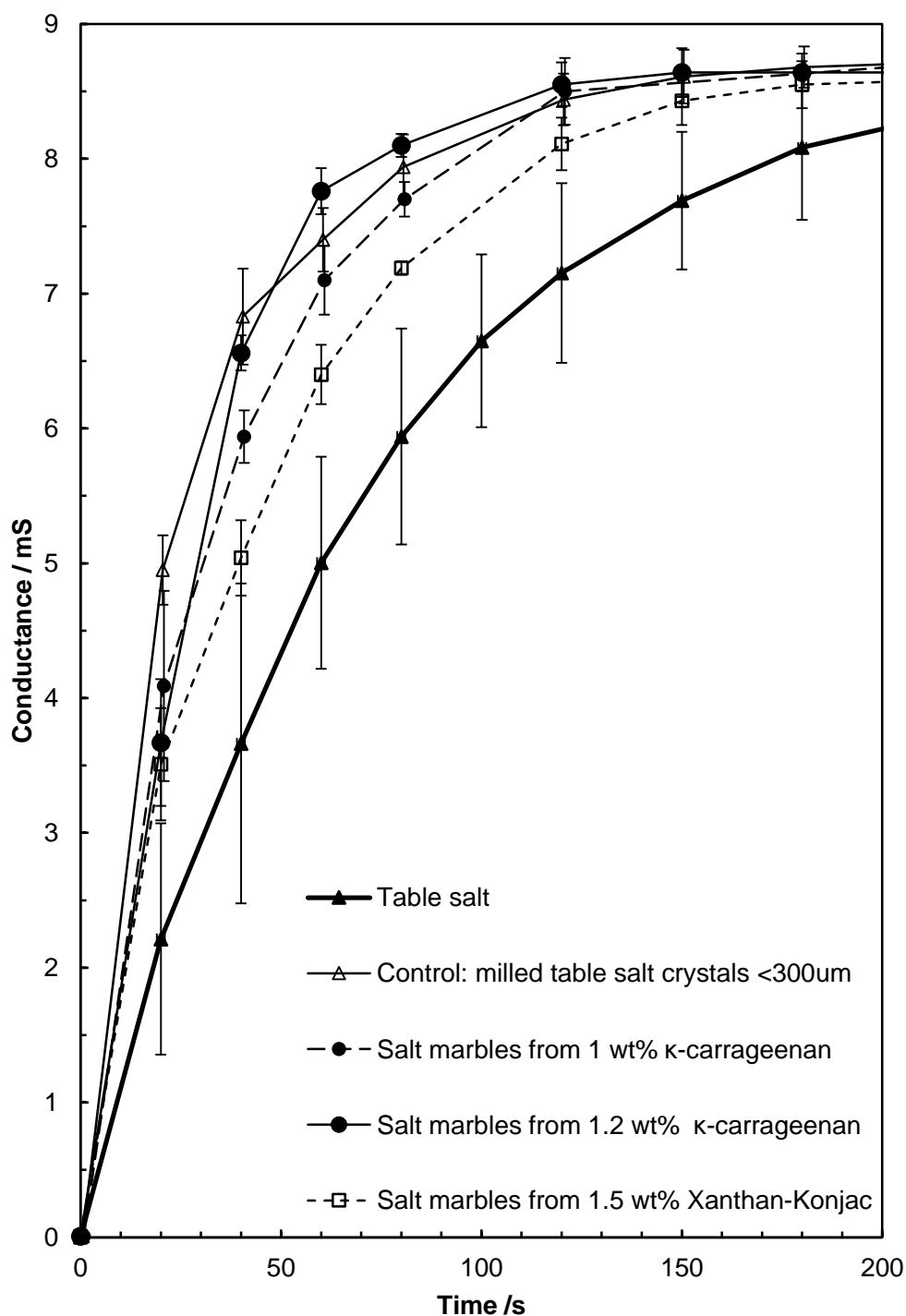


Figure 6.10. Conductivity of the aqueous medium vs time followed after the introduction of a fixed amount (0.2500 g) of table salt or alternatively hollow-shell salt marbles. The table salt particles had an average mean particle diameter of $280 \pm 100 \mu\text{m}$ and the milled salt crystals were $30 \pm 20 \mu\text{m}$.

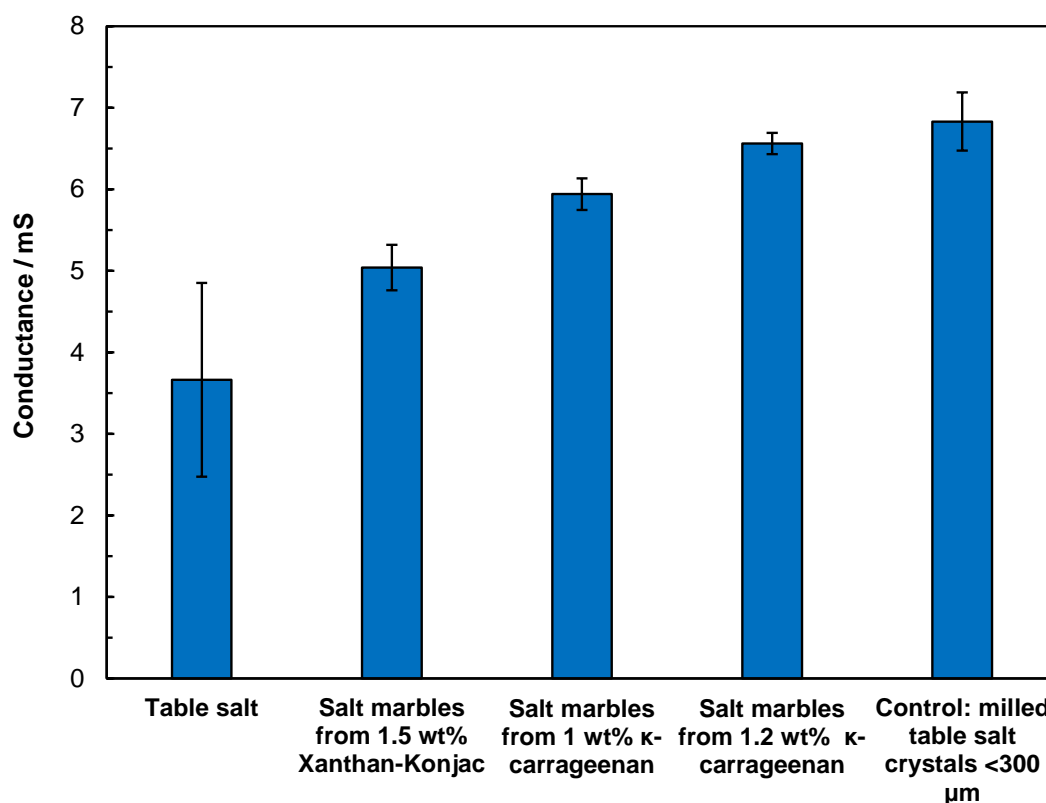


Figure 6.11. Graph showing the solution conductivity upon dissolution of different samples of salt or salt marbles 40 seconds after the addition of the sample (0.2500 g) into a fixed amount of water. The higher the conductivity of the solution the higher is the perception of saltiness for the consumer. The graph shows that compared to the ordinary table salt higher saltiness feel could be possibly delivered to the consumer using salt marbles produced by the hydrogel bead templating.

6.4 CONCLUSIONS

Salt marbles were produced by spray gelling hydrogels over microcrystalline salt powder followed by their separation by sieving. Compared to the table salt, the salt marbles release salt quicker upon dissolution in water, since the surface area of the salt from the solid microcrystals on the marble is much higher and easier to access and could be released faster than those ordinary salt crystals. Salt marbles hold a promise for a possible replacement of the conventional table salt. A reduced salt content would yield the same or higher rate of salt release. The marbles could be used as a healthy alternative for the consumer.

This product could be used to reduce the salt intake of consumer, by reduced quantity of salt used in the products, such as crisps, meat products and others. This Chapter showed only the preliminary results, which illustrate the technique for the salt marble preparation and their superior rate of salt release leading to the reduced overall salt content to trigger the same perception, compared to ordinary table salt.

However, there are several issues that need to be addressed further. For example, the high polydispersity of the produced marbles and their relatively large size calls for further improvements in the production of the hydrogel beads. This could be accomplished by using a more powerful atomizer instead of the conventional sprayer, as well as by better regulation of the temperature of the cold air which would improve the formation of hydrogel beads in an aerosol form. The additional properties of the salt marble such as porosity and mechanical strength need to be evaluated, using BET adsorption analysis and compressional strength analysis.

6.5 REFERENCES

1. C. Ayala, E. V. Kuklina, J. Peralez, N. L. Keenan, et al., Morbidity and Mortality Weekly Report, 2009, 58, 281.
2. A. Moshfegh, J. Goldman, J. Ahuja, D. Rhodes, et al., US Department of Agriculture, Agricultural Research Service, 2009.
3. L. A. Wyness, J. L. Buttriss and S. A. Stanner, Public Health Nutrition, 2012, 15, 254.
4. F. J. He and G. A. MacGregor, Cochrane Database of Systematic Reviews, 2004, Cd004937.
5. Unilever, Unilever Sustainable Living Plan: Progress Report 2011, 2011.
6. E. J. Lynch, F. Dal Bello, E. M. Sheehan, K. D. Cashman, et al., Food Research International, 2009, 42, 885.
7. H. Salovaara, Cereal Chemistry, 1982, 59, 427.
8. S. Girgis, B. Neal, J. Prescott, J. Prendergast, et al., European journal of clinical nutrition, 2003, 57, 616.
9. H. L. Meiselman and B. P. Halpern, Physiology and Behavior, 1973, 11, 713.
10. M. W. J. Noort, J. H. F. Bult, M. Stieger and R. J. Hamer, Journal of Cereal Science, 2010, 52, 378.
11. J. Busch, J. Keulemans, G. Van den Oever and F. Reckweg. Food composition, W. I. P. Organization, 2008.
12. S. Dieter, S. Franz-Theo and B. Helmut. Predominantly aqueous compositions in a fluffy powdery form approximating powdered solids behavior and process for forming same, U. P. Office, 1968.
13. P. Aussillous and D. Quéré, Nature, 2001, 411, 924.
14. C. Planchette, A. L. Biance and E. Lorenceau, Europhysics Letters, 2012, 97, 14003.

15. R. Murakami and A. Bismarck, *Advanced Functional Materials*, 2010, 20, 732.
16. B. P. Binks and R. Murakami, *Nature Materials*, 2006, 5, 865.
17. J. Tian, T. Arbatan, X. Li and W. Shen, *Chemical Communications*, 2010, 46, 4734.
18. M. Dandan and H. Y. Erbil, *Langmuir*, 2009, 25, 8362.
19. P. Aussillous and D. Quéré, *Proceedings of the Royal Society A: Mathematical, Physical and Engineering Science*, 2006, 462, 973.
20. T. H. Nguyen, Master Thesis, Monash University, 2009.
21. K. P. Hapgood, L. Farber and J. N. Michaels, *Powder Technology*, 2009, 188, 248.
22. S. Gaunt, S. J. Minter, E. E. Best and W. L. Nehmer. Sodium bicarbonate product, W. I. P. Organization, 2013.
23. S. J. Minter and S. Maude. Salt product, W. I. P. Organization, 2009.
24. Y. Zhang, B. Xie and X. Gan, *Carbohydrate Polymers*, 2005, 60, 27.
25. R. M. D. Soares, A. M. F. Lima, R. V. B. Oliveira, A. T. N. Pires, et al., *Polymer Degradation and Stability*, 2005, 90, 449.

Chapter 7. Development of Novel Soap-Hydrogel Formulations with Improved Sustainability

“I am a Count, not a Saint.”

Alexandre Dumas, The Count of Monte Cristo

In this Chapter it will be demonstrated how the original methodology of hydrogel slurry templating technique that was used in Chapters 3-5 can be tuned to the formulation of a soap composite. An overview for the need of new approaches in soap making is followed by the results obtained for the morphology, dissolution time and washing ability of the soap – hydrogel bead slurry composites produced. Here a new formulation of soaps based on hydrogel slurry composites is developed, which uses much less soap and allows minimisation of soap waste.

7.1 THE NEED FOR SOAP WASTE REDUCTION IN THE DEVELOPED WORLD

Soap is an important product used worldwide everyday day. Typically, the active part of a soap bar consists of a mixture of fatty acids, which act as surfactants in cleaning the dirt from skin. It has been well established that hand washing is crucial to remove pathogens and thus stop the spread of diseases.¹ On the other hand, it has been estimated that around 2.6 million bars of soap in the U.S. hotel rooms alone are discarded every day.² This essentially is a waste of resources used to produce this soap (i.e. oils, water, perfume, energy, etc.) and an environmental pollutant, where it could harm aquatic microorganisms like algae and affect river marine ecosystems.

Soap, together with shower gel are reported to contribute to 48 % of the total carbon footprint of Unilever products.³ Following the Sustainable Living Plans by Unilever⁴ the hydrogel templating technique could be applied in soap bars as a route to reduce waste, environmental damage and preserve ingredients used in the production of the soap bars. The cost of soap bar production could be reduced by templating hydrogels within the matrix of the soap and introducing porosity, or alternatively producing

composite soap-hydrogel meso-structured material, where the hydrogel acts as a filler. Significant part of the composite volume would still be the original soap, but another part would consist of a hydrogel (<5% polysaccharide and >95% water). Such bars could be used where the whole bar is usually not fully used, e.g. in private rooms of hotels and cruise ships. In addition to the reduction of cost to produce such soap bars, it would be beneficial for the environment as less soap would be discarded into the environment and the carbon footprint of soap bar production would be reduced. This strategy of reducing the soap content in the disposable soap bars at the expense of incorporating hydrogel micro beads into these composites would reduce the environmental impact of such household products upon their disposal. Such bars could be an attractive alternative to the currently available products.

A somewhat similar approach to the hydrogel slurry templating technique has been reported in the literature.⁵ The researchers reported encapsulation of various oils into beads shelled by resistant walls e.g. made from alginate, Agar or another material, and then mixing these beads into a pre-gel solution of Laponite XLG, which was then gelled by an addition of an electrolyte and then dispersing these gel matrixes homogeneously within the soap base. In the research reported in this Chapter, no oils or fragrances were encapsulated, but this could be potentially done in the follow-up studies. Also, the hydrogel was gelled and pre-blended before being mixed with the soap base and no articles were encapsulated in the hydrogel beads.

7.2 RESULTS

7.2.1 Adjustment of the Melting Points of Soap Composite

As seen in the previous Chapters, the disadvantage of using Xanthan-Konjac hydrogel is its relatively low melting point (around 45-50 °C). Above this temperature the beads of hydrogel melted and reformed a continuous matrix. To avoid this, the temperature of the hydrogel needed to be kept below its melting and thus the material with which the hydrogel is templated should ideally be in a liquid phase or at least workable below the melting temperature of the hydrogel. Soaps have relatively high melting temperatures, but their setting temperatures are within the desired range. However, it

would still be beneficial to lower the soap melting temperature so that the melting temperature of the used hydrogel is not reached during the composite preparation.

Firstly, the melting point of the soap base and the effect to this temperature by the addition of glycerol was analysed. Glycerol was used in order to add a moisturising effect to the soap bars and also to reduce the setting temperature of the soap base. In addition to this, since glycerol is a waste by-product of biodiesel production, there is an active research in the alternative uses of this chemical.⁶ The incorporation of glycerol from the biodiesel production in the soap base could be an attractive way of using this abundant side product of biodiesel production.

The melting and the setting temperatures of the soap base quoted by the supplier were 70 °C and 40 °C respectively. Solid soap was opaque, whereas soap that was molten into a liquid phase was transparent. This phenomenon was used in order to confirm the melting and setting temperatures of the soap. By measuring the UV-Vis absorption of the soap whilst lowering the temperature, the setting point of the soap base was determined. Below, a set of UV-Vis spectra of soap base with various amounts of glycerol (which reduces the setting temperature of the soap base) are presented (see Figure 7.1). Figure 7.1(a) shows soap base alone at various temperatures. It could be said that the setting temperature was 41 °C, since the absorbance at $\lambda \approx 300$ nm had increased compared to the samples at higher temperature i.e. the soap become opaque at 41 °C. Figure 7.1(b) shows the comparison of UV-Vis absorbance spectrum of the molten state soap samples with various ratios of glycerol. The addition of glycerol reduced the absorbance at $\lambda \approx 300$ nm, that way confirming that addition of glycerol lowers the setting temperature of the soap base. Figure 7.1(c) displays data at 40 °C for the control sample and 38 °C for samples with added glycerol. Three samples had a higher absorbance at $\lambda \approx 300$ nm, which were for the samples with 0 vol%, 20 vol% and 40 vol% glycerol content in the soap, and the sample with 60 vol% glycerol showed low absorbance at this wavelength. From this data it can be concluded that all but the 60 vol% glycerol content samples have solidified at this temperature. The setting temperatures determined by the change of absorbance (setting of the soap) are presented in Table 7.1.

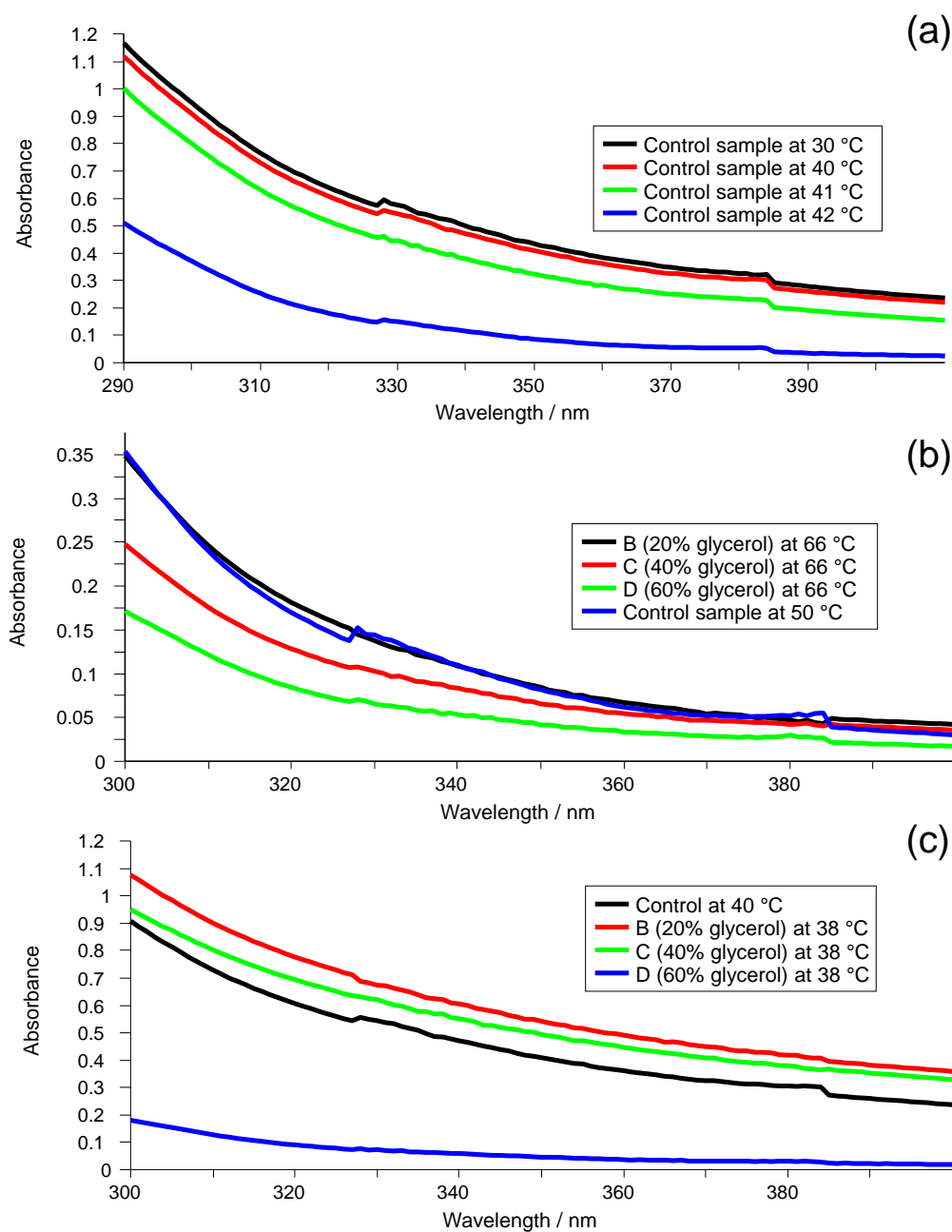


Figure 7.1. UV-Vis spectra of (a) raw soap at various temperatures (cooling down) as showed in the legend. The higher absorption recorded for samples at $T \leq 41$ °C correspond to the solidified sample; (b) samples at molten state: raw soap at 50 °C (blue) and soaps with varying glycerol content (B, C, D with 20 vol%, 40 vol%, 60 vol% glycerol respectively) at 66 °C. All graphs represent molten soap. (c) soap base at 40 °C (black) and soaps with varying glycerol content (B, C, D with 20 vol%, 40 vol%, 60 vol% glycerol respectively) at 38 °C. Only sample D showed low absorbance at this temperature, as it still was in a molten state.

Table 7.1. Composition and setting temperature range of soap base with added glycerol.

Sample ID	Soap content / %	Glycerol vol% / %	T _{setting} / °C
A (control)	100	0	40-42
B	80	20	38-42
C	60	40	38-40
D	40	60	36-38

Since soap in the composite creates a different environment compared to salt-fat base, the hydrogel formulation needed to be adjusted accordingly. As mentioned in the previous Chapters, there has been some research reported in the literature on the stability of the hydrogels with glycerol and various salts. It has been reported that Xanthan and Locust Bean Gum (LBG) or Xanthan and Konjac mixtures are stable in the presence of salt.⁷ One recipe included glycerol (12.7 wt%), NaCl (21.6 wt%), Xanthan gum (0.58 wt%) and LBG (0.25 wt%); another had glycerol (20 wt%), NaCl (10 wt%) and Xanthan and Konjac gums each 0.5 wt%.⁷ Other patents use various mixtures of Xanthan and LBG (i.e. 1:1). High viscosities have been achieved when a Xanthan-LBG ratio of 2 : 4 was used.⁸ Depending on the other conditions such as the total polysaccharide concentration or dissolution temperature, this ratio can change to 1 : 5 or 3 : 3.⁸ Also, pectin has been found to be stable at low pH and slightly salty solution of water.⁹

The effect of addition of glycerol to the hydrogel for the soap-gel composite was analysed. Composite samples of soap and gel are shown below in Figure 7.2. All samples (a-d) had a hydrogel : soap ratio of 1 : 1. The composition of Xanthan : Konjac 2 : 1 hydrogel is detailed in Table 7.2. It is not very clear from the image what ratio of glycerol : water should be used, but samples (a) and (d) seem to have structural advantages over the (b) and (c) as they look very similar to the soap base.

Table 7.2. Hydrogel composition for the soap-gel mixture.

	Glycerol / vol%	Water / vol%	Total gelling agent / wt%	NaCl/wt%
A	17	83	2.7	4.1
B	29	71	2.3	4.1
C	37	63	2.0	4.1
D	43	57	2.3	4.1

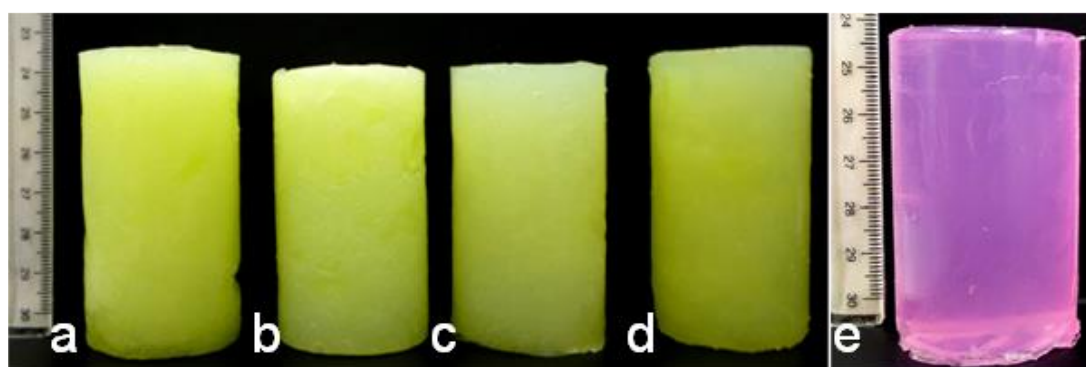


Figure 7.2. Images of (a-d) hydrogel (Xanthan - Konjac) templated soap composites after 4 hours of moulding. All samples had a hydrogel to soap ratio of 1 : 1 and gels contained fluorescein sodium salt dye. All hydrogels had glycerol, water and 4% sodium chloride present. Glycerol content was 17, 29, 37 and 43 vol% for a, b, c and d respectively. The mass of the gelling agent used accounts for 2.7, 2.3, 2.0 and 2.3 wt% for a-d samples. E is the control sample of soap base with Nile red dye.

7.2.2 Morphology Analysis of the Soap-Hydrogel Composites

The composites of hydrogel templated soap were analysed using confocal microscopy. The images obtained are shown in Figure 7.3. It was observed, that the individual phases (hydrogel beads and soap base) were still intact after moulding and solidification. This confirmed that the hydrogel did not melt as it was mixed with the hot soap solution. However, due to the high thickness of the samples (approximately 1 mm), the laser light was lost as the penetration was increased to larger than 100 μm depth due to the absorption and dissipation of the laser light by the hydrogel and soap phases.

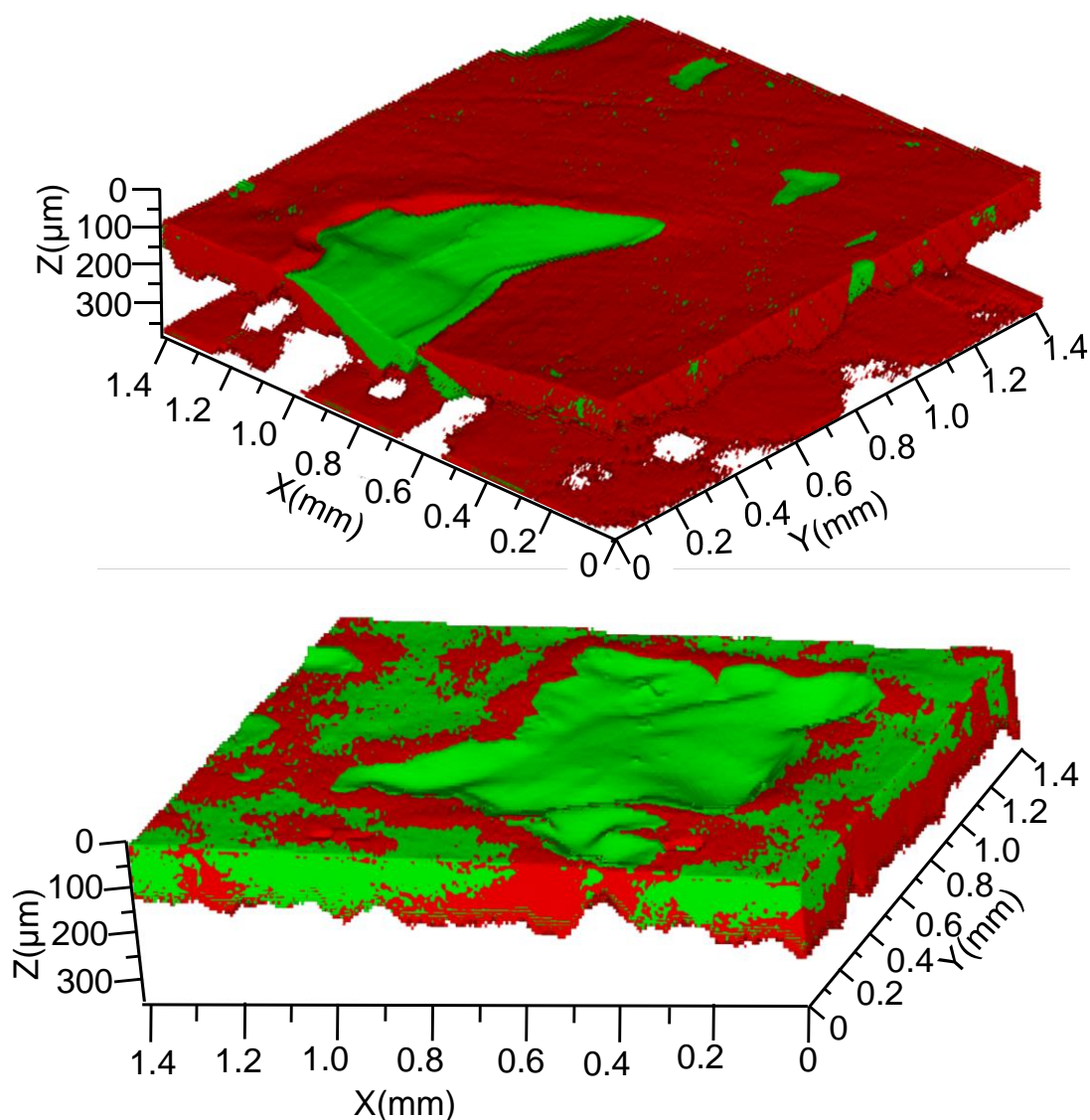


Figure 7.3. 3D Confocal laser scanning images reconstructing the structure of soap - hydrogel bead composite (50 vol%) with 2.7 wt% of the gelling agent and 17 vol% of glycerol within the hydrogel. Soap was stained with Nile Red and hydrogel with Fluorescein sodium salt, which correspond to the red and green stains respectively. z – stacking analysis was performed to obtain the images and the individual slice thickness was set to 10 μm. The sample cannot be analysed at deeper penetration (>100 μm) due to the light absorption and dissipation.

7.2.3 Dissolution Time of the Soap Composites

Soap composites were analysed and their dissolution times measured using a setup for the dissolution time measurements described in Chapter 2 Section 2.2.5. The beaker contained distilled water and all the soap samples were cut to have a height of 2 cm (diameter was 3.6 cm). The samples were placed in a cylinder-shaped mesh and left to stir for 20 hours at room temperature. The composition of the samples is detailed in Table 7.3. The difference between the samples in this case was not the hydrogel volume content (which was kept constant as well as the gelling agent concentration), but the glycerol-to-water ratio. The hydrogels in these experiments were blended using a Silverson homogeniser and additional water was added to facilitate this procedure, by adding extra lubrication between the hydrogel beads. The results of the dissolution experiments obtained are shown in Table 7.4. An image of the soap and soap - hydrogel composites after the experiment allowing to dry for 4 days is shown below in Figure 7.4. All samples (a-c) had a gel : soap ratio of 1:1. As can be seen from Figure 7.4 all samples retained their volume to a high extent. The gels in samples (b) and (c) were very viscous and sticky, due to the glycerol present within, but the structure of the composite did not swell in water more than the soap base. A conclusion can be made that the composites were as stable in stirred water at room temperature as the soap base and that the hydrogel may be capable to preserve the soap composite from a rapid disintegration.

Table 7.3. Hydrogel composition used in soap-hydrogel composites dissolution experiment.

	Water / g	Glycerol / g	Water (excluding extra added) / %	Total gelling agent / %
A	70+20 ^a	30	70	3
B	40+10 ^a	60	40	3
C	20+10 ^a	80	20	3
Control	n/a	n/a	n/a	n/a

^a– This volume after summation sign was added prior blending the mixture to facilitate blending and enhance hydrogel fragmentation. It contained proportionate amounts of water, glycerol and salt, same as the initial mixture for the gel.

Table 7.4. Size and weight change for the soap – hydrogel composites after the dissolution experiment. Composition of the samples is given in Table 7.3

	Sample height after 1 day drying / cm	Initial weight / g	Weight after 2 days / g	Diameter after 1 day / cm
A	2.0	23.0	22.2	3.4
B	2.0	20.9	18.8	3.5
C	1.8	23.8	19.8	3.3
Control	1.9	23.6	20.4	3.5



Figure 7.4. Images of (a-c) hydrogel (Xanthan - Konjac) templated soap stirred in water for 20 hours. All samples had a gel to soap ratio of 1:1, original sample height was 2 cm. Hydrogels phases were stained with fluorescein sodium salt dye, soap phase had Nile Red. Image taken after 4 days of drying under vacuum. Control sample was the soap base (without the dye or hydrogel).

7.2.4 Release of the Soap during Dissolution of the Soap-Hydrogel Composites

Various methods to assess the cleansing abilities of soaps are described in literature, e.g. measuring soap capabilities to remove dirt by immersing a dirty hand in a stirred solution of soap,¹⁰ antibacterial tests in vivo,¹¹ and others. Here it was not aimed to analyse the activity of the soap composites in great detail, so a simpler experiment was designed to assess how fast the soap is released from the soap-hydrogel composites. Samples of soap composites of fixed volume were dissolved at 40 °C as described in the previous section and the surface tension of surrounding aqueous solution was measured as a function of the sample dissolution time. The surface tension was measured using a drop shape analyser. After the monolayer coverage of the interface is reached, surfactant molecules concentrate in the solution until CMC (critical micelle concentration point), i.e. surfactant micelles start to form. The washing action of a soap is the highest when the solubility of the monomers (fatty acids) correspond to the CMC.¹² The CMC can be found by extrapolating the graphs of the surface tension vs. the time of the experiment for the sharp fall in the surface tension region and the plateau region.

To analyse and compare the relative washing abilities of the composites, a set of soap – hydrogel composites containing 25 vol%, 50 vol% and 75 vol% of hydrogel were prepared with a 2:1 Xanthan : Konjac hydrogel ratio and a total of 0.7 wt% or alternatively 4.0 wt% gelling agent present with 17 vol% glycerol. Composites with a hydrogel containing 0.7 wt% of the gelling agents are shown in Figure 7.5. The dissolution experiment was carried out, measuring the surface tension of the solution at various times. The data obtained are presented in Figure 7.6 below. The measurement of the pure soap concentration (in wt%) effect on the surface tension was carried out and presented in Figure 7.7.



Figure 7.5. Image showing soap-hydrogel composites with a total 0.7 wt% of gelling agent (Xanthan : Konjac 2:1). Soap base was stained with Nile Red and the hydrogel with fluorescein sodium salt.

The composites reduced the surface tension of water less as the volume of the hydrogel in the composite was increased. The CMC would thus take longer to reach by the more hydrogel containing composites. This suggests that the composites may underperform pure soap for hand-washing purposes, however the addition of the hydrogel increased the softness of the material, and thus the composites were easier to break in the hands. This would release more soap from the composite than the control sample. However, such experiments were out of the scope of this research and could be carried out in the future. Also a different surfactant could be used in the soap base, making it more effective than the current ingredients. Another factor for the possible contribution of the loss of washing action could be the lower active ingredient content within the composite samples, as part of the soap base was substituted with the hydrogel.

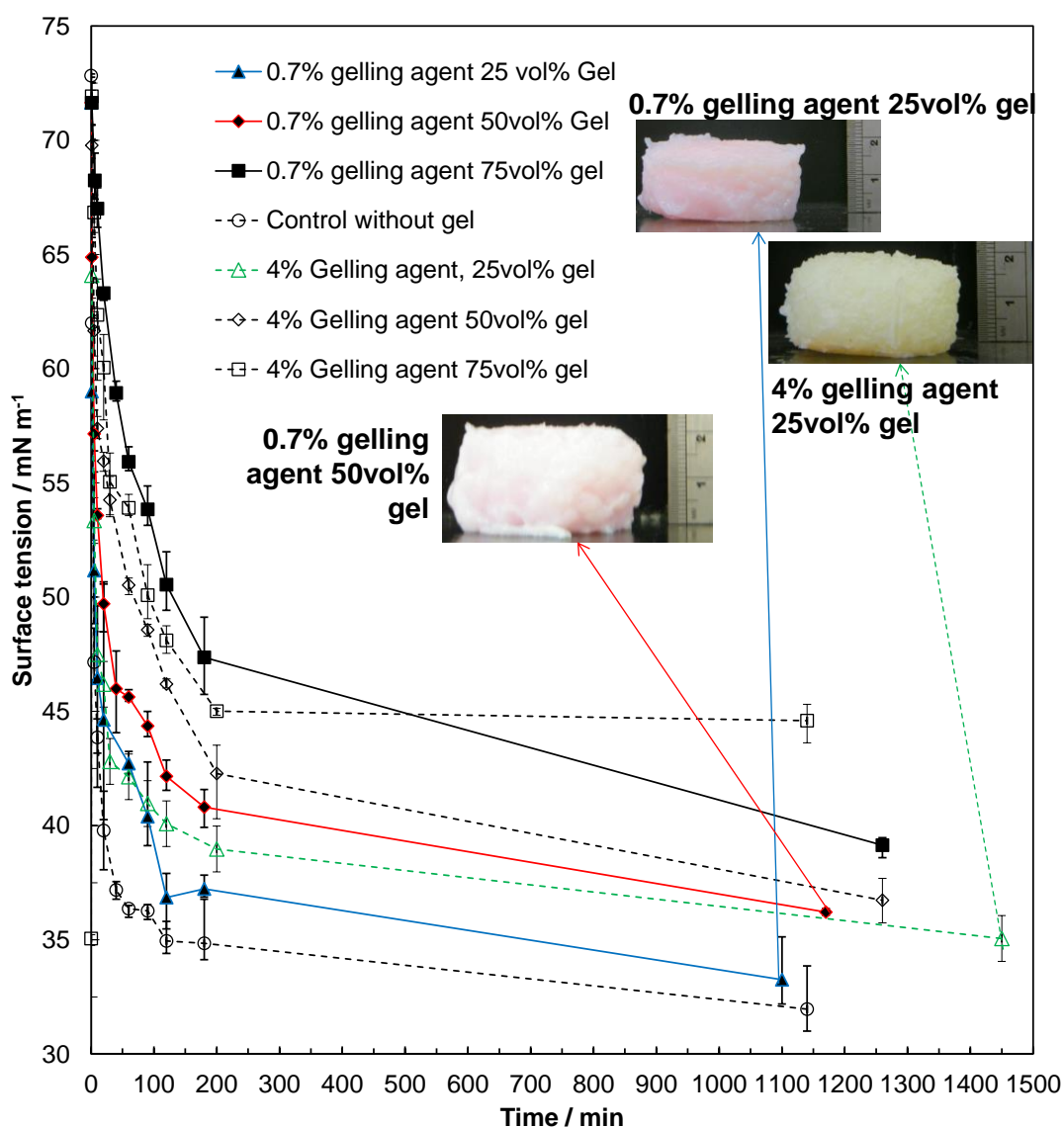


Figure 7.6. Graph showing the change in the surface tension as a function of the time of the sample dissolution experiment. The insets show the composite samples after dissolution experiment. Reduction of surface tension decreased as the vol% of the hydrogel and the gelling agent content were increased.

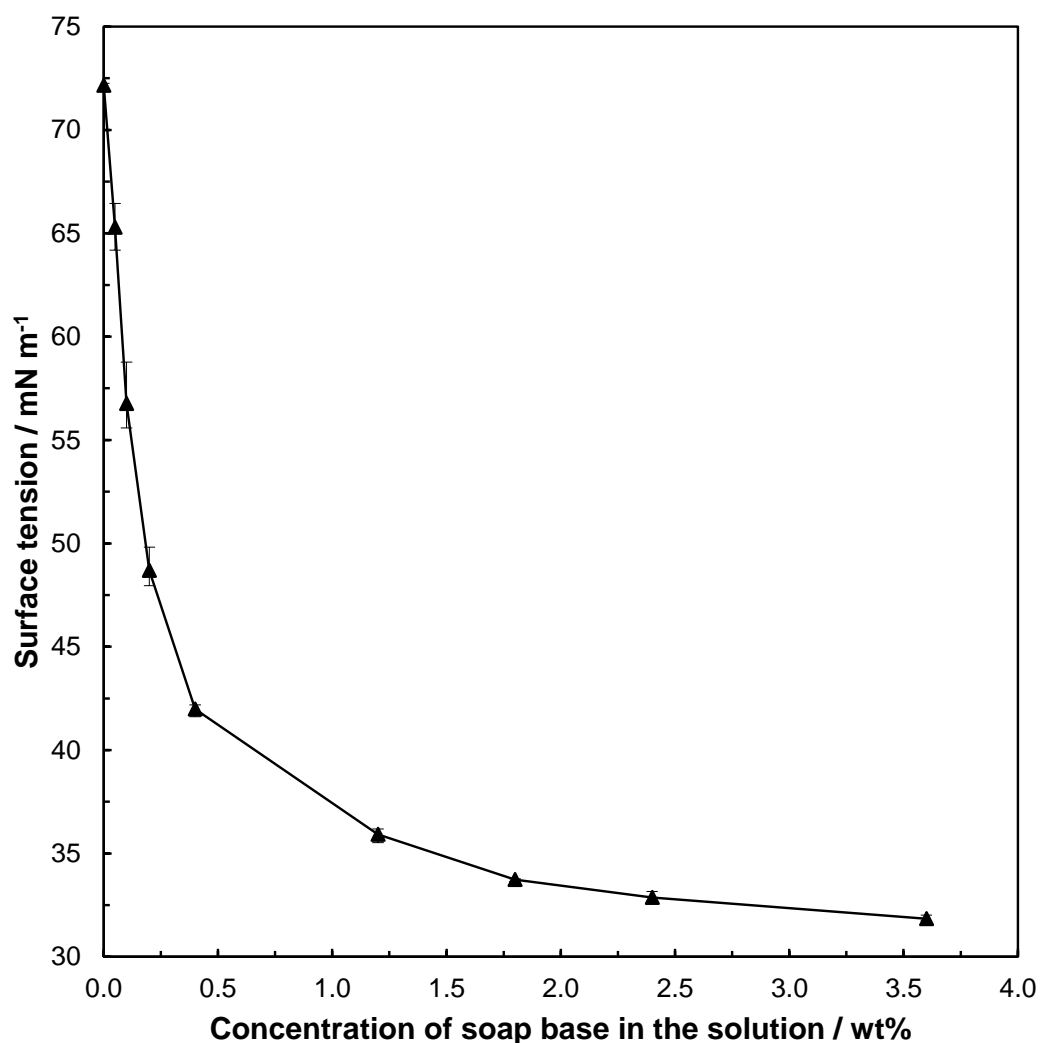


Figure 7.7. Surface tension of soap base as a function of its concentration in water.

The reduction in the gelling agent content (from 4 wt% to 0.7 wt%) in the hydrogel reduced the surface tension of the solution upon the dissolution of the composites, suggesting that the performance of the soaps composites bearing hydrogel with a lower gelling agent content would be greater. This could be due to the weaker structure of the filler (hydrogel) and water being able to dissolve it easier than the stronger 4 wt% Xanthan – Konjac hydrogel.

7.3 CONCLUSIONS

Hydrogel slurry templating technique was applied to produce soap composites. Unlike in previously described templating methodology, here the hydrogel was not evaporated, but left in as a filler. The challenge in this particular case was the

overlapping temperatures of the soap setting and hydrogel melting. The melting temperature was controlled by adding glycerol, while melting point of the hydrogel was set by the type of the gelling agent. By a careful setting of the temperatures on both the matrix (soap base with additional glycerol) and the filler (hydrogel beads) these were successfully mixed together and moulded. Confocal microscopy images showed that both the matrix and the filler were intact and the continuous phase was the soap base at 50 vol% of the hydrogel.

The composites were dissolved by adding them in a beaker of stirred warm water to imitate soap use. The surface tension of the water was measured upon dissolution of the soap-hydrogel composites. It was found, that as the hydrogel volume content was increased the reduction of the solution surface tension was smaller. This indicated, that the composites may be less capable to remove dirt from the surfaces compared to control samples. However, these composites ought to be tested using other methods reported in the literature, including *in vivo* analysis to generate data on their washing capabilities and the active component (soap base) mass should be equalised within the sets of samples. Finally, the incorporation of glycerol from the biodiesel production in the soap base could be an attractive way of using this abundant industrial side product.

7.4 REFERENCES

1. E. Lautenbach, K. F. Woeltje and P. N. Malani, Practical Healthcare Epidemiology, 3rd edn., The University of Chicago Press, Chicago, 2010.
2. J. Hattam, How Old Hotel Soap Can Save Thousands of Lives, <http://www.treehugger.com/green-food/how-old-hotel-soap-can-save-thousands-of-lives.html>, Accessed 24/7/2012, 2012.
3. Unilever, Unilever Sustainable Living Plan: Progress Report 2012, 2013.
4. Unilever, Unilever Sustainable Living Plan, <http://www.unilever.com/sustainable-living/>, Accessed 24/7/2012, 2012.
5. E. D. George. Soap with suspended articles, W. I. P. Organization, 2002.
6. G. L. Brett, Q. He, C. Hammond, P. J. Miedziak, et al., *Angewandte Chemie-International Edition*, 2011, 50, 10136.
7. C. Inoue, S. Silva Paes, M. E. Perrine, A. K. Popp, et al. Savoury Food Concentrate, U. P. Office, 2011, 20100143550.
8. J. A. Casas and F. García-Ochoa, *Journal of the Science of Food and Agriculture*, 1999, 79, 25.
9. I. A. Challen, S. East and G. R. Sanderson. Process for preparation of algin or pectin gels, U. P. Office, 1982.
10. Unilever, Unilever Sustainable Living Plan: Progress Report 2011, 2011.

11. C. Planchette, A. L. Biance and E. Lorenceau, *Europhysics Letters*, 2012, 97, 14003.
12. W. C. Presto and W. Preston, *The Journal of Physical and Colloid Chemistry*, 1948, 52, 84.

Chapter 8. Summary and Conclusions

“You can only grow by coming to the end of something and by beginning something else”

John Irving, The World According to Garp

Hydrogel slurry templating technique is a versatile route for the creation of composite and porous materials. This simple, green and cost-effective method is based on mixing of a slurry of hydrogel particles with a slurry of a matrix material, which is later solidified after the composite is moulded. In order to make a porous composite, the water from the hydrogel is evaporated without affecting the solidified matrix. The method offers control of the pore size through different hydrogel bead sizes, as the hydrogel beads are primarily serving only as a template over which the matrix can solidify. Nearly all of the initial hydrogel volume is replaced by air after allowing the water to evaporate from the composite, so the volume fraction of the hydrogel slurry directly influences the extent of porosity of the final composite. It was proved by a number of examples throughout this thesis that the technique can be easily modified to suit a variety of materials and is not limited to building and food industries.

In **Chapter 2** experimental techniques for the preparation of hydrogel, namely Xanthan – Konjac, κ -carrageenan, Gellan and polyacrylamide, their blending using different mixers are described. Also, preparation of cement, PDMS, gypsum, clay-cement, model bouillon cube (salt and fat mixture) and soap matrixes used to fabricate composites and the methods of preparation of the composites are outlined. It was found that in bouillon cube and soap composite preparations it was essential to control the temperature during the composite preparation as the hydrogel slurries were melting if the temperatures were too high. Another method of hydrogel templating, where the hydrogel was spray-gelled for the hollow-shell salt marbles preparation is described. At the end of the Chapter, the details of the equipment used for the sample visual, acoustic, texture, strength, dissolution and saltiness analysis are set out.

In **Chapter 3** the hydrogel slurry templating technique is applied for the preparation of porous cement, gypsum, clay-cement and PDMS composites. A non-ionic polyacrylamide hydrogel was used for the preparation of the former three types of composites, and Gellan gum was used for the fabrication of PDMS composites. The hydrogels were blended using hand-held blenders, which yielded a rather polydisperse-bead-size slurries of hydrogels with an average size of approximately 100 μm for polyacrylamide and 750 μm for Gellan. It was found, that the densities of porous cement composites dropped with respect to the control with up to 77 % reduction in density for initial 80 vol% of its volume substituted by the hydrogel. Similar reductions in densities were observed for PDMS composites. Clay-cement and gypsum samples, on the other hand, did not have such a significant reduction in densities due to the noticeable volume shrinkage of the composites, but still reached 57 % and 67 % respectively. Indeed, the cement and PDMS samples had only about 5 % of shrinkage with the hydrogel content being 80 vol% of the total volume of the composite, whereas talc-cement composites had 60 % volume shrinkage and in gypsum samples it was 65 % at the same hydrogel volume content. The compressional strength of the PDMS composites decreased by around 95 % for the samples with 80 vol% initial content of the hydrogel. All porous PDMS composites showed an elastic behaviour as they returned to their original volume after 24 hours if they were compressed.

Chapter 4 looks into the further optimisation of the methodology for the fabrication of cement and PDMS composites and targets the porous composites for the application in sound insulation panels. Highly porous PDMS samples templated with 70 vol% Gellan gum hydrogel and cement samples templated with 80 vol% of polyacrylamide hydrogel showed improvements in sound absorption throughout the analysed sound frequency range (200-2000 Hz), particularly improving the impedance between 200-400 Hz and 1200-1800 Hz frequency ranges. SEM images of cement samples with polyacrylamide showed fibrous domains within the pores of the composite, which, in addition to the classical methods of sound absorption, could be acting as viscous dampeners and thus reducing the amplitude of sound wave by passive absorbance of the sound energy. The hydrogel bead preparation methodology was improved by passing the hydrogel through a mincer with various pore size mincer plates. This

produced significantly less polydisperse bead size slurries with a much better average bead size control through the use of mincer plates with different hole sizes. The polyacrylamide hydrogel was replaced by naturally occurring Xanthan and Konjac gelling agents which together form a hydrogel resistant to a high salt content. Porous cement composites with different hydrogel bead size distributions were prepared and the differences in their acoustic absorbance properties with the same volume of the hydrogel were compared, showing significantly better absorption of the composites produced using smaller hydrogel beads (2 mm vs 3 mm mincer plate). The compressional strength of the porous cement composites decreased from 5 ± 1 MPa for the sample without hydrogel to 0.5 MPa for the 70 vol% hydrogel containing sample. The technique has a possibility to be used for the preparation of flame-resistant sound absorption panels.

Hydrogel slurry templating for the preparation of composite and porous model food products is presented in **Chapter 5**. Model bouillon cube base (without flavours and taste enhancers) consisting of palm oil and salt crystals (and in some cases starch) was templated over Xanthan – Konjac gum or κ -carrageenan hydrogel beads. A significant reduction in the composite density was detected after freeze-drying the composites. Porous composites had different texture and dissolution properties, with the increase in the initial hydrogel content and depending on the hydrogel used. Xanthan – Konjac hydrogel containing composites had an increase in their volume upon drying due to the expansion of the air bubbles trapped within the hydrogel during freeze drying. These composites showed an increase in both strength and dissolution time with hydrogel content < 35 vol% and a slight decrease above this volume fraction. Porous bouillon cubes with κ -carrageenan hydrogel beads had a decrease in the composite strength and dissolution time with the increase of the hydrogel content, with reduction in compressive strength by up to two times with an initial hydrogel volume fraction of 30-50 vol% depending on the sample preparation methods. The dissolution time of these composites was reduced by 2-3 times compared to samples without hydrogels. This reduction in strength and dissolution time of the bouillon composites had already attracted commercial interest to the hydrogel slurry templating technique and has a high potential in the application for these products.

Hollow-shell salt marbles preparation by templating salt microcrystals over hydrogel beads is described in **Chapter 6**. This methodology has the potential to reduce table salt intake by keeping the saltiness perception unchanged as the salt marbles dissolved faster compared to the ordinary table salt crystals. The marbles were prepared by spraying a hot hydrogel solution down a chilled column onto a bed of finely milled salt particles and, after covering the surface of the beads with salt, evaporating the water phase from the marble core. The methodology benefits from the use of different gelling agent concentrations, which influence the final size of the marbles (increase in the gelling agent content increased the marble size) as well as a possibility to modify the final size of the marbles with the use of different spraying machinery. Very recently released patents^{1, 2} show a high interest in the field of hollow-core salt production and the technique presented in Chapter 6 gives an alternative route for the production of such products.

Finally in **Chapter 7** the hydrogel slurry templating technology was applied to prepare composite soap-hydrogel bars without removing the water from the hydrogel phase. The idea behind the application of this technology is the need to reduce soap waste from soap bars in hotels. Replacing part of the soap volume with an environmentally friendly hydrogel would reduce the waste of soap. The composites were stirred in water to monitor the surface active component release vs time and a reduction in the release of surface active components was recorded for samples with an increase in the volume fraction of the hydrogel. However, since the composites were much softer, the release of active ingredients from the composites may be increased in the real hand washing procedure.

In summary, this thesis showed how a novel hydrogel slurry templating technique can be applied to produce a range of porous and composite materials, suited for food and personal care as well as construction industries. The use of this particular technique has the following key advantages:

- Use of naturally abundant hydrogels makes the methodology environmentally friendly for the introduction of porosity and change in texture, insulation, etc. Moreover, a wide scope of food-grade hydrogels is available, so the methodology can suit a number of composite food preparation requirements.

- The size of the pores can be selectively tuned for the particular requirement as the pore size is represented by the initial hydrogel bead size. This allows not only the fabrication of desired pore-size composites but also introduction of hierarchical porosity within the materials, leading to an improved texture and taste.

There is a large scope of further development of this technique. One of the outstanding flaw of the currently used hydrogel slurries is their bead size polydispersity. Additional methods for the preparation of hydrogel beads, which could be applied on an industrial scale production need to be developed for the better control of the beads size. Having batches of different bead size hydrogels could allow an incorporation of them to produce particular pore size cement composites, which could be later stacked into thicker walls for an even better sound insulation. It would also be interesting to study the structure of pores within the composites using mercury intrusion porosimetry, BET adsorption or even μ CT. For the increase in the strength of porous cements, it would be necessary to incorporate other particles, such as sand grains etc. to make the composites much stronger, as it is done in the preparation of concrete in laboratories focusing in the improvement of these materials.

The production of porous bouillon cubes using the current freeze drying procedure would not be implemented into industry due to the high costs associated with the procedure. Alternative methods of drying should be tested, such as drying in ovens at various temperatures or vacuum ovens. Also, it may not be necessary to produce porous bouillon cubes, but instead keep the hydrogel within the composite and gain the advantages of reduced strength of the composites and shorter dissolution time that way. Incorporation of various hydrophilic flavours within the hydrogel phase could be another interesting follow up study, together with monitoring of the release of these flavours by gas chromatography (GC-MS) and proton transfer reaction (PTR-MS).

Production of hollow-shell marbles using a specifically set spray drier, where particular size drops are sprayed into a cooled column onto a base of salt crystals which is dried by an air flow would result in a better control of the size of the marbles and could reduce the thickness of the salt shell. In other words, materials designed for the particular industry or purpose should be produced by the specialists of that field after

familiarising with the results outlined in this thesis. This will result in a much better quality of the composites, since the purpose of the work in this thesis was to develop the technique itself for a range of fields and explore the avenues in general, rather than to focus on a single application.

8.1 REFERENCES

1. S. Gaunt, S. J. Minter, E. E. Best and W. L. Nehmer. Sodium bicarbonate product, W. I. P. Organization, 2013.
2. S. J. Minter and S. Maude. Salt product, *W. I. P. Organization*, 2009.